AD-A046 542 NAVAL ENVIRONMENTAL PREDICTION RESEARCH FACILITY MON--ETC F/G 4/2
METEOROLOGICAL PHENOMENA OF THE ARABIAN SEA,(U)
MAR 77 L R BRODY

UNCLASSIFIED NEPRF-AR-77-01 NL

1 OF 2
AD
A046542

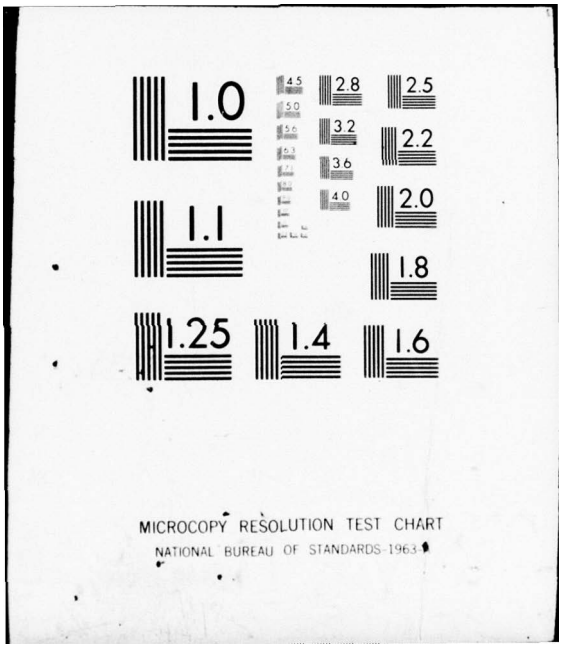
1.0
4.5
5.0
5.6
6.3
7.1
2.8
3.2
3.6
4.0
2.5
2.2
2.0
1.8
1.1
1.25
1.4
1.6
MICROCOPY RESOLUTION TEST CHART
NATIONAL BUREAU OF STANDARDS-1963-A

NEPRF APPLICATIONS REPORT
NEPRF-AR-77-01

(5) (14)

METEOROLOGICAL PHENOMENA OF THE ARABIAN SEA

(10) L. R. BRODY

(11) MARCH 1977 (12) 184p.

APPROVED FOR PUBLIC RELEASE
DISTRIBUTION UNLIMITED

NAVAL ENVIRONMENTAL PREDICTION
RESEARCH FACILITY
MONTEREY, CALIFORNIA 93940

UNCLASSIFIED

SECURITY CLASSIFICATION OF THIS PAGE *(When Data Entered)*

REPORT DOCUMENTATION PAGE		READ INSTRUCTIONS BEFORE COMPLETING FORM
1 REPORT NUMBER NEPRF APPLICATIONS REPORT AR-77-01	2. GOVT ACCESSION NO.	3. RECIPIENT'S CATALOG NUMBER
4. TITLE *(and Subtitle)* Meteorological Phenomena of the Arabian Sea		5. TYPE OF REPORT & PERIOD COVERED
		6. PERFORMING ORG. REPORT NUMBER
7. AUTHOR(s) L. R. Brody		8. CONTRACT OR GRANT NUMBER(s)
9. PERFORMING ORGANIZATION NAME AND ADDRESS Naval Environmental Prediction Research Facility Monterey, CA 93940		10 PROGRAM ELEMENT, PROJECT, TASK AREA & WORK UNIT NUMBERS NAVENVPREDRSCHFAC WU 086:2-2
11. CONTROLLING OFFICE NAME AND ADDRESS Naval Air Systems Command Department of the Navy Washington, D.C. 20361		12 REPORT DATE March 1977
		13. NUMBER OF PAGES 196
14. MONITORING AGENCY NAME & ADDRESS*(if different from Controlling Office)*		15. SECURITY CLASS. *(of this report)* UNCLASSIFIED
		15a. DECLASSIFICATION/DOWNGRADING SCHEDULE

16. DISTRIBUTION STATEMENT *(of this Report)*

Approved for public release; distribution unlimited.

17. DISTRIBUTION STATEMENT *(of the abstract entered in Block 20, if different from Report)*

18. SUPPLEMENTARY NOTES

19. KEY WORDS *(Continue on reverse side if necessary and identify by block number)*

Arabian Sea	Satellite meteorology
Indian Ocean	Climatology
Tropical meteorology	Subtropical cyclones
Monsoon meteorology	Western disturbances
Tropical cyclones	Low-level jet

20. ABSTRACT *(Continue on reverse side if necessary and identify by block number)*

This document, the product of extensive literature research, provides a single and comprehensive reference text for the operational forecaster in the Arabian Sea and Gulfs of Aden and Oman. It contains extensive climatological information, descriptions of significant meteorological phenomena and relevant forecasting aids, discussions of

DD FORM 1 JAN 73 1473 EDITION OF 1 NOV 65 IS OBSOLETE S N 0102-014-6601

UNCLASSIFIED

SECURITY CLASSIFICATION OF THIS PAGE *(When Data Entered)*

20. Abstract (continued)

meteorological conditions affecting various regional ports, and a representative assortment of typical weather sequences depicted by both satellite imagery and conventional data.

General information on the large-scale Asian monsoon and its relationship to the Arabian Sea region is presented. Also discussed are the significant meteorological phenomena associated with time and space variations in the Arabian Sea monsoon; forecasting aids and typical weather sequences are provided. Seasonal progressions of weather events are discussed; variations from normal conditions are described in first-hand reports from observers in the field.

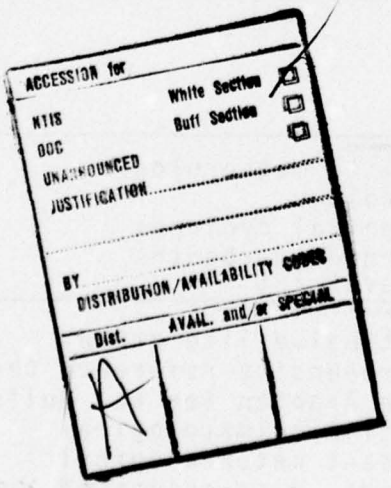

CONTENTS

1. INTRODUCTION

Despite the increasing importance of the Arabian Sea as a region of naval and maritime interest, the operational meteorologist's forecasting efforts are frequently hindered by a lack of comprehensive, readily available information on regionally significant meteorological phenomena. Conventional data are also sparse in some areas, and present numerical forecasting schemes are unable to model accurately the low-latitude monsoon circulation.

This document is designed to serve, as nearly as possible, as a single reference text for forecasters in the Arabian Sea region. Two other publications are recommended in support of the information provided herein: Handbook for Forecasters in the Bay of Bengal, Cuming, 1973; and Climatic Summaries for Major Indian Ocean Ports and Waters, U.S. Naval Weather Service Command, 1974a (see References).

The Cuming Handbook provides detailed descriptions of the general monsoon circulation and defines general flow features found in the Arabian Sea as well as the Bay of Bengal. The NWSC Climatic Summaries is the Navy forecaster's best single source of surface climatological information. (Although several charts from this latter work are included herein to compliment climatological information from other sources, the complete Climatic Summaries will still be of great value to the forecaster.)

Figure 1-1, a locator map of the geographical areas and features addressed in this document, depicts the Arabian Sea to 5°N and the Gulfs of Oman and Aden. Also shown is the Indian Ocean off the Somali and Kenya coasts (to about 5°S), an area of considerable importance to studies of the Arabian Sea monsoon. Two areas shown on the map, the Persian Gulf and Red Sea, are not discussed because the weather that affects them is significantly different from the monsoonal nature of the Arabian Sea. These areas will be addressed in future NEPRF studies.

The format of this publication makes important climatological information and forecasting aids readily available for operational use:

Section 2 -- Summary of information on the larger scale Asian monsoon and its relationship to the Arabian Sea region.

Section 3 -- Detailed descriptions of significant meteorological phenomena associated with time and space variations of the Arabian Sea monsoon. Also forecasting rules and typical weather sequences (related satellite photographs and analyses contained in Appendices B and C).

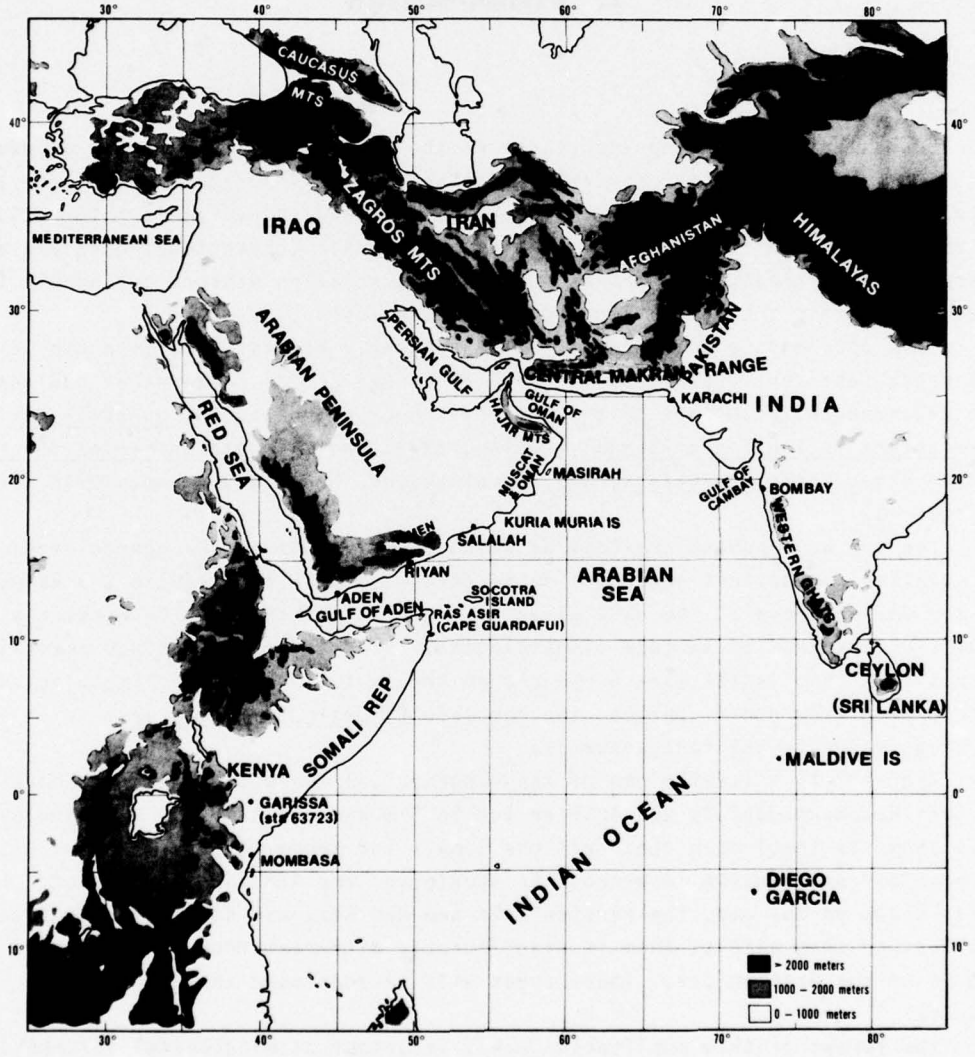

Figure 1-1. Locator map of the Arabian Sea.

Section 4 -- Information from preceding sections incorporated into a seasonal progression of Arabian Sea weather events (climatological charts showing expected normal seasonal conditions contained in Appendix A).

Variations from expected normal conditions are discussed in Section 3 and first-hand descriptions of such phenomena by observers in the field are presented. Also described in this section are meteorological conditions affecting various ports; included, for example, is a special study of forecasting high winds at Karachi, Pakistan. (This Karachi port study, to be published in Typhoon Havens Handbook for the Western Pacific and Indian Oceans, S. Brand and J. Blelloch, is summarized in Appendix D.)

Once information in earlier sections is studied, Section 4 will serve as a reference source for both normal conditions and significant deviations from normal for each of the Arabian Sea's four monsoon seasons.

As in any survey study where conditions are variable and data in some cases are sparse, certain operational questions necessarily have been left unanswered, e.g., refractive effects (but see Rosenthal, 1976, in References). Also, some of the forecasting aids described herein may not always be one hundred percent effective. Accordingly, users of this handbook are urged to provide their comments on its utility as well as their suggestions for incorporating additional materials, so that subsequent updating will reflect actual experiences from the field.

2. THE MONSOON REGIME

2.1 MONSOONAL REGIONS CRITERIA

The Arabian Sea is generally considered to be in that area of the world where the name "monsoon" was first used (Huschke, 1959) to signify a seasonal wind regime in which surface winds blow persistently from one general direction in summer and just as persistently from a markedly different direction in winter. Other significant meteorological phenomena are not included in the term's definition, although Indian meteorologists use "monsoon" to indicate a wet summer versus a dry winter over the Indian subcontinent (Cuming, 1973).

The most satisfactory criteria for determining whether a region is monsoonal have been developed by Ramage (1971), who defines the monsoon area as encompassing regions with January and July surface circulations in which:

(1) The prevailing wind direction shifts by at least 120° between January and July;

(2) The average frequency of prevailing wind directions in both January and July exceeds 40%;

(3) The mean resultant winds in at least one of the two months exceed 3 m sec^{-1}; and

(4) Fewer than one cyclone-anticyclone alternation occurs every two years in either January or July in a 5° latitude-longitude rectangle.

These criteria indicate that for a region to be considered monsoonal, there must be highly persistent winds from different directions in summer and winter. In addition, the fourth criterion excludes areas in which the seasonal wind shift only reflects a movement in the mean tracks of moving systems.

This is not to say, however, that fronts do not affect a monsoon region. For example, the South China Sea experiences strong cold surges several times each winter (Kindle *et al.*, 1969), and cold fronts also push into the northern Arabian Sea several times each winter (see Para. 3.4).

Thus the monsoon area defined by Ramage, with "squaring off," is enclosed between 35°N and 25°S and between 30°W and 170°E. This area, which encompasses the entire Arabian Sea, is shown in Figure 2-1.

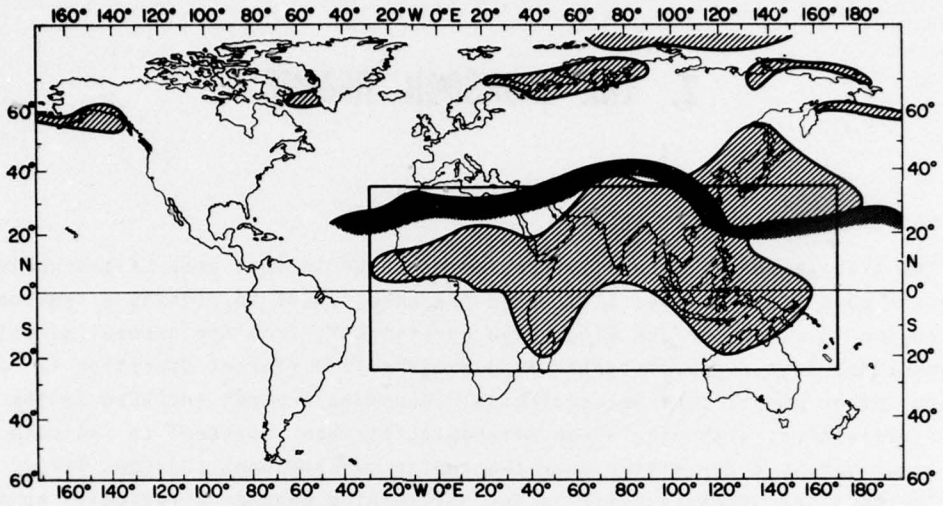

Figure 2-1. Delineation of the monsoon region. Hatched areas are defined by criteria 1, 2 and 3 from Para. 2.1, while the heavy line marks the northern limit of criterion 4. The rectangle encloses the monsoon region (from Ramage, 1971).

2.2 SEASONAL VARIATION OF THE ARABIAN SEA MONSOON

The fundamental causes of the monsoon's seasonal variations are the temperature gradients established between land and sea -- where continents border oceans, large temperature differences (and thus pressure differences) occur (Ramage, 1971). In addition, the shapes and topographical features of the continents surrounding the Arabian Sea (see Figure 1-1), as well as variations in sea-surface temperatures, all interact to produce the unique features of the Arabian Sea monsoon.

In winter, the low heat capacity of land relative to sea causes the surface air over southern Asia to be colder than that over the sea (see Figure 2-2a). This in turn produces a gradient of air pressure which causes surface air to flow southward over the Arabian Sea (see Figure 2-2b). However, the huge Siberian polar anticyclone, source of the cold monsoon surges of the South China Sea (Kindle et al., 1969) and potential source for surges into the Arabian Sea, is effectively cut off from the Arabian Sea by the Himalayas and the contiguous mountain ranges of Afghanistan and Iran (Ramage, 1969). Thus the Arabian Sea winter monsoon is noted for only moderate northeasterly flow -- the surface

wind roses for January in Figure A-2 of Appendix A exemplify this fact. To the rear of disturbances moving eastward south of the Himalayan Massif, winds do increase as cold air moves off the Arabian Peninsula over the northern Arabian Sea. It should also be noted that the African continent has the effect of causing the northeast monsoon to extend into the Southern Hemisphere. Radiational cooling over both the Sahara Desert and Arabian Peninsula, along with radiational heating over the Kalahari Desert (located about 20°S over Africa), results in a north-south pressure gradient at the surface across the equator over eastern Africa (see Figure 2-2b). As a consequence, a flow of air from north to south extending out to 400 n mi off the coast sets up across the equator (Ramage, 1971).

During summer the reverse process occurs. An intense heat low is formed over the Arabian Peninsula, southern Iran, Pakistan and northern India, due to strong radiational heating (see Figure 2-3). Again, as in winter, the Himalayas, the Zagros Mountains of Iran and the Caucasus seal off regions to the south from possible invasion by cold air, thus allowing the heat low to be the dominant weather feature. The southwest monsoon of the Arabian Sea is therefore much more intense than the northeast monsoon (Ramage, 1971). The effects of the African land masses are again felt on the monsoon regime during the summer. In contrast to winter, radiational cooling produces high pressure over the Kalahari Desert. Radiational heating causes low pressure over the Sahara Desert and Arabian Peninsula, and the resulting south-north pressure gradient (see Figure 2-3) sets up a southerly flow across the equator. Because of cold upwelling off the Somali coast, the southwest monsoon is intensified further. Also affecting this cross-equatorial flow, with possible consequences to the entire monsoon circulation, is the phenomenon called the "low-level jet" -- this is discussed in detail in the following section.

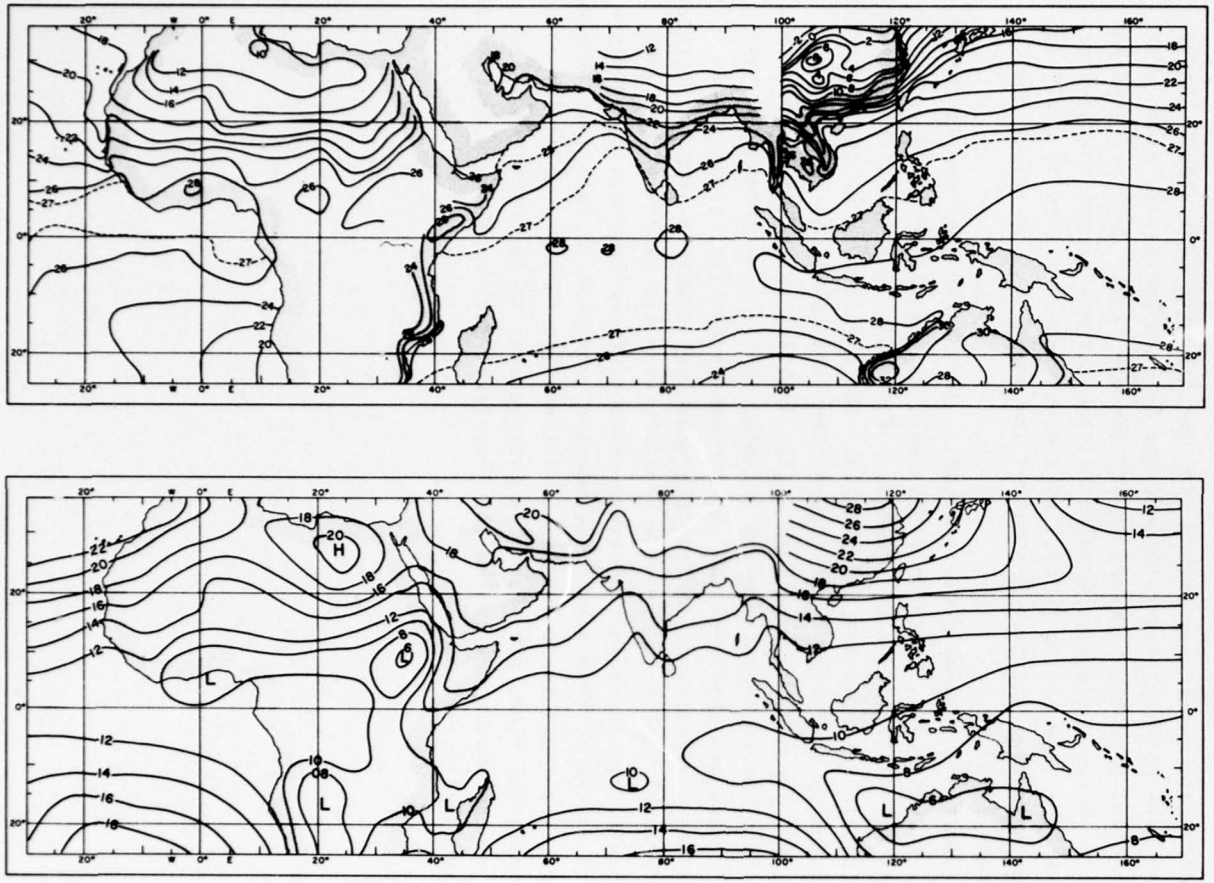

Figure 2-2. Temperatures and pressures for January: (a) mean surface temperature over land, and sea surface temperature over water, in °C; (b) mean sea level pressure in mb (from Ramage, 1971).

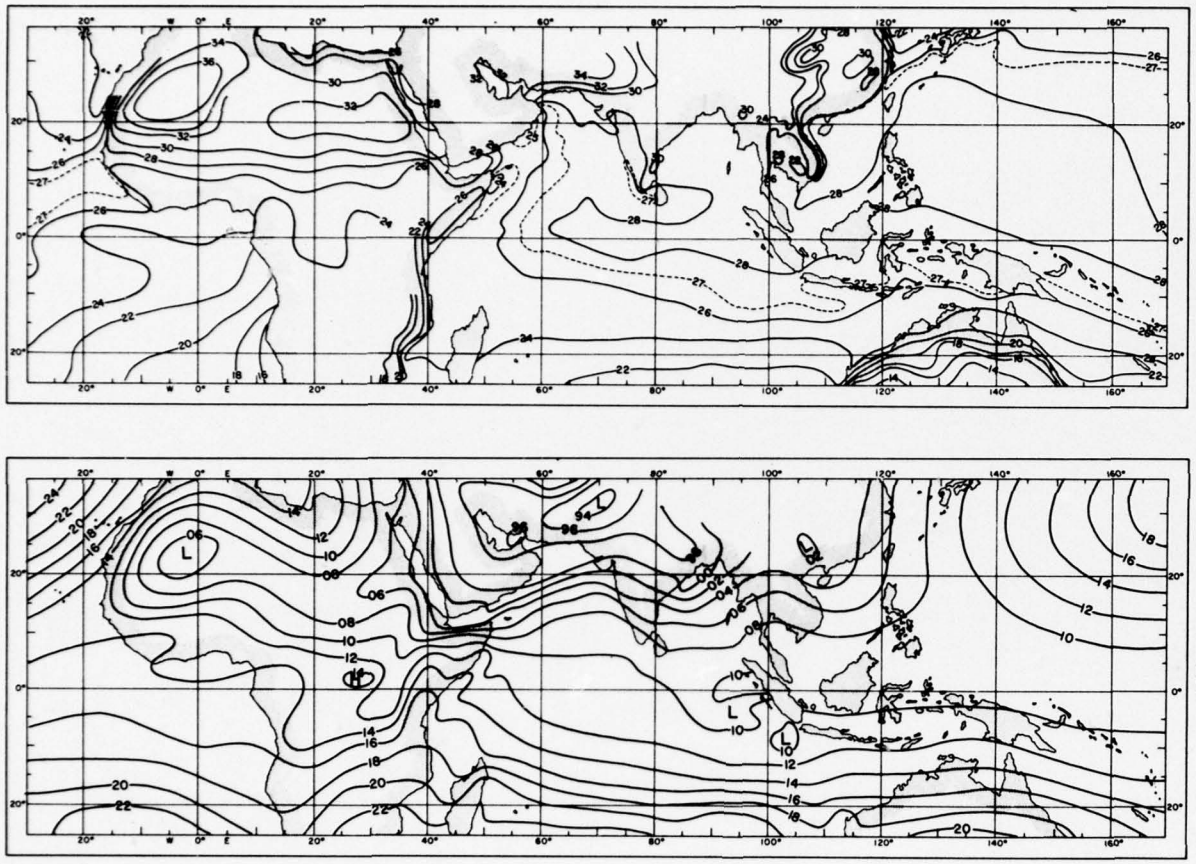

Figure 2-3. Temperatures and pressures for July: (a) mean surface temperature over land, and sea surface temperature over water, in °C; (b) mean sea level pressure in mb (from Ramage, 1971).

3. METEOROLOGICAL PHENOMENA AFFECTING THE ARABIAN SEA*

3.1 LOW-LEVEL JET

During the summer monsoon season, the surface southwesterlies of the Somali coast waters are one of the strongest and most-sustained wind systems on earth (Ramage, 1971). An example can be seen in the July surface wind roses in Figure A-8a, which show the winds to be gale force (> 33 kt) 28% of the time in the *Socotra Is.* climatic area (Figure A-1a shows locations of the climatic areas referenced in italics). This section describes the winds that are part of the low-level jet, cites possible causes for the jet's fluctuations and discusses the effects of the jet and its fluctuations on the monsoon regime of the Arabian Sea.

3.1.1 Description

Findlater (1966, 1967) was the first investigator to document the existence of a strong low-level jet stream from a southerly direction over the flat arid lands in the eastern part of equatorial Kenya. This jet stream, which attains speeds in its core of 50 to 100 kt, is usually centered at about 5000 ft (1.5 km) and is found to occur between the months of April and October though most commonly from June through August. Findlater (1969) also demonstrated that the high-speed flow occurs in the same geographical areas along the western edge of the monsoon system of the Indian Ocean. It is so persistent that it shows up strongly in the mean monthly airflow charts at 3000 ft (1 km) for June through September (A-19a through A-22a).

By using pilot balloon soundings south of the equator, Findlater (1969) revealed that the jet stream is not always a single core of high-speed flow, but often is made up of a series of segments. Examples of this are seen in Figures 3-1a, b, which show low-level jets on two different days; it should be noted that these two charts are not for a constant level since there is vertical and horizontal variation in the location of the jets.

---

*References are made in this section to illustrations contained in Appendixes A, B and C. For brevity within text, these references will often appear simply as the referenced figure's number, e.g., (A-1) (B-2), rather than in the longer form (see Figure A-1) (see Figure B-2).

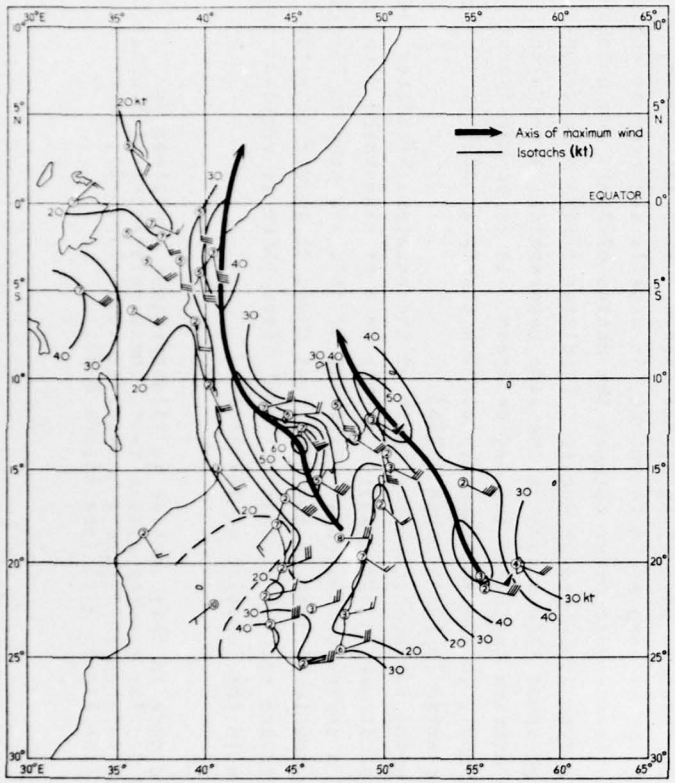

Figure 3-1a. Low-level jet streams from the southeast (26 June 1966). Each plot represents the highest wind speed recorded on each pilot balloon ascent, with the height of the maximum wind (in 1000's of feet) shown at the point of the wind arrow (from Findlater, 1969).

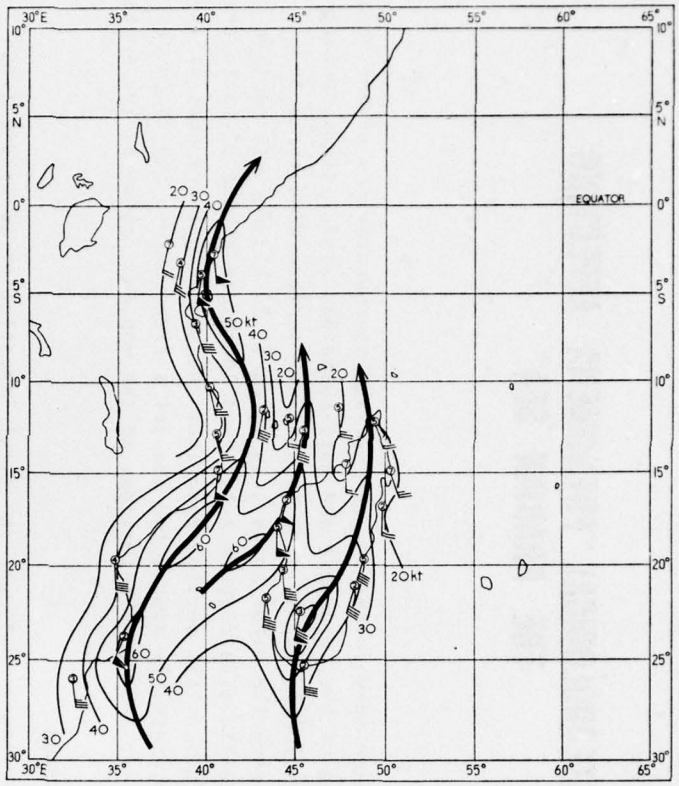

Figure 3-1b. Low-level jet streams from the south (26 July 1966). The method of plotting is the same as in Figure 3-1a (from Findlater, 1969).

3.1.2 Relationships to Upwelling off the Somali Coast

As can be seen from the mean 3000-ft flow for the months June through August (A-19a through A-21a), the low-level jet has a secondary maximum just to the east of the Socotra Islands. This feature is even more pronounced at the surface as shown by the wind roses for June through August (A-7a through A-9a).

The occurrence of the strong surface flow parallel to the Somali coast causes a net transport of water off the coast, and thus an upwelling of cold bottom water which begins in May. This upwelling is most evident on the mean sea-surface temperature charts shown in Figures A-31f, g, h for the months of June through August at about 10°N along the Somali coast. The upwelling increases the pressure gradient between sea and land by cooling the coastal waters, and thus the surface southwesterlies are made even stronger (Ramage, 1971). East of the region of cold water, thermal wind considerations (see Figure 3-2) also cause the upwelling to intensify the winds aloft and thus intensify the low-level jet (Saha, 1974).

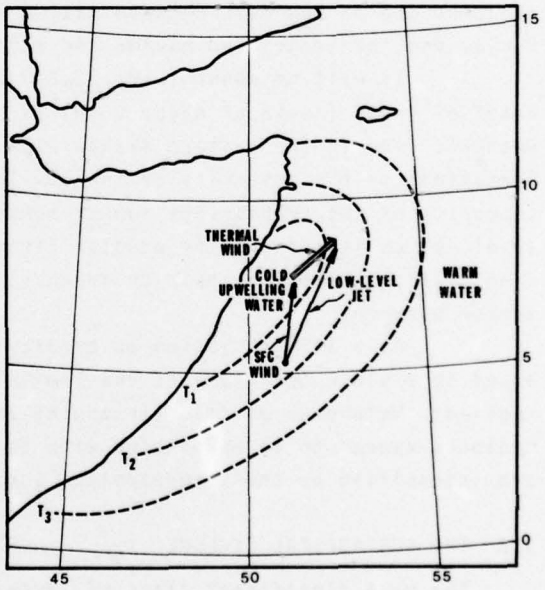

Figure 3-2. Thermal wind relationship showing the effect of cold upwelling water off the Somali coast on the intensity of the low-level jet.

3.1.3 Relation between Low-Level Jet and Intensity of Monsoon Circulation

Findlater (1969) also found what appears to be one of the few forecasting aids useful for predicting changes in the Arabian Sea summer monsoon, by relating changes in the low-level jet as it crossed the equator to rainfall over western India. (Variations in jet intensity at the equator are easily monitored because the jet stream is locked in position by rising ground to the west as shown in Figure 3-3.) His methodology is described below.

Cross-equatorial flow at Garissa, Kenya, (see locator map, Figure 1-1) was calculated for each day by adding the speeds in knots of the winds at the 3,000-, 4,000- and 5,000-ft levels. The values obtained were smoothed by producing overlapping five-day means. Further smoothing was accomplished by forming overlapping means of three successive values. The values thus obtained were referred to by Findlater as the cross-equatorial index. Rainfall data over western India were utilized by adding the daily rainfall at four representative stations and then calculating overlapping five-day totals.

Figure 3-4 shows the comparison between the cross-equatorial index and the rainfall of western India for a two-month period during the height of the summer monsoon. The two curves follow each other very closely with a lag of about one to two days between maxima and minima of the index at Garissa, Kenya, and the associated maxima and minima of rainfall over western India.

It will be shown (Para. 3.2.3) that increased rainfall along the west coast of India (south of about 20°N) is associated with increased surface westerly flow in the eastern Arabian Sea. It therefore seems possible that the variations in the intensity of the low-level jet have an effect on the overall intensity of the Arabian Sea summer monsoon. Careful monitoring of the low-level jet as it crosses the equator (from data at Garissa, Kenya, pilot-balloon wind station 63723) may help to forecast intensifications of the Arabian Sea summer monsoon.

At a 1974 symposium on tropical meteorology in Nairobi, Findlater was asked to explain the cause of the low-level jet observed over Kenya. He replied: "Outbreaks of cold air coming around the southern subtropical anticyclones appear to be associated with the jet, and these (the low-level jets) are intensified by the topographical constant of Africa."

3.2 THE SUBTROPICAL CYCLONE

The most significant class of large-scale cyclonic circulations affecting the Arabian Sea during the summer monsoon is the subtropical cyclone. This system is also called "mid-tropospheric cyclone" because its circulation first appears in the mid-troposphere, although it may subsequently extend downwards and be detectable in the surface pressure pattern (see Cuming, 1973).

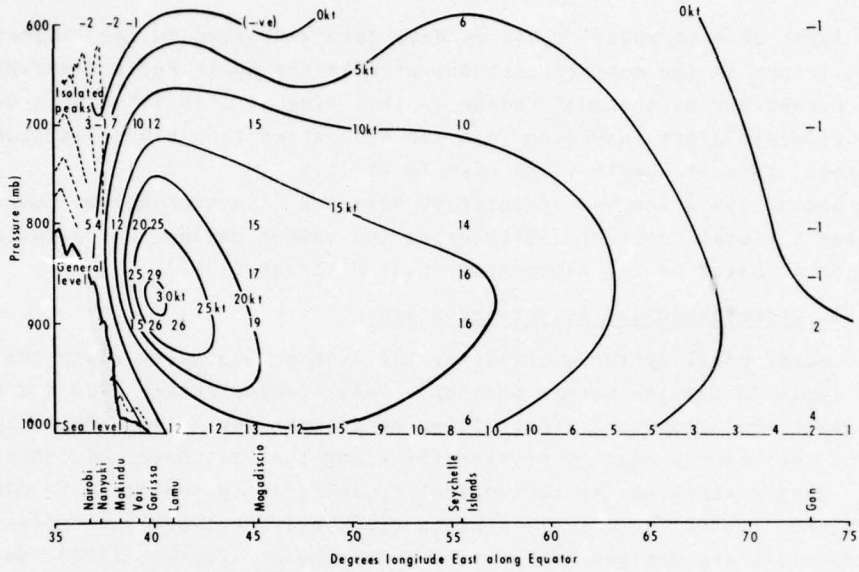

Figure 3-3. Mean meridional flow at the equator in July (from Findlater, 1974).

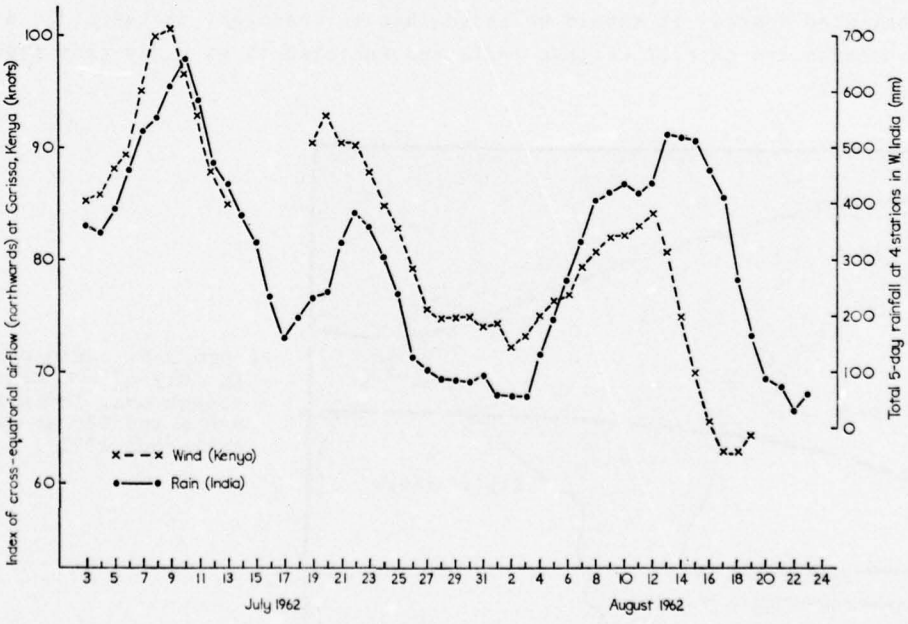

Figure 3-4. Cross-equatorial airflow at Garissa, Kenya, in relation to rainfall at four stations in western India (smoothed values) (from Findlater, 1969).

Two types of subtropical cyclones have been discussed in the literature. The first occurs in the eastern portions of both the North Pacific and North Atlantic Oceans during the cool season -- this type is associated with cut-off pools of cold air aloft intruding into the subtropics from higher latitudes, and the Kona storm of Hawaii is an example of it.

The second type, the one of interest here and discussed below, commonly occurs near the west coast of India during the summer monsoon. The following description is based on the documentation of Atkinson (1971).

3.2.1 Description and Associated Weather

Subtropical cyclones affecting the Arabian Sea occur along the west coast of India during the summer monsoon. They develop between 700 and 500 mb in the upper level (monsoon) trough lying across the northeast Arabian Sea and are one of the major producers of rainfall along the west coast of India.

When describing the subtropical cyclone, it is important to contrast the difference in the large-scale monsoon circulation between two regions: the Bay of Bengal, where monsoon depressions are frequent (Cuming, 1973); and the Arabian Sea, where these depressions do not occur during the summer monsoon. This basic difference is found in the mean position of the monsoon trough over the Indian subcontinent, shown in Figure 3-5 for July at 900 meters and 500 mb. Locations of the trough positions at these two levels were determined from the resultant wind field. It should be noted that in the mean, the vertical slope of the monsoon trough over western India and Pakistan is markedly less than over eastern India.

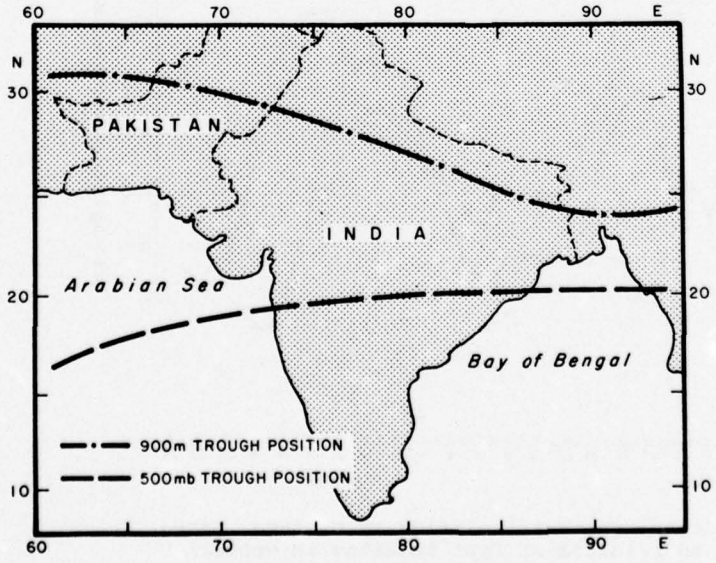

Figure 3-5. Mean positions in July of the monsoon trough over India at 900 m and 500 mb (from Atkinson, 1971).

This shallow vertical slope of the monsoon trough over the eastern Arabian Sea and western India is also visible in the north-south cross-section of the resultant wind field for July shown in Figure 3-6. In addition, this cross-section shows that above 400 mb, where the trough disappears, a steady easterly regime prevails to the south of the subtropical ridge. The tropical easterly jet is evident near 100 mb south of 20°N, while the mid-latitude westerly maximum occurs north of 35°N near the 200-mb level.

The differences between the Bay of Bengal and eastern Arabian Sea described above for July can also be seen on climatological charts (A-20, A-28).

An example of a persistent subtropical cyclone occurred near Bombay during the period 1-10 July 1963. This system was studied in detail and composite wind, pressure, temperature, moisture and weather distributions associated with this system were prepared. Figure 3-7 shows the composite kinematic analyses for the near-surface (500-900 meters) and 600-mb levels. A composite of the vertical motion and cloud distribution associated with the cyclone is shown in Figure 3-8. The cyclonic circulation is well developed at 600 mb, while the only evidence of the circulation affecting the near-surface layer is the weak trough near the coast. The composite temperature fields show the cyclone to be colder than the environment at 700 mb and warmer than the environment at 500 mb.

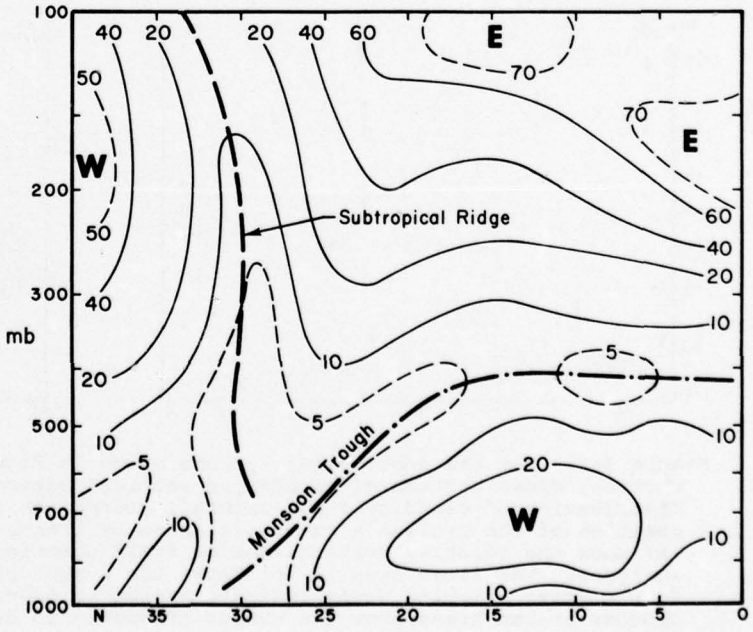

Figure 3-6. North-south cross section of the July resultant wind speeds (kt) and directions (east or west) along western India (from Atkinson, 1971).

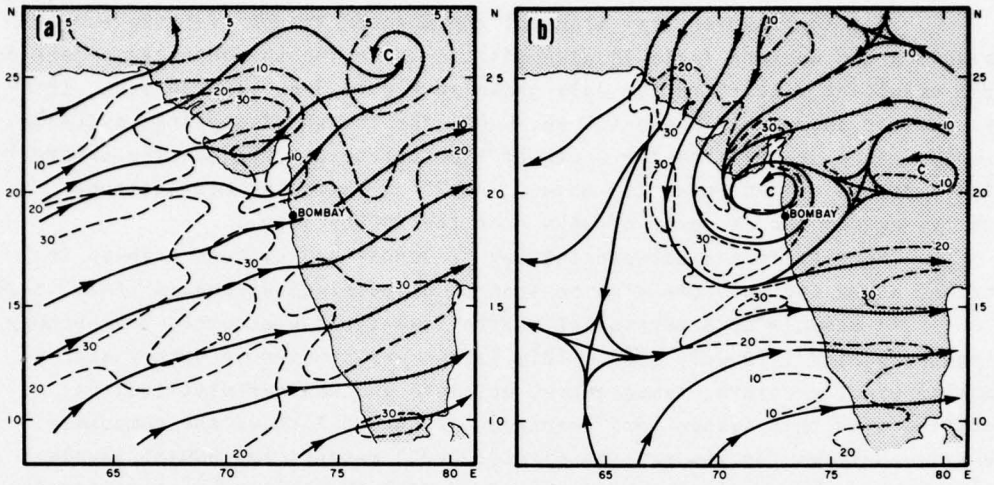

Figure 3-7. Composite kinematic analyses for (a) a near-surface layer (500-900 m) and (b) the 600-mb level showing a well developed subtropical cyclone over western India during July 1963. Solid lines are streamlines and dashed lines are isotachs in kt (from Atkinson, 1971).

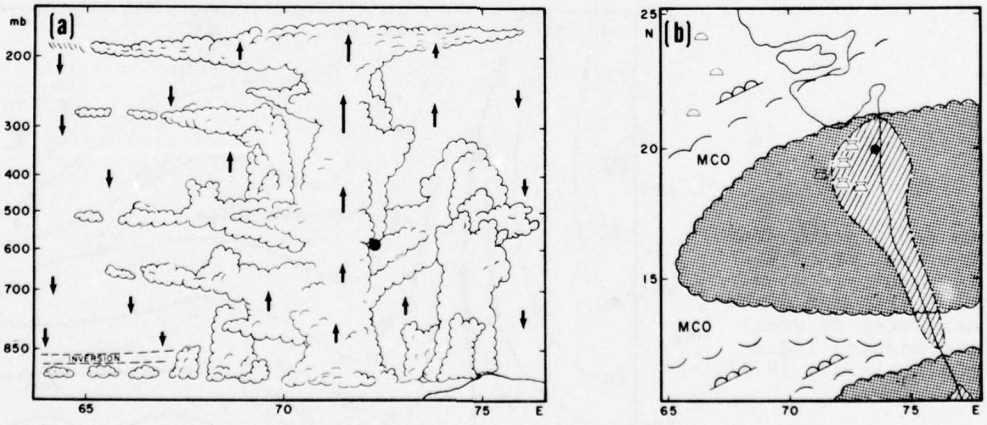

Figure 3-8. For the subtropical cyclone shown in Figure 3-7: (a) east-west vertical cross section of clouds and vertical motion, and (b) horizontal distribution of cloudiness and rainfall around the cyclone. The 600-mb position of the cyclone's center is shown by the heavy dot. Arrows in (a) show the relative vertical-motion field computed from composite wind analyses. The lined area in (b) shows the extent of rainfall exceeding four cm/day; stippled areas indicate broken to overcast middle or high clouds; broken areas show the extent of broken to overcast low clouds (from Atkinson, 1971).

A dynamic explanation (not necessary to cite here) may be given to show that such subtropical cyclones cannot be maintained in a steady state without cumulus convection. This explanation is also consistent with the observed evidence that the most severe weather and greatest vertical cloud development are to the west of the cyclone center (see Figure 3-8).

3.2.2 Relationship to Large-Scale Monsoon

Over the Arabian Sea, subtropical cyclones are the dominant weather features during the summer monsoon and cause much of the summer rains in western India (Atkinson, 1971). It is generally observed that while these cyclones are active, a heavy overcast extends westward out to about 500-700 n mi from the west coast of India (Ramamurthy, 1972).

Although not dealing directly with the subtropical cyclone, Ramamurthy (1972) deduced important information on its relationship to the summer monsoon system by comparing differences between spells of weak monsoon and strong monsoon. Rainfall data along the west coast of India were used to differentiate the spells, which were chosen such that the mean rainfall per day was about twice the normal for strong cases and about 30% of normal for weak cases. In a more recent study, Jambunathan and Ramamurthy (1974) analyzed streamline and isotach charts for various levels over the Arabian Sea during both a period of strong and a period of weak monsoon. These charts are shown in Figures 3-9 through 3-12 for the surface, 850-mb, 700-mb and 500-mb levels, respectively. The isotach analyses represent only the zonal component of the wind (westerly winds-positive).

The strong monsoon case was analyzed using all available Monsoon Experiment (MONEX) data for the period 4-8 July 1973 (Figures 3-9a to 3-12a). The weak monsoon case using the same data covered the period 19-25 June 1973 (Figures 3-9b to 3-12b). Thus, instead of choosing a typical day for each type, the authors used a period of five to seven days to obtain the maximum data coverage. It must be stressed that only during the MONEX 1973, was there a wide enough coverage of upper winds over the Arabian Sea for these analyses to be made.

Several conclusions of value to forecasters resulted from these two studies:

(1) The maximum velocity of the low-level winds appears to be about 50-55 kt in both strong and weak monsoon conditions over the western Arabian Sea. This wind maximum is found in both cases in the longitudinal belt between 55°E and 60°E near latitude 12°N. However, during the strong monsoon the level of maximum winds is about 900 mb, while during the weak monsoon it is about 950 mb. It is interesting to note that these speeds are much higher than the mean maximum wind of 35 kt analyzed by Findlater (1971a) in July and shown at 3000 ft in Figure A-20a. It was also reported by Jambunathan and Ramamurthy (1974) that

this low-level maximum wind occurred just below or in the layer of a pronounced low-level inversion.

(2) The effect of the perturbations of the strong monsoon (i.e., subtropical cyclones) is to cause an intensification of the SSE-NNW pressure gradient over the eastern half of the Arabian Sea south of about 20°N as shown in Figure 3-13. This increased pressure gradient causes surface SW/W winds to be much stronger off the west coast of India during strong monsoon conditions (compare Figures 3-9a and 3-9b).

(3) The westerlies are strong through a much greater depth of the atmosphere in the eastern Arabian Sea during periods of strong monsoon. This relation is evident from the streamline and isotach analyses for the 850-mb through 500-mb levels shown in Figures 3-10, 3-11, and 3-12.

(4) Variations in the strength of the low-level flow over the Arabian Sea are not correlated to the intensity of the heat low centered in Pakistan. This result is quantitatively seen in Figure 3-14, which shows the latitudinal variation of sea level pressure from 8° to 28°N for both weak and strong monsoon conditions. In both cases, the pressure at 28°N, near the center of the heat low, is approximately the same. However, the strongest pressure gradient during the weak monsoon is north of 23°N, while during the strong monsoon the strongest pressure gradient is between 21° and 13°N. The wind analyses in Figure 3-9 show the same differences between weak and strong monsoons. In the case of the weak monsoon there is a wind maximum along the extreme northwest coast of India with light winds to the south (see Figure 3-9b). On the other hand, during strong monsoon conditions the westerlies are light north of 20°N and relatively strong along the remainder of the west Indian coast (see Figure 3-9a).

(5) Many, but not all, of the strong monsoon cases are caused by developing subtropical cyclones. During the strong monsoon analyzed in Figures 3-9a through 3-12a, there appears to be a closed cyclonic eddy throughout the lower troposphere near the Gulf of Cambay, which indicates that a subtropical cyclone was associated with the strong monsoon of 4-8 July 1973.

(6) Overcast conditions over the Arabian Sea extend westward to about 500-700 n mi off the west coast of India during strong monsoon cases. This increased cloud cover is attributed to the direct and indirect dynamical processes of the monsoon circulation rather than to the orographic effects caused by the increased westerly flow crossing the Western Ghats. Figures 3-15 and 3-16 show satellite photographs of cases of strong and weak monsoons, respectively. The extension of the cloud cover over the eastern Arabian Sea during strong monsoon is very evident in Figure 3-15. It is also quite possible that a subtropical cyclone was responsible for this extensive cloud cover.

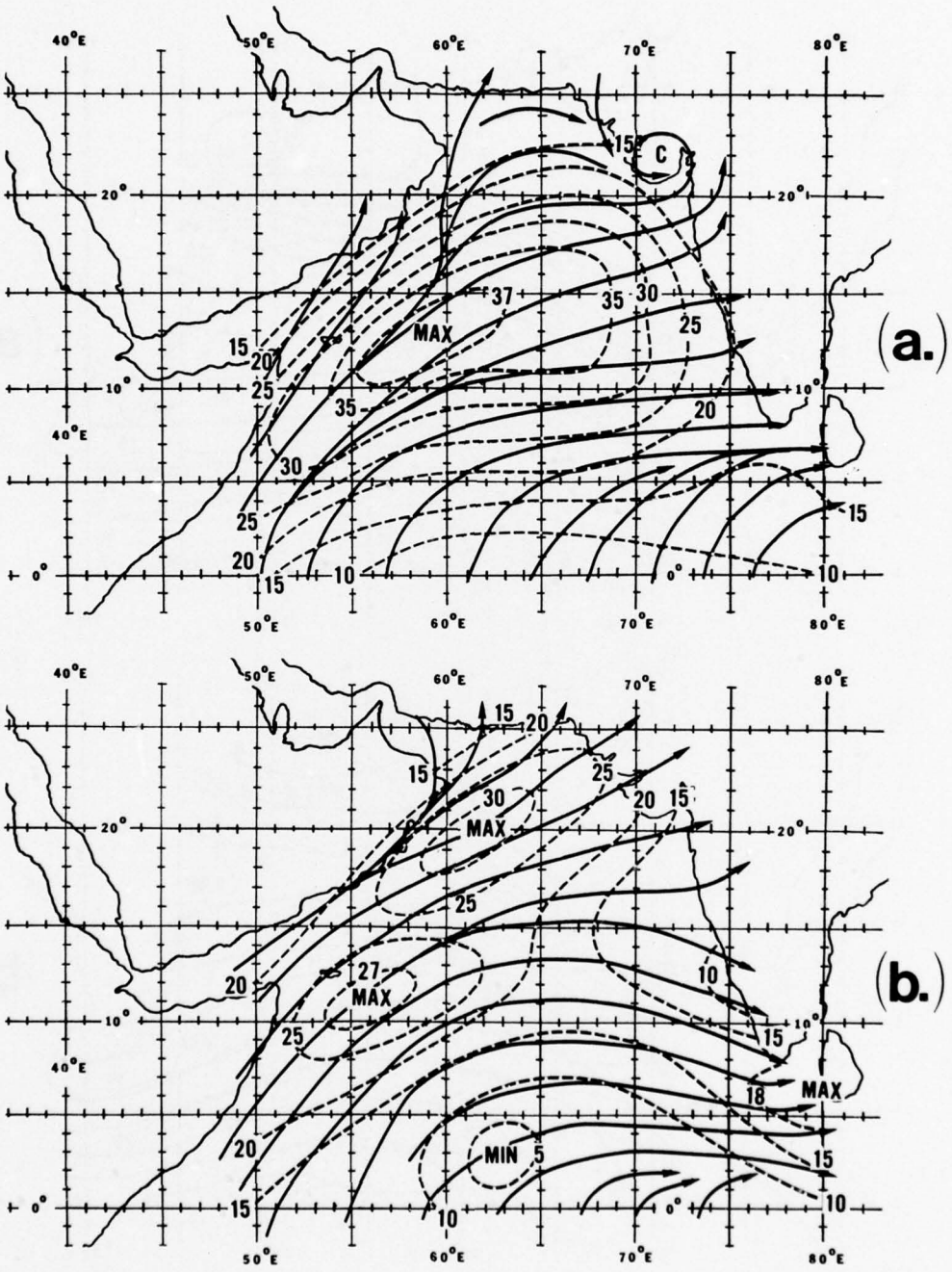

Figure 3-9. Streamlines and isotachs (zonal component only in kt) for surface during (a) strong monsoon conditions 4-8 July 1973 and (b) weak monsoon conditions 19-25 July 1973 (after Jambunathan and Ramamurthy, 1974).

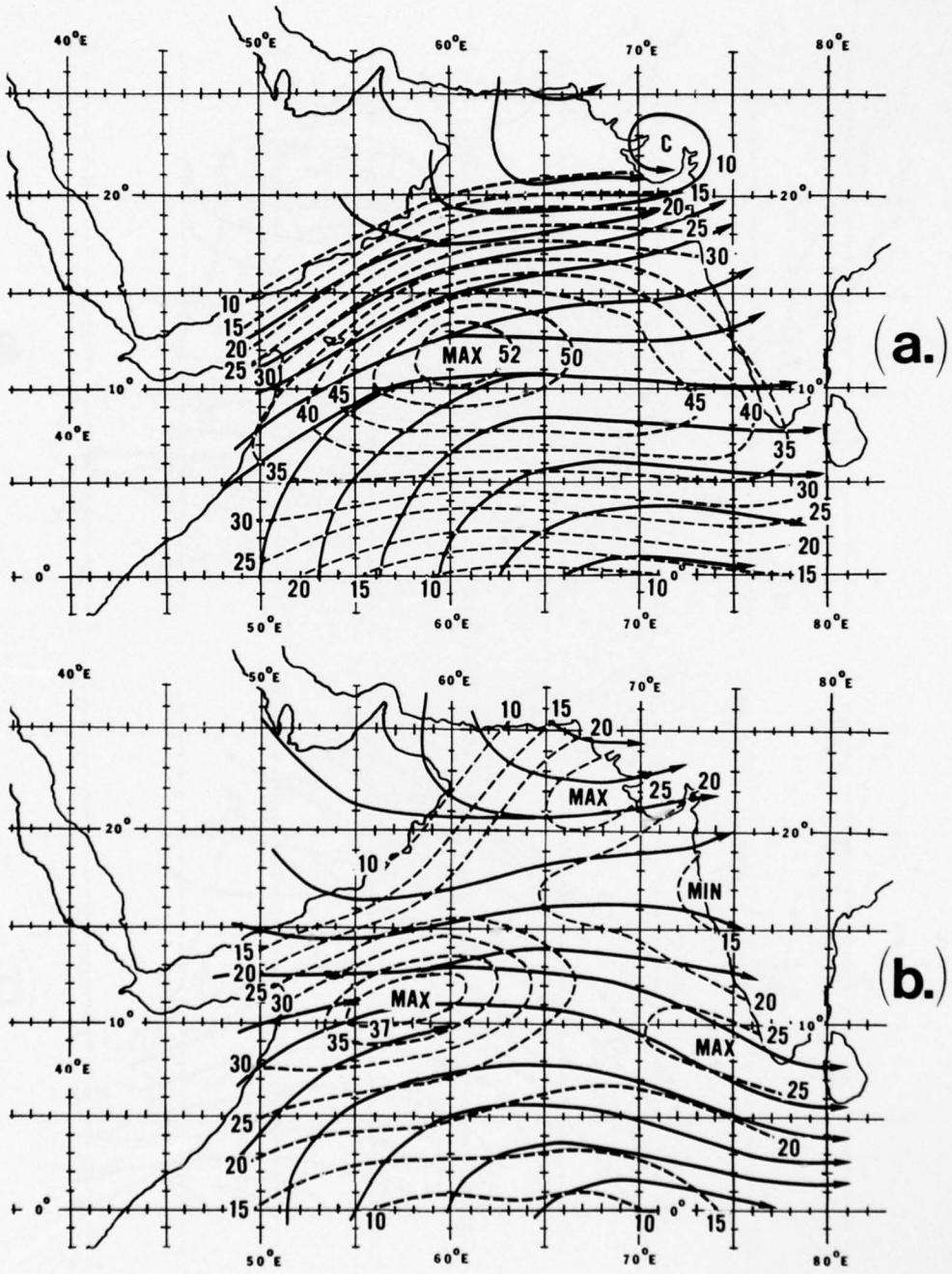

Figure 3-10. Streamlines and isotachs (zonal component only in kt) for 850 mb during (a) strong monsoon conditions 4-8 July 1973 and (b) weak monsoon conditions 19-25 June 1973 (after Jambunathan and Ramamurthy, 1974).

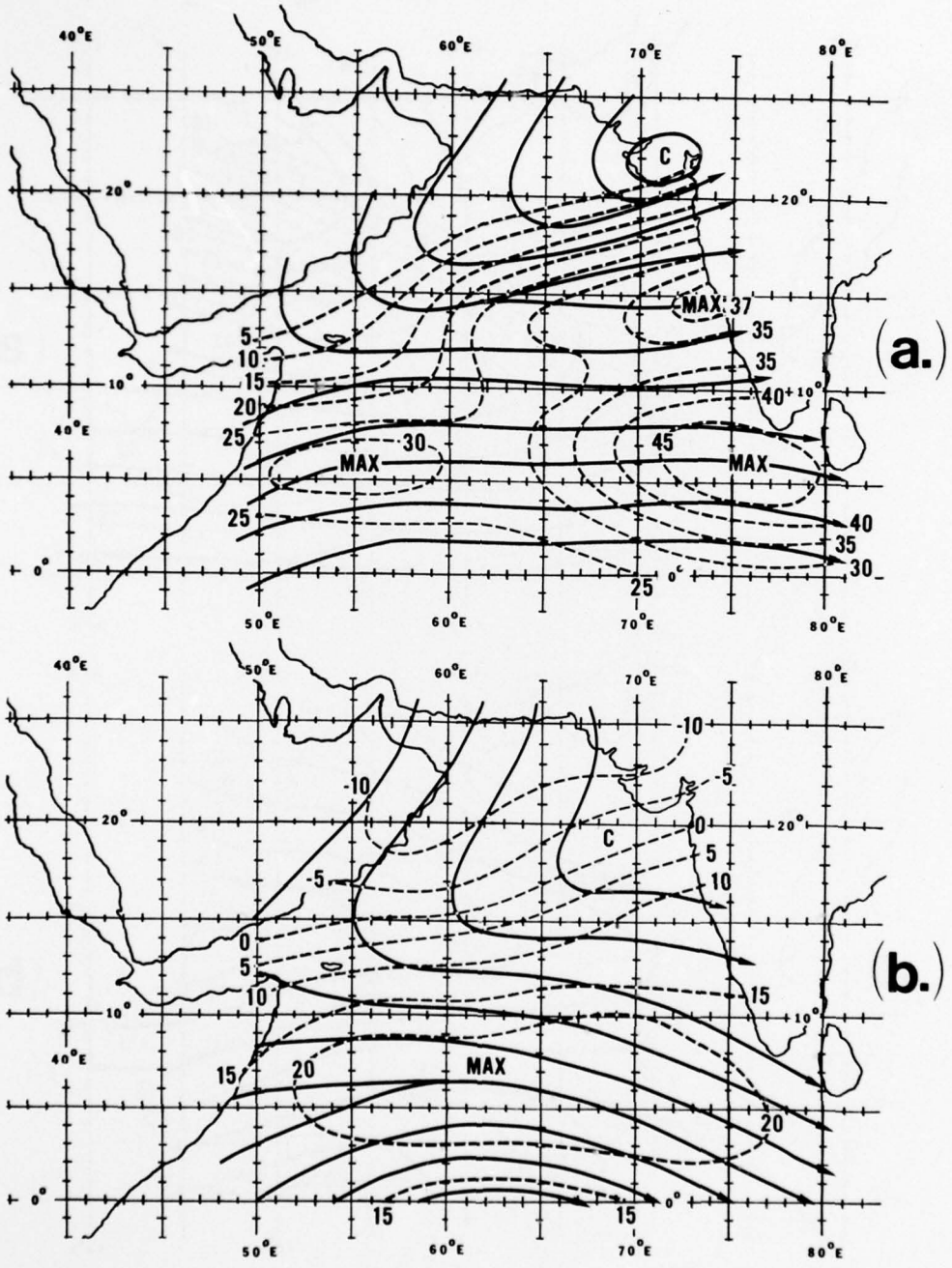

Figure 3-11. Streamlines and isotachs (zonal component only in kt) for 700 mb during (a) strong monsoon conditions 4-8 July 1973 and (b) weak monsoon conditions 19-25 June 1973 (after Jambunathan and Ramamurthy, 1974).

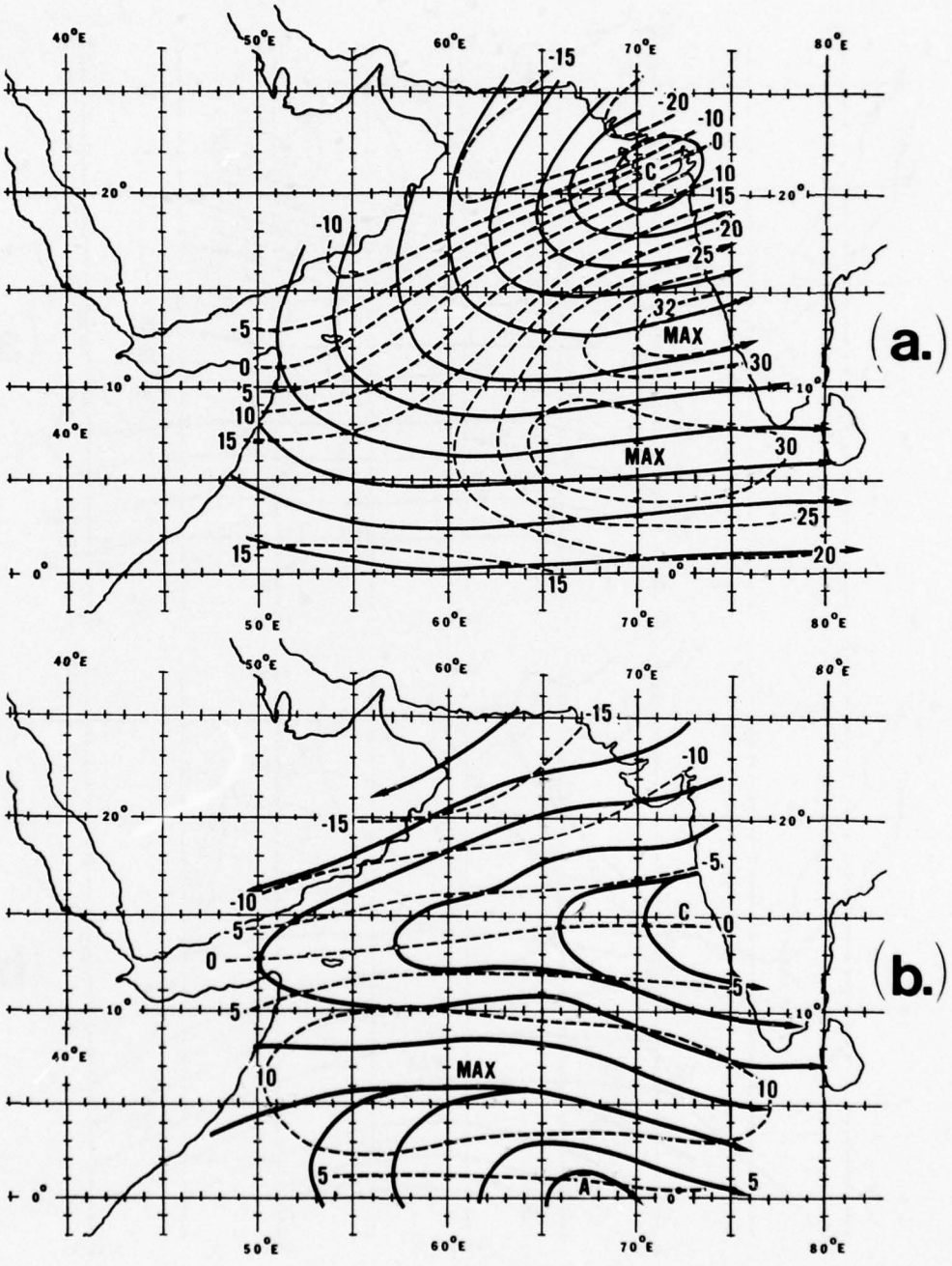

Figure 3-12. Streamlines and isotachs (zonal component only in kt) for 500 mb during (a) strong monsoon conditions 4-8 July 1973 and (b) weak monsoon conditions 19-25 June 1973 (after Jambunathan and Ramamurthy, 1974).

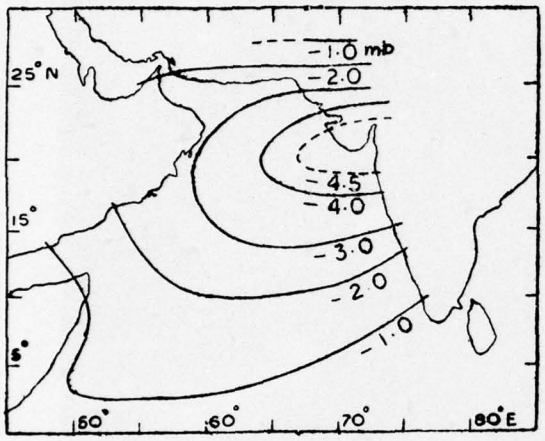

Figure 3-13. Isopleths of mean pressure differences (mb) between strong and weak Arabian Sea monsoon (from Ramamurthy, 1972).

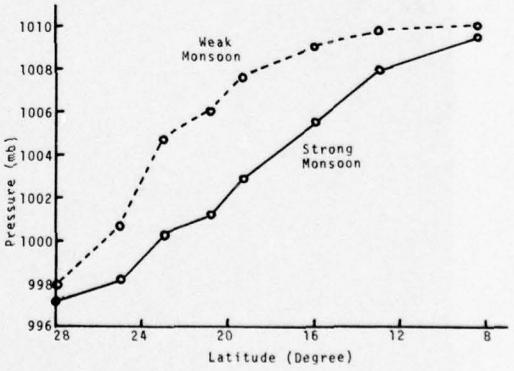

Figure 3-14. Mean pressure during spells of strong and weak Arabian Sea monsoon (after Ramamurthy, 1972).

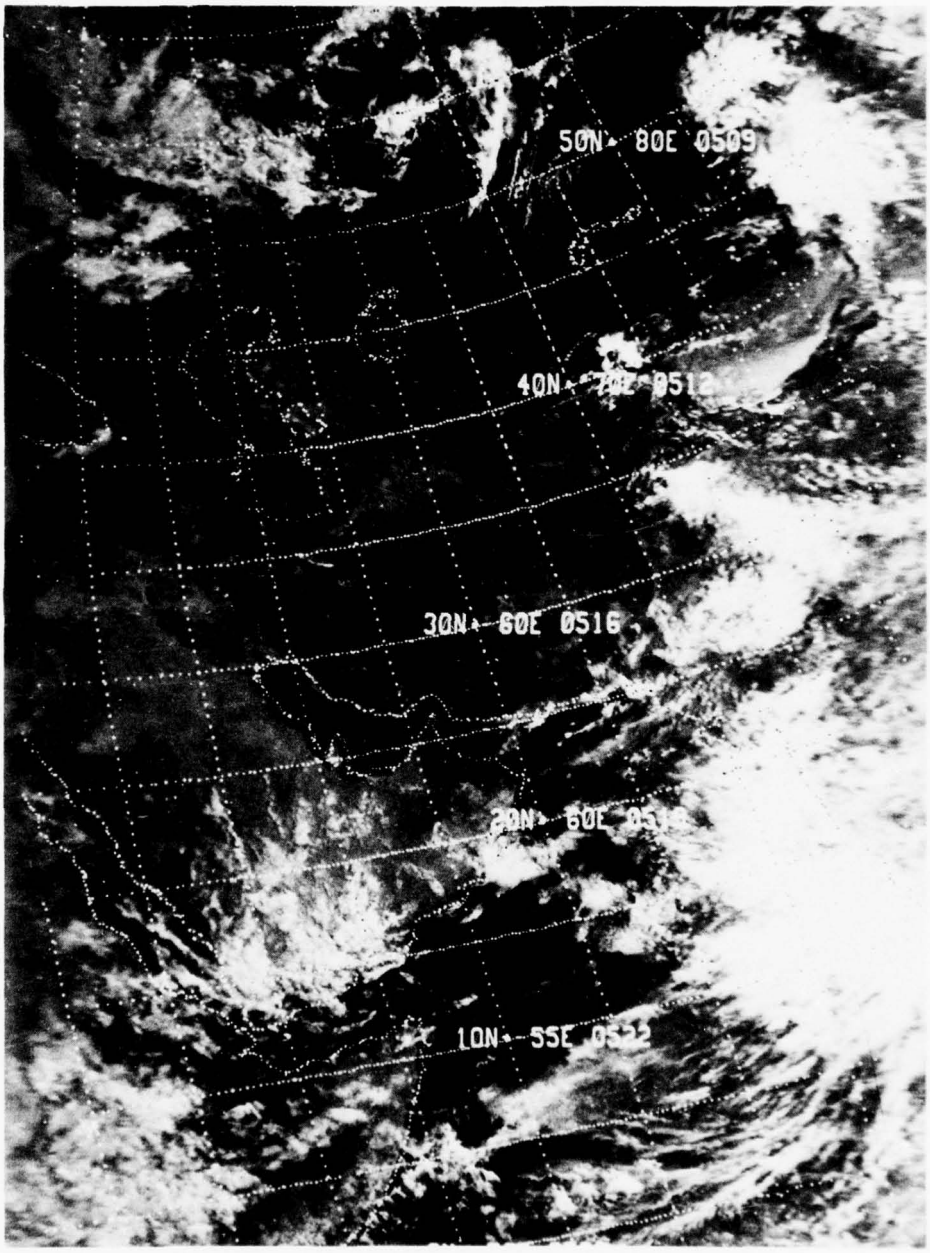

Figure 3-15. Satellite photograph showing strong monsoon in the eastern Arabian Sea, 0455 GMT 3 August 1974 (NOAA-2).

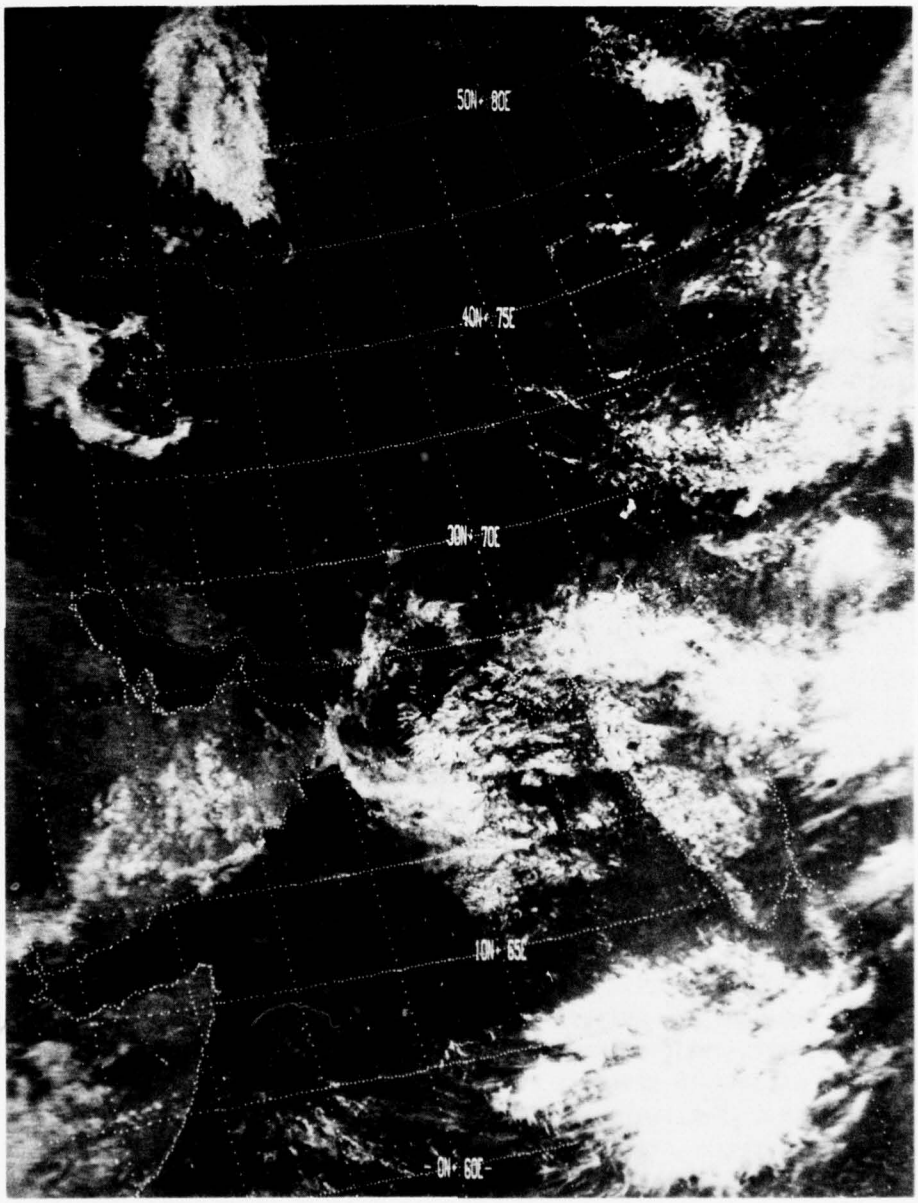

Figure 3-16. Satellite photograph showing weak monsoon in the eastern Arabian Sea, 0523 GMT, 25 August 1973 (NOAA-2).

3.2.3 Possible Aids for Forecasting Subtropical Cyclogenesis

As is the case for most low-latitude phenomena, few aids for forecasting subtropical cyclogenesis are available in the literature. However, several investigators -- Ramage (1971), Ramamurthy (1972) and Desai (1967) among them -- feel that there is a relationship with the monsoon depression of the Bay of Bengal. (For a complete description of this depression, see Cuming, 1973.)

Ramage (1971) hypothesizes that a significant incursion of deep moist air is a prerequisite for development of a subtropical cyclone. His reasoning is that the supply of moisture from the west is so limited by the subsidence inversion over the Arabian Sea, that cyclogenesis can occur only in situations where moisture is available from the south or east. Because these conditions are usually met only with monsoon depressions, the forecaster would be advised to look for the development of a subtropical cyclone with increased rains, cloudiness and surface winds in the eastern Arabian Sea during periods of monsoon depressions in the Bay of Bengal or northeastern India.

It is also possible that other processes lead to increased intensity of the Arabian Sea monsoon and possible subtropical cyclogenesis. As described in Para. 3.1.3, Findlater (1969) found a one- to two-day lag between the cross-equatorial index over eastern Africa and rainfall over western India.

3.3 TROPICAL CYCLONES

Although tropical cyclones do not commonly occur in the Arabian Sea region, they do have a significant effect on regional weather. Despite the infrequency of their occurrence along the Arabian coast, where they influence the weather on an average of only once in three years, their associated torrential rains make up a significant part of the total rainfall. During the 25-year period 1943 to 1967, a quarter of the total rainfall at the city of Salalah (locator map, Figure 1-1) was associated with tropical cyclones (Caplinger, 1971). In addition, their winds and associated sea conditions make the tropical cyclone the most dangerous single meteorological event affecting the Arabian Sea. For these reasons the forecaster must remain vigilant during those periods of the year when tropical cyclones have been observed. Paragraphs 3.3.1 through 3.3.3 provide statistical information on storm occurrence, discuss the necessary criteria for development of tropical cyclones, and show typical storm sequences as recorded by satellite coverage of Arabian Sea tropical cyclones.

3.3.1 Statistical Information

The standard conventions on intensities of tropical cyclones are used throughout this handbook:

Tropical depression -- Winds less than 34 kt

Tropical storm -- Winds of 34-63 kt

Hurricane (typhoon) -- Winds greater than 63 kt

These values may be contrasted with those used in the North Indian Ocean by the Indian Meteorological Department:

Tropical Depression -- Winds less than 34 kt

Moderate cyclonic storm -- Winds of 34-47 kt

Severe cyclonic storm -- Winds of 48-63 kt

Severe cyclonic storm with a core of hurricane winds -- Winds greater than 63 kt

As noted by Atkinson (1971), the Arabian Sea is the least active of the various development regions for tropical storms. Figure 3-17 indicates that only about 1% of the world's tropical cyclones of tropical storm or greater intensity develop in the Arabian Sea, as opposed to 5% in the Bay of Bengal (which is of similar area). The rarity of tropical storms is also indicated by the fact that during a recent 17-year period, none were observed in seven of these years (see Figure 3-18), while a maximum of three tropical storms were observed in only two of the years (Atkinson, 1971). However, in a more recent four-year study using only satellite data (Sadler and Gidley, 1973), it was noted that the occurrence of tropical storms in the Arabian Sea might be more frequent than indicated from previous climatology, especially in southwestern areas where virtually no data are available. During this shorter study, two tropical storms entered Somali and another decayed just off the Somali coast.

As discussed in Para. 3.3.2 (see following), those tropical cyclones that do develop are found primarily during the spring and autumn transition seasons. This bimodal distribution for both tropical depressions and storms is shown in Table 3-1, which lists the frequency (number) of tropical cyclones that reached only depression intensity and tropical cyclones that reached at least storm intensity. Also compared are the long term averages based on the Indian Meteorological Department summaries for the period 1891-1970, and averages based entirely on satellite data for the period 1967-1970 (Sadler and Gidley, 1973). The same bimodal relationship is present in the case of tropical cyclones that reached hurricane intensity, as shown in Figure 3-19 (which was constructed by using overlapping five-day means).

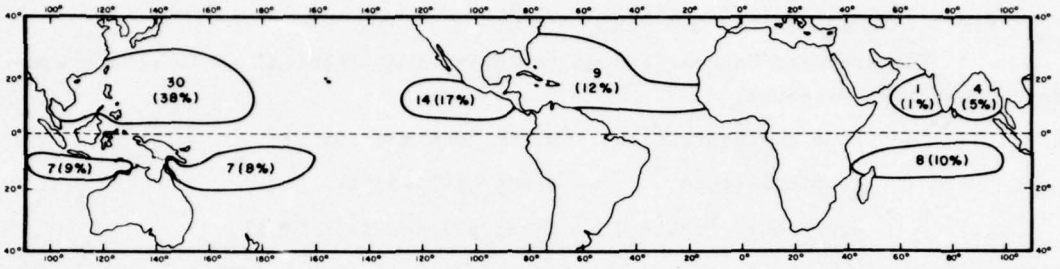

Figure 3-17. Average annual number (and percent of global total) of tropical cyclones of tropical storm or greater intensity in each development area (from Atkinson, 1971).

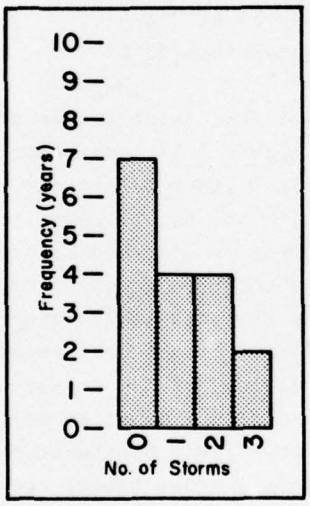

Figure 3-18. Frequency distribution of the annual number of tropical storms in the Arabian Sea during the period 1951-1967 (from Atkinson, 1971).

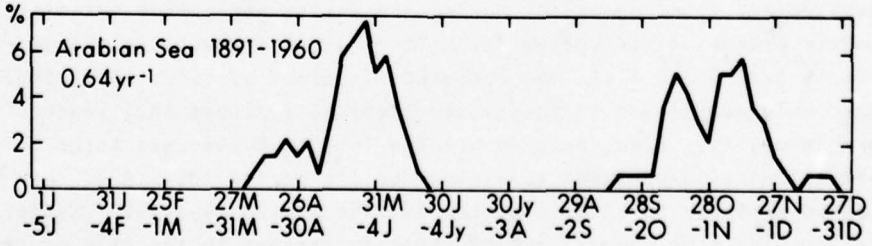

Figure 3-19. Overlapping five-day mean frequencies of tropical cyclones of hurricane intensity expressed as percentages of the annual total for the Arabian Sea (from Ramage, 1974).

The rarity of tropical storms is quite apparent in Table 3-1, which shows that only 92 tropical cyclones reached storm intensity in the 80-year period (excluding the months of July and August), a frequency of 1.15 storms per year (Sadler and Gidley (1973) showed a frequency of 1.25 storms per year). Only a little more than half of these tropical storms, 0.64 per year, reached hurricane intensity (Ramage, 1974).

Table 3-1. Number and frequency (cyclones per year) of those tropical cyclones which reach (a) depression intensity only and (b) tropical storm intensity. Figures are based on Indian Meteorological Department summaries for the period 1891-1970 and on satellite data for the period 1967-1970 (Sadler and Gridley, 1973).

MONTH	1891-1970				1967-1970*			
	DEP.		T.S.		DEP.		T.S.	
	No.	Freq.	No.	Freq.	No.	Freq.	No.	Freq.
January	3	.04	2	.02	2	.50	0	0
February	0	0	0	0	2	.50	0	0
March	1	.01	0	0	0	0	0	0
April	2	.02	5	.06	0	0	0	0
May	9	.11	16	.20	1	.25	1	.25
June	18	.22	15	.19	2	.50	0	0
September	8	.10	5	.06	0	0	0	0
October	21	.26	19	.24	7	.72	1	.20
November	15	.19	26	.33	3	.60	4	.80
December	5	.06	4	.05	4	.80	0	0
Jan-Jun Sep-Dec	82	1.01	92	1.15	21	3.87	6	1.25

*Also October 1971, November 1966 and December 1966.

Although statistics of storm movement in the Arabian Sea are quite limited, the U.S. Naval Weather Service Command (1974a) has published useful charts that show mean monthly tracks of tropical cyclones which reached at least storm intensity. These charts for the peak tropical storm months of April, May, June, October and November are provided in Figure A-35. These charts depict both storm constancy (likelihood in percent that a storm will approximately follow the mean track) and frequency for five-degree squares. The actual storm tracks are shown monthly for the period 1891 through 1970 in Figure A-36.

Referring to the tracks shown in Figure A-35, it can be seen that tropical storms south of about 15°N generally move in a northwesterly direction well off the western coast of India. North of 15°N this track splits, with some of the storms moving westward while others move northward. It is emphasized that only a very small sample is used in these statistics, which causes the observed high values of the constancy.

3.3.2 Tropical Storm Development

Although some of the tropical storms shown in Figure A-36 have crossed the Indian subcontinent and regenerated in the Arabian Sea (see also Sadler and Gidley, 1973), the majority of tropical storms found in the Arabian Sea also develop there. This suggests an investigation of probable causes of storm development to explain the spring and autumn transition season storm maxima.

The prerequisites for the development of intense tropical cyclones, as stated by Palmen and Riehl (Ramage, 1971), are:

(1) "Sufficiently large sea or ocean areas with the temperature of the sea surface so high (above 26 to 27C) that an air mass lifted from the lowest layers of the atmosphere (with about the same temperature as the sea) and expanded adiabatically with condensation remains considerably warmer than the surrounding undisturbed atmosphere at least up to a level of about 12 km. (Some evidence suggests that the absolute value of the sea-surface temperature may not be critical, but rather that the horizontal gradient of the sea-surface temperature should be small over distances of several hundreds of kilometers.)

(2) The value of the Coriolis parameter larger than a certain minimum value, thus excluding a belt of the width of about 5 to 8 degrees latitude on both sides of the equator.

(3) Weak vertical wind shear in the basic current, thus limiting formation to latitudes far equatorwards of the subtropical jet stream.

(4) A pre-existing low-level disturbance (areas of bad weather and relatively low pressure).

(5) Upper-tropospheric outflow above the surface disturbance."

Ramage (1974) argues convincingly that these conditions are only met in the Arabian Sea when the near-equatorial trough is found over the water north of 5° to 8°N, i.e., condition (2) above. (For reference, the near-equatorial trough is the large-scale trough of low pressure lying east-west between the subtropical high pressure belts of the Northern and Southern Hemispheres.) The near-equatorial trough then coincides with the warmest sea surface. Ramage shows there is a negative correlation between sea-surface temperature change and 24-hour changes of surface pressure, that is, as the sea-surface temperature rises, the surface pressure falls.

From this simple explanation, one might expect the near-equatorial trough to move smoothly northward and southward with the sun. In fact, over the Arabian Sea, the near-equatorial trough weakens and disappears in the spring as a heat trough develops over the Indian subcontinent and reappears in autumn as the land-anchored heat trough fills. This discontinuous movement of troughs is shown in Figure 3-20.

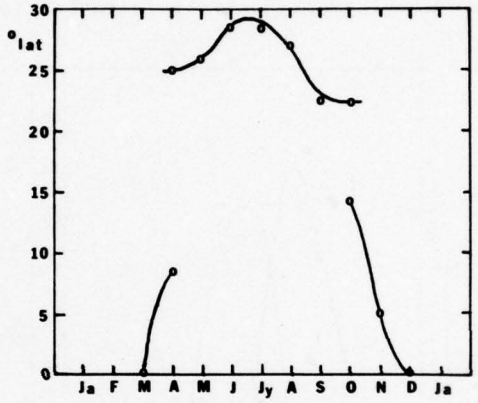

Figure 3-20. Mean annual variation in the latitude of the near-equatorial trough along 58.5°E (after Ramage, 1974).

As derived from the relationship between the near-equatorial trough and tropical storm development proposed by Ramage (1974), the annual variation in tropical storm development -- and thus tropical storm occurrence -- is as follows:

(1) During the winter monsoon, the fresh northeast winds cause a relatively deep mixed layer in the Arabian Sea and, along with minimum solar insolation, a sea-surface temperature minimum (see Figure 3-21). Thus no surface trough can be found north of the equator, as shown in Figure 3-20. However, by March, both the Arabian Peninsula and India begin to warm, weakening the northeast monsoon. This causes the ocean-mixed layer to decrease (see Figure 3-21). At the same time, decreased cloudiness combines to increase insolation, thus contributing to rapid sea-surface warming.

(2) With the near-equatorial trough now (April) over the central Arabian Sea (see Figure 3-20), tropical cyclone development and frequency increase. By mid-May, the heat low over Pakistan becomes dominant even though at times a near-equatorial trough with associated tropical storm development is still found over the Arabian Sea. With this heat low, the southwesterlies increase, causing the mixed layer to deepen, and as cloudier skies counteract increased solar radiation, the sea-surface temperature falls to a minimum by August.

(3) With the surface trough (a heat low in this case) over land to the north of the Arabian Sea from late June to early September, almost no tropical cyclones occur in the Arabian Sea. By the start of autumn the land is cooling and the winds, mixed-layer depth and cloudiness decrease (see Figure 3-21). Despite the opposing trend in solar radiation, sea-surface temperatures increase, reaching a secondary maximum in October and November. Thus the near-equatorial trough reforms over the sea as shown in Figure 3-20 and tropical storm development/activity reaches a secondary peak.

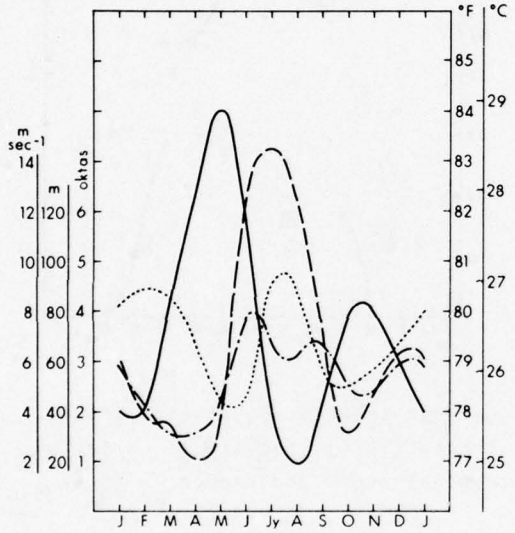

Figure 3-21. Mean annual variation of sea surface temperature (°C, solid line), surface wind speed (m sec^{-1}, dashed line), depth of ocean-mixed layer (m, dotted line) and cloudiness (oktas, dot-dash line) for small area centered at 11.5N, 58.5E (Arabian Sea) (from Ramage, 1974).

3.3.3 Examples of Tropical Storms in the Arabian Sea

Two typical examples of tropical storm development and movement as depicted by NOAA-3 visual data are discussed here to familiarize the forecaster with these processes. Both of the tropical cyclones reached only tropical storm intensity, although usually about one out of every two tropical storms reaches hurricane intensity in the Arabian Sea. The April 1974 storm had peak winds of 60 kt on 15 April, while the May 1974 storm reached 50 kt on 20 May. The storm tracks are shown in Figure 3-22; satellite photographs are presented in Appendix B as Figures B-1 through B-9.

The April sequence (B-1 through B-4) appears to have developed in the vicinity of a strong near-equatorial trough (note east-west cloud mass between 5°N and 10°N on Figure B-1 over the Arabian Sea). This extensive convective activity is generally believed to exist just to the equatorial side of the

near-equatorial trough with relatively clear skies within the trough (see Para. 3.3.2). By 13 April (B-2), an organized cloud mass is present, supporting the analyzed tropical depression indicated in Figure 3-22. Development is seen to continue throughout the sequence with the cyclone reaching tropical storm intensity on 15 April (B-4). This storm maintained a northerly track throughout its history and generally conformed to the typical mean track shown in Figure A-35a.

The development of the May case (B-5 through B-9) also appears to have been associated with a near-equatorial trough. Cloudiness over the Arabian Sea south of 15°N (B-5) indicates the presence of the near-equatorial trough near 15°N at time of development of the tropical storm. This cyclone rapidly reached tropical storm intensity on 18 May (B-6), moving westward to the Gulf of Aden by 21 May (B-9). This tropical storm followed one of the typical mean tracks for May shown in Figure A-35b and would have caused serious problems for ships in the Gulf of Aden.

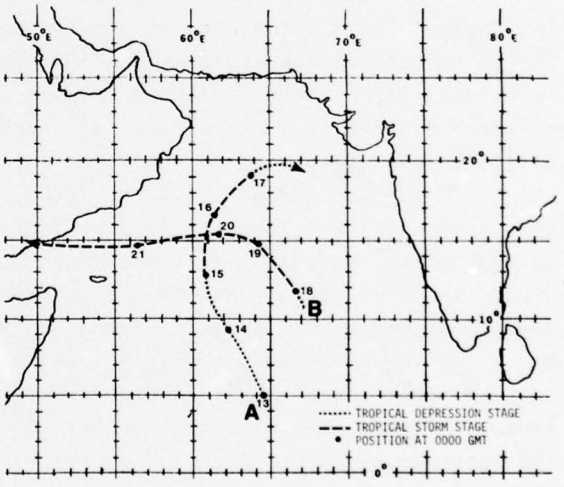

Figure 3-22. Tropical storms that originated in the Arabian Sea during the spring transition season of 1974. Storm A, 13-17 April; and storm B, 17-21 May (from Mariners Weather Log, 1974).

3.4 WESTERN DISTURBANCES

Although the major mountain chains north of the Arabian Sea -- including the Himalayas, the Zagros Mountains of Iran and the Caucasus (locator map, Figure 1-1) -- cut off strong surges of cold air from the north during the winter monsoon, cold fronts with associated dust storms do affect the weather of the northern Arabian Sea several times each winter. Most of these cold fronts are associated with "western disturbances" (terminology of the Indian

Meteorological Department), which appear to move from the Mediterranean region across southwest Asia toward India (Snead, 1968). This section describes these disturbances primarily from a satellite point of view and includes typical case studies and forecasting hints.

3.4.1 Statistical Information

The most extensive study of western disturbances has been made by Bhaskara Rao and Moray (1971), who analyzed satellite data covering the region from 40°E to 90°E and 15°N to 60°N for the years 1967 and 1968. Based on the satellite cloud pictures, the various cloud forms moving eastward across the area under consideration were classified into five types:

(1) Systems with a Vortex (V)
(2) Latitudinal Bands (LB)
(3) Meridional Bands (MB)
(4) Overcast cloud Masses (OM)
(5) Broken Amorphous cloud area (BA)

The vortex type (V) is typical of the extratropical cyclone of mid-latitudes. It is associated with a strong upper-level, short-wave trough (negative Small Scale Disturbance (SD Center*)) and, although this type is relatively rare in the region, it causes strong cold frontal passages over the northern Arabian Sea. An example of the V type over Iraq is seen in the satellite photograph and SD analysis in Figures C-1a and C-1c respectively.

The latitudinal band type (LB) is appropriately named -- the cloud band is generally oriented in a west-southwest to east-northeast direction. A survey of the synoptic situations associated with the LB type shows that the cloud band lies roughly in the section of the upper-level flow from trough to downstream ridge. An example of the LB type appears in Figure C-4a.

The meridional band type (MB) generally lies to the east of a surface low. In most cases, a well marked upper-level trough-ridge system similar to type V is found. As with type LB, the cloud band lies at some position between the upper-level trough line and downstream ridge line in the region of positive vorticity advection (see Figure 3-23b). The surface chart, Figure 3-23a, shows that type MB often has an active cyclone associated with it, and in the case depicted there is an obvious strong cold front moving out over the northern Arabian Sea.

---

*For a complete description of the scale and pattern separation fields of Fleet Numerical Weather Central, see U.S. Naval Weather Service (1975).

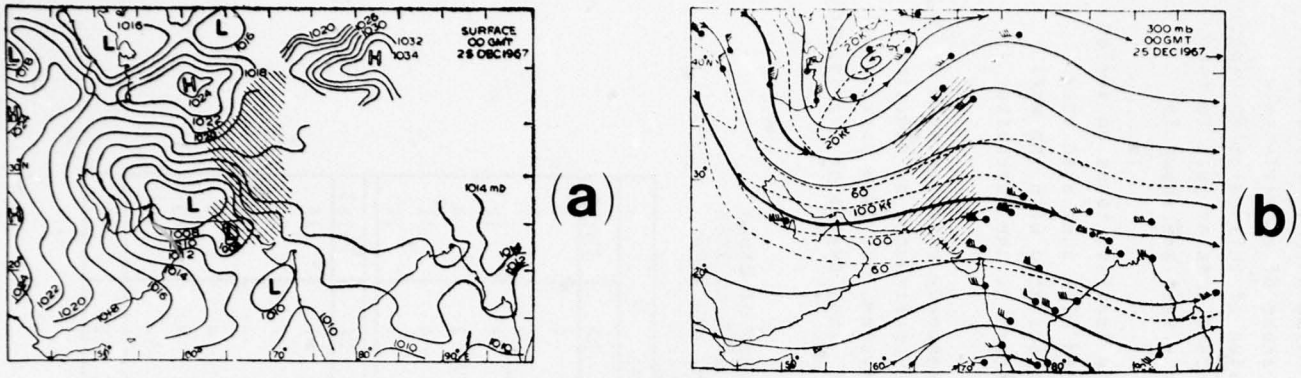

Figure 3-23. Surface (a) and 300 mb (b) charts showing meridional band (MB) type cloud system. The shaded areas correspond to the cloud system. (from Bhaskara Rao and Moray, 1971).

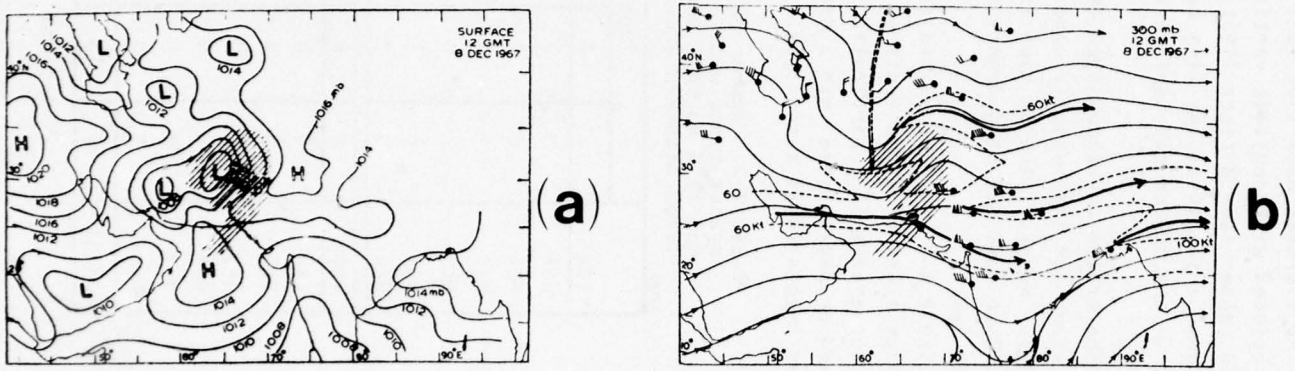

Figure 3-24. Surface (a) and 300 mb (b) charts showing overcast cloud mass (OM) type cloud system. The shaded areas correspond to the cloud system. (from Bhaskara Rao and Moray, 1971).

The overcast mass type (OM) appears as a "comma-shaped" cloud mass and is associated with positive vorticity advection ahead of a small-scale negative SD center (see Bittner (1971) for a discussion of this relationship). In most cases, a sea level low lies beneath the overcast area or just to the west of it -- the 300 mb and surface charts for such a case are shown in Figure 3-24.

The broken amorphous type (BA), as the name implies, takes on varied forms and sizes and the synoptic conditions associated with them also vary considerably. However, the BA type is not usually associated with the well defined surface lows and cold fronts that are of concern to the forecaster in the Arabian Sea.

Table 3-2 provides an indication of the frequency of occurrence of these various types of cloud systems. The table was constructed by counting the first appearance of a particular type of cloud system, but if a particular type evolved or degenerated into a different type of cloud system on a following day, it was recounted as a new type.

Table 3-2. Number of first occurrences of cloud system types within the area from 40°E to 90°E and 15°N to 60°N for the years 1967 and 1968 (from Bhaskara Rao and Moray, 1971).

	Type of Cloud System					
1967	V	LB	MB	OM	BA	Total
Jan	0	0	3	4	2	9
Feb	0	2	6	5	4	17
Mar	1	4	1	2	4	12
Oct	2	0	1	2	3	8
Nov	1	1	4	1	4	11
Dec	0	3	1	3	7	14
1968	V	LB	MB	OM	BA	Total
Jan	0	0	1	7	6	14
Feb	1	3	2	3	7	16
Mar	0	0	0	4	8	12
Oct	2	0	0	2	4	8
Nov	2	0	2	1	8	13
Dec	2	0	0	6	9	17
Total	11	13	21	40	66	151

V - Systems with a Vortex
LB - Latitudinal Bands
MB - Meridional Bands
OM - Overcast cloud Masses
BA - Broken Amorphous cloud area

Because of the inherent limitations in counting the number of occurrences in this manner (e.g., more than one type of cloud system can occur during a given sequence), the data in Table 3-2 do not give the actual frequency of western disturbances for the various months. However, some indication of the likelihood of cold frontal passages can be obtained by analyzing the types separately. As noted in Para. 3.4.2 following, both the V and MB types are usually associated with strong surface cyclogenesis leading to cold frontal passages into the northern Arabian Sea. Because of the difficulty of combining these two columns from Table 3-2, a conservative estimate of the maximum number of occurrences can only be made by adding the maximum number in 1967 from one of the two columns (16 type MB) to the maximum in 1968 (7 type V). Thus this sample of two years would indicate that about 11 surges per year, a significant number, would be a reasonable estimate.

3.4.2 Typical Case Studies With Forecasting Hints

Two case studies of strong cold fronts moving out over the northern Arabian Sea are presented. These cases appear to be rather typical of the events that lead up to the cold frontal passages and their effects on the local weather. Both of these cases have been studied by Perrone (pending NEPRF report), who investigated the shamal (see Huschke, 1959) in the Persian Gulf and developed several forecasting aids.

The first case covers the period 24-26 January 1974 (C-1 through C-3). As noted in Para. 3.4.1, the satellite photograph on 24 January (C-1a) indicated a type V pattern with the vortex at about 32°N, 42°E. It has been shown from DMSP data in this case that explosive deepening of a surface low, which is a positive indication of a cold surge, is taking place to the east of the vortex with lines of strong convective activity over the Persian Gulf. The high clouds extending from about 20°N, 40°E across the Persian Gulf in Figure C-1a are likely associated with the subtropical jet stream which is normally found crossing the Persian Gulf during the winter season (see Figure 3-25). Reiter (1975) believes that interaction between the subtropical jet and polar jet is a necessary condition for rapid cyclogenesis in these latitudes.

The strong upper trough with associated negative SD center shown over Iraq in Figures C-1b and C-1c must continue moving eastward to western Iran, leading to northwesterly flow over the Persian Gulf, if a strong cold front is to cross the Arabian Peninsula and enter the Arabian Sea. It appears that the strong northwesterly airstream to the west of the trough is responsible for forcing cold air southward over the normal barrier formed by the mountains of Turkey and western Iran and onward into Syria, Iraq and the northern Arabian Peninsula -- the forecaster must therefore have an accurate forecast of the movement of these strong upper troughs (negative SD centers).

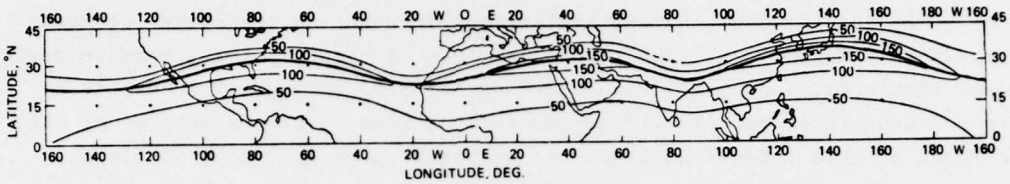

Figure 3-25. Mean subtropical jet stream for winter 1955-1956. Isotach analysis at 200-mb surface. Isotachs are drawn for every 50 kt. The mean latitude of the jet axis is 27.5°N (from Reiter, 1969).

By 25 January the surface cold front has reached the southeast coast of the Arabian Peninsula, as clearly indicated by both the satellite photograph and the wind data plotted on the surface analysis (C-2a and C-2d). A good indication of the duration of the cold surge is the speed of movement of the upper trough, so as long as the upper trough remains over western Iran, the cold surge continues. It is believed that subsidence, which occurs within the western portion of the trough, helps to increase the pressure gradient along the southern coast of the Arabian Peninsula. Once the upper trough moves eastward, the subsidence lessens, the pressure gradient relaxes, and the winds diminish. Thus the continued rapid movement of the strong upper trough shown by comparison of Figures C-2b and C-1b indicates that the surge will only last one or two days. It should be noted that strong dust storms (as indicated by both the plotted data in Figure C-2d and the DMSP data) are very common following the cold fronts -- a description of such a dust storm in the wake of a cold front is found in Section 4.1.

On the last day of this sequence, although the cold front has continued moving southeast across the Arabian Sea (extending from point A to point B in Figure C-3a), conditions have changed dramatically to the north and now indicate a weakening of the cold surge. At 500 mb the upper trough has moved to about 72°E (C-3b, C-3c) and the flow over the Arabian Peninsula and Persian Gulf has turned westerly as another trough approaches from the west. Thus the surface high cell over the Arabian Peninsula with resulting strong pressure gradient to the south, which is necessary for a continuation of the surge, is weakening (Figure C-3d).

The second case covers the period 15-19 January 1973, although the surge continued beyond the later date, and is a typical example of an extended cold surge over the northern Arabian Sea (C-4 through C-8). The upper level flow (C-4b, 5b, 6b, 7b, 8b) did not turn northwesterly over the northern Arabian Peninsula until 18 January. The sequence shown on the three preceding days emphasizes the difficulty of forecasting the necessary flow pattern for the

surge. The deep 500-mb trough on 15 January in the eastern Mediterranean basin, with associated negative SD center (C-4b, C-4c), weakened as it moved eastward over Syria and Iraq on 16 January (C-5b, C-5c). This change in the intensity and configuration of the trough delayed the strong advection of deep cold air southward over the northern Arabian Sea.

It should be noted that the subtropical jet was well defined on 15 January as indicated by the band of high clouds crossing the Persian Gulf in a southwest-northeast direction (C-4a). It was this cloud band that caused the satellite picture to be designated type LB in Para. 3.4.1. The fact that cyclogenesis did not take place on this day emphasizes the point that a strong subtropical jet is not a sufficient requirement for storm development (see Reiter (1975)).

Although the cold front reached the south coast of the Arabian Peninsula on 17 January (note thin cloud lines between points A and B on Figure C-6a), the cold surge did not extend far out into the northern Arabian Sea until 18-19 January (note narrow cloud bands between points A and B on Figures C-7a and C-8a). Thus the major penetration of cold air over the northern Arabian Sea occurred in conjunction with the shift to northwesterly of the 500-mb flow over the Arabian Peninsula (C-7b, C-8b). Again, as was the case during the January 1974 cold surge, blowing dust was evident at some of the coastal stations (C-7d, C-8d).

It is interesting to note that both of the typical cases described above occurred during January at the height of the winter monsoon. The strongest and most persistant cold surges occur during the last half of December, January, February and early March. In November and early December, the upper westerlies are generally positioned too far north for deep troughs to penetrate south of the mountains of Turkey -- the cold surges during this period tend to be short-lived and relatively weak, although they do indeed occur (see Section 4.1). In late March and April, on the other hand, while troughs in the upper westerlies frequently do reach well southward, the upper air flow tends to be neither sufficiently meridional nor sufficiently intense to advect enough cold air southward across the mountain barriers to the north. Also, because of the strong heating of the cold air over the Arabian Peninsula, cold surges which do occur over the northern Arabian Sea tend to be weak and short-lived.

3.5 MESOSCALE PHENOMENA

Local wind regimes along the coastline of the Arabian Sea must be considered important because of both the complexity of the orographic features of the land masses and the strong differential heating at these low latitudes. Although literature on the subject is generally scarce, the following subsections outline some of the information that is available.

3.5.1 Diurnal Effects

Atkinson (1971) provides a comprehensive description of possible diurnal effects in tropical regions. As expected, diurnal wind changes in the tropics are most pronounced near coastlines where strong differential heating takes place. A sea breeze generally develops a few hours after sunrise, continues during the daylight hours and dies down after sunset. Later a land breeze appears and continues until after sunrise. The sea breeze may extend up to 30-60 n mi inland, but the seaward range of the land breeze is much smaller. The vertical extent of the sea breeze is 1300-1400 meters (4300-4600 ft), with the maximum speed at a few hundred meters above the ground due to surface friction. In contrast, the land breeze is usually only a few hundred meters deep.

A study made from pilot-balloon observations for Djakarta (Indonesia) is also described by Atkinson (1971), and the results should be of general application (see Figure 3-26). The analyses on this diagram show the speed of the onshore/offshore winds at various levels as a function of time. It can be seen that the surface sea breeze blows from about 1000 to 1900 LT, reaching a maximum strength in mid-afternoon. Due to surface frictional effects, the sea breeze appears earlier and at greater intensity above the ground. Maximum depth of the sea breeze, about 1300 meters (4300 ft), is reached near 2100 LT after it has died at the surface. Near the surface, the land breeze that occurs after dark is much weaker than the sea breeze.

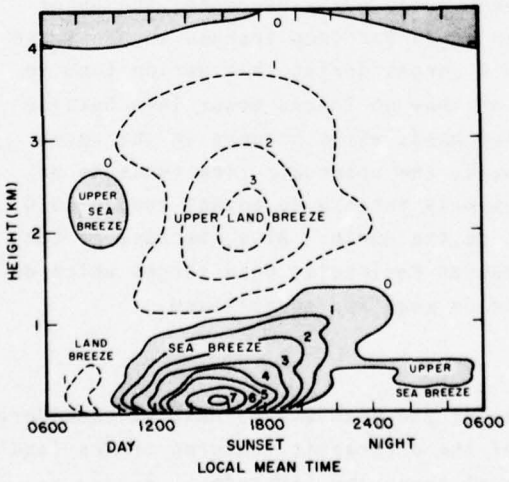

Figure 3-26. Velocity isopleths (m sec^{-1}) for the land-sea breeze in Djakarta. Shaded area indicates onshore flow and unshaded area indicates offshore flow (from Atkinson, 1971).

Of great interest in the Arabian Sea region are the occurrences of land-sea breezes when they are reinforced by upslope-downslope wind regimes. These upslope-downslope winds, commonly referred to as mountain-valley winds, have been observed and studied mostly in the mountainous regions of mid-latitudes. To the shipboard meteorologist, however, these circulations are of primary importance when the mountains are found along such coastlines as those bordering the Gulf of Aden and to a lesser extent the Gulf of Oman. The mountain-valley winds are the results of the temperature differences between the heated/cooled mountain slopes and the air at the same altitude over nearby valleys/water surfaces. During the day the heat of the mountain slopes causes the air over these surfaces to rise, while at night the reverse circulation with downslope winds occurs due to radiational cooling of the same slopes. These circulations are well developed on slopes facing the sun and weak on shady slopes. The thickness of the upslope wind layer is generally 100-200 meters (300-600 ft) with characteristic speeds of 2 to 4 m sec^{-1} (4-8 kt). The nocturnal downslope wind is shallower with lower velocities.

One of the best documented cases of land-sea breezes and upslope-downslope wind regimes reinforcing each other is found in the Red Sea/Gulf of Aden region (Flohn, 1965).

Along the coast of the Gulf of Aden, steep escarpments rise abruptly a short distance inland. During the summer monsoon, generally fair skies allow a maximum of surface heat for the combined land-sea, upslope-downslope effects to occur. Figure 3-27 shows the resultant surface wind directions over the Gulf of Aden area for two daytime periods (0600-0800 LT and 1200-1500 LT) during July and August, the peak summer monsoon months. The resulting gradient-level flow in the Gulf of Aden during July and August is from the west-southwest (A-20a and A-21a). During the morning hours (0600-0800 LT), downslope/land breezes prevail and cause convergence over the water, while by afternoon (1200-1500 LT), upslope/sea breezes prevail and cause divergent surface winds over the water and convergence inland. (This same type of combining upslope-downslope/sea-land breeze circulation was observed in a recent study (Brody and Godfrey, 1971) along the coast of the South China Sea.) It would also be expected that strong diurnal wind changes could affect the Gulf of Oman region because of its coastal mountains.

Finally, diurnal wind changes should be expected along most of the coastal Arabian Sea because of the large differential heating along the coast under clear skies. Only during the cloudy summer monsoon of western India will the diurnal wind regimes be of minimal importance in forecasting the coastal winds.

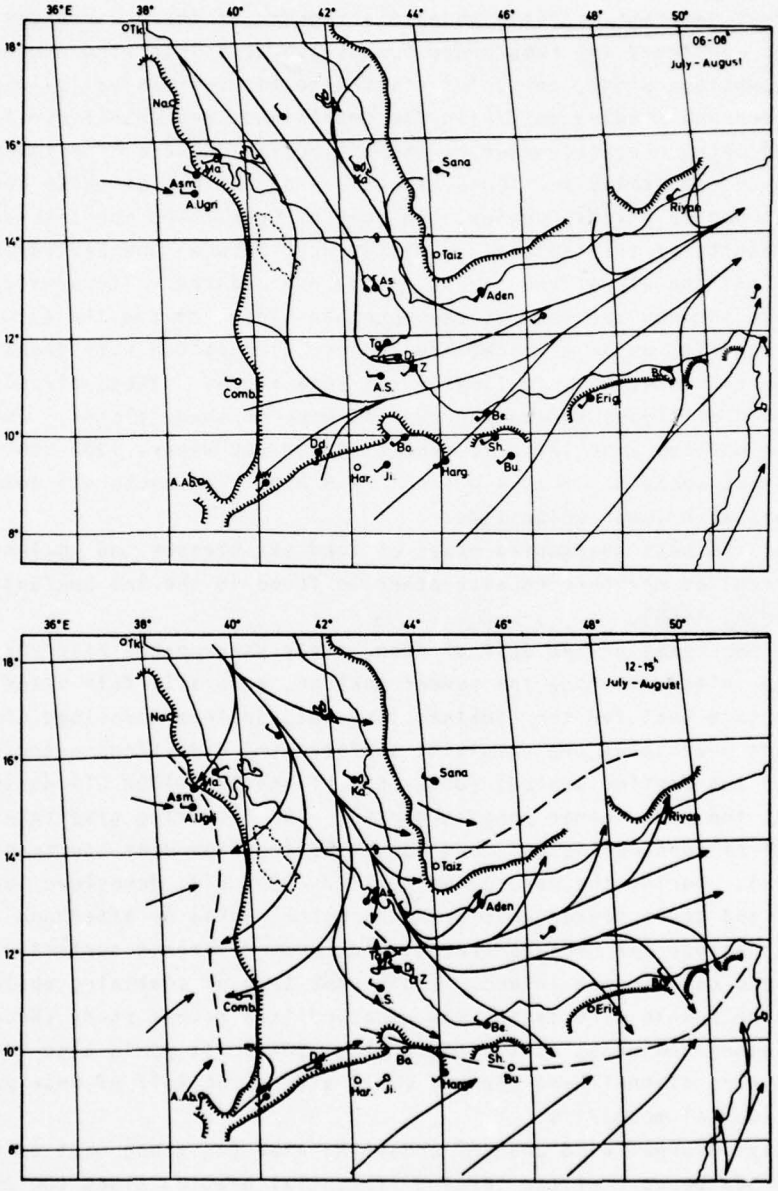

Figure 3-27. Streamlines and resultant surface winds in the southern part of the Red Sea Trench and Gulf of Aden, July and August: (a) early morning, nighttime circulation; (b) early afternoon, daytime circulation (broken lines are convergence zones) (from Flohn, 1965).

3.5.2 The Mesoscale Eddy of Ras Asir (Cape Guardafui)

During the summer monsoon of the western Arabian Sea, the region near Ras Asir (see locator map, Figure 1-1) is in the vicinity of the strong low-level jet described in Para. 3.1. As indicated by Figures A-7b, A-8b and A-9b, the surface winds in this region are very strong from the south and southwest. However, within this region near Ras Asir is a mesoscale eddy which has a great influence on the surface flow.

Figure 3-28 shows the mean surface position of the eddy. It is centered between Ras Asir and Alula on the northwestern edge of the main monsoon (Figure 3-29), and is partly caused by the topography of the area (Figure 3-30). In Figure 3-28, the diameter of the closed circulation appears to be only about 100 n mi, but its influence appears to deform the surface flow over a much wider area out to about 250 n mi. Also of interest is an area of light mean surface winds to the northwest side of the eddy.

Findlater (1971) has investigated the eddy, and based on his data its most important features are:

(1) The eddy is linked to the topography of Ras Asir. The small ridge of hills to the south of Alula (Figure 3-30) has higher mean wind speeds within the southwest flow at the hills' eastern end, favoring eddy formation on the leeward side.

(2) The eddy is evident only in the summer months and is sufficiently persistent to show in mesoscale analysis for the months of June through September (Figure 3-28).

(3) The eddy is of mesoscale dimensions with a diameter of 100 n mi at the surface, but it influences an area out to 250 n mi as seen in the surface wind field (Figure 3-28).*

(4) The eddy extends upward to between 500-1000 m (1600-3300 ft) with a slope to the northeast. This can be deduced, for example, from the doppler radar winds shown in Figure 3-31.

---

*An example of surface wind changes associated with this mesoscale eddy is given in Section 4.3.

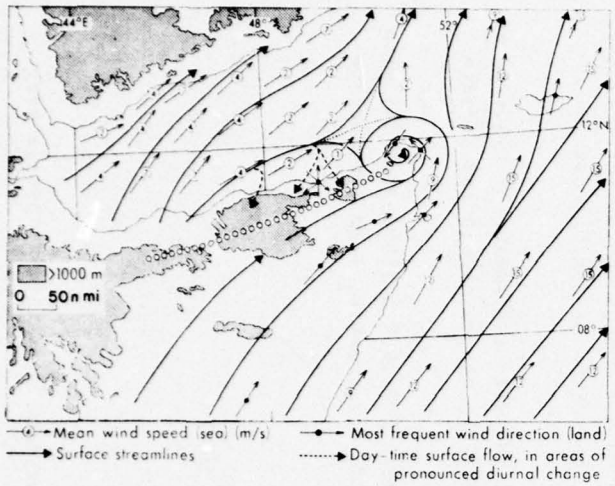

Figure 3-28. Mean surface flow in July (line of circles indicates sea breeze convergence zone) (from Findlater, 1971b).

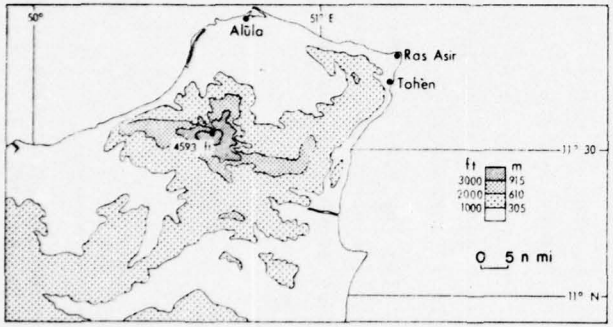

Figure 3-30. Topography of area (from Findlater, 1971b).

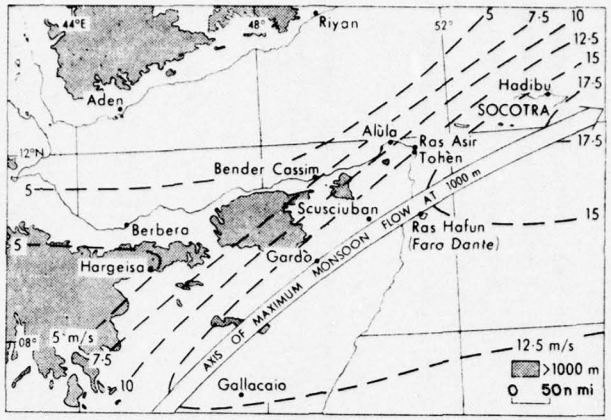

Figure 3-29. Mean flow at 1000 m in July, and location of stations (from Findlater, 1971b).

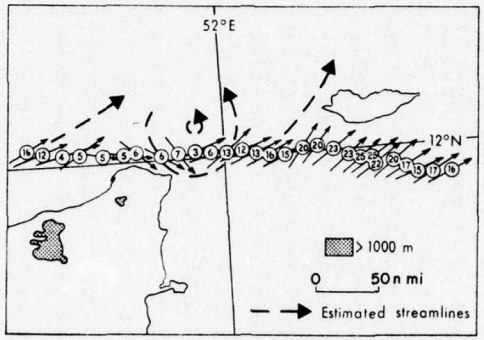

Figure 3-31. Doppler radar winds at 560 m on 1 September 1964 near Ras Asir. Aircraft position is marked by circles; wind speeds in m sec^{-1} are cited in the circles; small arrows indicate wind directions (from Findlater, 1971b).

4. SEASONAL PROGRESSION OF THE ARABIAN SEA MONSOON*

This section describes the typical sequences of weather events that occur during the four basic seasons of the Arabian Sea region. Climatological charts supporting the discussions are presented in Appendix A, and it is recommended that the reader refer to them frequently for a clearer visualization of the subject. Included in this appendix are monthly charts of surface wind roses for both the Arabian Sea and Gulf of Aden; airflow charts at 3000 and 10,000 ft; and streamline analyses for the months of January, May, July and October for the 500-mb, 300-mb and 200-mb levels. Also included are climatological charts of such significant meteorological parameters as mean cloud amounts, mean air and sea-surface temperatures, visibilities (less than 2 n mi), tropical storm tracks and sea heights.

Interpretation of the sea height charts, which are presented in two formats, requires some explanation. In the first, the frequencies of sea waves greater than or equal to 10 feet were constructed from data in various volumes of the Summary of Synoptic Meteorological Observations published by the U.S. Naval Weather Service Command. This sea wave data (A-33) includes only waves generated by the local winds in the vicinity of the observer. Also, the heights are the "significant" heights -- the average of the one-third-highest sea waves. The second format (A-34) provides isoline analyses of the mean "significant" wave heights (U.S. Naval Weather Service Command, 1974a). Data on these analyses include both sea and swell waves. If both are present in an observation, only the higher of the two is used. However, if only one of the wave groups is observed, either sea or swell, this one group is used in the summary.

Although climatological information for various ports is not included in Appendix A, this information is easily obtained from Climatic Summaries for Major Indian Ocean Ports and Waters (U.S. Naval Weather Service Command, 1974a). It must be emphasized that although several illustrations from the Summaries have been reproduced in this document for the convenience of the reader, reference to the Summaries themselves is a necessity for the operational forecaster in the Arabian Sea.

---

*References are made in this section to illustrations contained in Appendixes A, B and C. For brevity within text, these references will often appear simply as the referenced figure's number, e.g., (A-1) (B-2), rather than in the longer form (see Figure A-1) (see Figure B-2).

In the following discussions of seasonal events, information in Section 3 is frequently referenced. In this way, emphasis can be placed on important variations from the normal in both time and space as well as on possible aids to the forecasting of significant meteorological phenomena.

4.1 THE WINTER MONSOON - DECEMBER THROUGH MARCH

Because of the extensive mountain barrier to the north of the Arabian Sea, the region's winter monsoon is much weaker than the northeast monsoon of the South China Sea (Cuming, 1973), as is also the case in the Bay of Bengal. The surface wind roses (A-2, A-3, A-4, A-13) show wind speeds on the average under 10 kt over the northern Arabian Sea and under 21 kt in the south. With these relatively light winds, sea heights are generally low (A-33, A-34) -- only along the Somali coast are the mean wave heights greater than 4 ft. However, and probably due to the cold surges (see Para. 3.4.2), locally wind-generated waves do reach 10 ft at times (<5% frequency) in the western Arabian Sea. It is also quite likely that behind an extremely strong cold front, winds and seas in the northern Arabian Sea reach much higher values. (The example shown in Figures C-1 through C-3 is probably such a case.) Wind directions during the winter monsoon are generally from the northeast. The easterly winds in the Gulf of Aden are directed by the channeling effect of the mountains on either side of this gulf.

There is an important exception to the simple wind pattern just described for the normal winter monsoon. This variation occurs in the two northern areas of the Arabian Sea, *North Gulf of Oman* and *Sonmiani* (see Figure A-1a for locations of italicized areas), where the winds are generally light and variable. LT Paul Grisham, meteorologist aboard USS HANCOCK (CVA-19), observed these conditions during November-December 1971 and explained the phenomenon as being associated with an induced lee low pressure trough in the northeast flow as the air crossed the mountain ranges of southern Iran and Pakistan. Grisham reported that as the ship approached the trough line (mean position shown in Figure 4-1), the winds became light and variable.

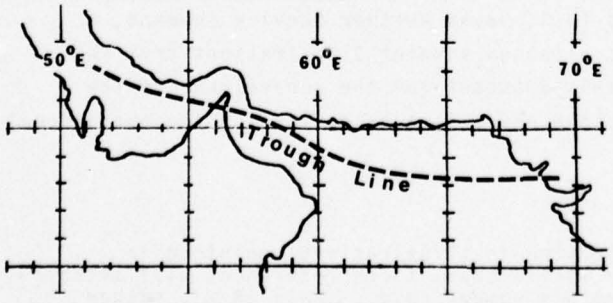

Figure 4-1. Mean position of lee low pressure trough in northeast flow during the winter monsoon season.

During the winter monsoon, cloud amounts are generally small and visibilities are good over the Arabian Sea (A-30a, A-32a, b). The cloud amounts increase southward, however, with a maximum at 5°N near the position of the weak Northern Hemisphere near-equatorial trough (see Figures A-14, A-15, A-16 and A-25 for lower troposphere positions of this trough during winter).

Although the mean cloud amounts are higher over the Bay of Bengal then over the Arabian Sea during the winter monsoon (A-30a), somewhat more low-level cumulus and stratocumulus are observed over the Arabian Sea, especially south of 20°N. This cloudiness is generally found between 60-65°E spreading out toward the south-southwest and south. Figure 4-2 for 27 January 1974 shows an excellent example of this cloudiness. Gurunadham (1971) attributes this rather semipermanent cloudiness to the cold dry air that travels toward the south over the northern Arabian Sea and picks up moisture by evaporation from a relatively warm water surface that is about 1°C warmer than the air, especially during the first half of winter (A-31). The cold air is associated with cold surges (rare in the Bay of Bengal) following western disturbances (see Para. 3.4.2). In this regard, it will be interesting to note that the satellite photograph in Figure 4-2 was taken one day after the cold surge shown in Figures C-1 through C-3. Gurunadham believes that an indication of the strength of the cold air invading the Arabian Sea, and thus of the wind strength, is the increased density of the small packed cells of clouds, often in bands, that spread out in the direction of the low-level winds.

Another common weather phenomenon of the northern Arabian Sea is the occurrence of dust associated with cold fronts moving off the Arabian Peninsula (see Para. 3.4.2). LT Grisham on USS HANCOCK reported such a situation during November 1973:

> "The heavy dust which enveloped the northern Arabian Sea was not detected by marine observers for a period of about six to eight hours after the cold frontal passage (about midnight local time). The earlier sunset revealed an otherwise clear sky to be quite red, indirectly indicating dust to be present in the atmosphere. The passage of the dry front was determined with reasonableness by a marked drop in dew point temperature, a sharp wind shift and increase in wind speed and, most importantly, by surface analysis continuity.
>
> Shortly after daybreak a heavy cloud was detected on the western horizon by observers aboard a USN unit. This rapidly-moving cloud appeared to be fog, even though a check of the measurable parameters indicated that the air was much too dry to support such a phenomenon. Within an hour of the first sighting, the ship was enveloped by dust which reduced horizontal visibility to two miles and slant range visibility to 1/2 mile. The tops were measured by aircraft to be 8500 feet and further indicated that the dust was continuous at least 300 nm in all directions. The next day showed visibilities of 5-7 miles. The atmosphere was not clean for about one week."

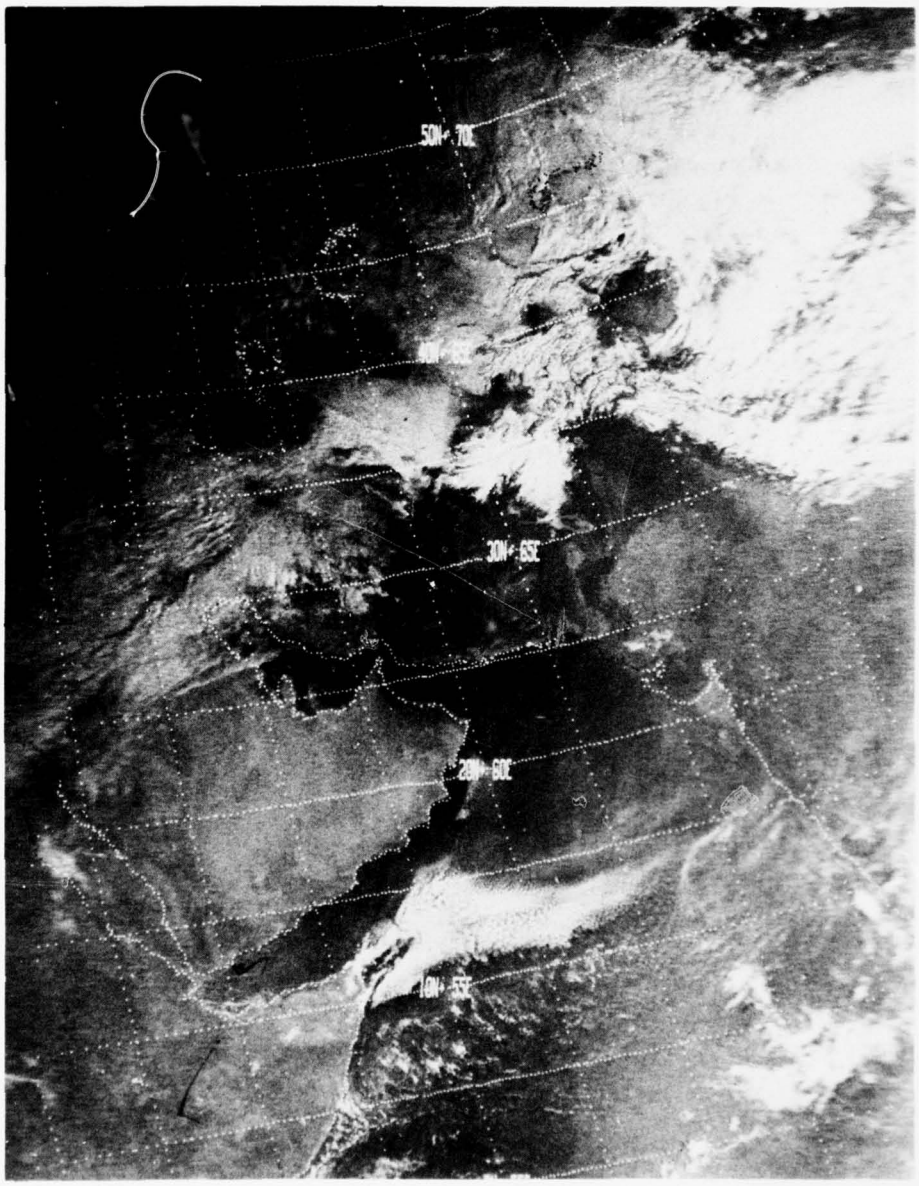

Figure 4-2. Satellite photograph showing typical cloudiness in the Arabian Sea region during the winter monsoon. 0451 GMT 27 January 1974 (NOAA-2).

Although wind speeds in this case reached only 15-20 kt, it is quite likely that gale force winds might be expected in stronger situations (see example in Appendix C). It has been shown that high-resolution DMSP data are very useful as indicators of the horizontal extent of such a dust storm.

Similar cases of dust and dust haze, but covering a much more extensive area, are documented in the literature. In one notable case, a cold wave and extensive dust haze covered practically the whole of India during the second week of February, 1950.

Cold fronts associated with western disturbances and moving out over the northern Arabian Sea have been known to cause other changes in the normal winter monsoon weather. Observers aboard USS HANCOCK noted that cold fronts on two occasions resulted in the development of a well-defined surface high pressure cell over the northern Arabian Sea separate from the high pressure cell to the north. With this change in the pressure pattern, southerly winds accompanied by cloudiness were observed along the southeast coast of the Arabian Peninsula. However, the cloudiness lost its vertical characteristics on moving into the area of the high, and was observed in that region to be stratocumulus capped by a strong inversion at about 4000 feet.

Rain, though rare, is another effect seen in conjunction with slow-moving cold fronts during the winter monsoon. Observers aboard USS ENTERPRISE (CVN-65) reported that during a five-day period in the Gulf of Oman in January 1975, two weak western disturbances crossed the Persian Gulf. The associated slow-moving cold fronts moved southeastward across the Gulf of Oman causing 1000 ft ceilings and rain.

Among mesoscale effects to be expected are land/sea breezes along the Arabian Sea coastlines (see Para. 3.5.1), such as those at the port of Mombasa, Kenya, where observers on USS ENTERPRISE reported a strong sea breeze regime during the winter monsoon. Although Mombasa is south of the equator, radiational cooling over the Arabian Peninsula coupled with radiational heating over the Kalahari Desert causes the northeast flow of the winter monsoon to affect this region (see surface wind roses in Figures A-2a, A-3a, A-4a and A-13a). The winter monsoon flow is so enhanced by the afternoon sea breeze at Mombasa that the northeasterlies increase to 18-25 kt each afternoon.

Tropical cyclones during the winter monsoon are extremely rare, and only during December have such storms been recorded. Figure A-36j shows their tracks.

4.2 THE SPRING TRANSITION SEASON - APRIL THROUGH MAY

During April and May, changes in the surface flow which were first discernible in the latter half of winter (February, March), take place rapidly. These changes are associated with both the slow northward movement of the near-equatorial trough and the development of a strong heat trough over the Arabian Peninsula and Indian subcontinent (between 20°N and 30°N).

At the surface (A-5), the winds in the northern Arabian Sea even by April have turned westerly in response to the developing heat trough. Over the southern half, the winds during April generally remain northeasterly as the near-equatorial trough is normally still located to the south. An exception is the *Somali Coast SE* area, most of which is south of the near-equatorial trough (A-17a). Wind speeds in all cases are light during April. It is only along the extreme northern coast, in response to the developing heat trough, that winds greater than 21 kt appear in the wind rose summaries. These summaries, of course, do not indicate the occurrence of the relatively rare tropical storm with its much stronger winds. It is interesting to note that the winds over the Gulf of Aden shown in Figure A-5b have continued easterly. However, it should be remembered that the diurnal effects are present near the shores (see Para. 3.5.1).

By May, the effect of the continental heat trough on the surface winds (A-6) has become dominant except for the southern areas -- *Arabian Sea SW*, *Arabian Sea S* and *Arabian Sea SE* -- which are still occasionally under the influence of the near-equatorial trough. Wind speeds have increased markedly along the Somali coastal region where winds greater than 33 kt are reported and probably are related to the development of the low-level jet (see Para. 3.1.2). In conjunction with these speed increases, the frequency of locally generated sea heights greater than 10 ft are showing marked increases in the western Arabian Sea (A-33a). The easterly winds in the Gulf of Aden are still present in May, but speeds have become extremely light. In the area *N Gulf of Oman* the winds are variable, a condition which appears to persist throughout the summer season.

The mean location of the near-equatorial trough aloft during the spring transition season, with its slow northward movement at both 3000 and 10,000 ft, is shown in Figures A-17 and A-18. Note that along the eastern coast of equatorial Africa, marked changes take place in the lower troposphere as the low-level jet becomes established in May (see Para. 3.1.3).

Skies are generally clear and visibility good during the spring transition season. Comparing Figures A-30a and A-30b, it can be seen that except in the region of the near-equatorial trough, the skies are actually clearer in spring than during the winter. Although sea-surface temperatures have shown marked increases (A-31), the sea is no longer warmer than the air -- thus the low cumulus and stratocumulus common during the winter have decreased.

The major meteorological events of the spring transition season (and the autumn transition season as well) are tropical storms. Generally speaking, as long as the near-equatorial trough remains over the sea, and the farther it moves from the equator as during the spring, the more often tropical cyclones will develop in it (see Para. 3.3.2). It must be remembered that this near-equatorial trough does not move continuously northward, but changes locations and intensities from day to day. Also, as the heat trough to the north develops, the near-equatorial trough tends to weaken and finally disappear by the summer monsoon season. Preferred tracks of tropical storms are shown in Figures A-35a through A-35c for the months of April through June. The actual tracks for this same period are found in Figures A-36b through A-36d.

Examples of two tropical storms that developed in the Arabian Sea during the spring transition season are discussed in Para. 3.3.3 (see Appendix B for satellite pictures). To give the forecaster an indication of what effect these tropical storms had on the otherwise calm sea experienced during the spring (A-34d, A-34e), a study by Brand et al. (1973) was used to estimate sea heights at the time of maximum intensity of each storm. The combined sea height, a parameter defined as the square root of the sum of the squares of the "significant" sea and swell height, was used in this study. As suggested for analysis of South China Sea tropical cyclones, the average radii of the 9- and 15-ft isopleths of combined sea height for Arabian Sea tropical cyclones were similarly reduced by 20% of the expected values of western North Pacific storms. Asymmetry considerations described in the study were also included. The final results are shown in Figures 4-3a and 4-3b for both the 9-ft and 15-ft isopleths.

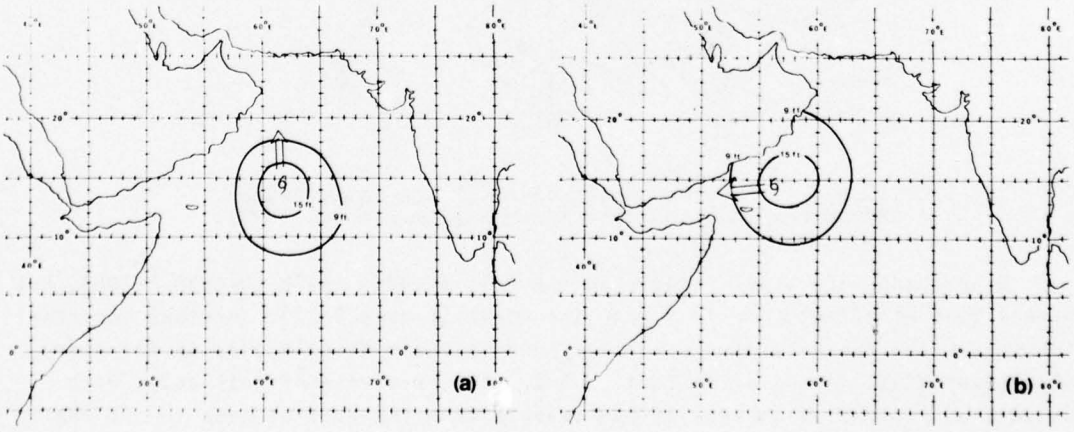

Figure 4-3. Combined sea height around two tropical storms (9- and 15-foot isopleths) obtained from equations modified for asymmetry in Brand et al., 1973: (a) 0000 GMT 15 April 1974 and (b) 0000 GMT 21 May 1974.

It can be seen in Figure 4-3b that ships leaving the Gulf of Aden would probably have experienced combined sea heights of at least 9 ft on 21 May 1974. (High winds associated with tropical cyclones are rare at the port of Karachi, Pakistan (see Appendix D), until June, a summer monsoon month, when tropical cyclones influence this port.)

4.3 THE SUMMER MONSOON - JUNE THROUGH SEPTEMBER

From the standpoint of surface winds (used in the definition of the monsoon given in Para. 2.1), the summer monsoon of the Arabian Sea is firmly established by June. Indian meteorologists who define the monsoon by the start of the rainy season along the west coast of India, use a later date shown in Figure 4-4.

Surface winds (A-7 through A-10) reach a maximum during July with the highest speeds reported off the northern Somali coast where frequencies of winds greater than 33 kt occur up to 28% of the time (see areas *Somali Coast NE*, *Socotra Is.* and *Arabian Sea SW*). These winds are associated with the combined effect of the low-level jet and cold upwelling of water off the Somali coast (see Para. 3.1.2). Excellent sources of forecasts in this region are the shipping broadcasts issued by the East African Meteorological Department.

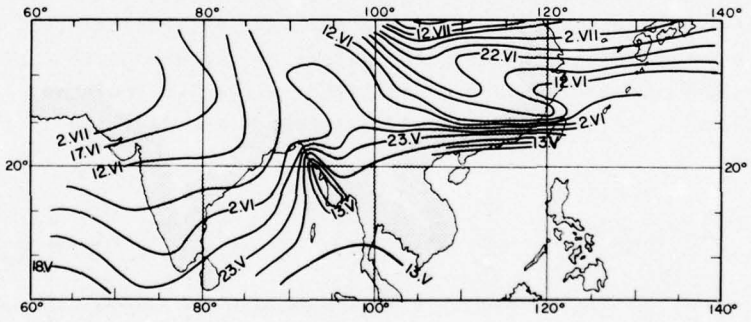

Figure 4-4. Average onset dates of the rainy season. Roman numerals indicate months (from Ramage, 1971).

Wind speeds are usually lower in the Gulf of Aden (A-7b through A-10b), but strong diurnal effects are felt near the coast (Figure 3-27). Another important feature in the vicinity of the Gulf of Aden is the mesoscale eddy at Ras Asir (Cape Guardafui) discussed in Para. 3.5.2. The existence of this eddy, with associated rapid wind changes as one travels from the Gulf of Aden to off the Somali coast, is documented by observers aboard USS CHICAGO (CG-11) transiting the area in Summer 1974:

"Winds throughout the Gulf of Aden were from the southwest at 15 to 25 kt increasing to a higher average of 20 to 30 kt when a high seas warning for the northern Arabian Sea was in effect. The only exception to this was found at the anchorage area approximately 15 miles north of Cape Guardafui, where an eddy effect produced southeasterly winds averaging 10 to 15 kt or less. This continued until CHICAGO passed through 52°E, at which time the southwesterly winds again prevailed. After rounding Cape Guardafui the winds increased as expected to 30 to 40 kt with gusts to 45 kt from the southwest."

As the persistent strong winds would indicate, sea heights in the Arabian Sea during the summer monsoon are high. Figure A-33 shows the the frequency of locally driven sea heights greater than or equal to 10 ft, which occur over 40% of the time in the areas of *Socotra Is.* and *Arabian Sea SW*. The analyses in Figures A-34f, g, h show that the mean significant wave heights (including swell) are 10-11 ft in this same general area from June through August, and it is quite possible that these results might even be on the low side. During the period 4 July to 7 August 1974, while USS CHICAGO was stationed along the Somali coast, observers reported combined significant sea heights of 12 ft or greater (up to 17 ft) 80% of the time.

The upper-level flow during the summer monsoon consists of deep westerlies up to 500 mb along the west coast of India (A-28a). Also a major feature is a shallower but strong low-level jet extending across the equator over Kenya and off shore in the vicinity of Cape Guardafui (A-19 through A-22). Note that although these analyses show the near-equatorial trough near the entrance of the Gulf of Oman at 3000 ft and sloping southeastward with increasing height to a line at 10,000 ft from approximately 20°N along the west coast of India to the vicinity of Cape Guardafui, the surface (heat) trough's usual summer location over land prevents the development of tropical cyclones (Ramage, 1974).

During June the near-equatorial trough occasionally reintensifies over the Arabian Sea and leads to tropical cyclogenesis. Figure A-36d shows that tropical cyclones reaching storm intensity in June generally develop off the west coast of India and move northwestward to the vicinity of Karachi, Pakistan, where they cause high winds (see Appendix D). It should be noted, however, that the high winds at Karachi during July and to a lesser extent in August and September (Appendix D) are associated with the remnants of monsoon depressions that developed in the Bay of Bengal (see Cuming, 1973).

The mean cloud cover for July shown in Figure A-30c displays the results of the essential differences in the monsoon regime between the eastern and western sections of the Arabian Sea. Near the western coast of India, large-scale upward motion causes general cloudiness to prevail along with frequent

showers and periods of rain that reduce visibilities (A-32a). To the west, large-scale subsidence (Ramage, 1971) keeps this cloudiness to a minimum. The reductions in visibility in the Gulf of Aden (A-32b) and western Arabian Sea (A-32a) are reported to be caused by haze, dust and some light fog. The occurrence of dust over the Gulf of Aden was considered a serious problem by observers aboard USS CHICAGO who reported:

> "The most significant meteorological phenomenon of the Gulf of Aden is the continual presence of fine dust in the air. Within a few hours of entering the Gulf of Aden, a layer of dust had coated the outside of the ship. The major problem with the dust was in the clogging of air filters and inlet ducts, a problem partially solved by taping cheese cloth over all topside inlets. This is not an optimum solution as the high winds continually tore the tape loose."

The probable cause of this persistent dust are the occurrences of numerous mesoscale dust storms that develop over land and move out to sea during the evening hours. These dust (sand) storms are similar to the "haboobs" which affect Khartoum (Ramage, 1971). In the case of the Gulf of Aden, strong convective activity is initiated in the coastal mountains during the afternoon along the convergence zones shown in Figure 3-27b (Atkinson, 1971). These zones are caused by the upslope sea breezes associated with the daytime heating (see Para. 3.5.1). Outflows from the convective systems pick up large amounts of dust (sand) as they move seaward and dissipate during the evening. At Aden (see locator map, Figure 1-1), these storms usually begin about sunset and at times blow hard until 2200 LT. The air becomes so thick with sand that visibility is sharply reduced. The only forewarning of these dust storms is a dense sand cloud appearing to the northward and northwestward of the port an hour or two before sunset. The wind then blows hard from the north, starts to decrease and finally becomes calm in about one to two hours. After a short interval, the wind blows hard from the south for another two hours before the storm ends (Port Directory, Volume VI, Indian Ocean). These dust/sand conditions appear to be almost daily events during the summer monsoon, not only at Aden but also to the east at Riyan (U.S. Naval Weather Service Command, 1974a).

The strong upwelling of cold water off the Somali coast during the summer monsoon is evident in Figures A-31f through A-31i. As expected, the coldest temperatures occur during July when the surface winds are strongest. Unlike a situation such as that off the coast of California, fog is not associated with the cold upwelling. Ramage (1971) attributes this lack of fog off the Somali coast to strong low-level divergence in the southwesterly flow which brings a strong subsidence inversion down to the surface, ensuring a supply of dry air adequate to prevent fog formation.

As is emphasized by several researchers (e.g., Cuming, 1973; Ramage, 1971; and Ramage et al., 1969), the features of the summer monsoon are not constant phenomena -- large variations in wind, cloudiness and precipitation patterns are observed from day to day. For example, two basic variations in the summer monsoon are described in Para. 3.2.2. These basic patterns, called strong and weak monsoon, are compared by the differences in flow (Figures 3-9 through 3-12) and by differences in cloud cover and rainfall (see satellite pictures in Figures 3-15 and 3-16). Fortunately there are some useful forecasting aids available to anticipate these changes. Findlater (1969) described changes in the strength of the low-level jet over Garissa, Kenya, and what appeared to be a one- to two-day lag in the rainfall (surface wind and cloudiness) along the west coast of India (see Para. 3.1.3).

Still another feature that appears related to the intensity of the summer monsoon is the development of the subtropical cyclone. A likely prerequisite for subtropical cyclogenesis -- with consequent increased wind, cloudiness and rain associated with strong monsoon conditions -- is the existence of a monsoon depression in the Bay of Bengal or northeastern India (see Para. 3.2.3). In a negative sense, there does not appear to be a relationship between the central pressure of the heat trough over Pakistan and the variations of winds, cloudiness and precipitation over the Arabian Sea (see Para. 3.2.2).

4.4 THE AUTUMN TRANSITION SEASON - OCTOBER THROUGH NOVEMBER

As the amount of insolation received over the Northern Hemisphere decreases as summer progresses into autumn, the heat trough over Pakistan and vicinity weakens and the near-equatorial trough again reappears over the Arabian Sea (Ramage, 1974). With the near-equatorial trough over the water, the occurrence of tropical cyclones reaches a secondary maxima for the year (see Para. 3.3.2). Typical tracks of tropical storms for October and November are shown in Figures A-35d and A-35e. The actual tracks of tropical cyclones that reached storm intensity are shown in Figures A-36h and A-36i. As discussed more fully in Appendix D, these tropical storms do occasionally affect the port of Karachi, Pakistan.

As indicated by the surface wind roses shown in Figure A-11, the October surface winds are again light and variable over most of the Arabian Sea as they were in April. In the Gulf of Aden the winds have again become easterly. However, it would be expected that intensifications of the near-equatorial trough (see Adler, et al., 1970) -- with or without tropical cyclogenesis -- will lead to periods of increased northeasterly winds over most of the Arabian Sea north of the trough, as is the case in the South China Sea. On the other hand, cold frontal passages during October should be extremely rare (as noted by Perrone, publication pending), so increases in the northeasterlies over the northern Arabian Sea from this source are not to be expected.

By November (A-12), the surface northeasterlies over the Arabian Sea are well established although speeds are generally still moderate (less than 22 kt). In the Gulf of Aden the prevailing easterlies have also increased and will remain the dominant wind flow until the end of the spring transition season. As is the case during the winter monsoon, the winds in the two northernmost areas -- *N Gulf of Oman* and *Sonmiani* -- are light and variable due to their proximity to the lee trough (see Figure 4-1) described in Para. 4.1. Increases in the intensity of the monsoon flow during November are related not only to tropical storm development and near-equatorial trough intensification, but also to passages of cold fronts into the northern Arabian Sea (described by observer aboard USS HANCOCK, Para. 4.1). These cold surges, however, are likely to be only short-lived (one to two days) in comparison to the winter monsoon surges (see Para. 3.4.2).

Cloud cover during autumn, as in spring, has reached a minimum (A-30d). Although water temperatures are very high (A-31j, A-31k), little if any cool air is advected out over the sea to cause the increased cumulus and stratocumulus common during the winter. With the generally clear skies, diurnal effects should predominate along all coasts (see Para. 3.5.1).

Visibilities during autumn are generally very good (A-32). The only exceptions would be the effects of tropical storms and dust storms related to cold frontal passages off the Arabian Peninsula. Due to the generally light winds during this season, sea heights (A-33, A-34) are again minimal.

REFERENCES

Adler, R. F., L. R. Brody, and W. L. Somervell, Jr., 1970: A preliminary survey of SEASIA fall transformation season weather. NAVWEARSCHFAC Tech. Paper No. 10-70.

Atkinson, G. D., 1971: Forecaster's guide to tropical meteorology. Air Weather Service Tech. Report 240.

Bhaskara Rao, N. S. and P. E. Moray, 1971: Cloud systems associated with western disturbances: A preliminary study. Indian J. Met. Geophys., 22, 3, 413-420.

Bittner, F. E., 1971: Forecasting horizontal weather depiction fields by satellite and numerical products. FAMOS TM 3-71.

Brand, S., J. W. Blelloch and D. C. Schertz, 1973: State of the sea around tropical cyclones in the western North Pacific Ocean. ENVPREDRSCHFAC Tech. Paper No. 5-73.

Brody, L. R., and R. A. Godfrey, 1971: Surface wind characteristics over RVN coastal waters during December through March. NAVWEARSCHFAC Tech. Paper No. 1-71.

Caplinger, R. L., 1971: Weather regimes of the Arabian Sea area: A handbook for the carrier meteorologist. Thesis, U.S. Naval Postgraduate School, Monterey, CA.

Cuming, M. J., 1973: Handbook for forecasters in the Bay of Bengal. ENVPREDRSCHFAC Tech. Paper No. 7-73.

Desai, B. N., 1967: The summer atmospheric circulation over the Arabian Sea. J. Atmos. Sci., 24, 216-220.

Findlater, J., 1966: Cross-equatorial jet streams at low level over Kenya. Met. Mag., 95, 353-364.

Findlater, J., 1967: Some further evidence of cross-equatorial jet streams at low level over Kenya. Met. Mag., 96, 216-219.

Findlater, J., 1969: A major low-level air current near the Indian Ocean during the northern summer. Quart. J. R. Met. Soc., 95, 362-380.

Findlater, J., 1971a: Mean monthly airflow at low levels over the western Indian Ocean. Geophys. Mem., London., 16, 115, 53 pp.

Findlater, J., 1971b: The strange winds of Ras Asir (formerly Cape Guardafui). Met. Mag., 100, 46-54.

Findlater, J., 1974: The low-level cross-equatorial air current of the western Indian Ocean during the northern summer. Weather, 29, 11, 411-416.

Flohn, H., 1965: Studies on the meteorology of tropical Africa. Met. Inst., Univ. of Bonn, Bonner Met. Abhandl, Heft 5, 1965, 58 pp.

Gurunadham, G., 1971: Clouds over Arabian Sea during winter. Indian J. Met. Geophys., 22, 3, 429-432.

Huschke, E. H., 1959: Glossary of meteorology. Boston: American Meteorological Society, 638 pp.

Indian Meteorological Department, 1964: Tracks of storms and depressions in the Bay of Bengal and the Arabian Sea 1877-1960. New Delhi, 167 pp.

Jambunathan, R. and K. Ramamurthy, 1974: Wind field in the lower and middle troposphere over the Arabian Sea during the southwest monsoon 1973. Indian J. Met. Geophys., 25, 3 and 4, 403-410.

Kindle, E. C., L. R. Brody, J. R. Bocchieri, S. Brand and R. F. Adler, 1969: The diagnosis and prediction of SEASIA northeast monsoon weather. Navy Weather Research Facility, NWRF 12-0669-144.

Ramage, C. S., 1969: Indian Ocean surface meteorology. Oceanogr. Mar. Biol. Ann. Rev., 7, 11-30.

Ramage, C. S., 1971: Monsoon meteorology. New York: Academic Press, 296 pp.

Ramage, C. S., 1974: Monsoonal influences on the annual variations of tropical cyclone development. ENVPREDRSCHFAC Tech. Paper No. 12-74.

Ramage, C. S., L. R. Brody, R. F. Adler, and S. Brand, 1969: A diagnosis of the summer monsoon of southeast Asia. NAVWEARSCHFAC Tech. Paper No. 10-69.

Ramage, C. S. and C. V. R. Raman, 1972: Meteorological atlas of the international Indian Ocean expedition, Vol. 2, upper air. Washington, D.C.: National Science Foundation.

Ramamurthy, K. M., 1972: On the activity of the Arabian Sea monsoon. Indian J. Met. Geophys., 23, 1, 1-14.

Reiter, E. R., 1969: Atmospheric transport processes, Part 1: Energy transfers and transformations. AEC Critical Review Series, USAEC Report TID-24868.

Reiter, E. R., 1975: Handbook for forecasters in the Mediterranean; weather phenomena of the Mediterranean basin; Part 1: General description of the meteorological processes. ENVPREDRSCHFAC Tech. Paper No. 5-75.

Rosenthal, J., 1976: Refractive effects guidebook (REG). Monterey, CA: Naval Environmental Prediction Research Facility.

Sadler, J. C., 1975: The upper tropospheric circulation over the global tropics. Dept. of Meteorology, Univ. of Hawaii, UHMET-75-05.

Sadler, J. C. and R. E. Gidley, 1973: Tropical cyclones of the North Indian Ocean. ENVPREDRSCHFAC Tech. Paper No. 2-73.

Saha, K., 1974: Some aspects of the Arabian Sea summer monsoon. Preprints, Part I, Int. Trop. Met. Meeting, 31 Jan-7 Feb 1974, Nairobi, Kenya.

Snead, R. E., 1968: Weather patterns in southern West Pakistan. Worcester, MA: Clark Univ., AD685-975.

U.S. Naval Weather Service Command, 1971: Summary of synoptic meteorological observations, southwest Asian coastal marine areas, Vols. 3, 4, 5.

U.S. Naval Weather Service Command, 1974a: Climatic summaries for major Indian Ocean ports and waters. NAVAIR 50-1C-63.

U.S. Naval Weather Service Command, 1974b: Summary of synoptic meteorological observations, East African and selected island coastal marine areas. Vols. 1, 3, 4, 6.

U.S. Naval Weather Service Command, 1975: U.S. Naval Weather Service numerical environmental products manual. NAVAIR 50-1G-522.

APPENDIX A

CLIMATOLOGICAL CHARTS FOR THE ARABIAN SEA AND GULF OF ADEN

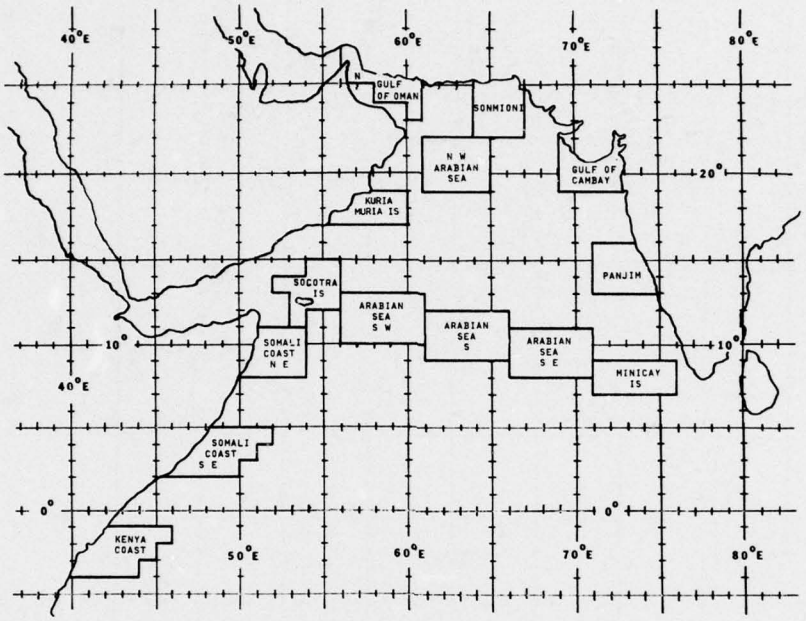

(a.)

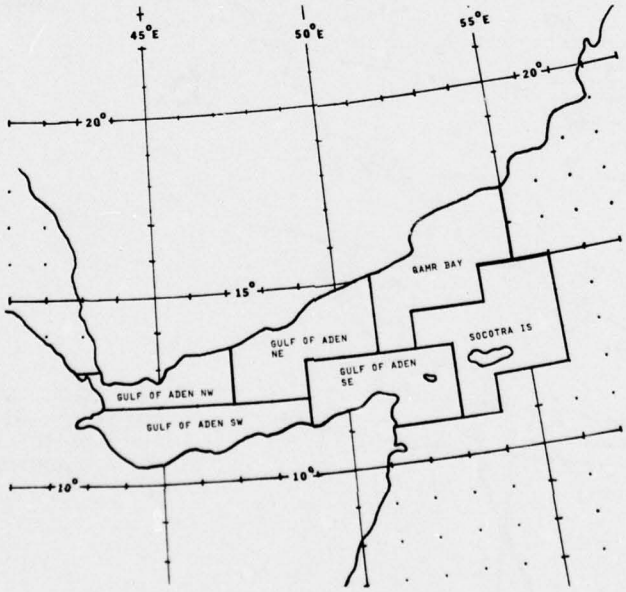

(b.)

Figure A-1. Climatic areas used for surface wind roses, sea heights and visibilities: (a) Arabian Sea and (b) Gulf of Aden.

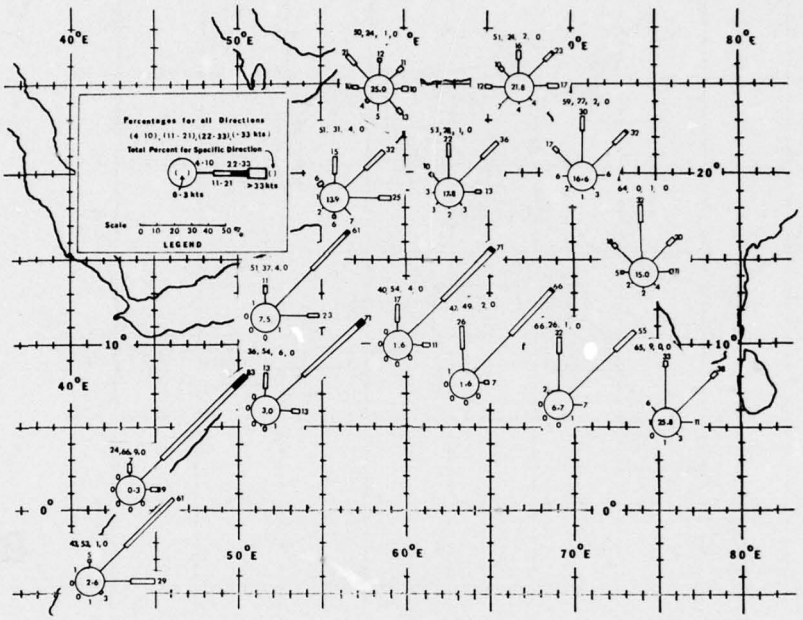

(a.)

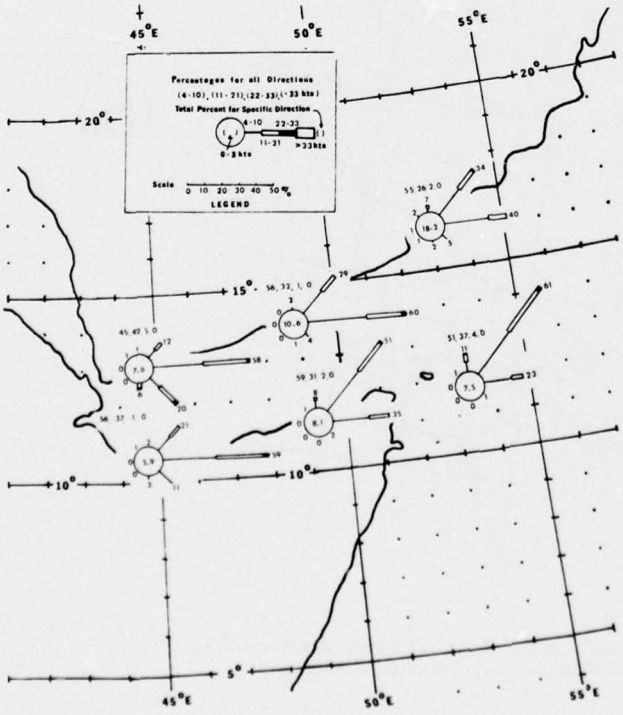

(b.)

Figure A-2. Surface wind roses for (a) the Arabian Sea and (b) the Gulf of Aden, January.

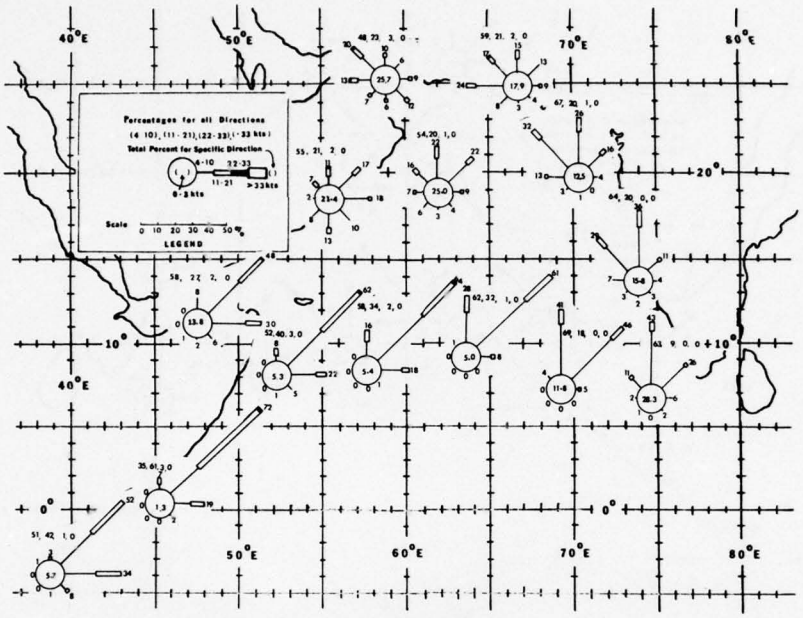

(a.)

(b.)

Figure A-3. Surface wind roses for (a) the Arabian Sea and (b) the Gulf of Aden, February.

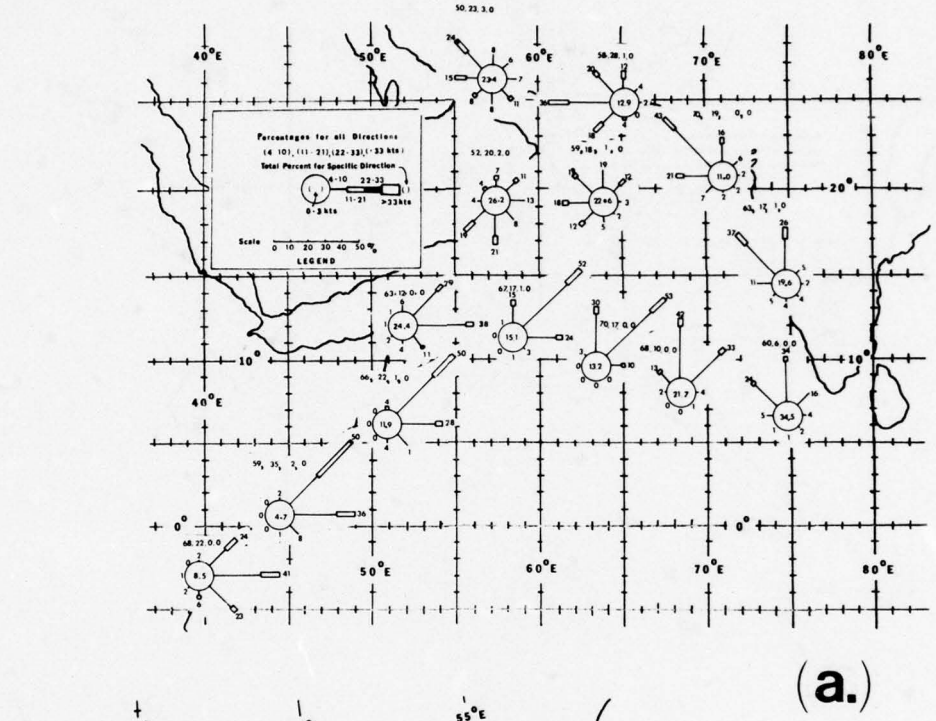

(a.)

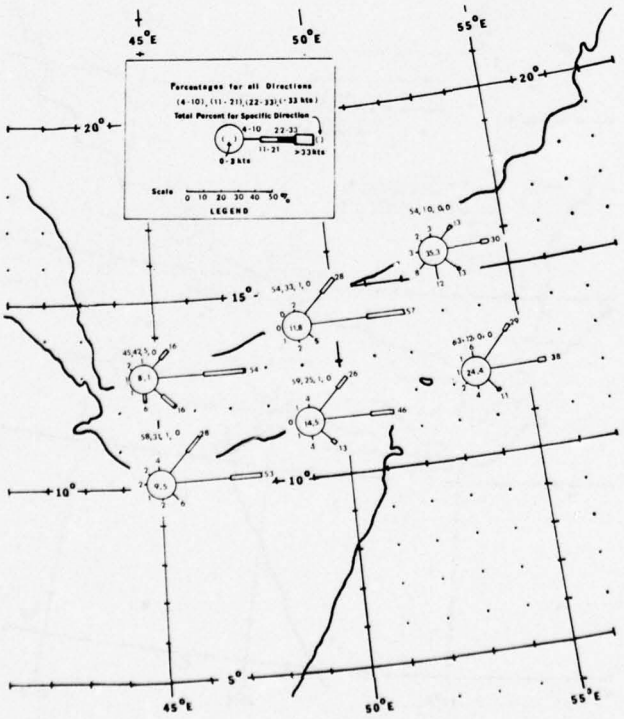

(b.)

Figure A-4. Surface wind roses for (a) the Arabian Sea and (b) the Gulf of Aden, March.

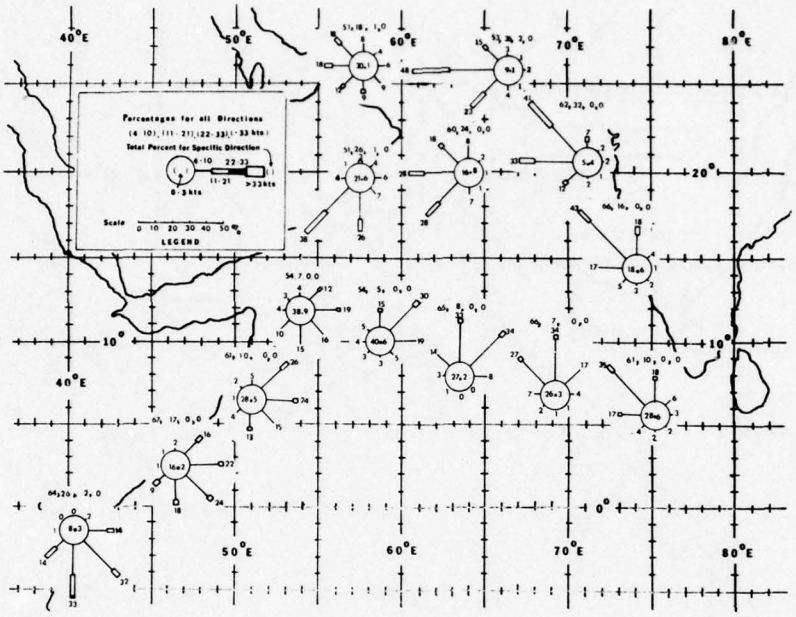

(a.)

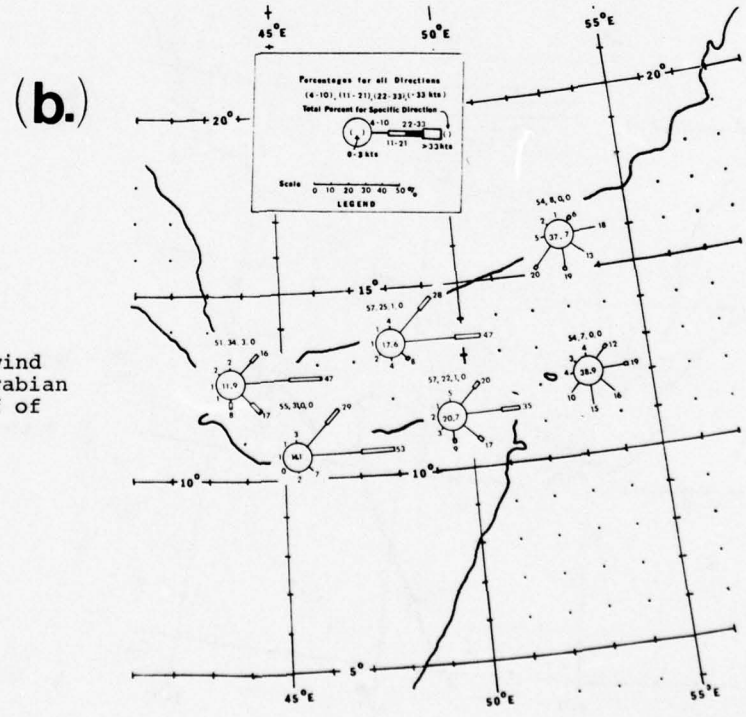

(b.)

Figure A-5. Surface wind roses for (a) the Arabian Sea and (b) the Gulf of Aden, April.

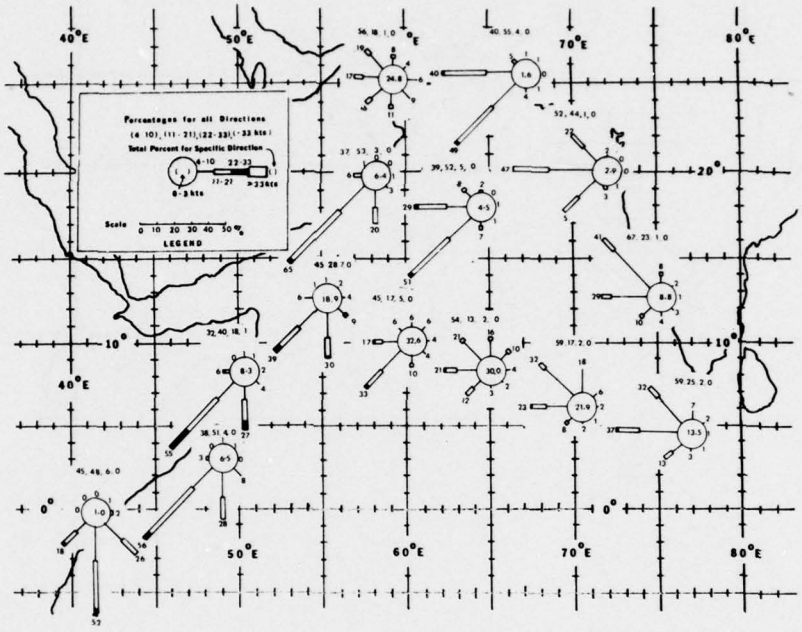

(a.)

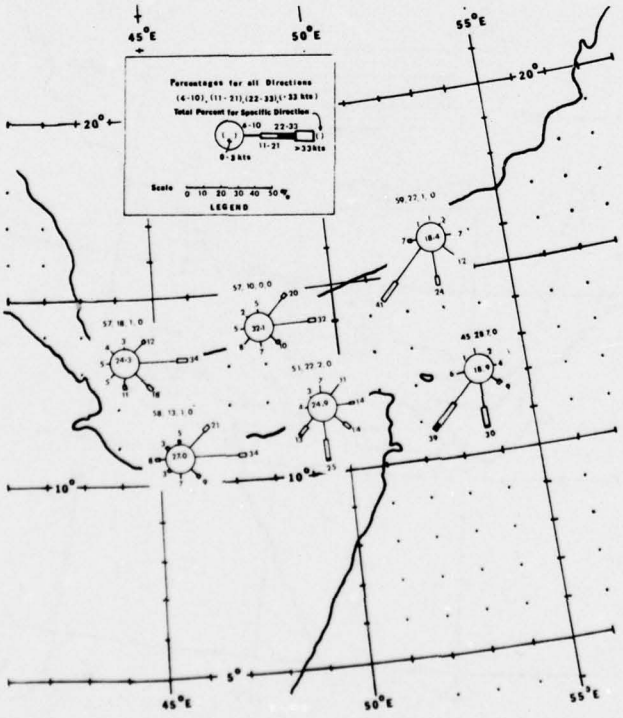

(b.)

Figure A-6. Surface wind roses for (a) the Arabian Sea and (b) the Gulf of Aden, May.

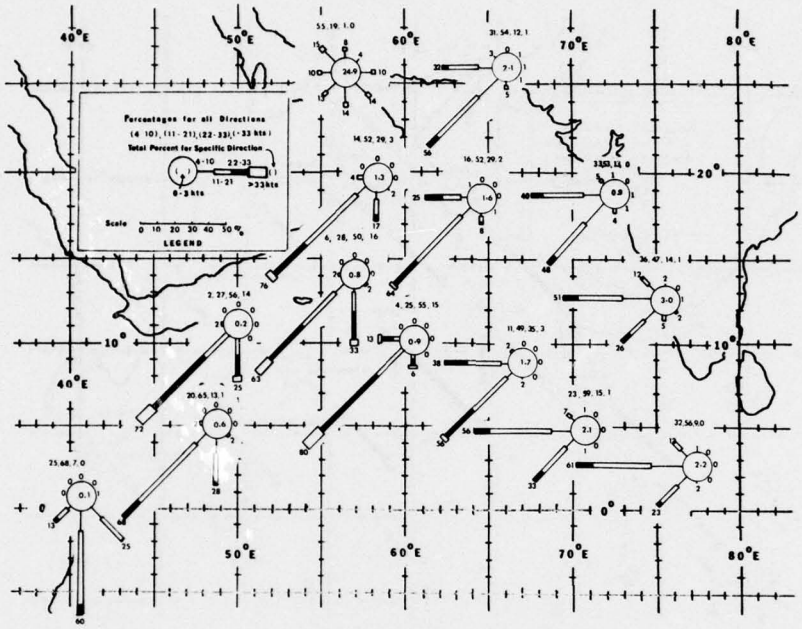

(a.)

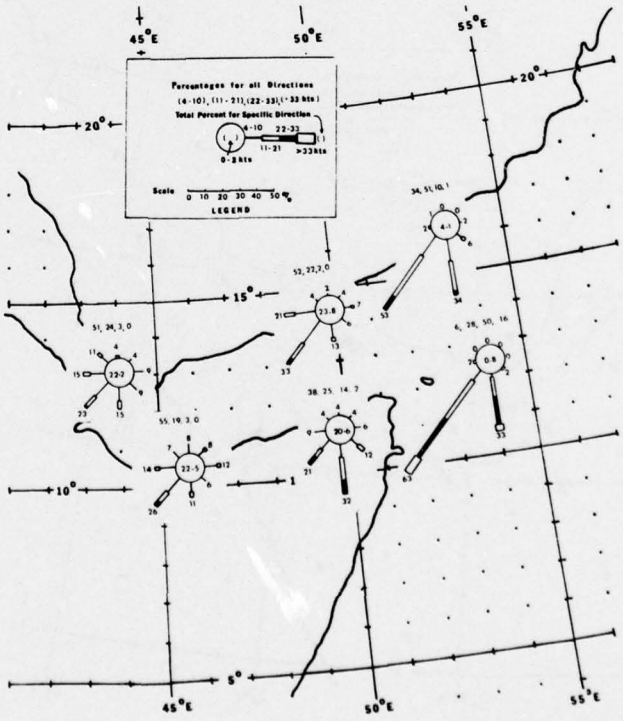

(b.)

Figure A-7. Surface wind roses for (a) the Arabian Sea and (b) the Gulf of Aden, June.

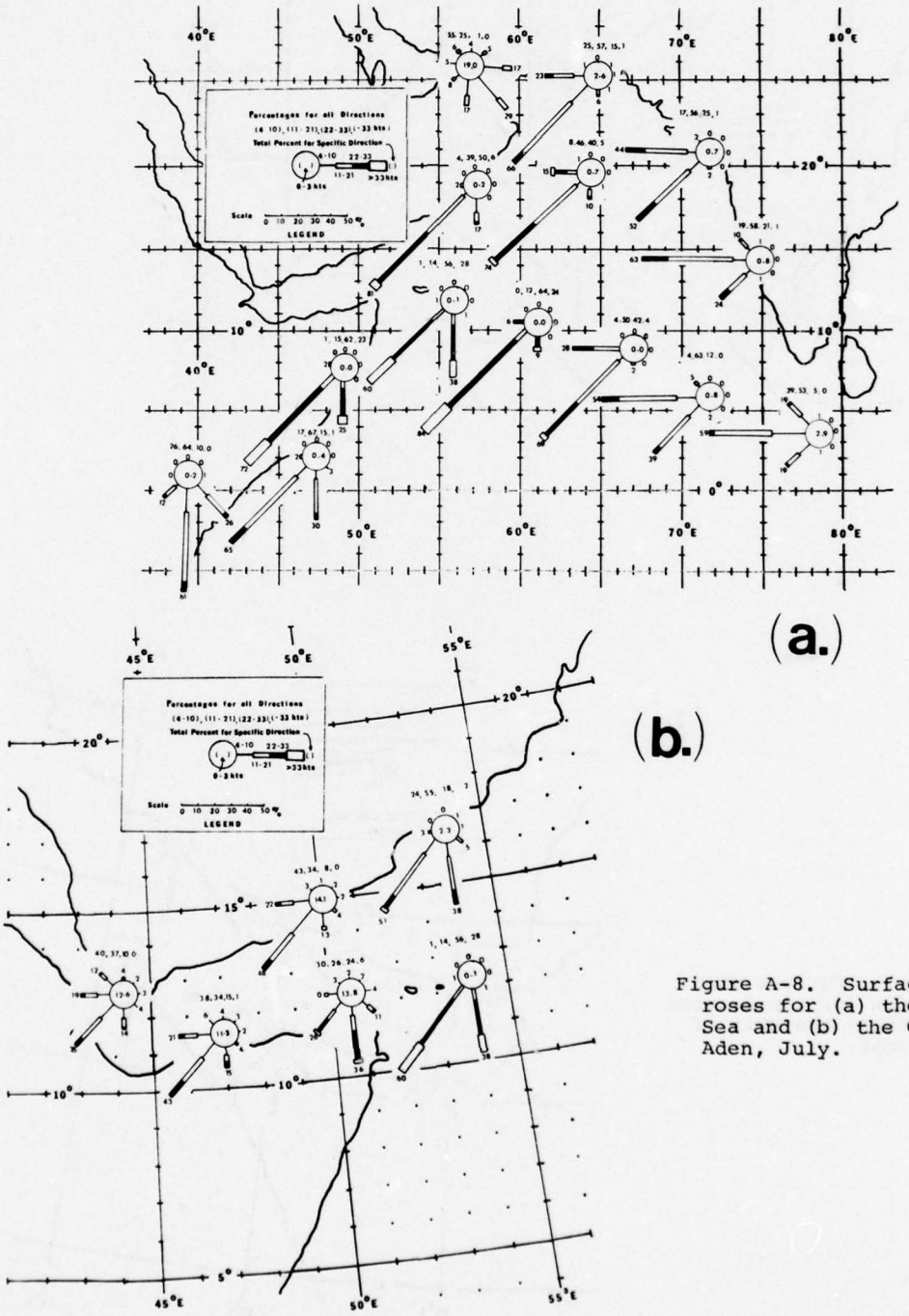

Figure A-8. Surface wind roses for (a) the Arabian Sea and (b) the Gulf of Aden, July.

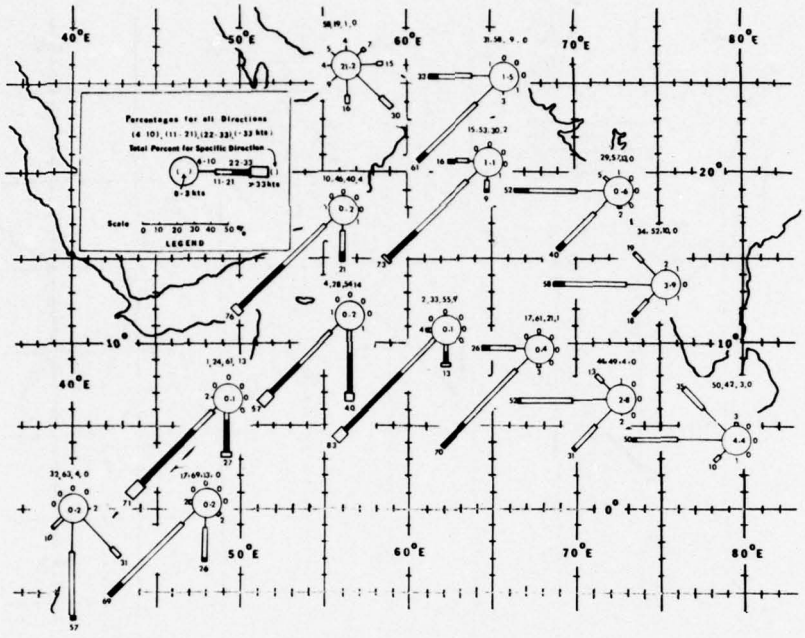

(a.)

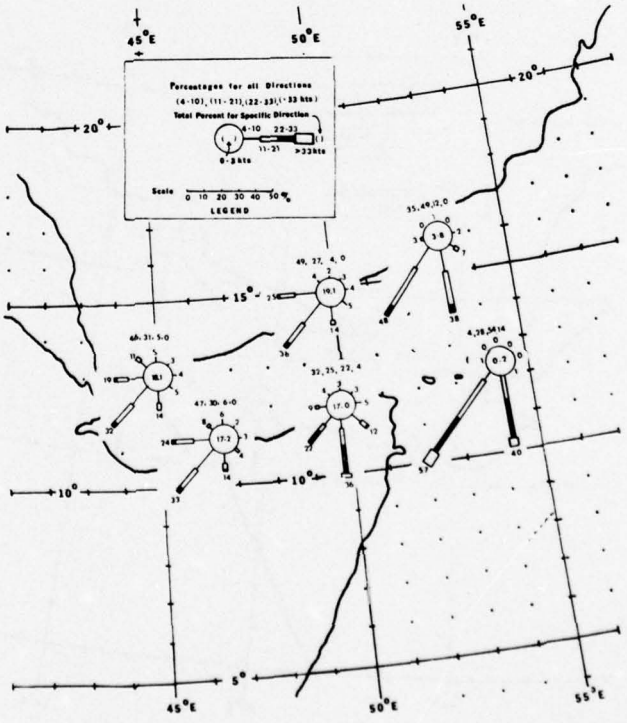

(b.)

Figure A-9. Surface wind roses for (a) the Arabian Sea and (b) the Gulf of Aden, August.

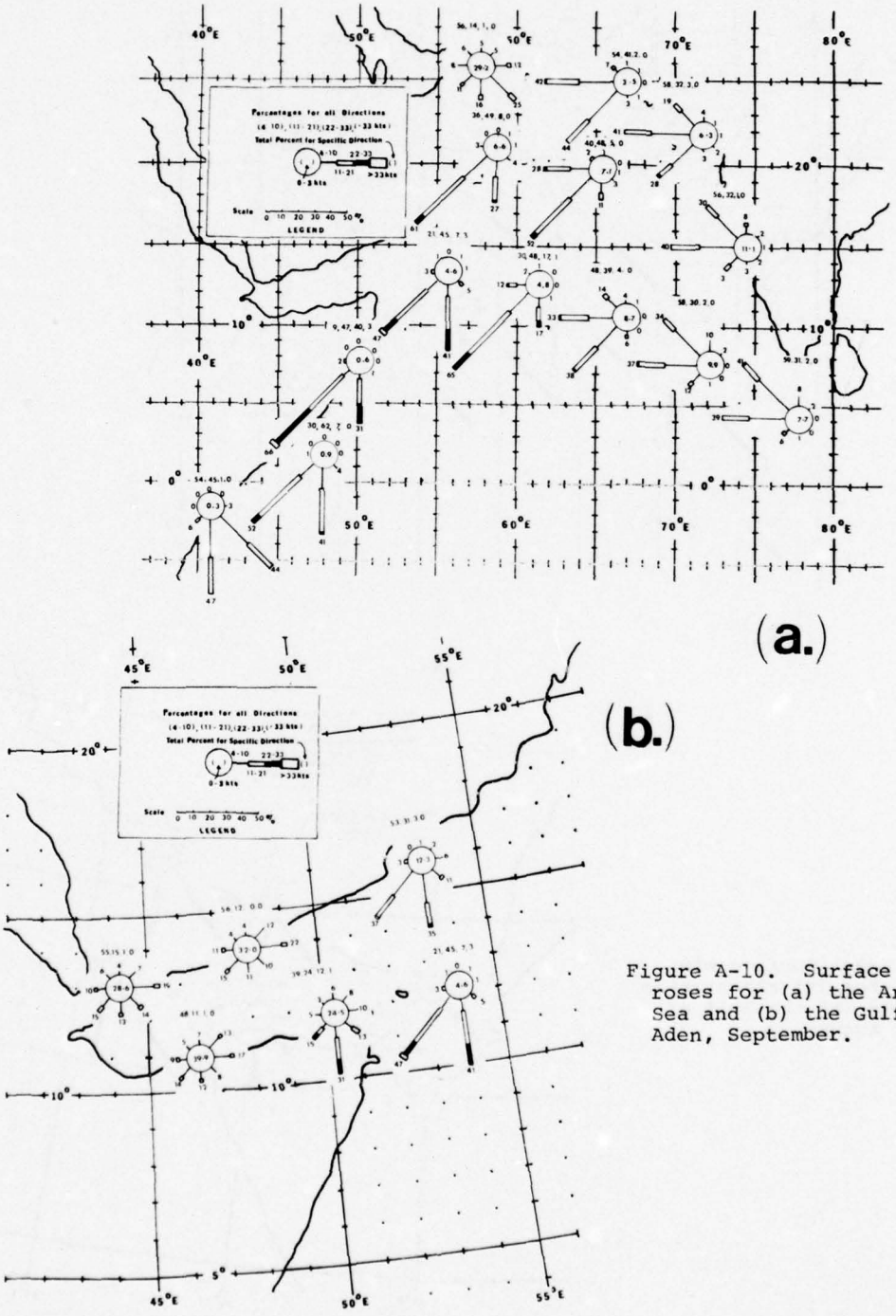

Figure A-10. Surface wind roses for (a) the Arabian Sea and (b) the Gulf of Aden, September.

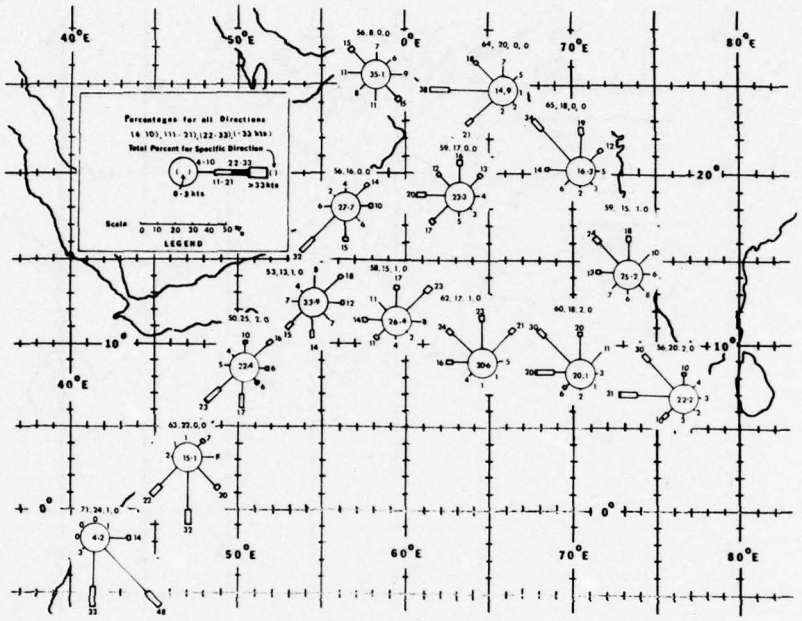

(a.)

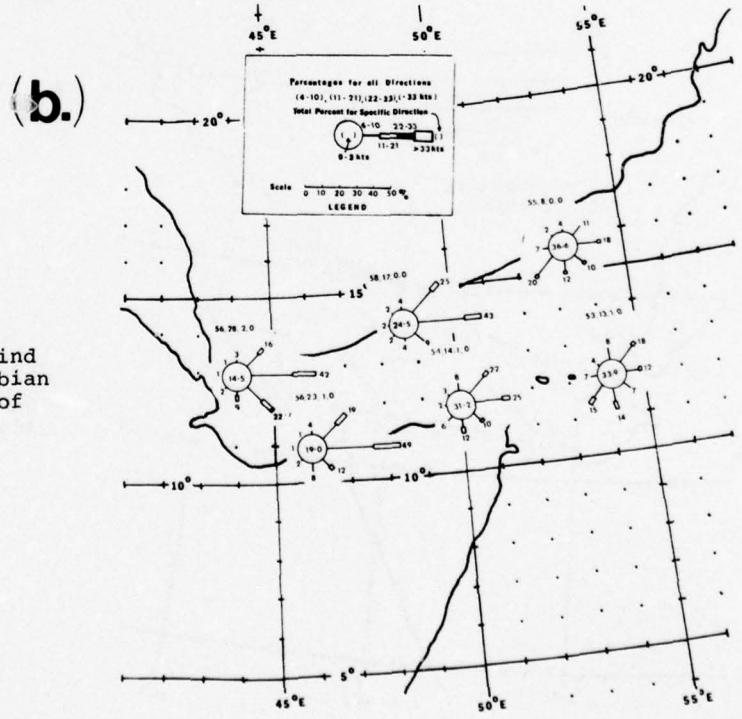

(b.)

Figure A-11. Surface wind roses for (a) the Arabian Sea and (b) the Gulf of Aden, October.

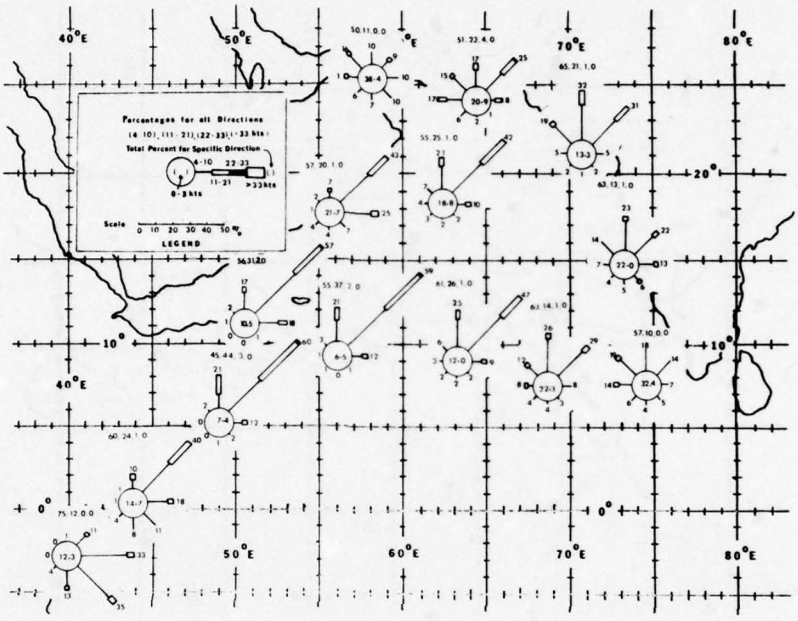

(a.)

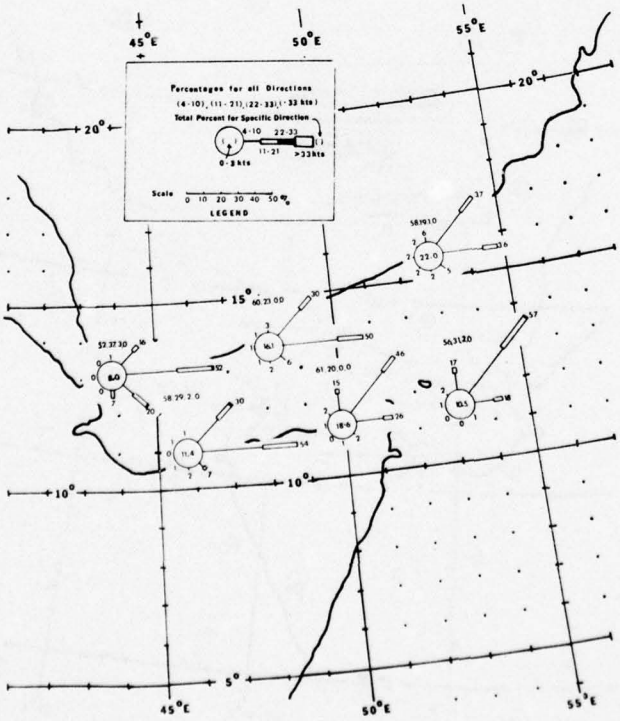

(b.)

Figure A-12. Surface wind roses for (a) the Arabian Sea and (b) the Gulf of Aden, November.

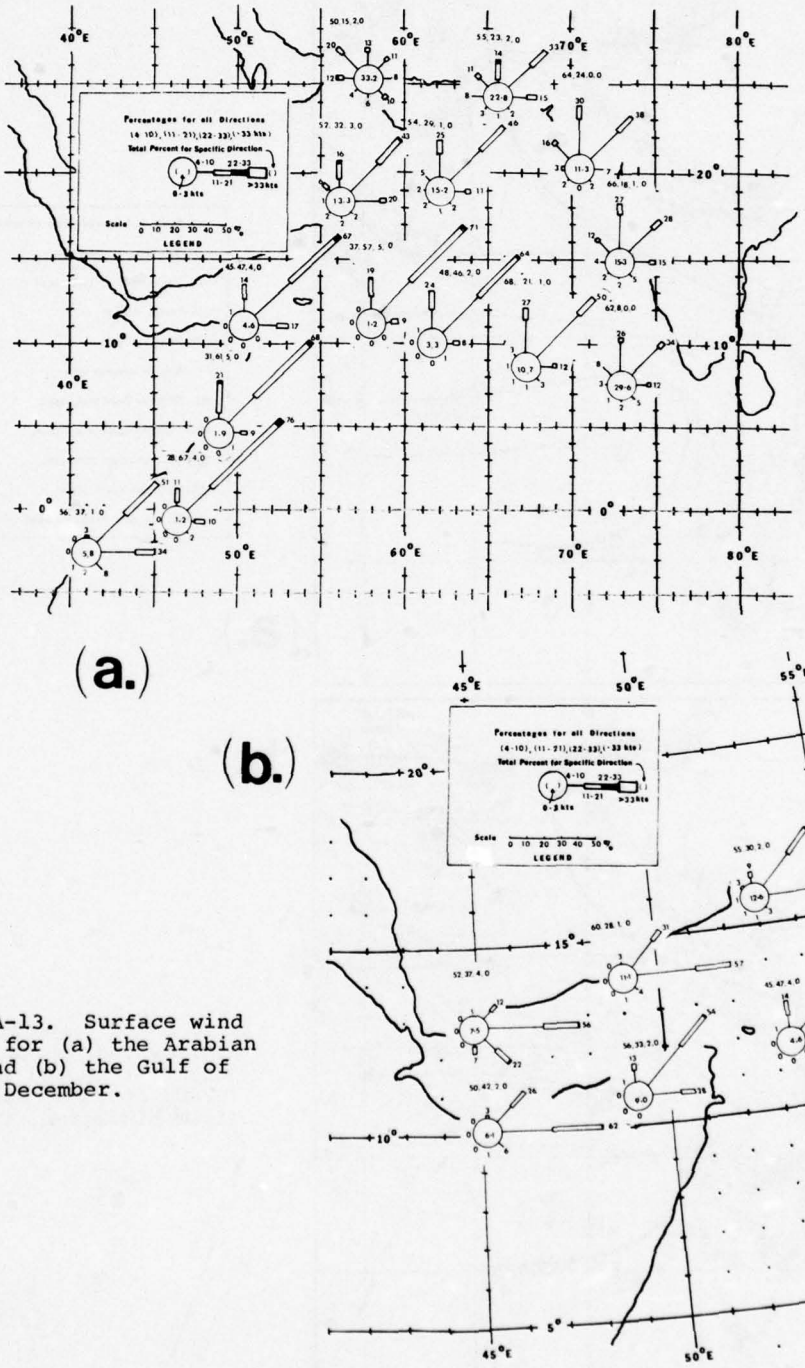

Figure A-13. Surface wind roses for (a) the Arabian Sea and (b) the Gulf of Aden, December.

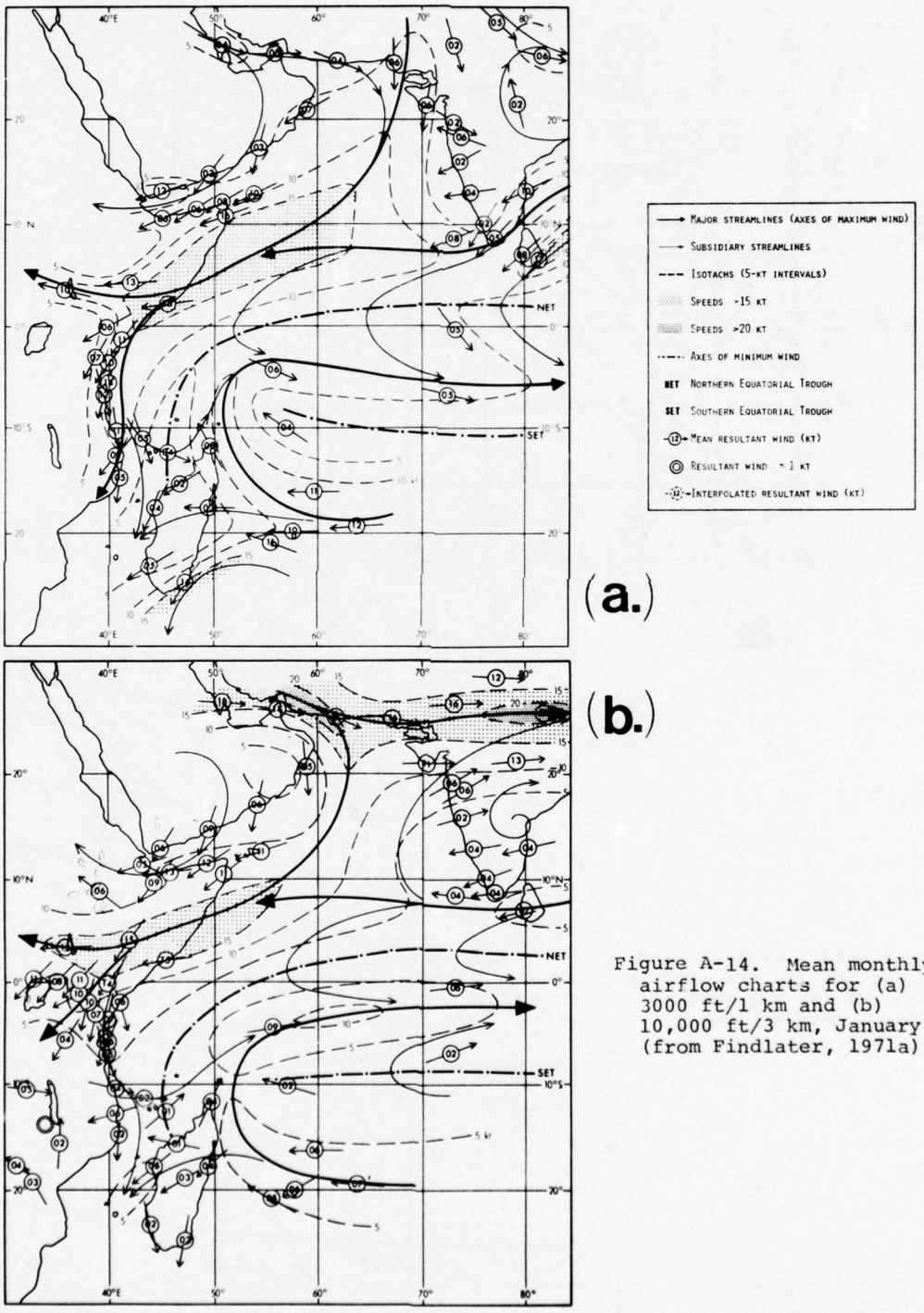

Figure A-14. Mean monthly airflow charts for (a) 3000 ft/1 km and (b) 10,000 ft/3 km, January (from Findlater, 1971a).

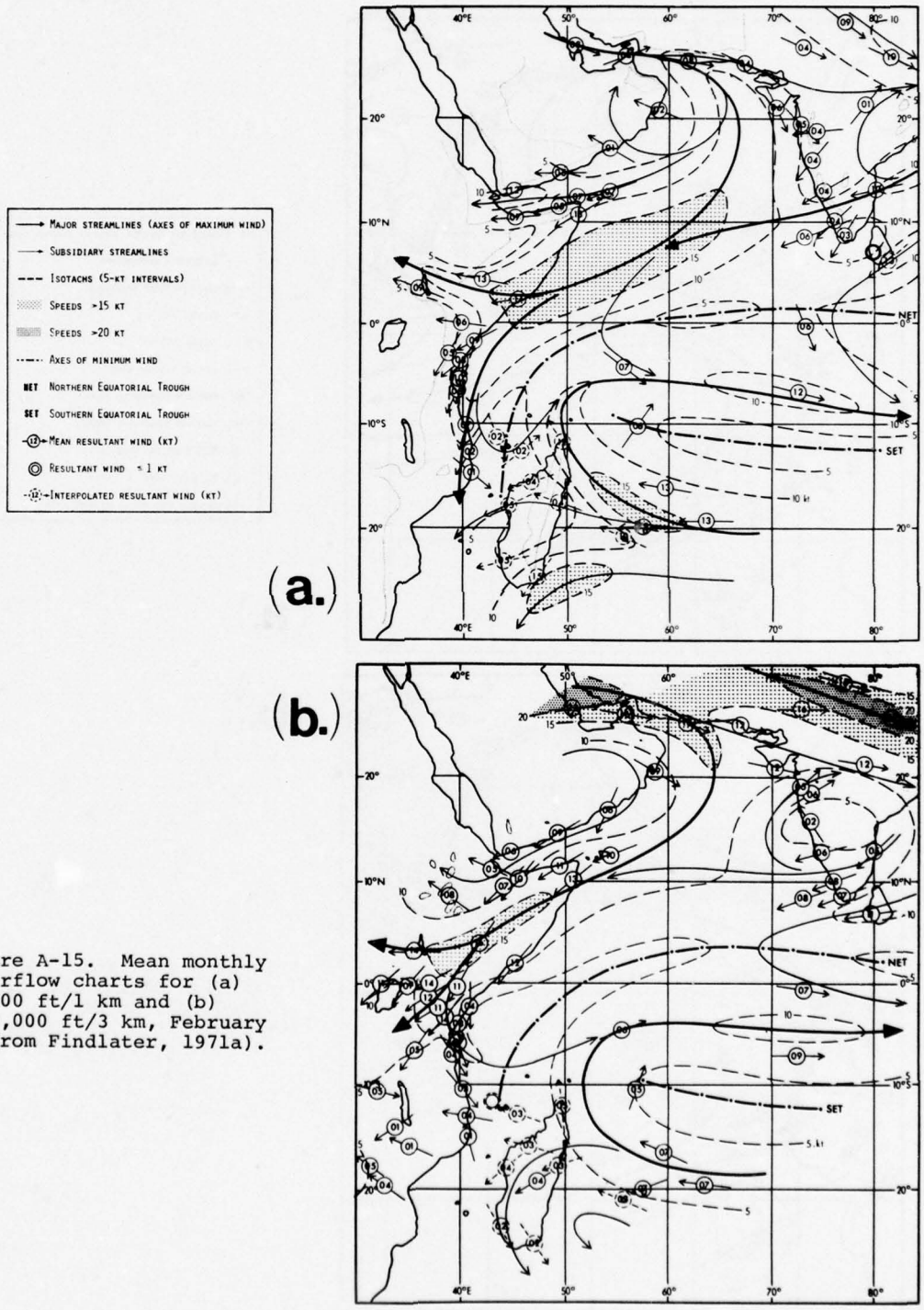

Figure A-15. Mean monthly airflow charts for (a) 3000 ft/1 km and (b) 10,000 ft/3 km, February (from Findlater, 1971a).

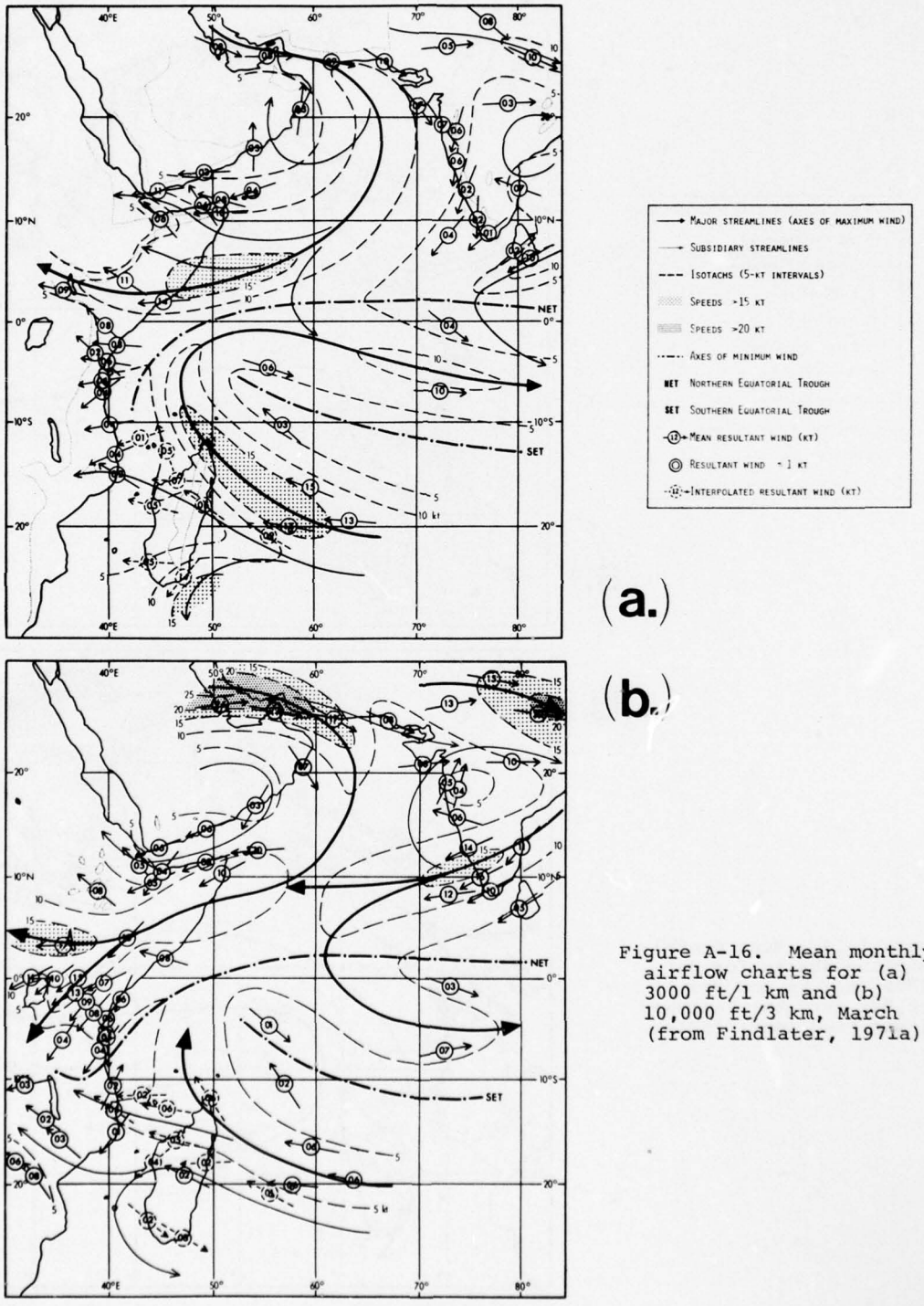

Figure A-16. Mean monthly airflow charts for (a) 3000 ft/1 km and (b) 10,000 ft/3 km, March (from Findlater, 1971a).

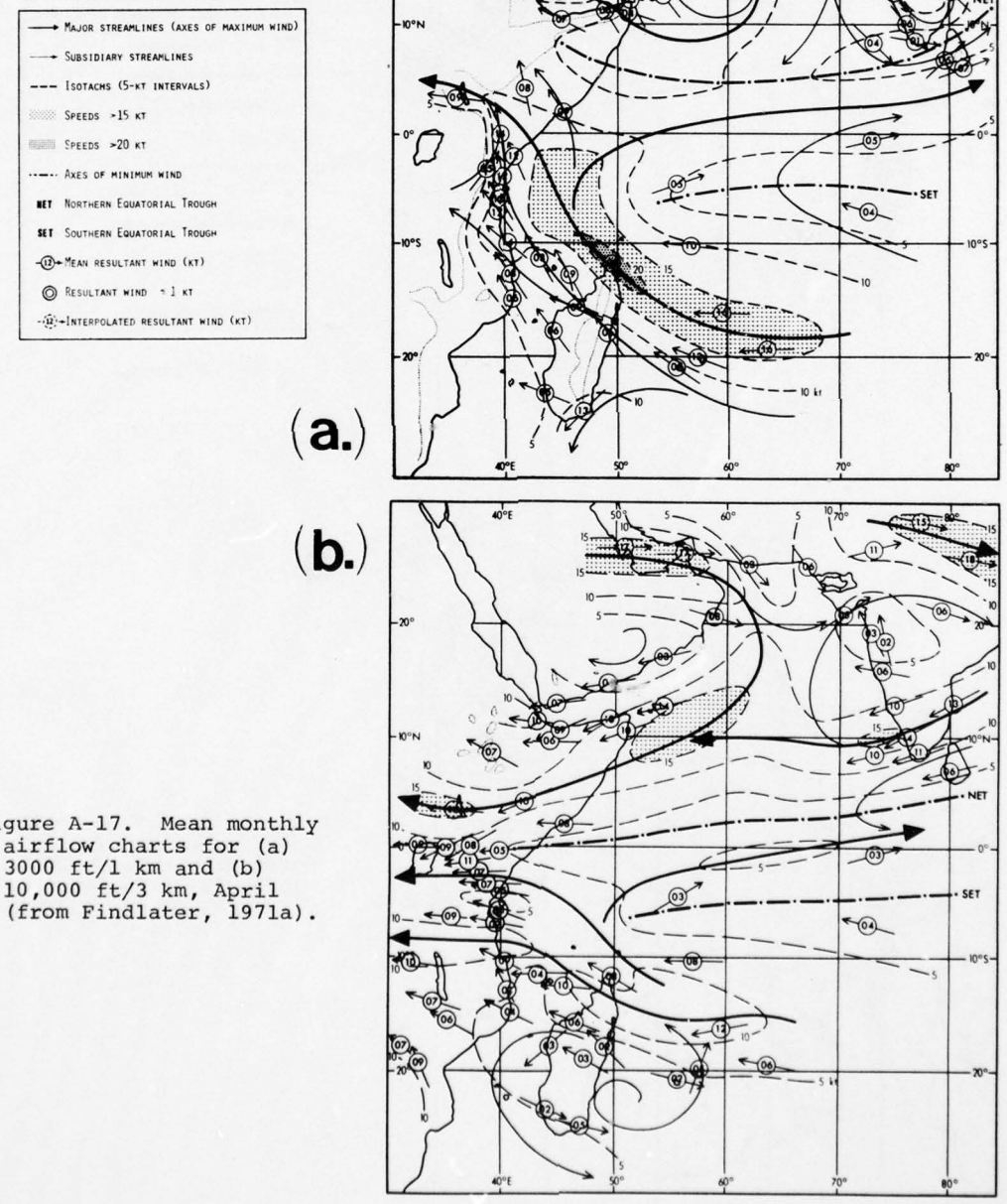

Figure A-17. Mean monthly airflow charts for (a) 3000 ft/1 km and (b) 10,000 ft/3 km, April (from Findlater, 1971a).

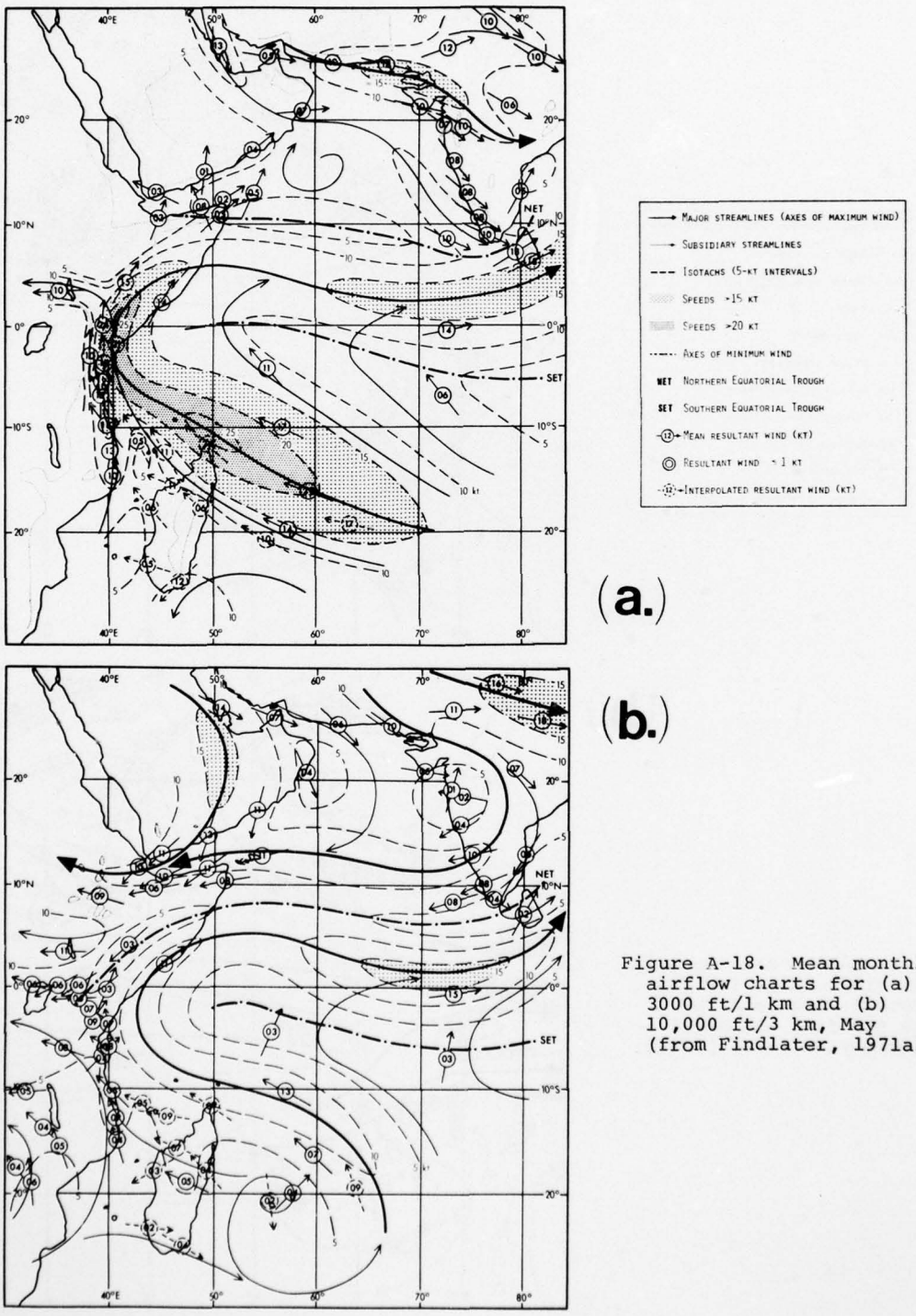

Figure A-18. Mean monthly airflow charts for (a) 3000 ft/1 km and (b) 10,000 ft/3 km, May (from Findlater, 1971a).

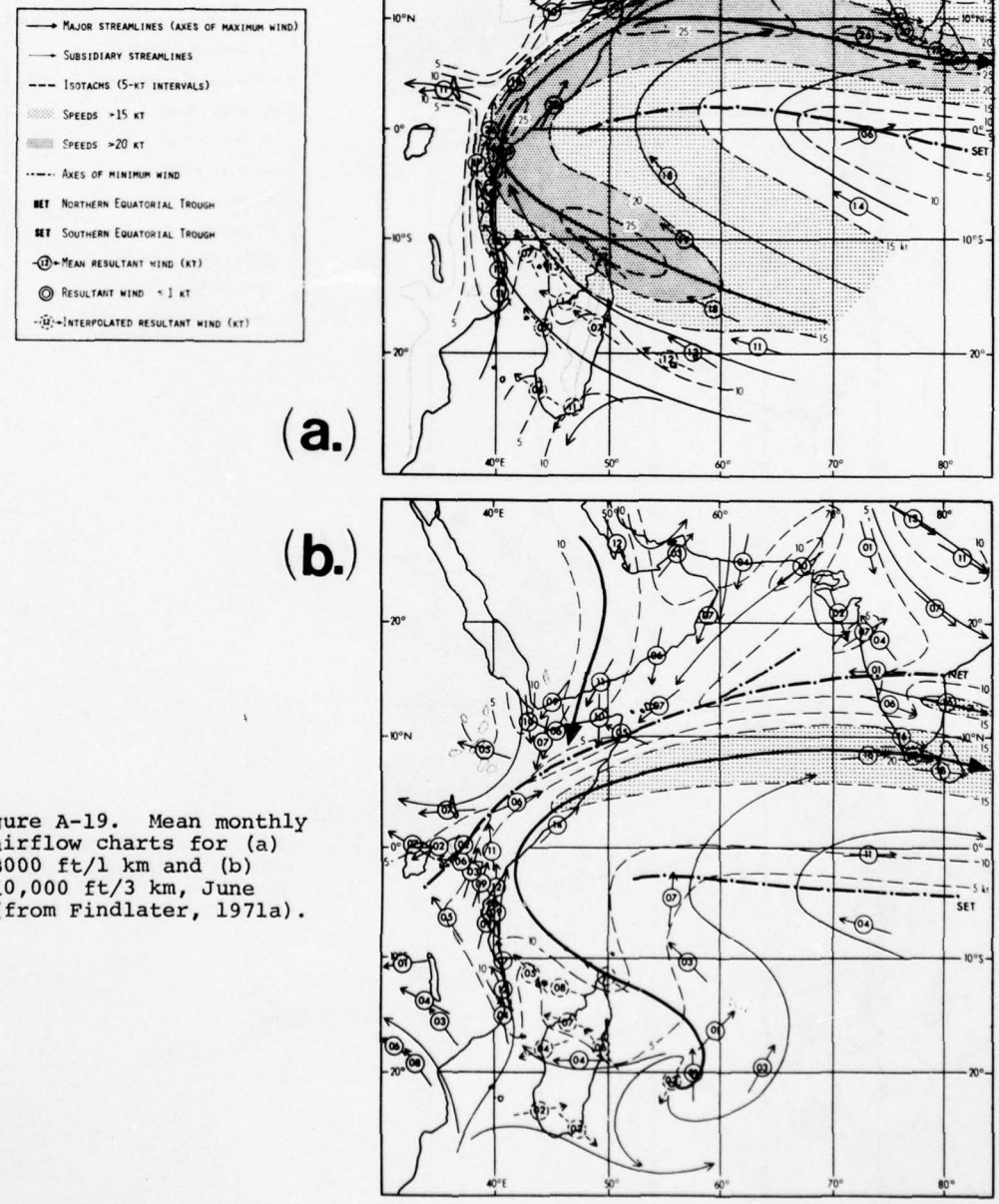

Figure A-19. Mean monthly airflow charts for (a) 3000 ft/1 km and (b) 10,000 ft/3 km, June (from Findlater, 1971a).

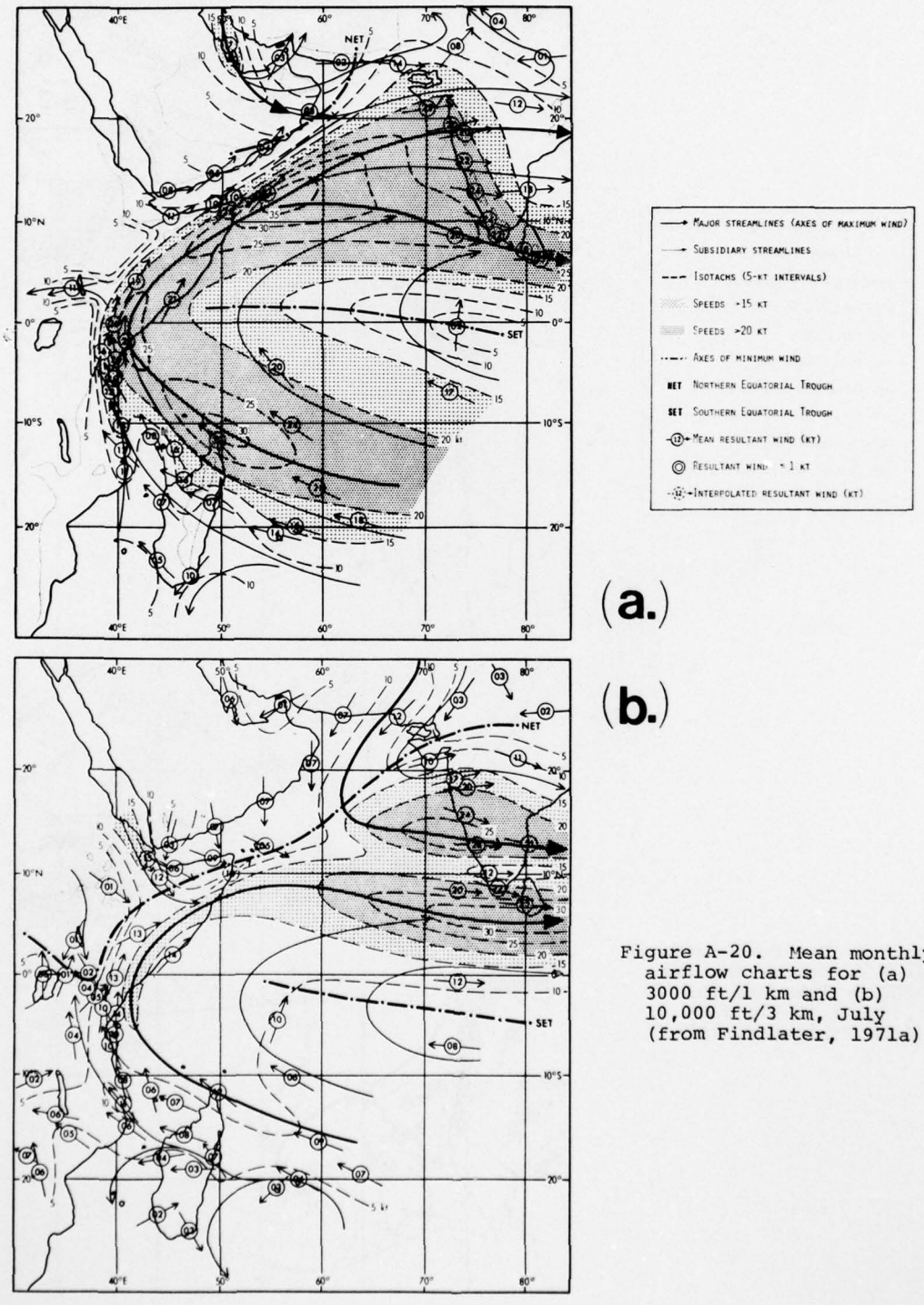

Figure A-20. Mean monthly airflow charts for (a) 3000 ft/1 km and (b) 10,000 ft/3 km, July (from Findlater, 1971a).

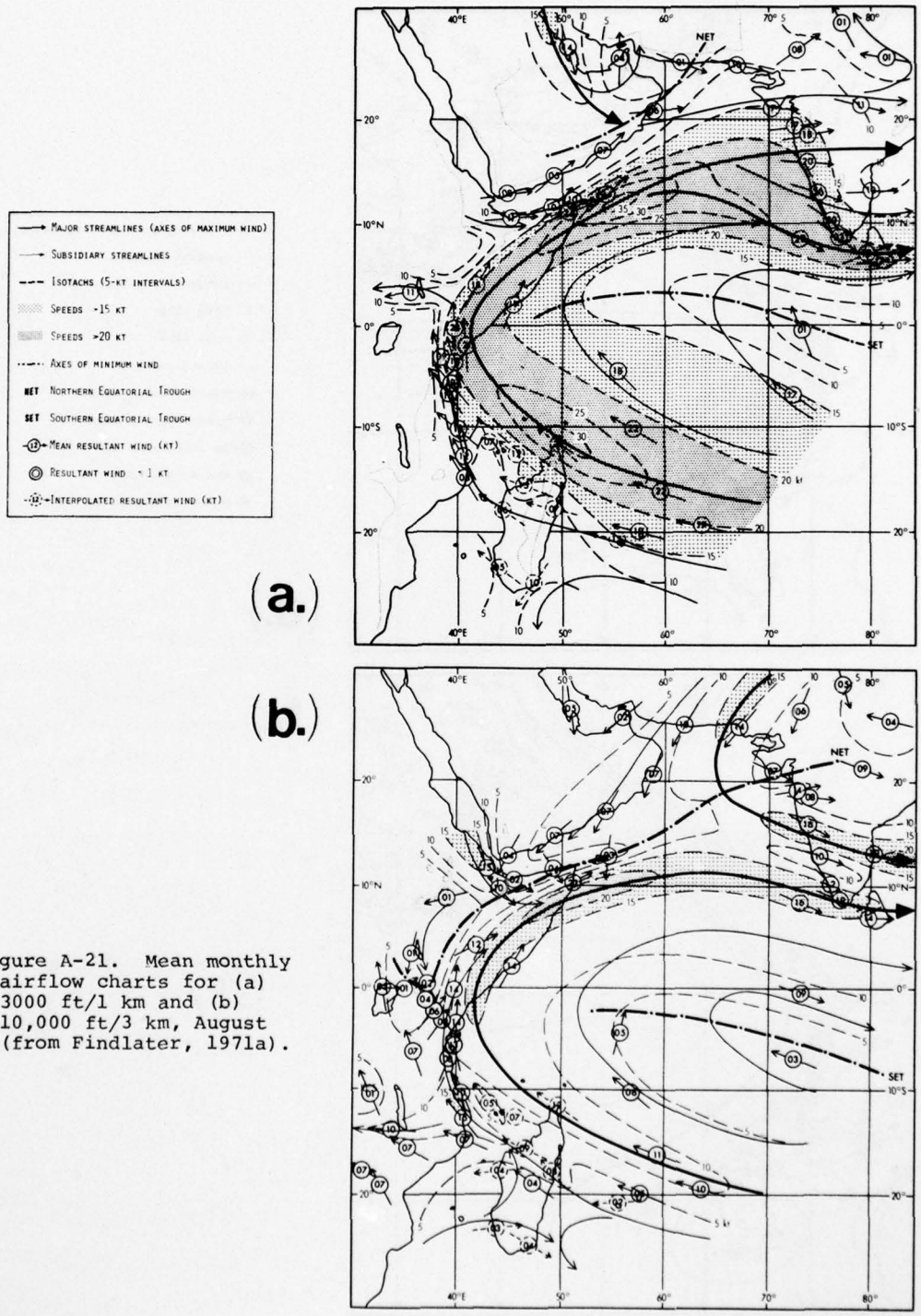

Figure A-21. Mean monthly airflow charts for (a) 3000 ft/1 km and (b) 10,000 ft/3 km, August (from Findlater, 1971a).

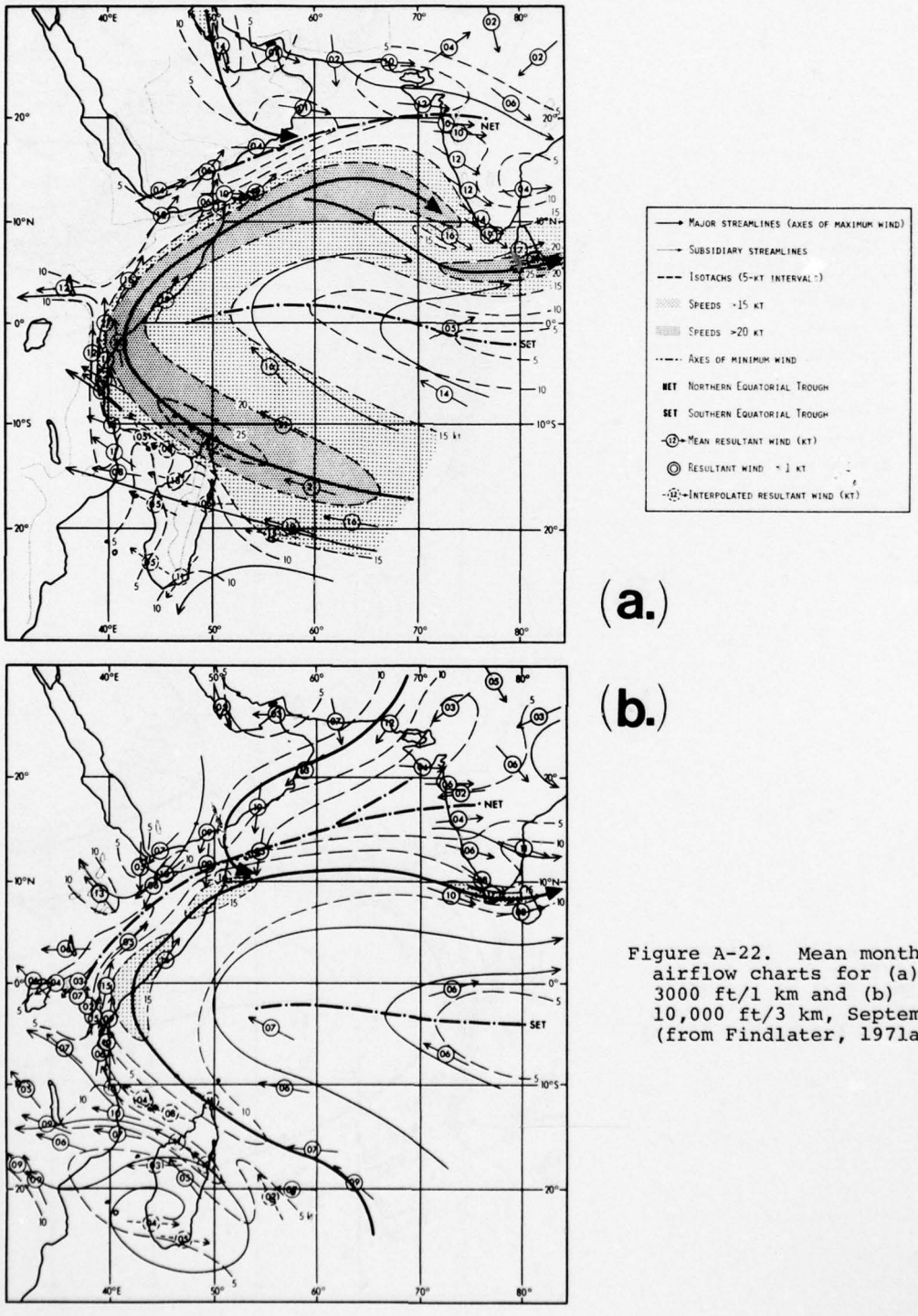

Figure A-22. Mean monthly airflow charts for (a) 3000 ft/1 km and (b) 10,000 ft/3 km, September (from Findlater, 1971a).

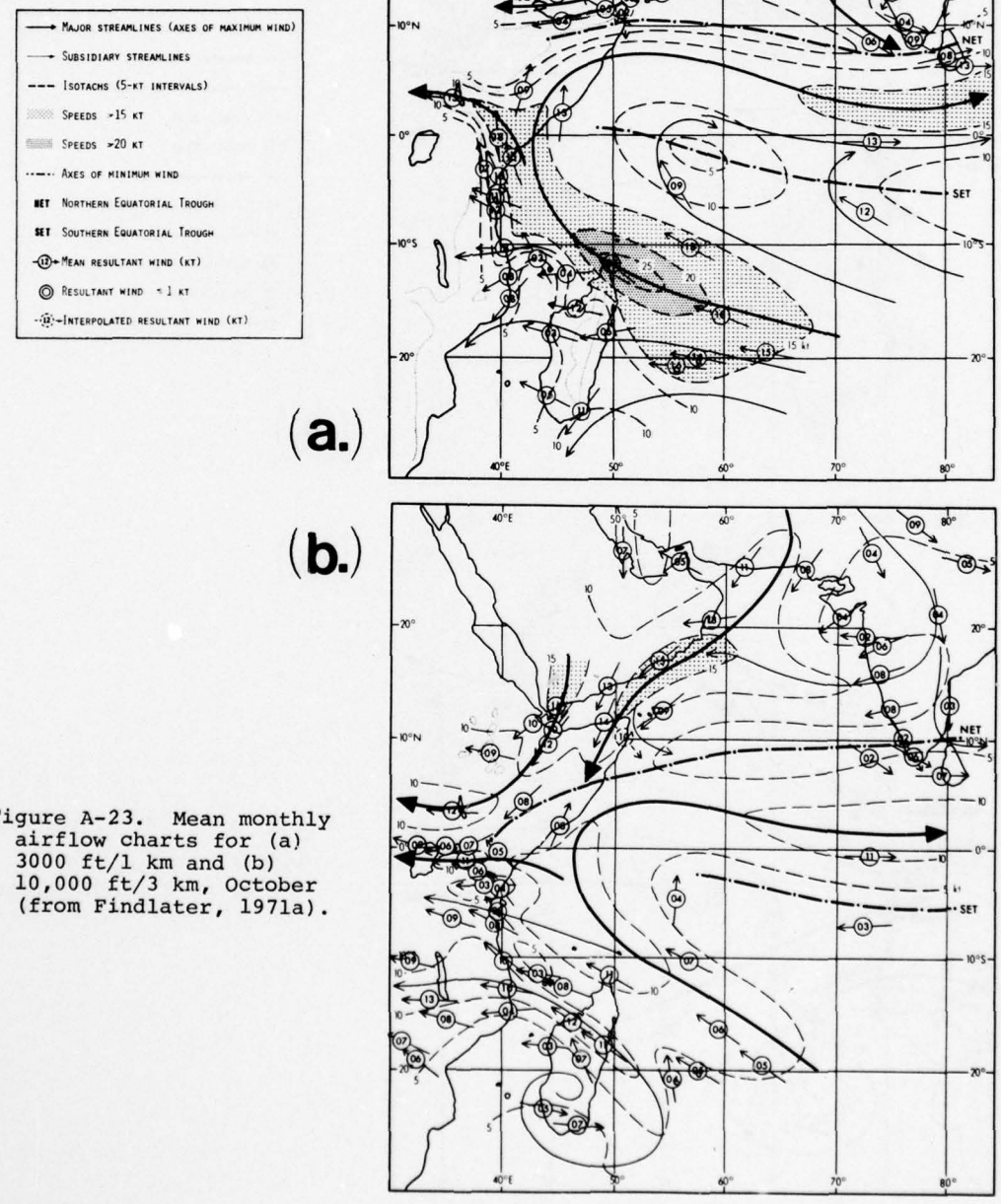

Figure A-23. Mean monthly airflow charts for (a) 3000 ft/1 km and (b) 10,000 ft/3 km, October (from Findlater, 1971a).

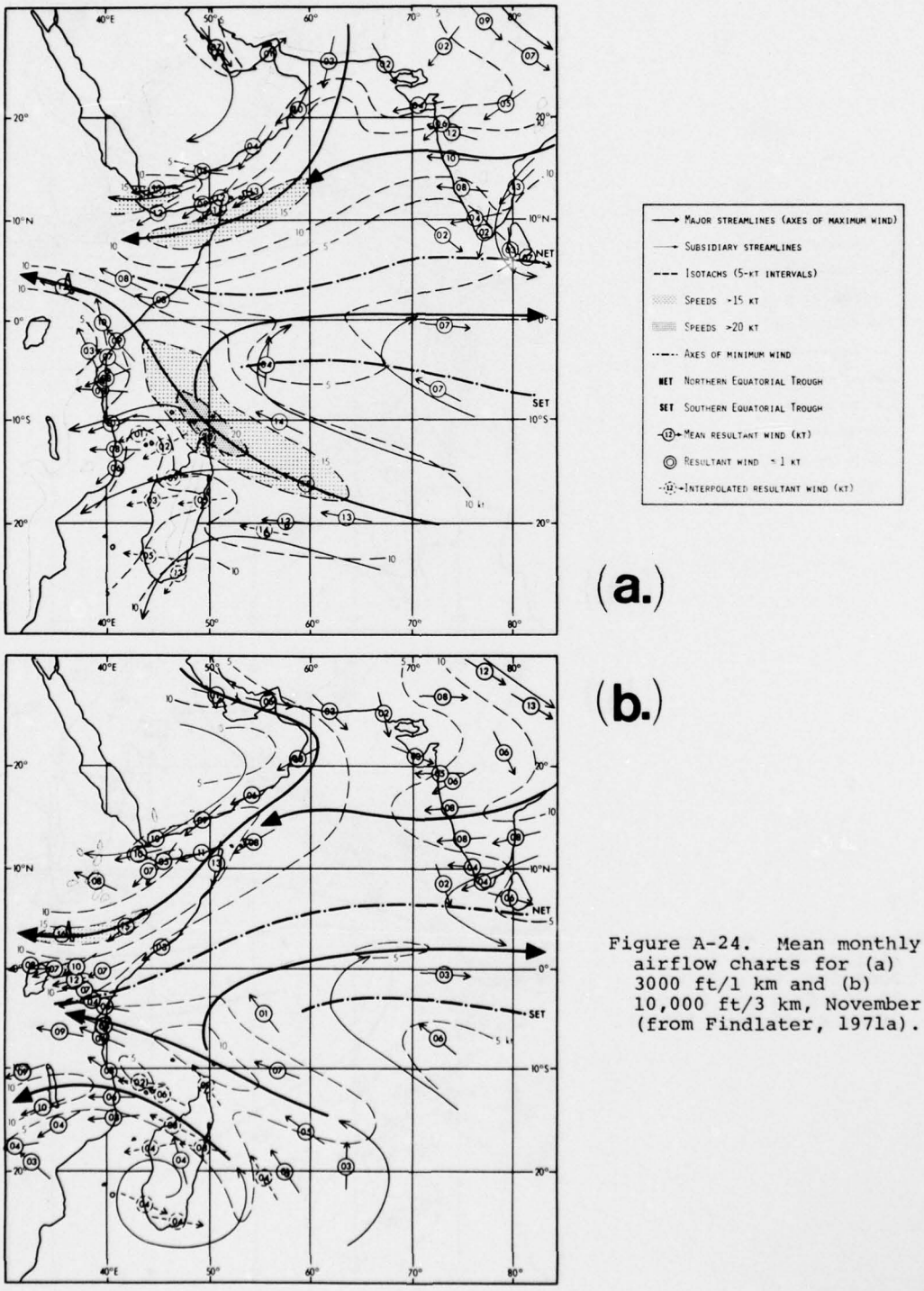

Figure A-24. Mean monthly airflow charts for (a) 3000 ft/1 km and (b) 10,000 ft/3 km, November (from Findlater, 1971a).

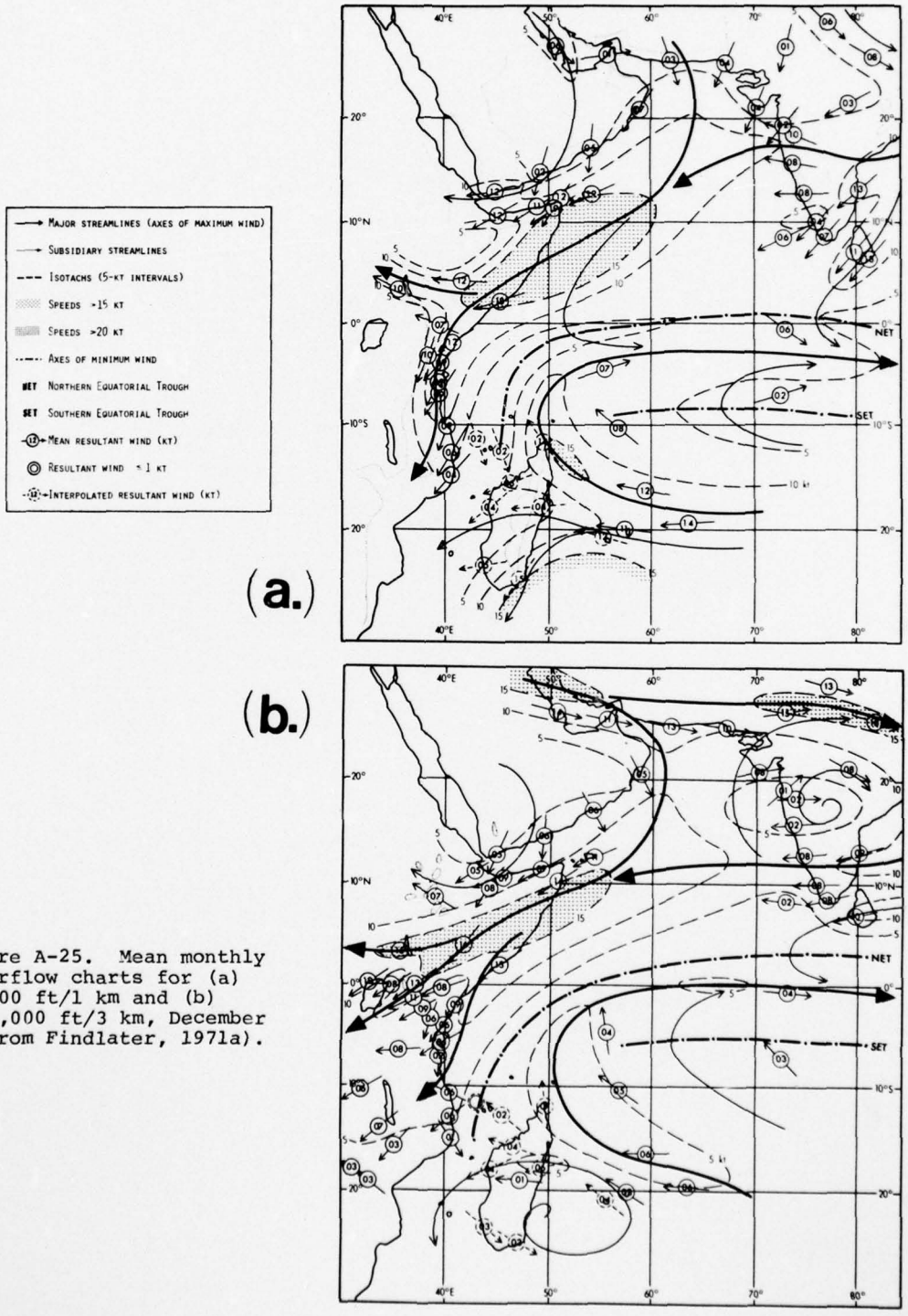

Figure A-25. Mean monthly airflow charts for (a) 3000 ft/1 km and (b) 10,000 ft/3 km, December (from Findlater, 1971a).

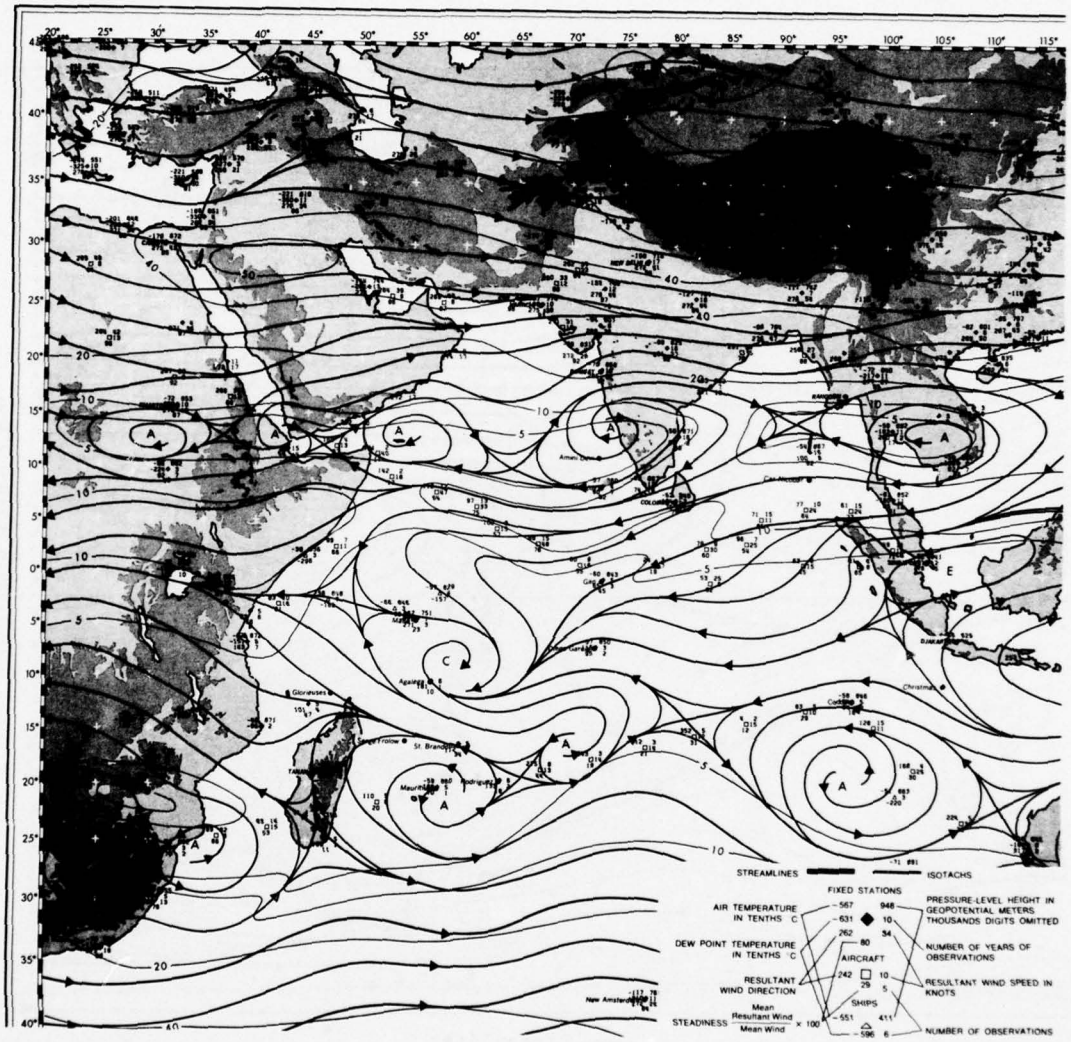

Figure A-26. Mean monthly constant pressure charts for January. (a) 500 mb (from Ramage and Raman, 1972). (b) 300 mb and (c) 200 mb (from Sadler, 1975).

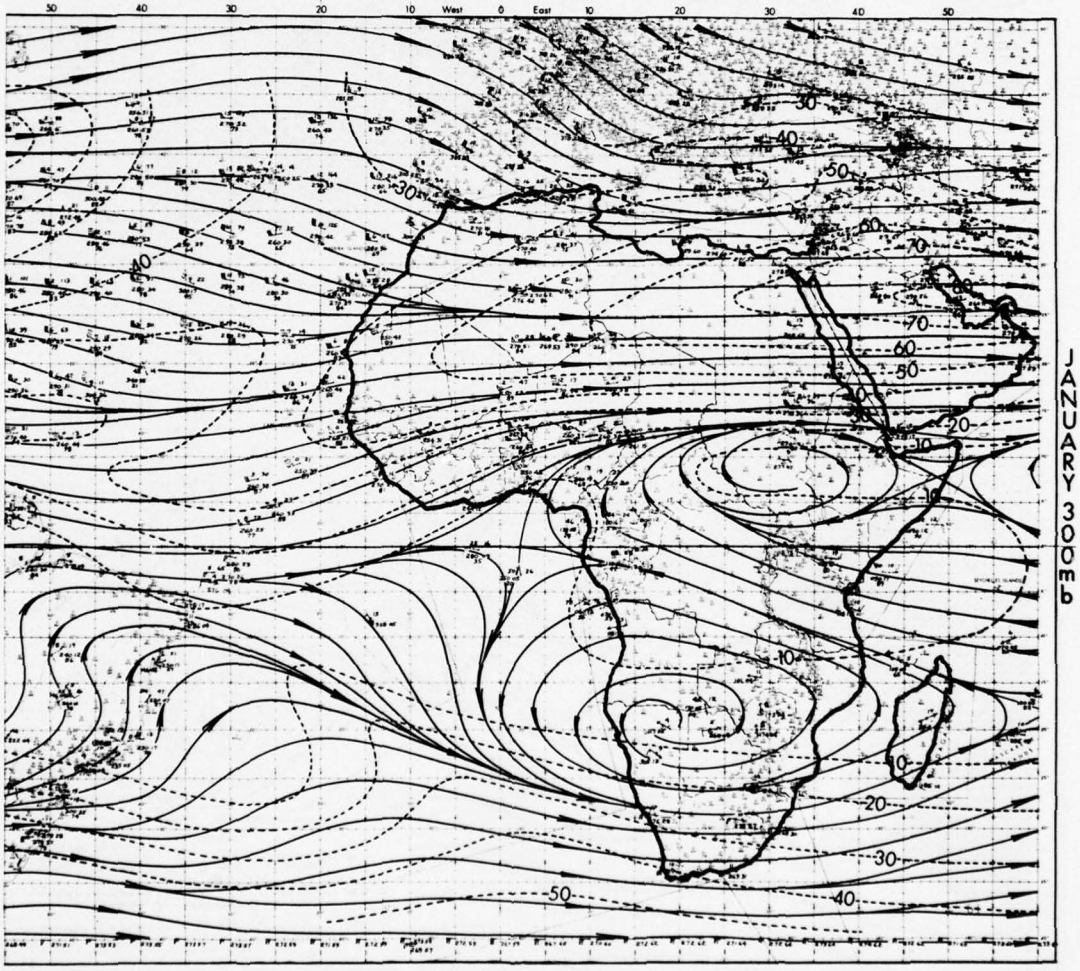

Figure A-26, continued. (b) 300 mb, January.

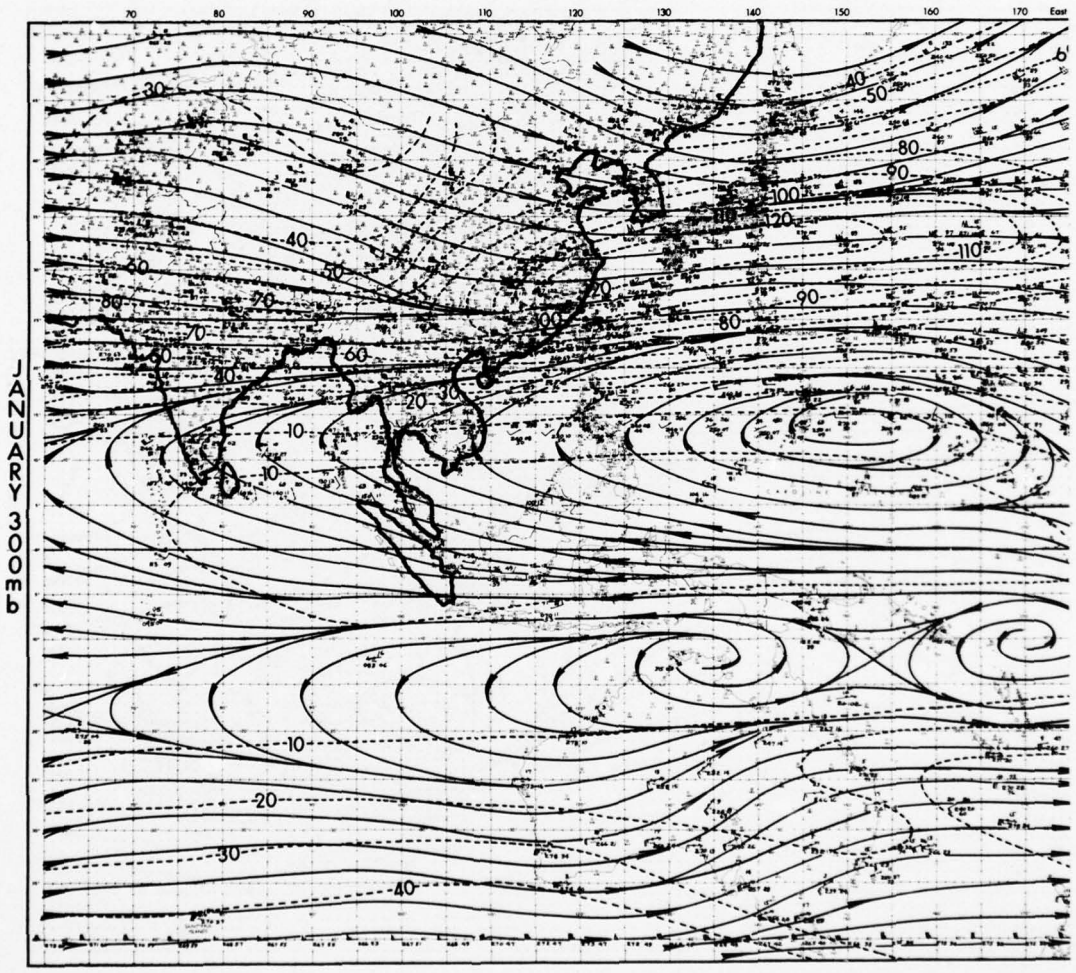

Figure A-26, continued. (b) 300 mb, January.

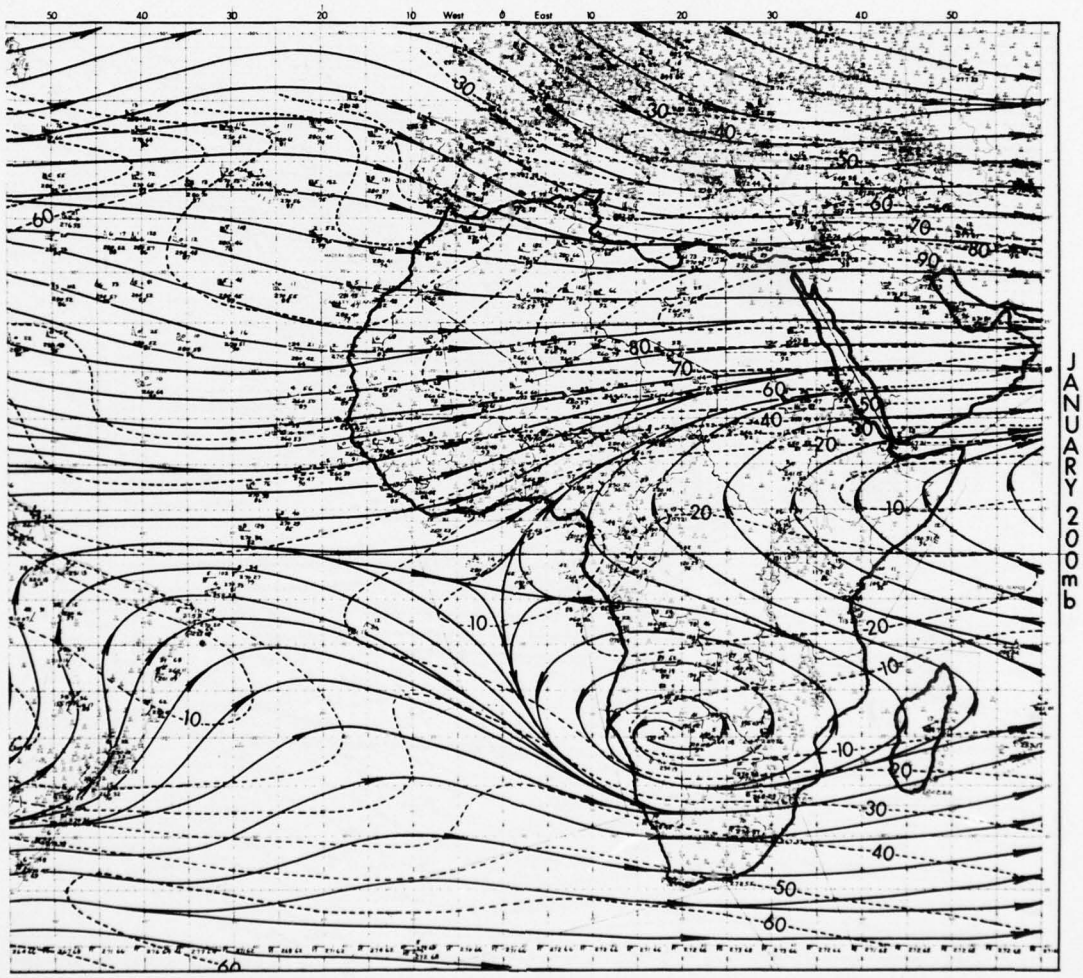

Figure A-26, continued. (c) 200 mb, January.

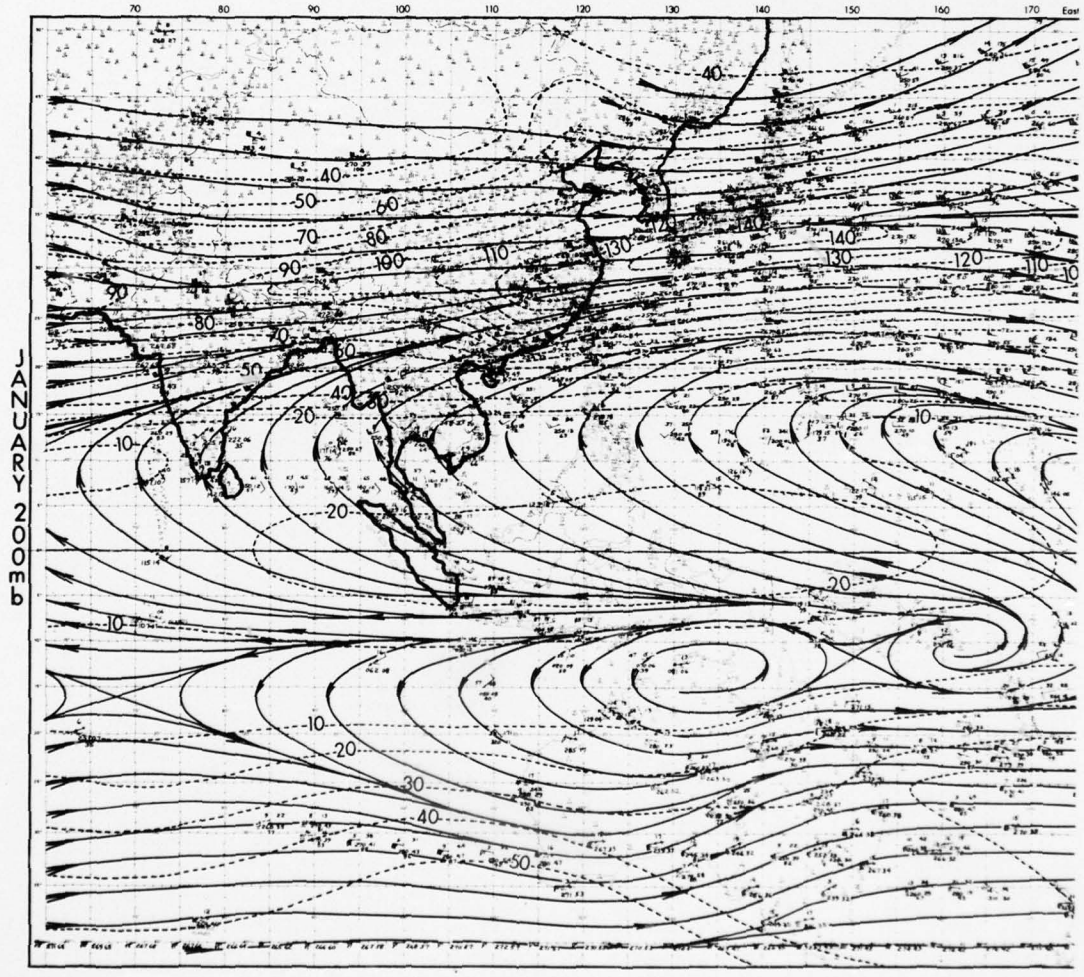

Figure A-26, continued. (c) 200 mb, January.

AD-A046 542 NAVAL ENVIRONMENTAL PREDICTION RESEARCH FACILITY MON--ETC F/G 4/2
METEOROLOGICAL PHENOMENA OF THE ARABIAN SEA,(U)
MAR 77 L R BRODY
UNCLASSIFIED NEPRF-AR-77-01 NL

2 OF 2
AD
A046542

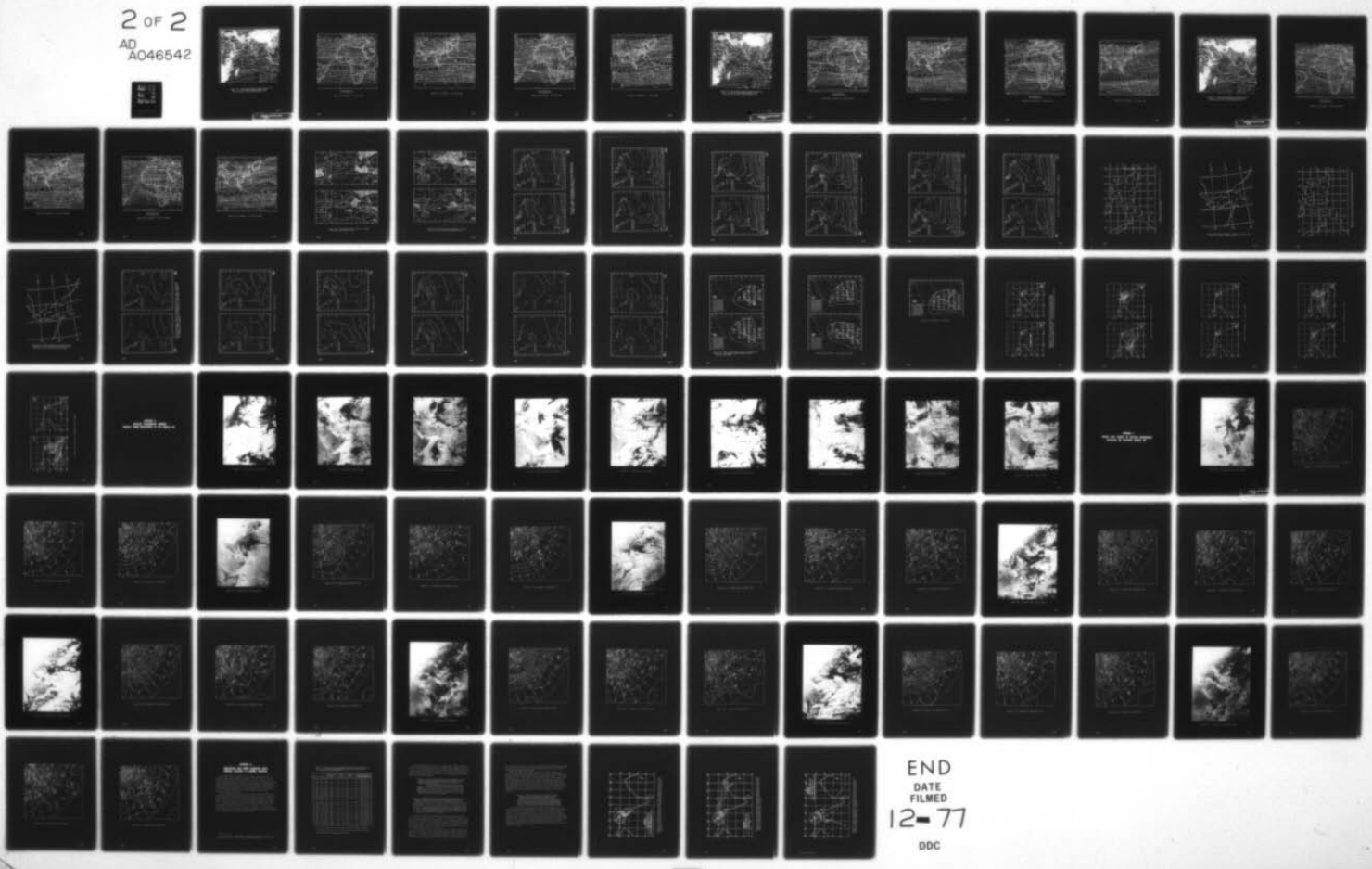

END
DATE
FILMED
12-77
DDC

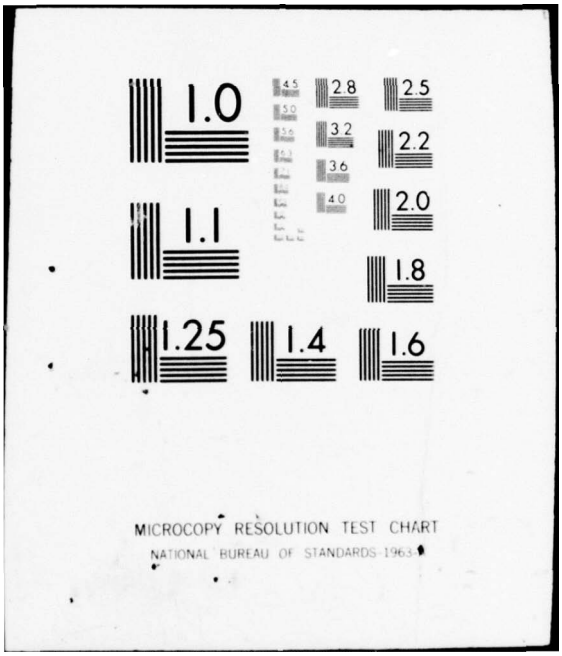
1.0
1.1
1.25
1.4
1.6
1.8
2.0
2.2
2.5
2.8
3.2
3.6
4.0
4.5
5.0
5.6
MICROCOPY RESOLUTION TEST CHART
NATIONAL BUREAU OF STANDARDS-1963-A

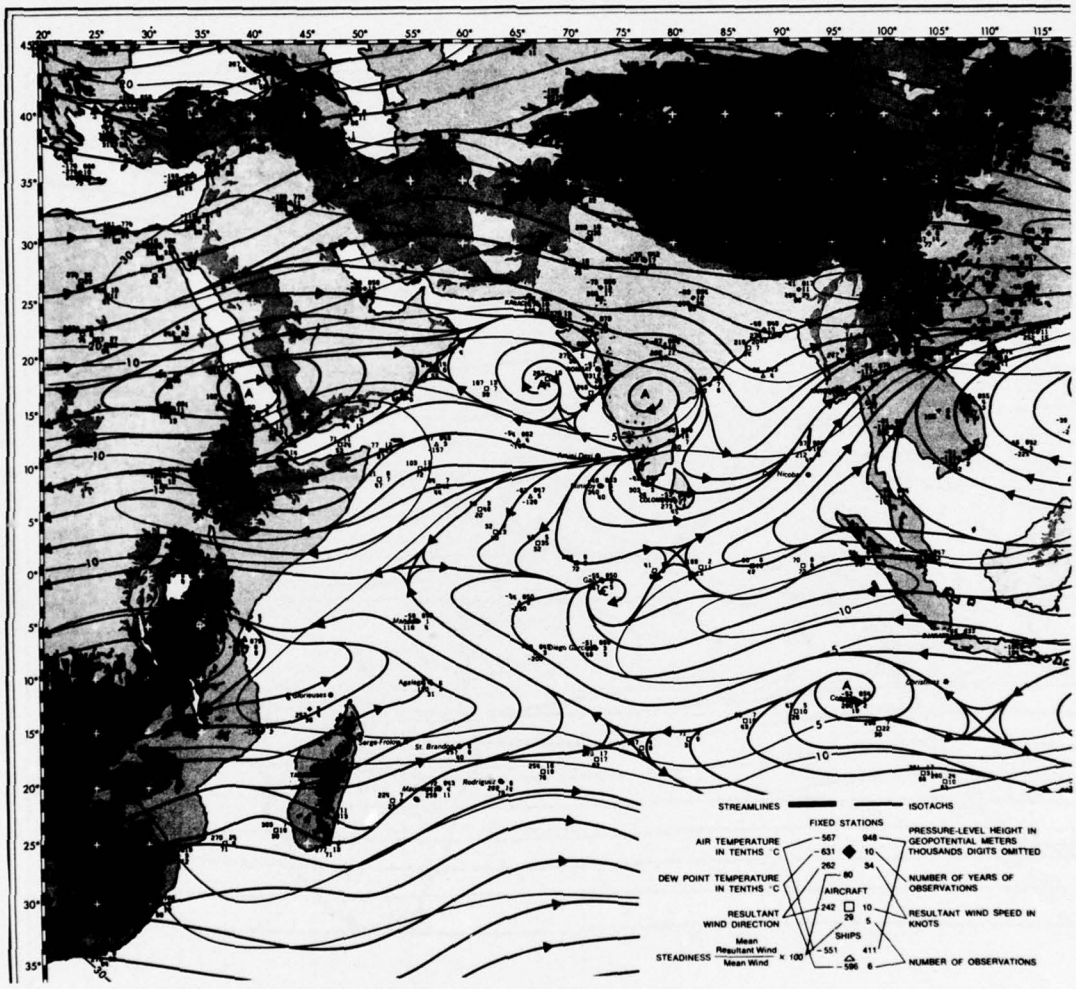

Figure A-27. Mean monthly constant pressure charts for May. (a) 500 mb (from Ramage and Raman, 1972). (b) 300 mb and (c) 200 mb (from Sadler, 1975).

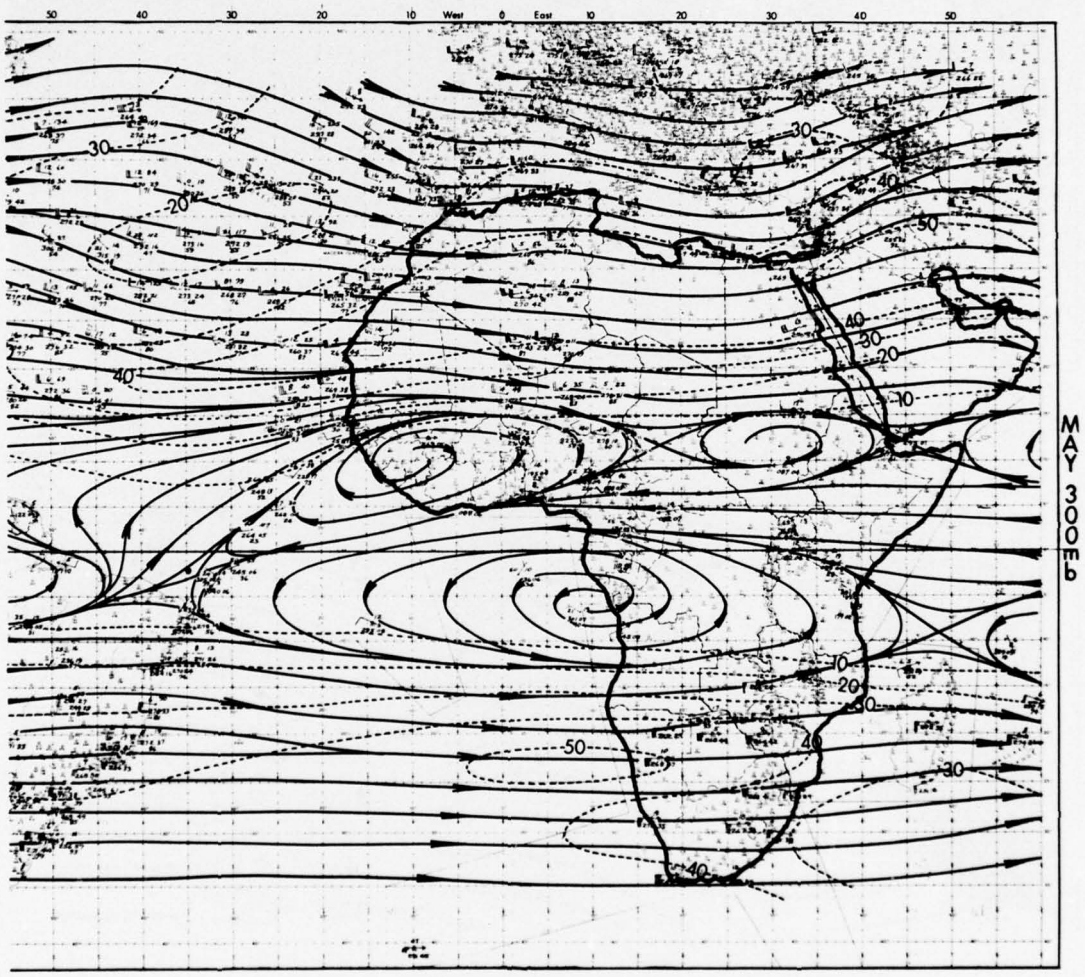

Figure A-27, continued. (b) 300 mb, May.

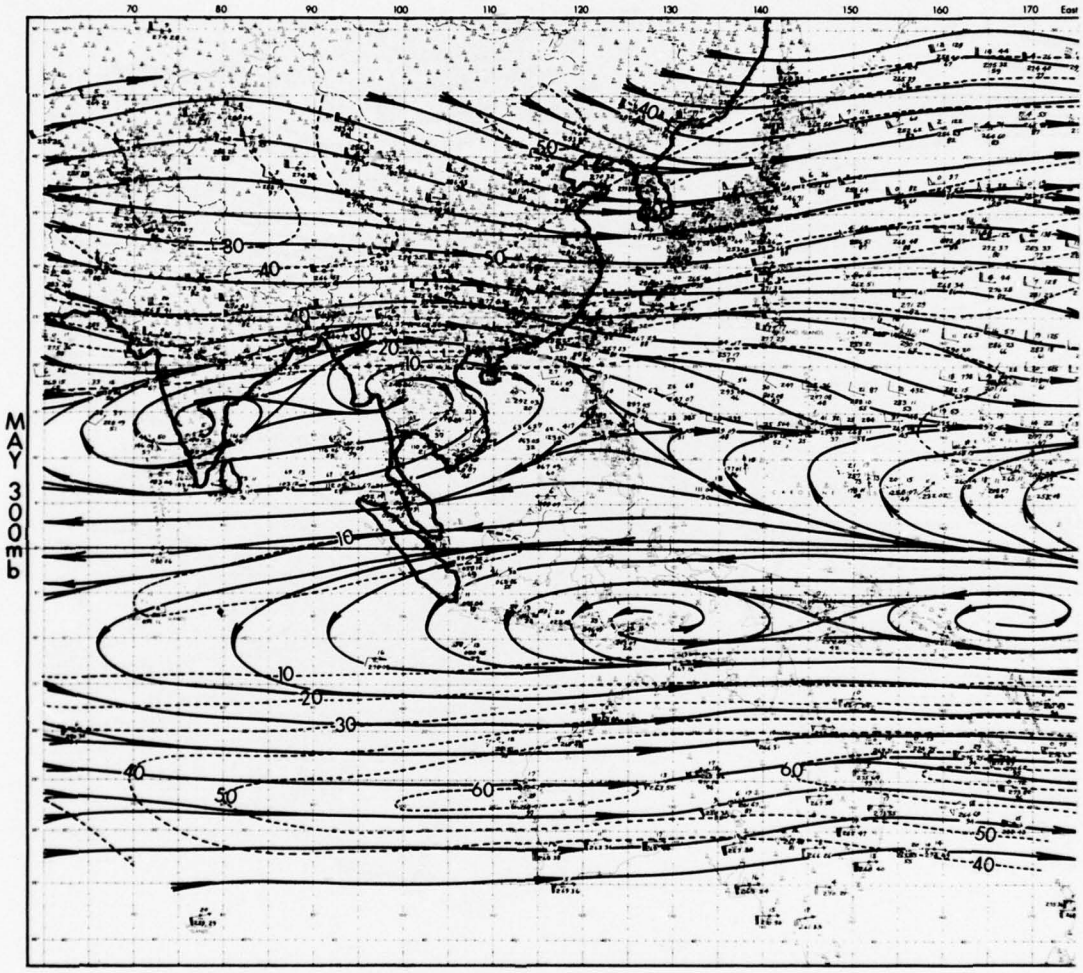

Figure A-27, continued. (b) 300 mb, May.

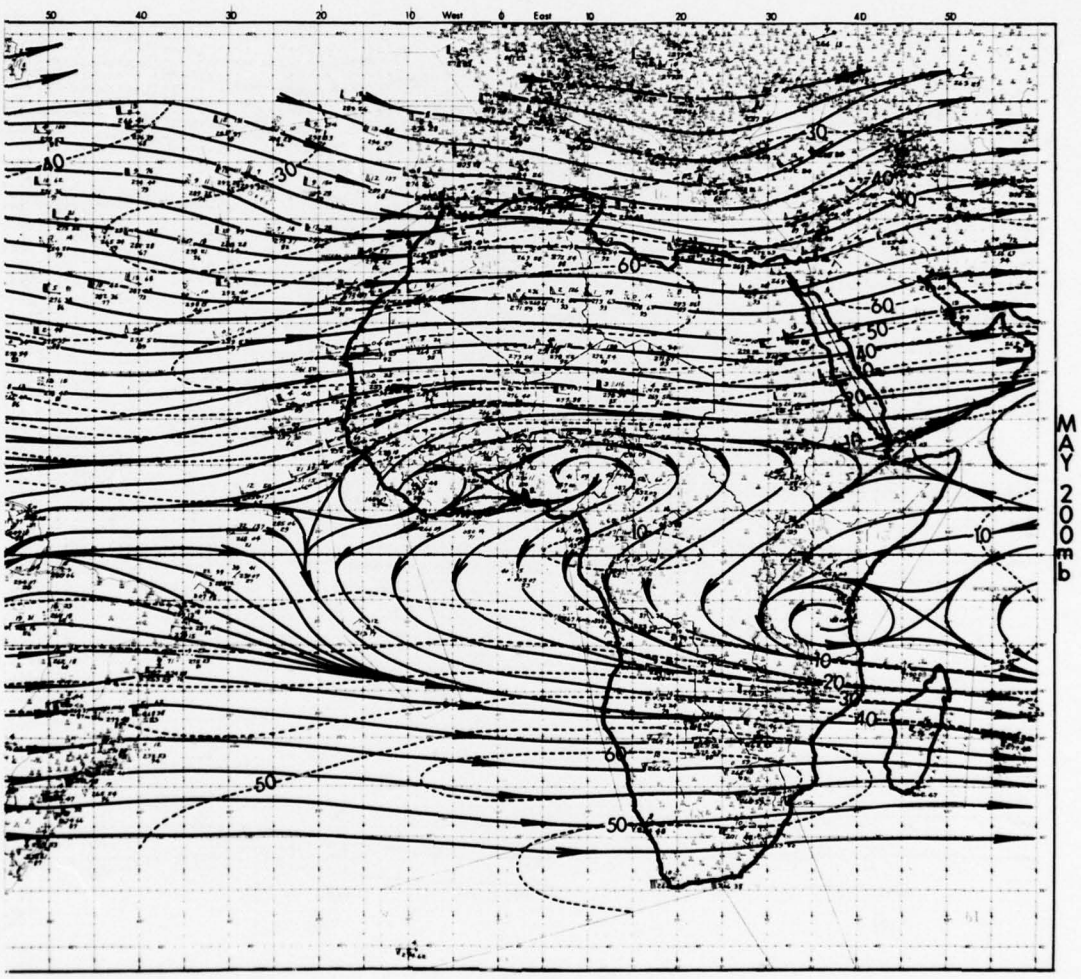

Figure A-27, continued. (c) 200 mb, May.

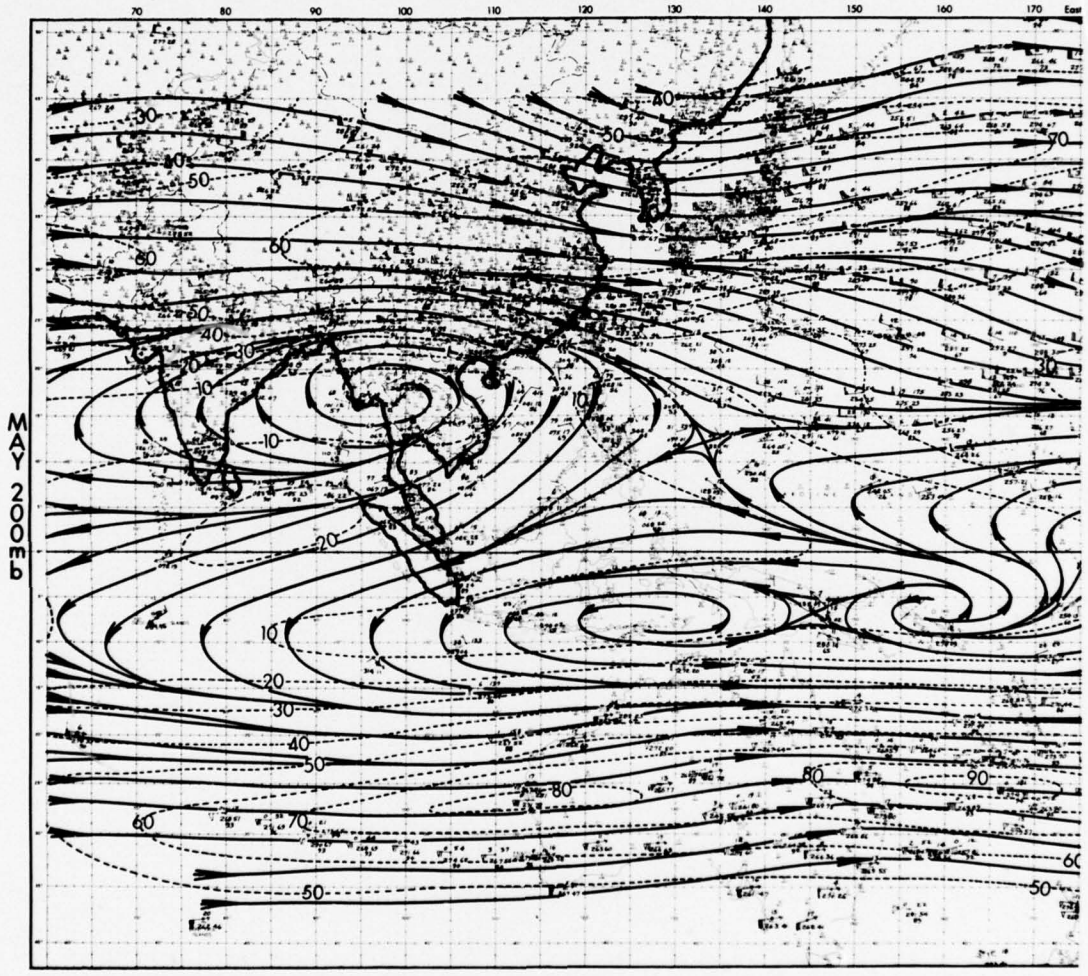

Figure A-27, continued. (c) 200 mb, May.

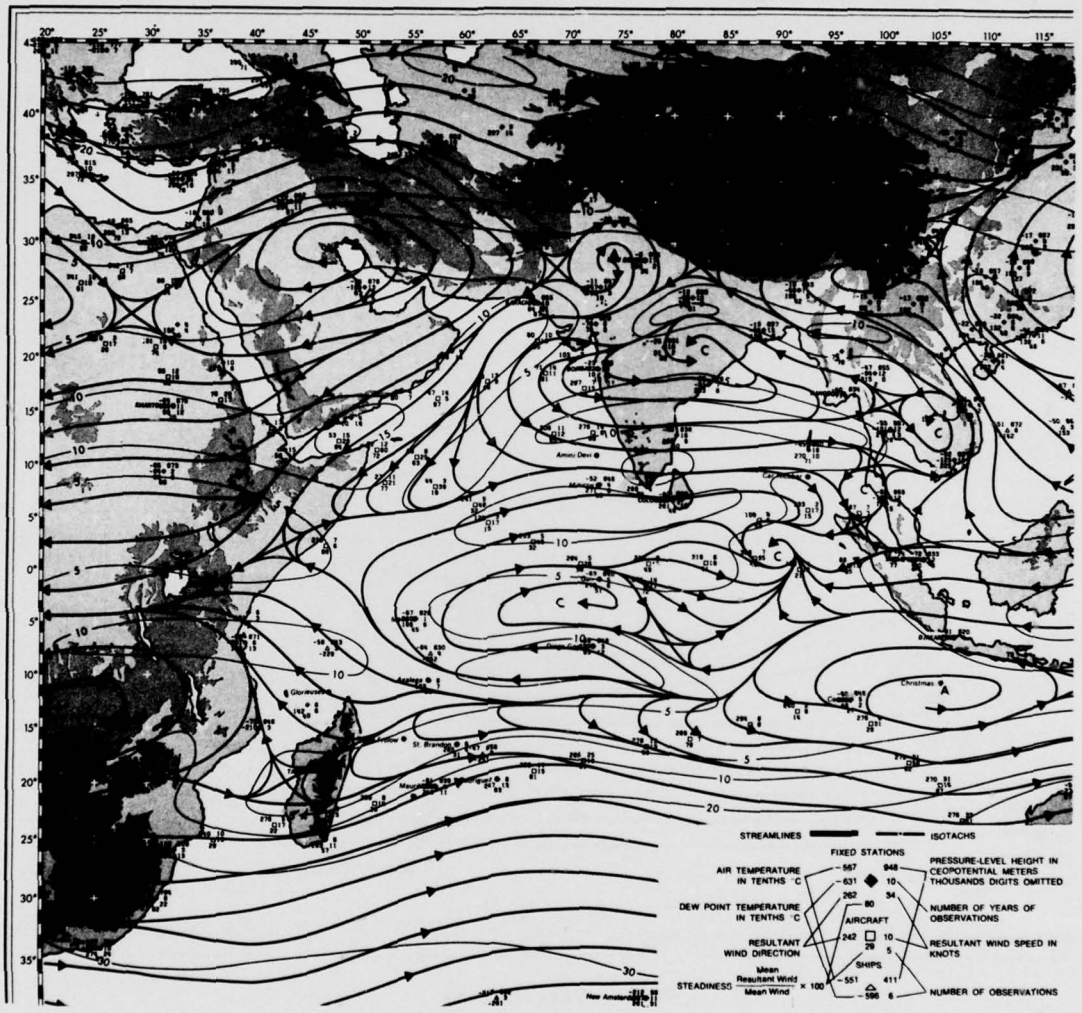

Figure A-28. Mean monthly constant pressure charts for July. (a) 500 mb (from Ramage and Raman, 1972). (b) 300 mb and (c) 200 mb (from Sadler, 1975).

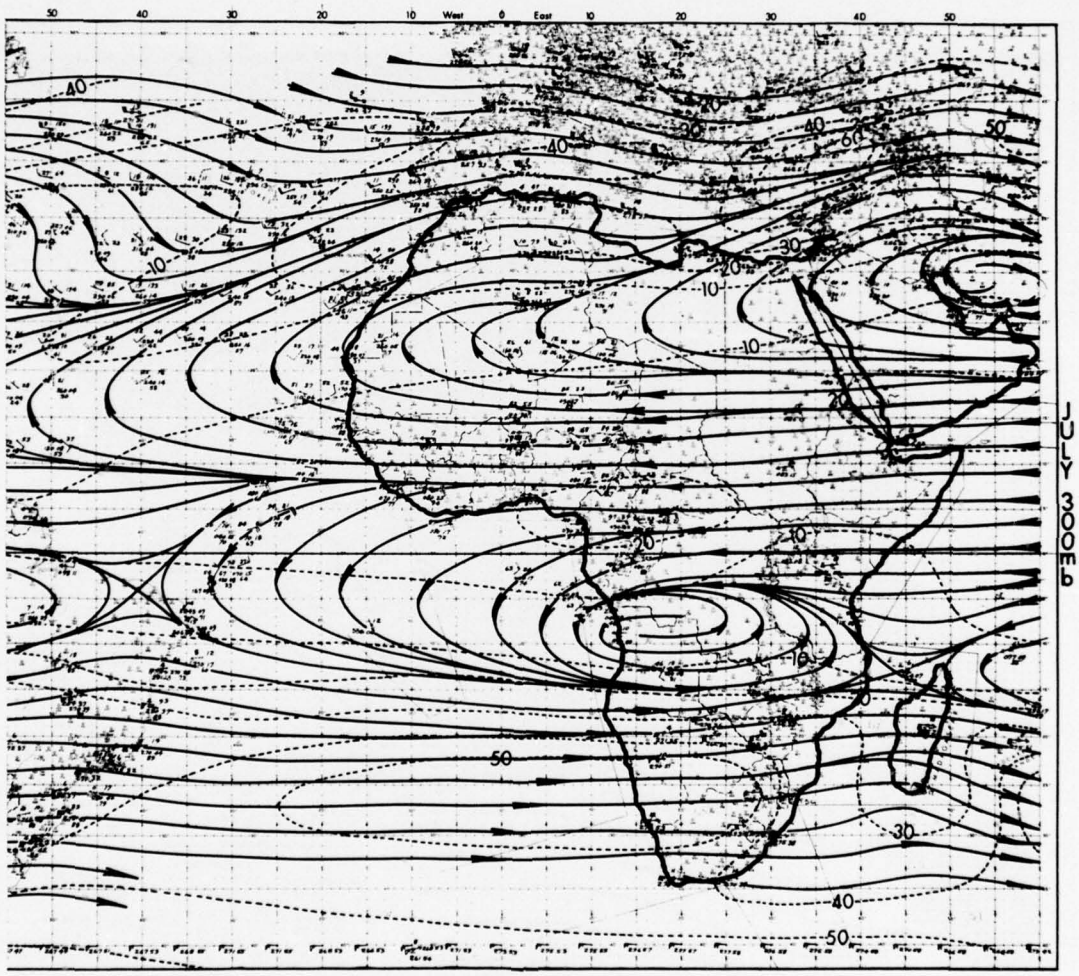

Figure A-28, continued. (b) 300 mb, July.

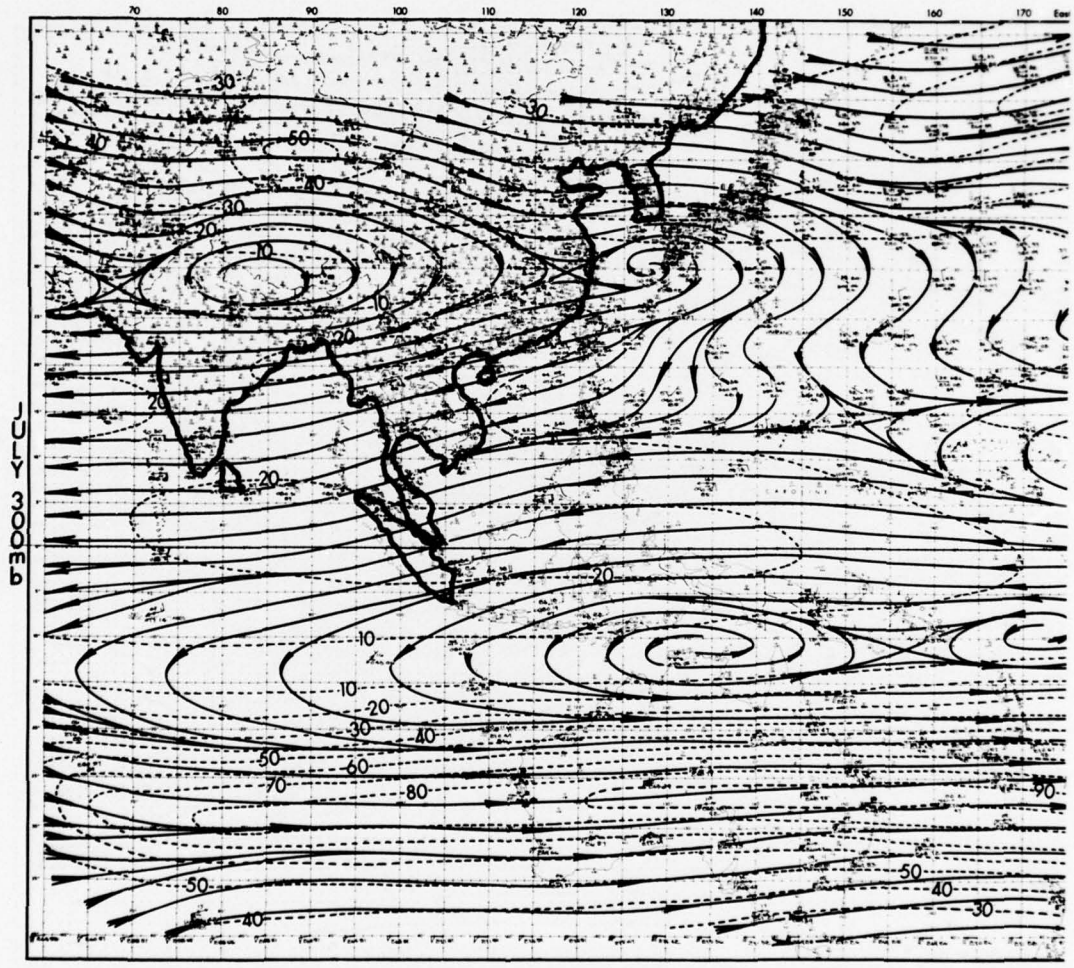

Figure A-28, continued. (b) 300 mb, July.

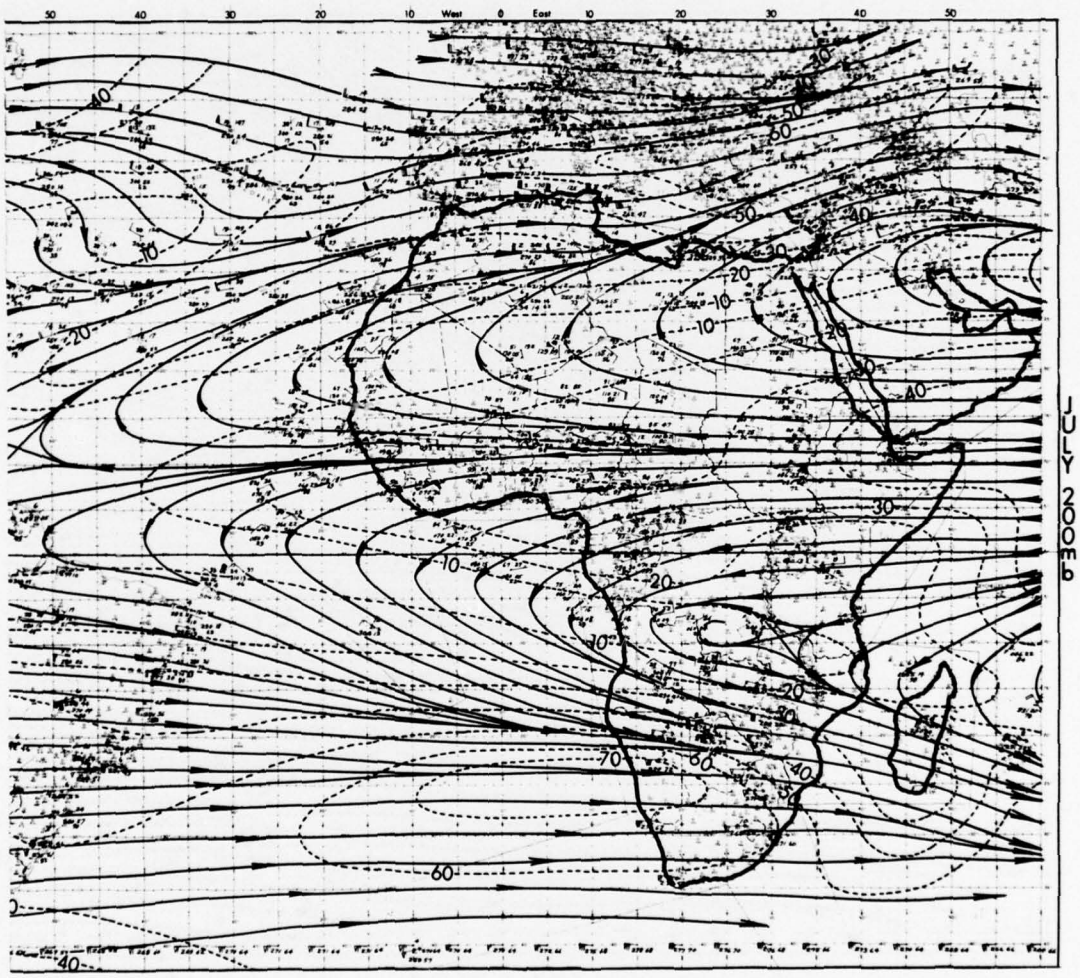

Streamlines
Isotachs (kt)

Figure A-28, continued. (c) 200 mb, July.

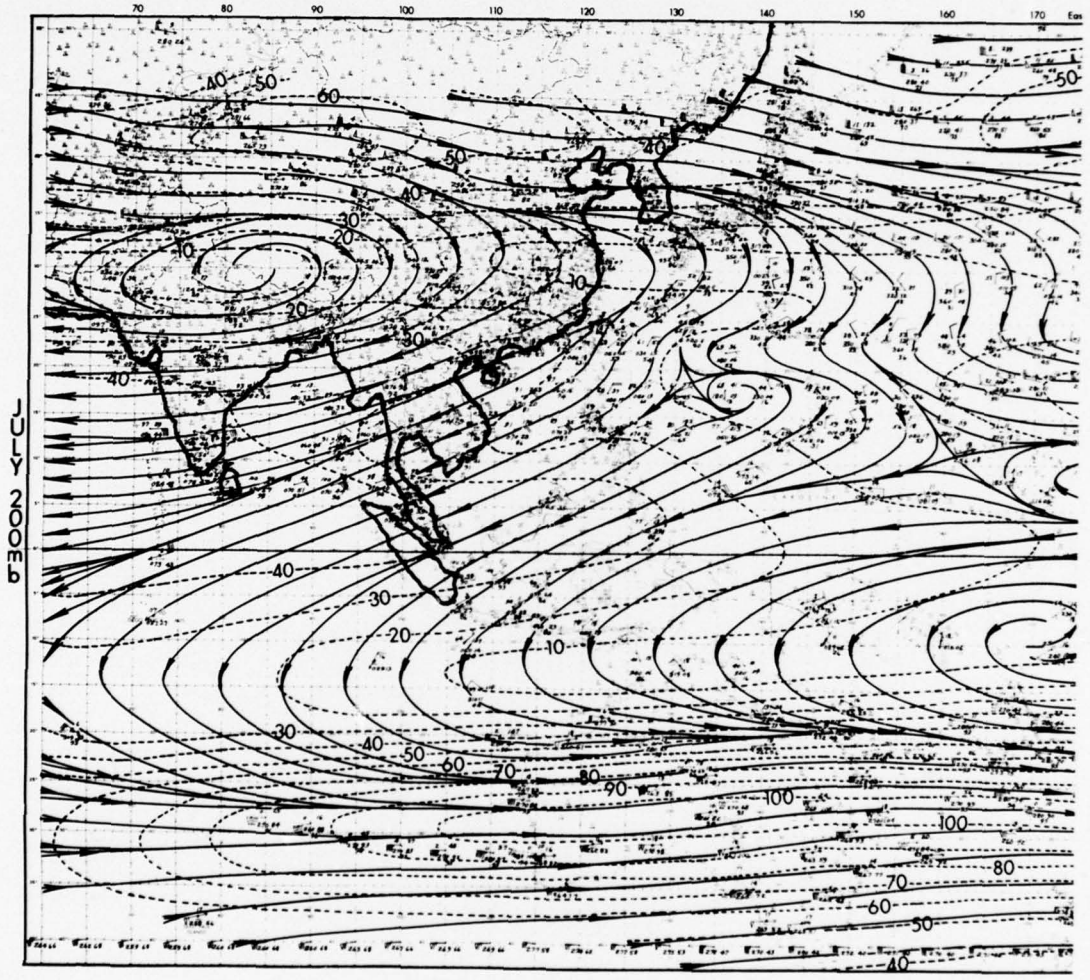

Figure A-28, continued. (c) 200 mb, July.

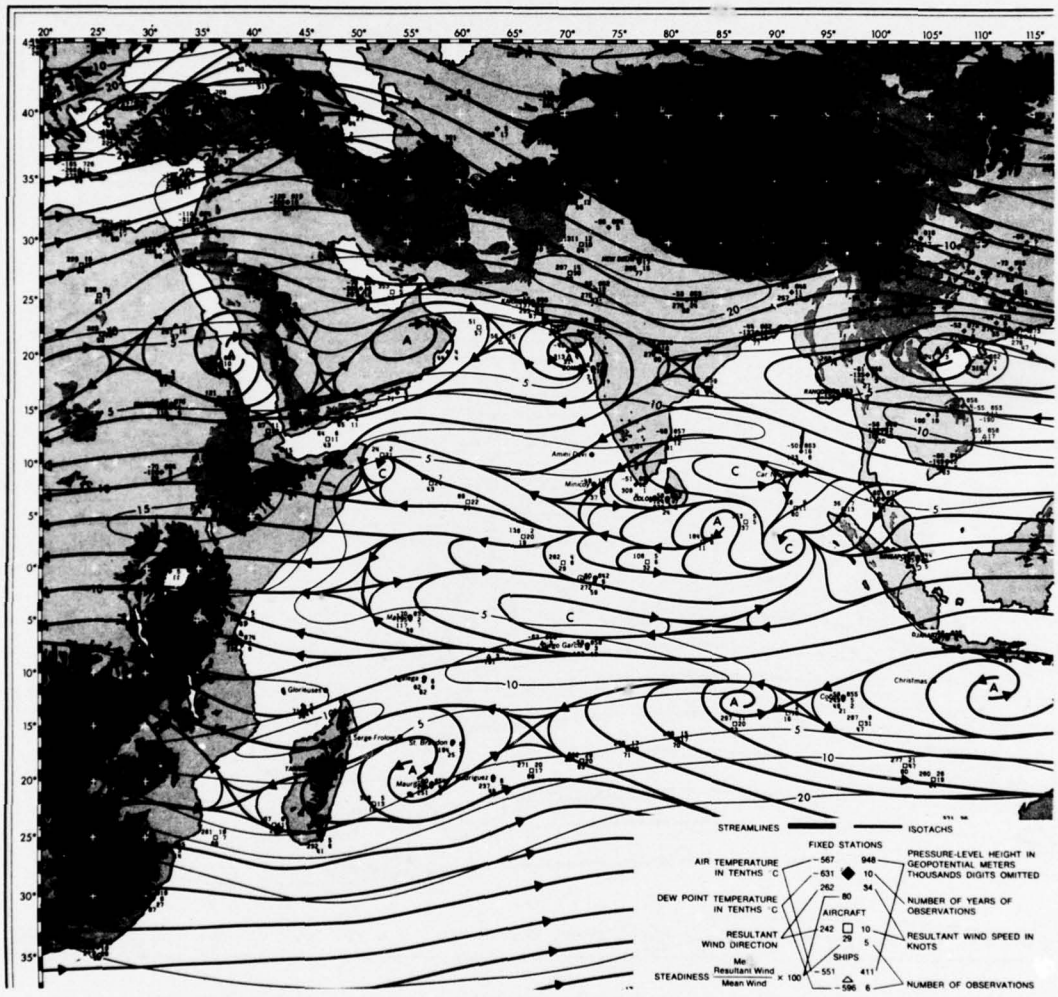

Figure A-29. Mean monthly constant pressure charts for October. (a) 500 mb (from Ramage and Raman, 1972). (b) 300 mb and (c) 200 mb (from Sadler, 1975).

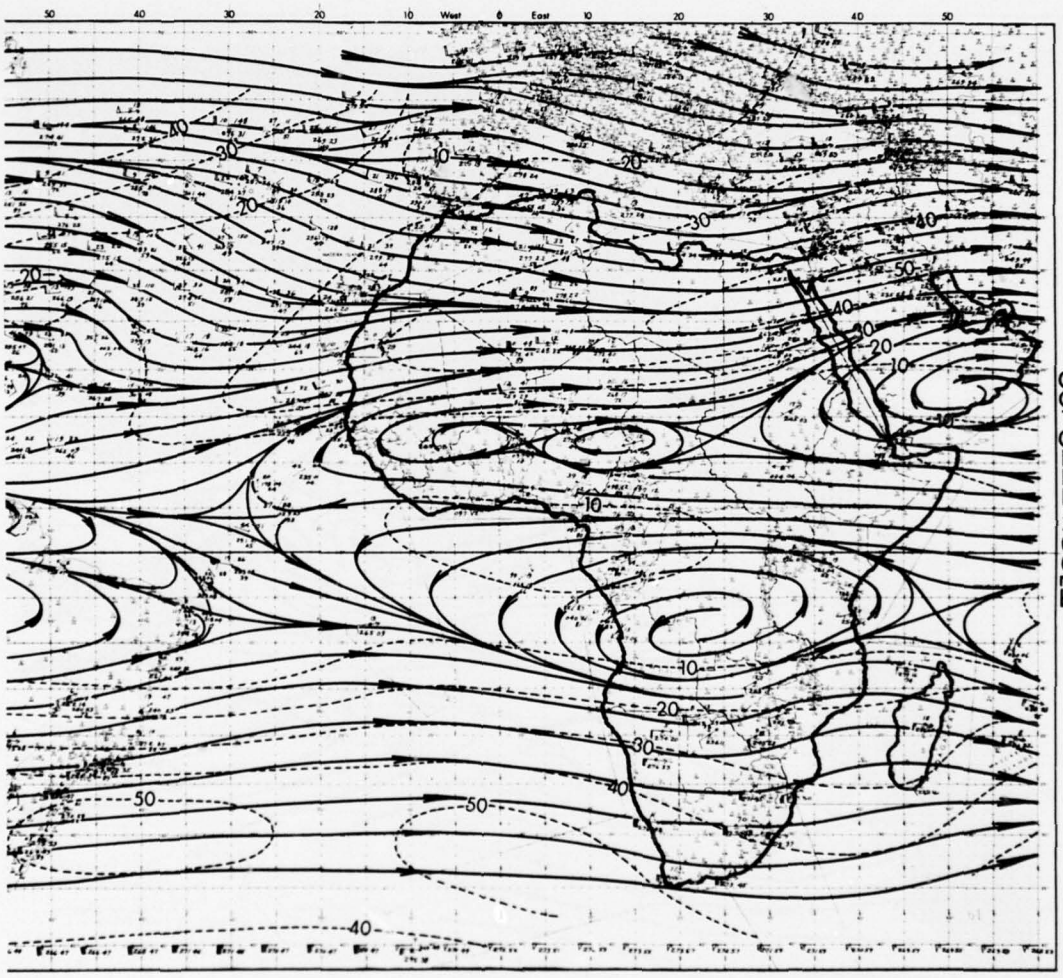

Figure A-29, continued. (b) 300 mb, October.

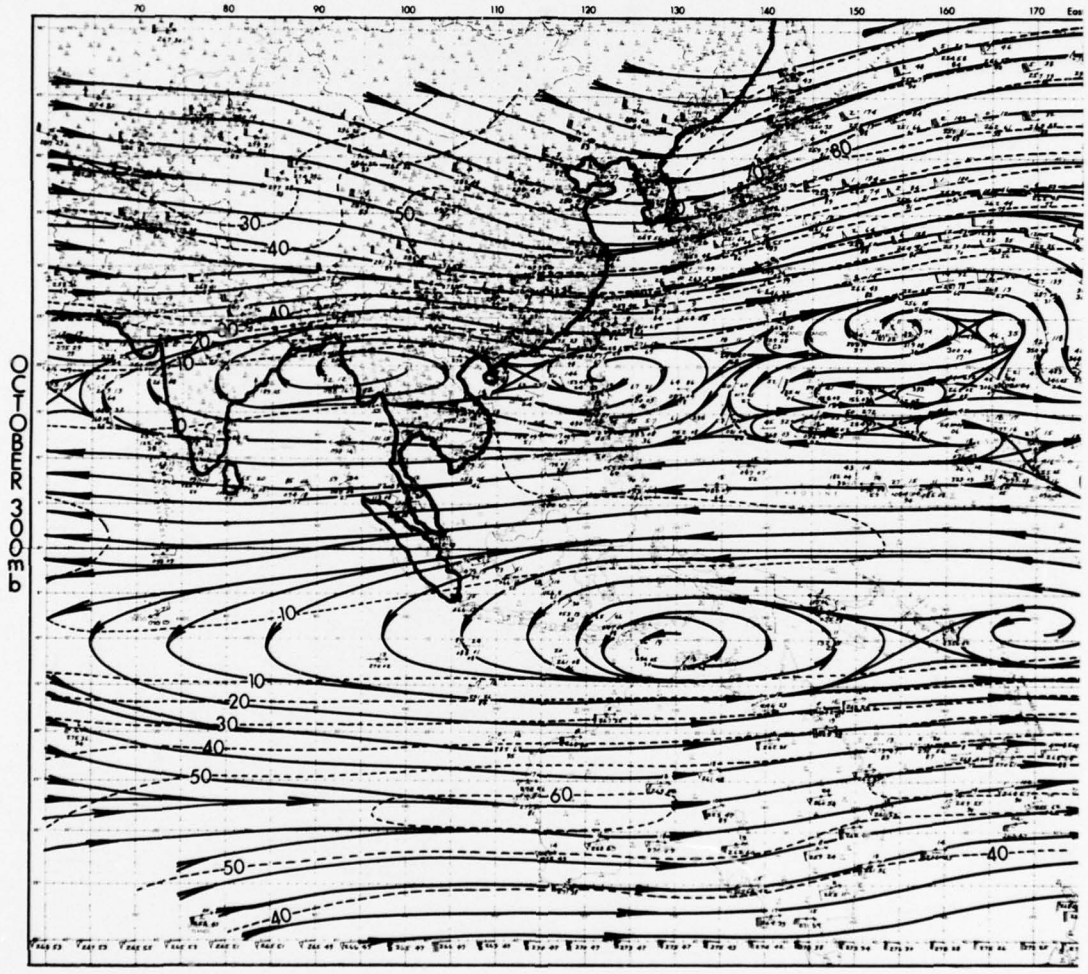

Figure A-29, continued. (b) 300 mb, October.

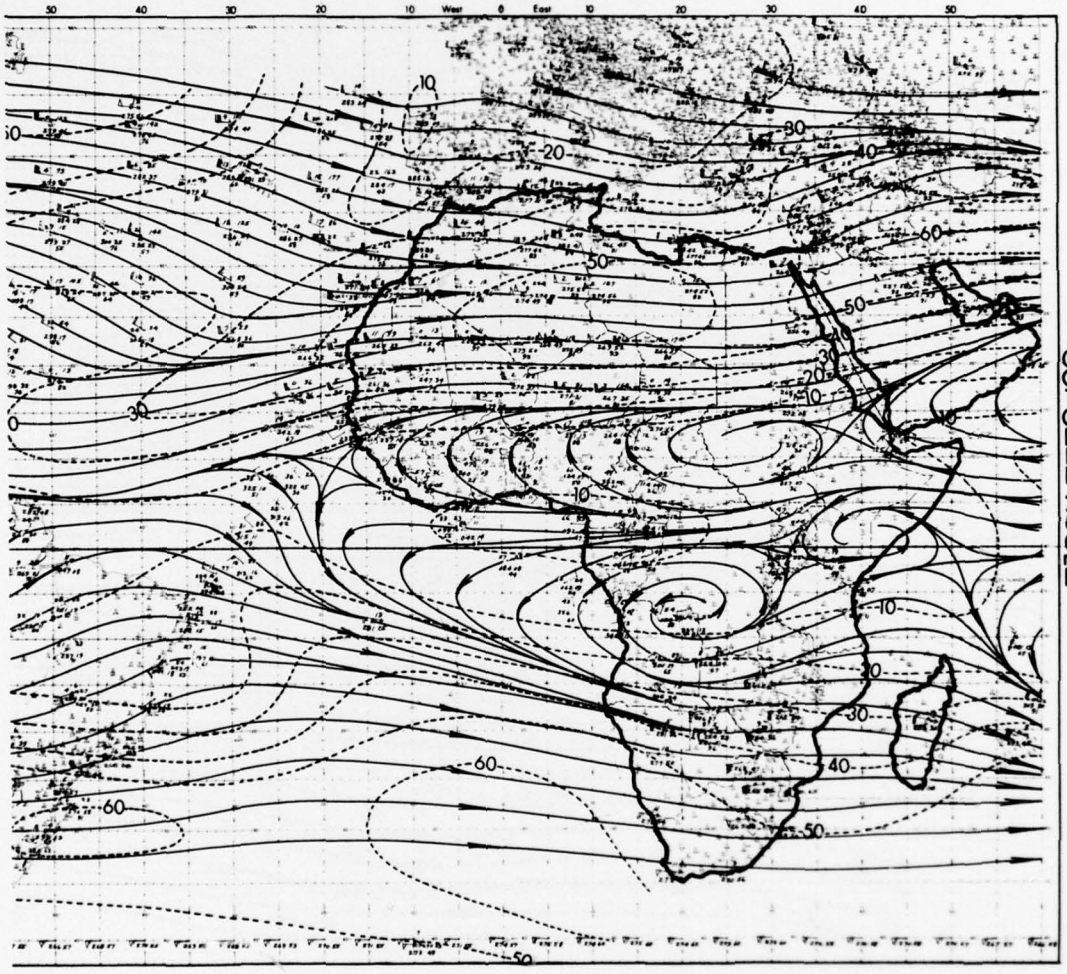

Figure A-29, continued. (c) 200 mb, October.

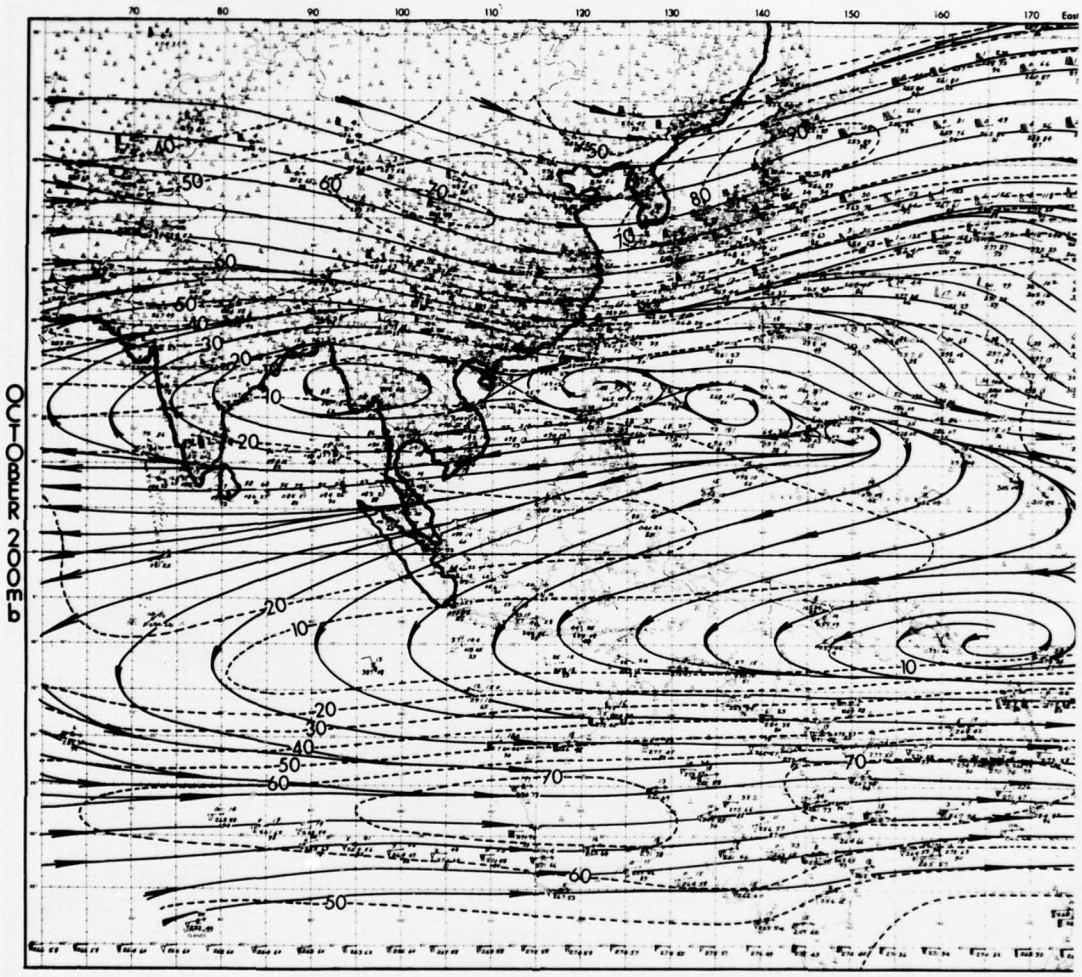

Figure A-29, continued. (c) 200 mb, October.

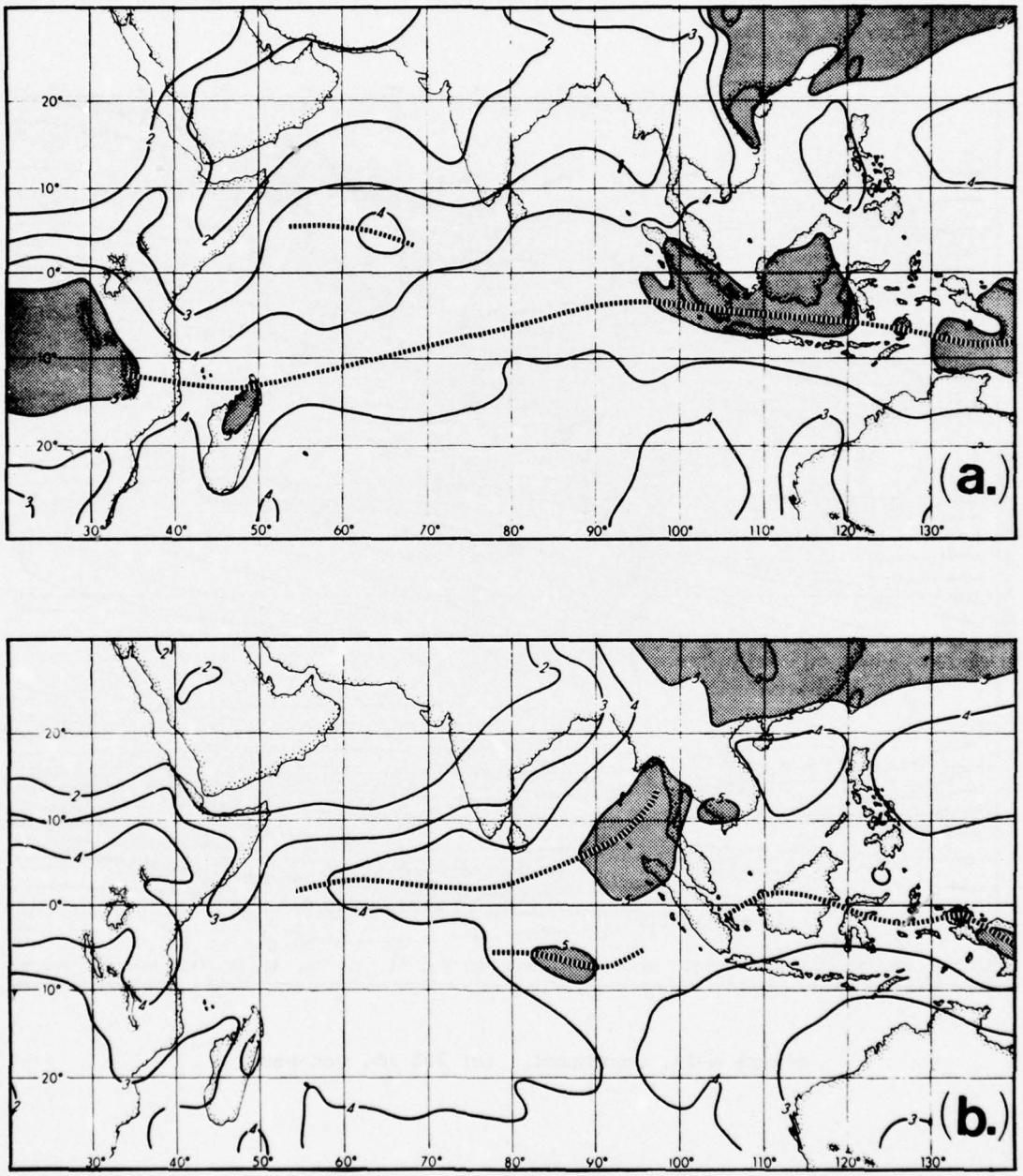

Figure A-30. Mean cloud amount in oktas: (a) January and (b) May (from Cuming, 1973).

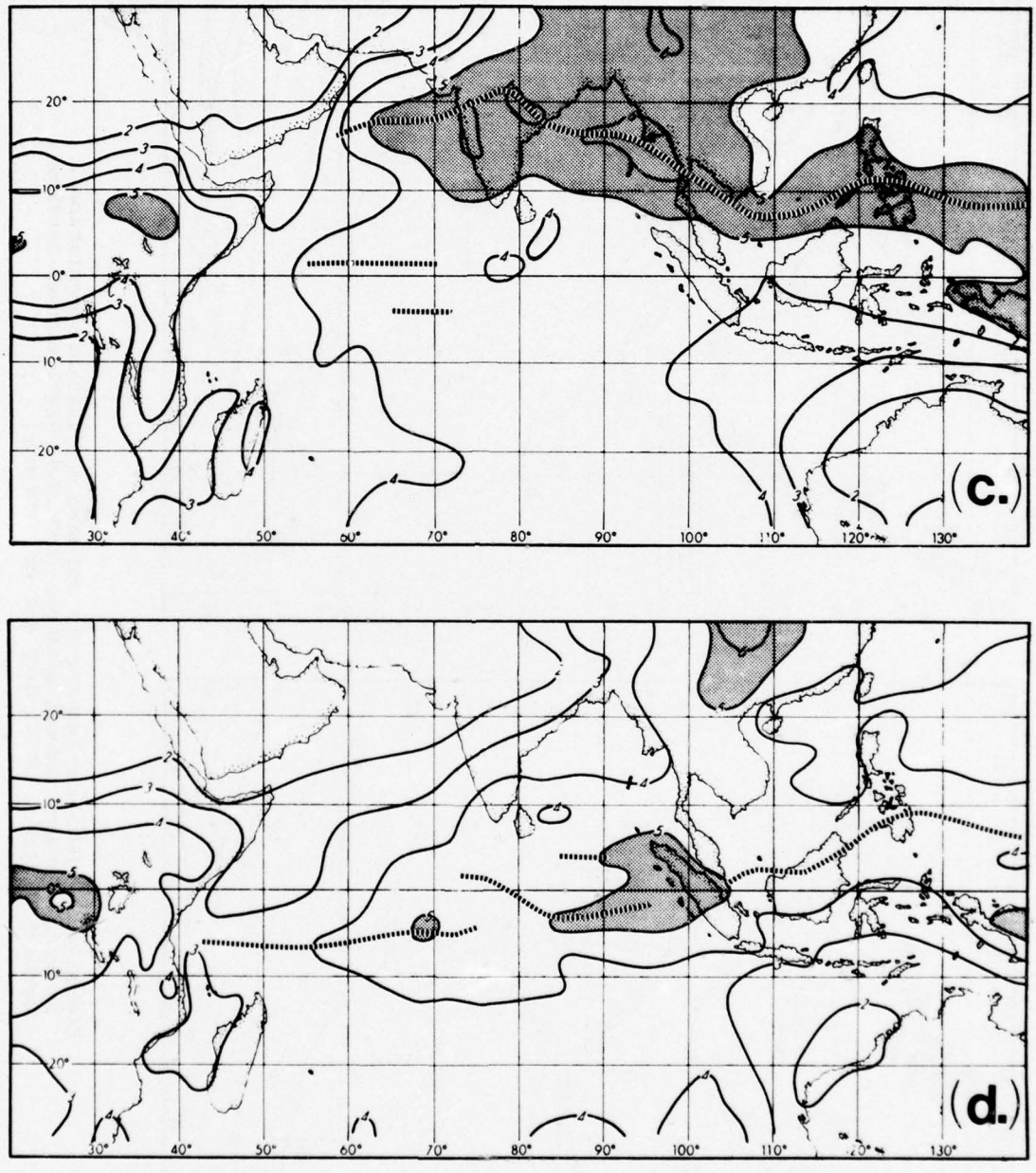

Figure A-30, continued. Mean cloud amount in oktas: (c) July and (d) October (from Cuming, 1973).

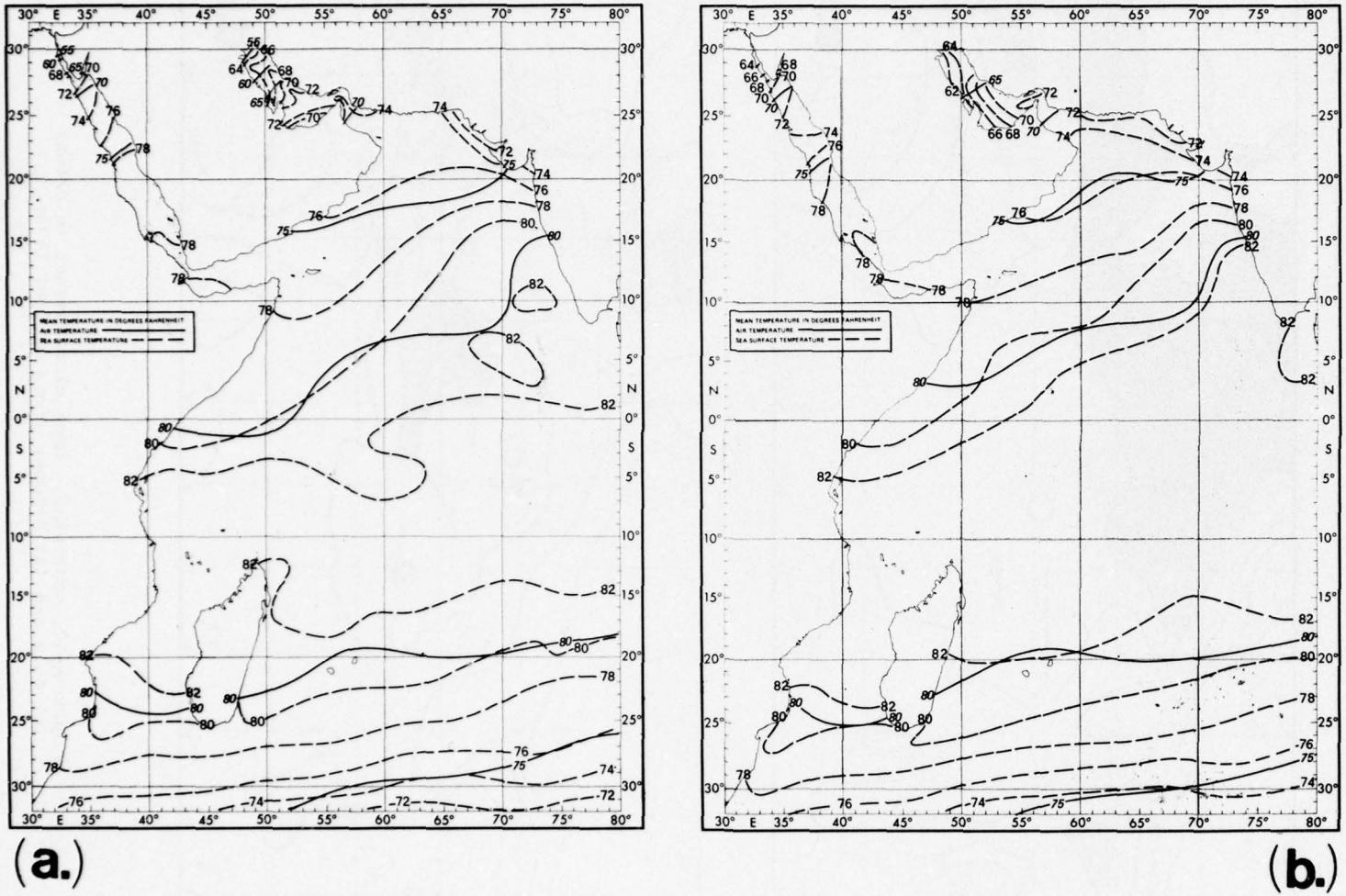

Figure A-31. Mean air temperature and mean sea surface temperature, by month, January through December (from U.S. Naval Weather Service Command, 1974a). (a) January and (b) February.

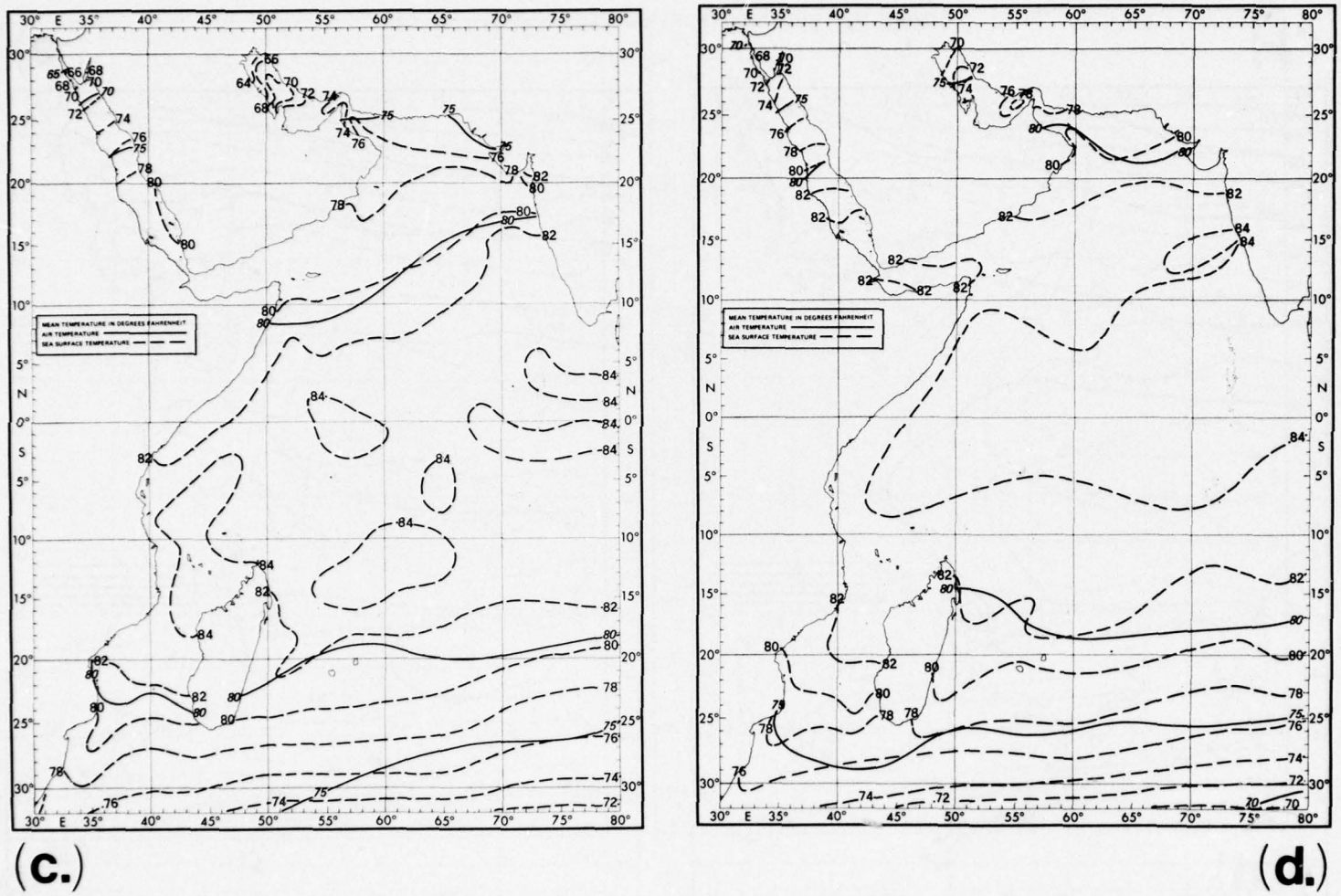

Figure A-31, continued. (c) March and (d) April.

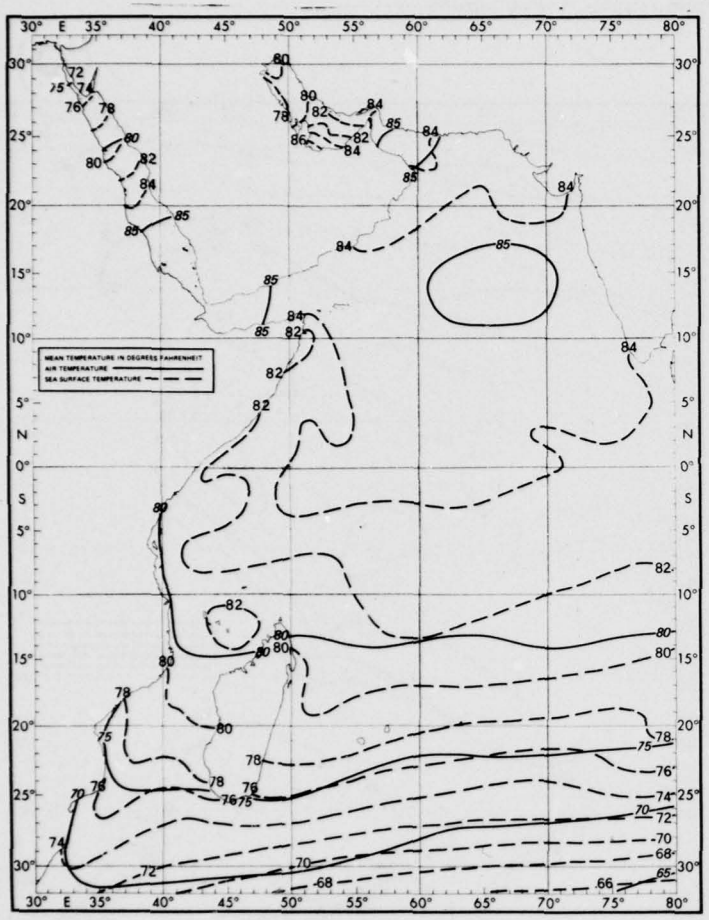

(e.)

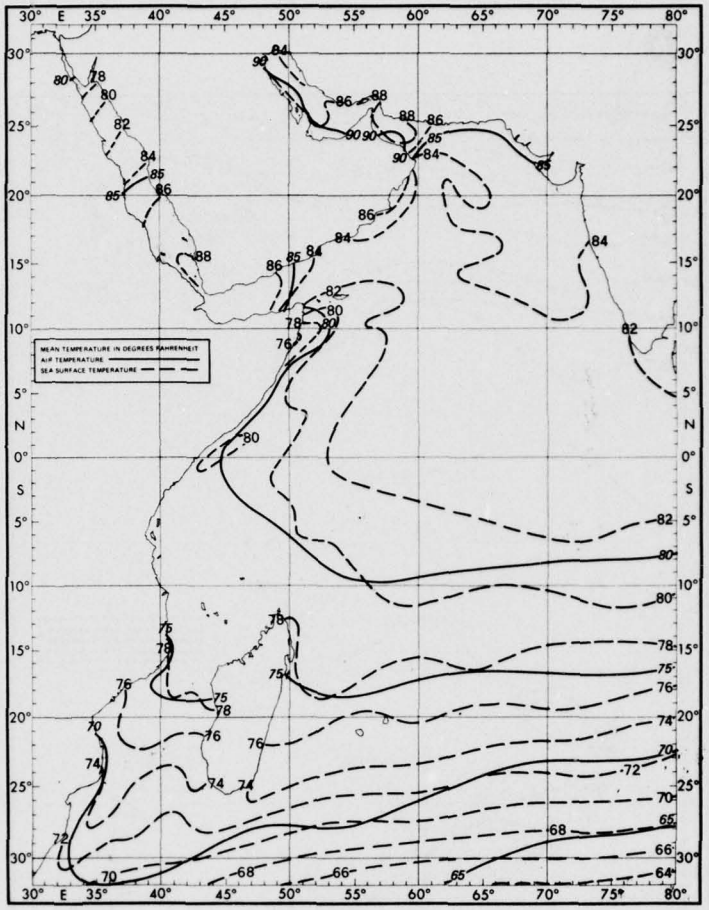

(f.)

Figure A-31, continued. (e) May and (f) June.

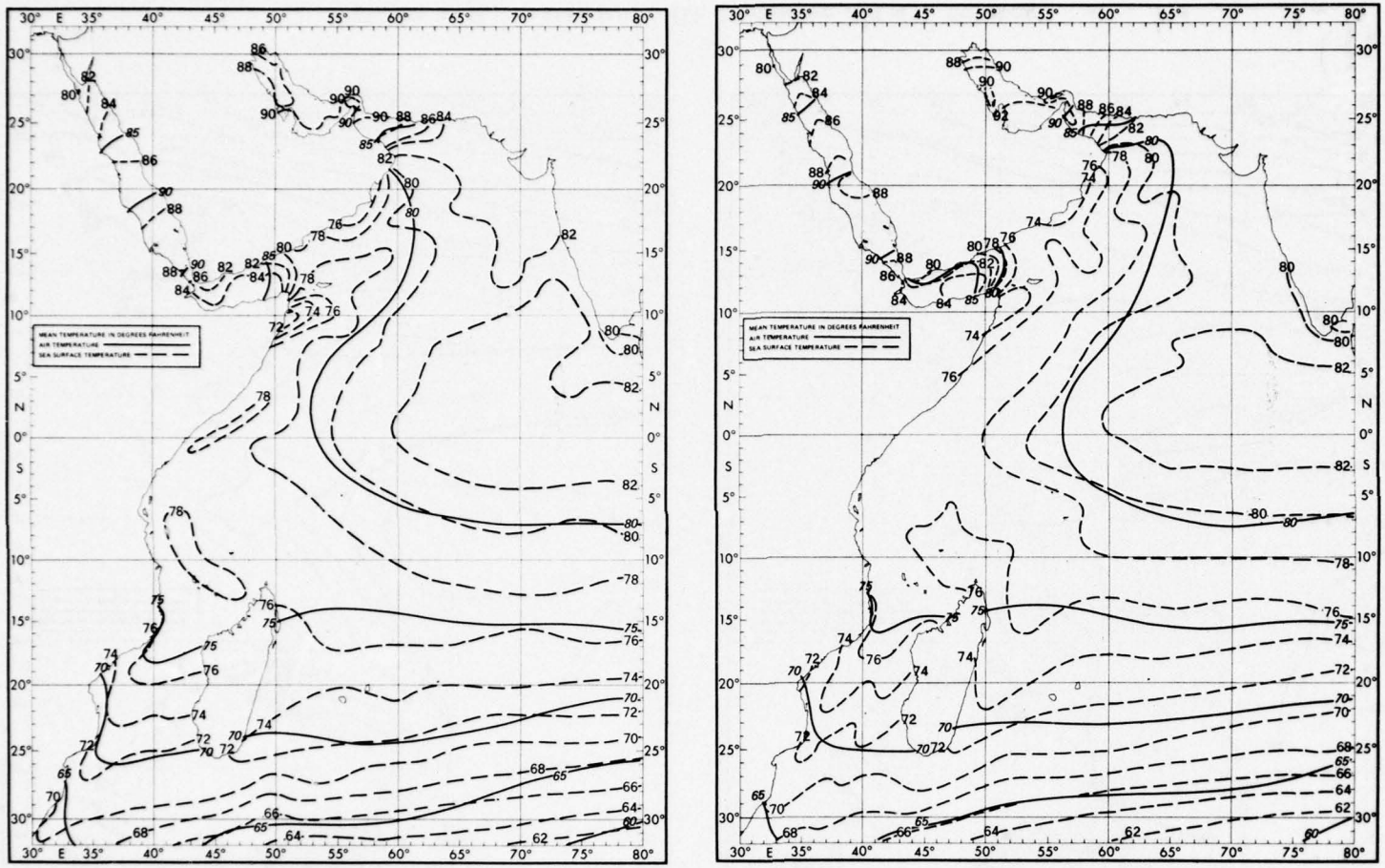

(g.) (h.)

Figure A-31, continued. (g) July and (h) August.

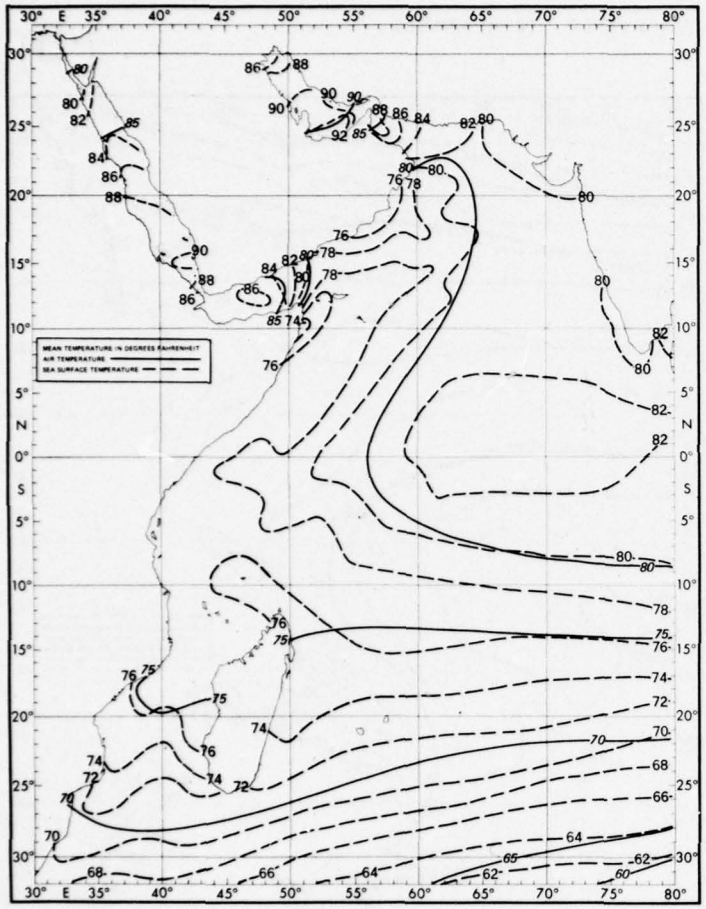

(i.)

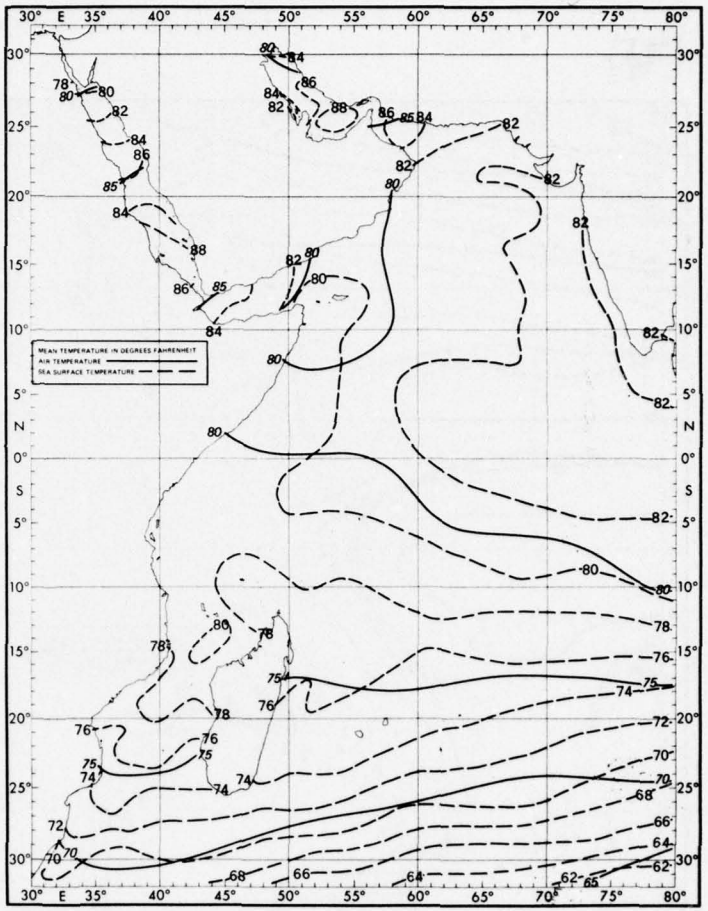

(j.)

Figure A-31, continued. (i) September and (j) October.

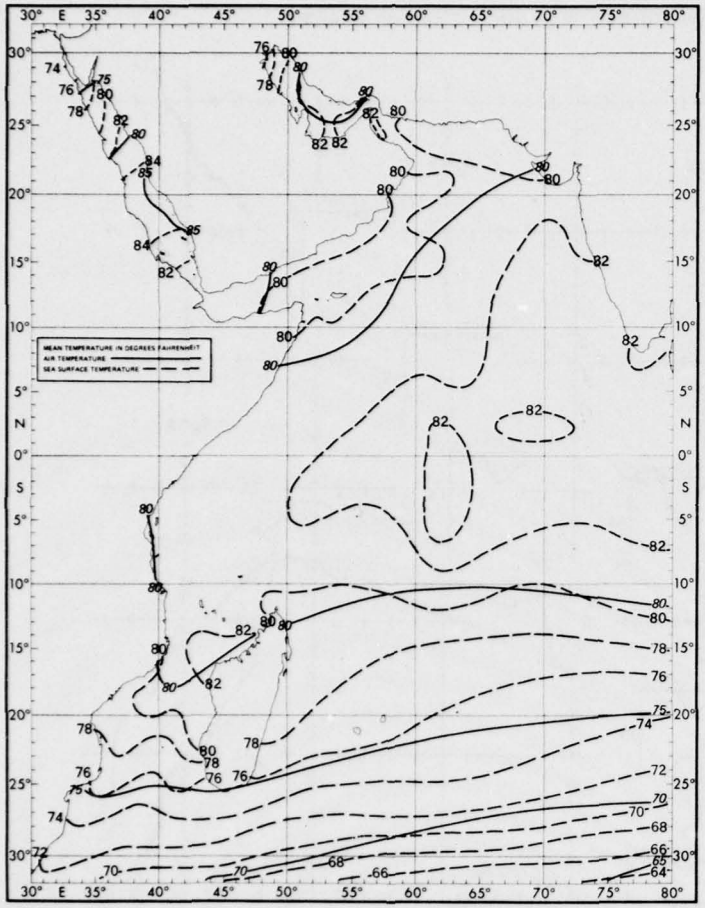

(k.)

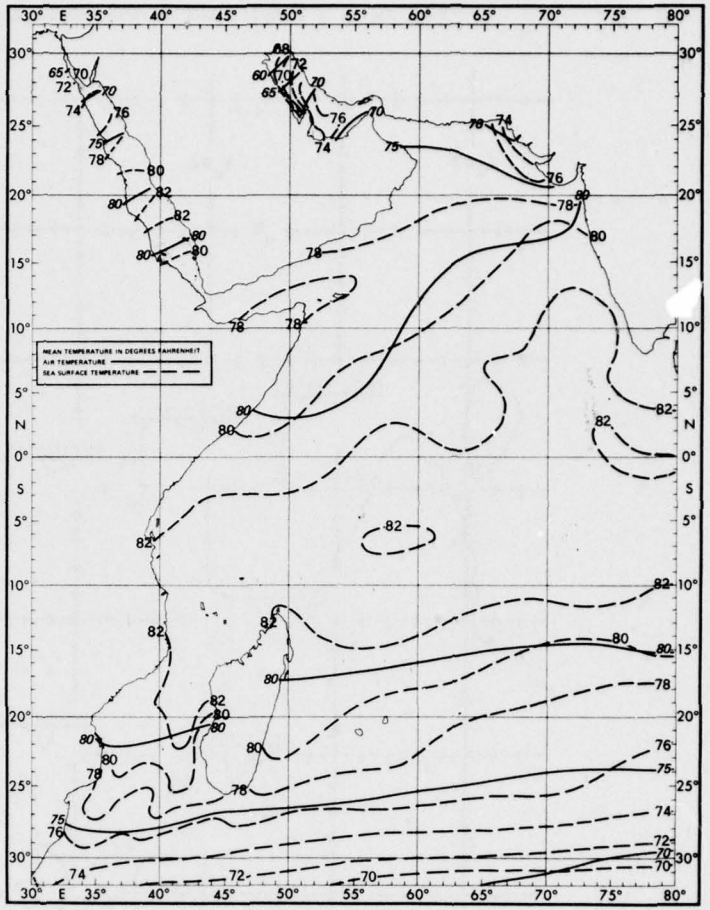

(l.)

Figure A-31, continued. (k) November and (l) December.

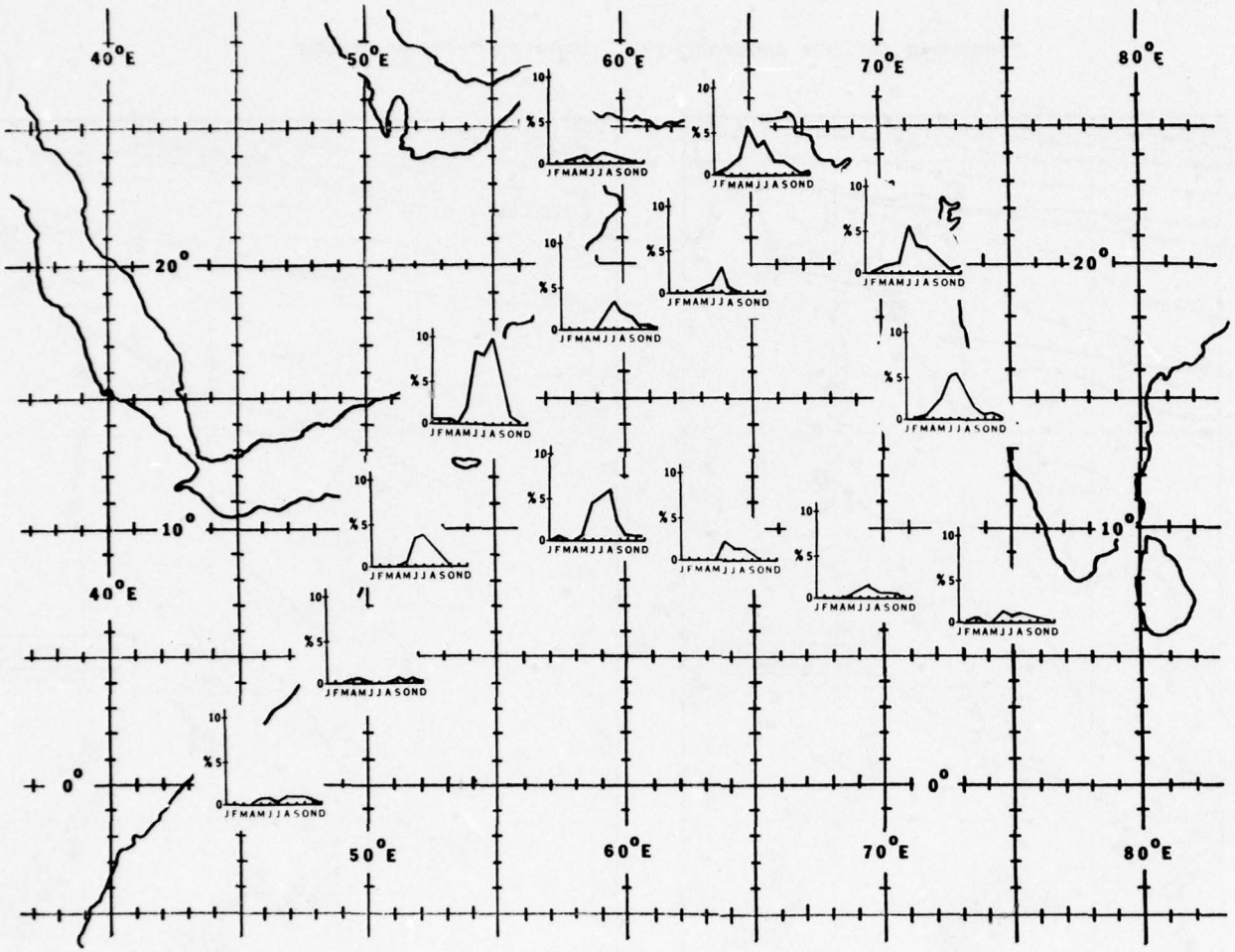

Figure A-32a. Percent frequency of visibilities less than 2 n mi for the Arabian Sea, by month.

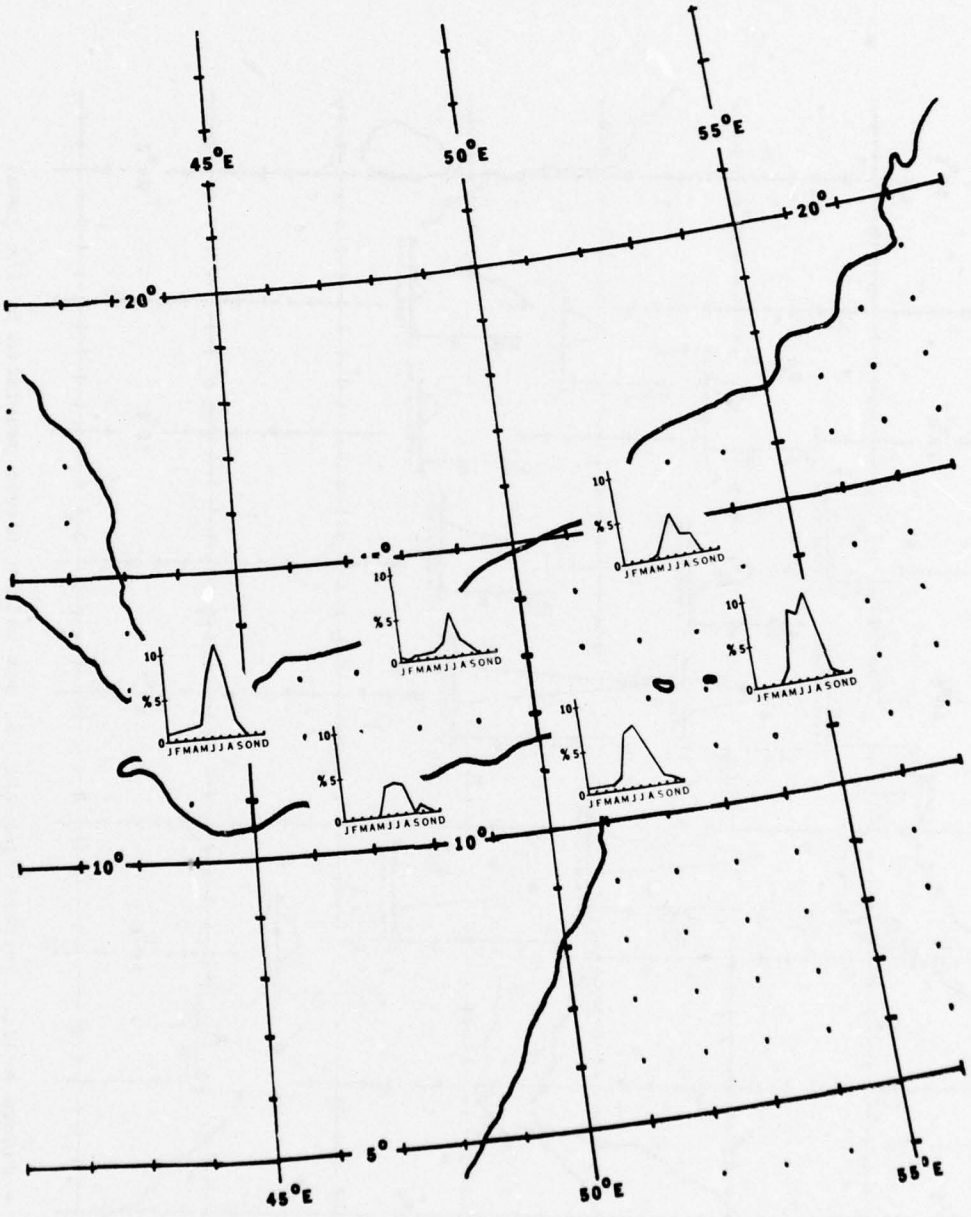

Figure A-32b. Percent frequency of visibilities less than 2 n mi for the Gulf of Aden, by month.

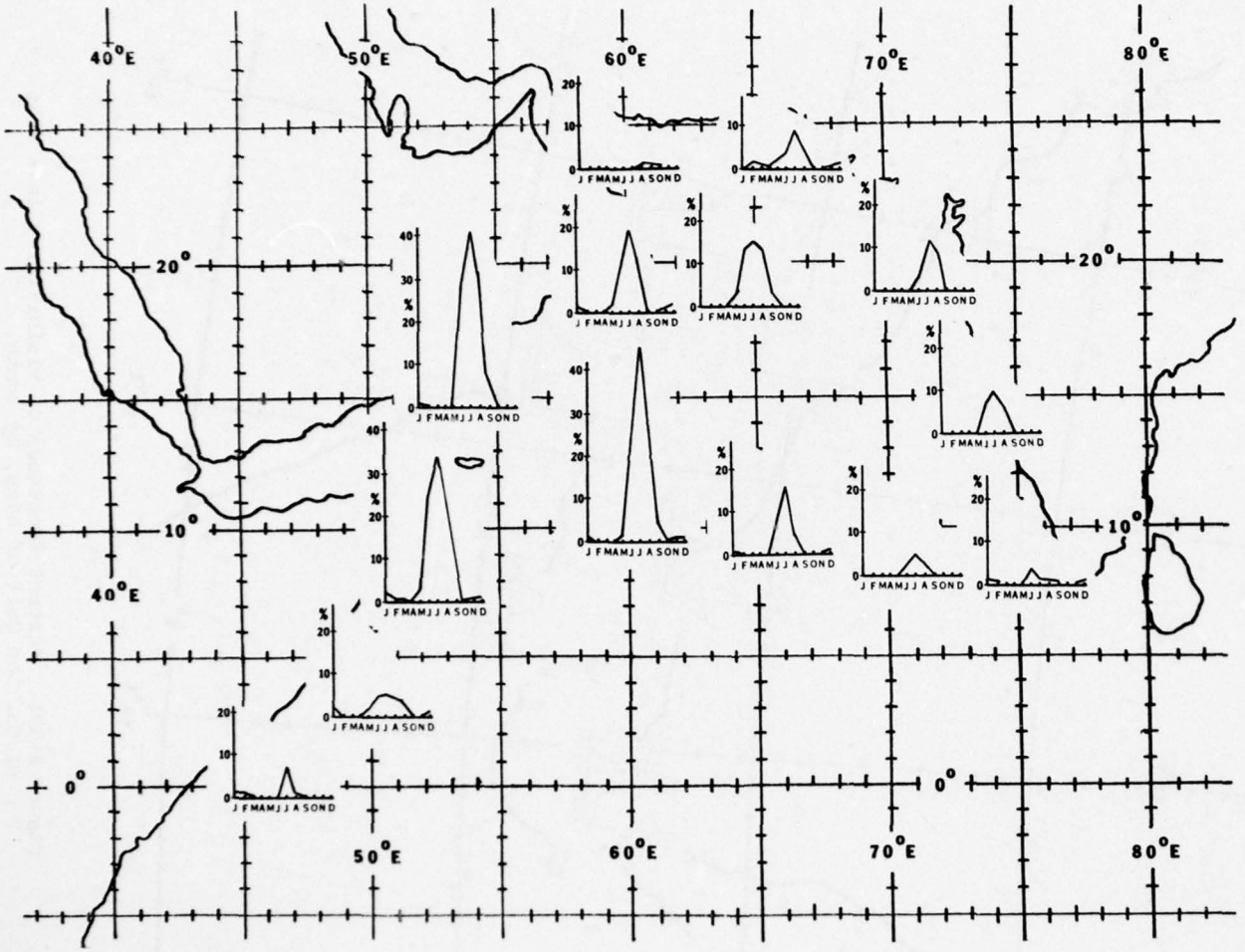

Figure A-33a. Percent frequency of sea height (waves generated by the local winds only) greater than or equal to 10 ft for the Arabian Sea, by month.

Figure A-33b. Percent frequency of sea height (waves generated by the local winds only) greater than or equal to 10 ft for the Gulf of Aden, by month.

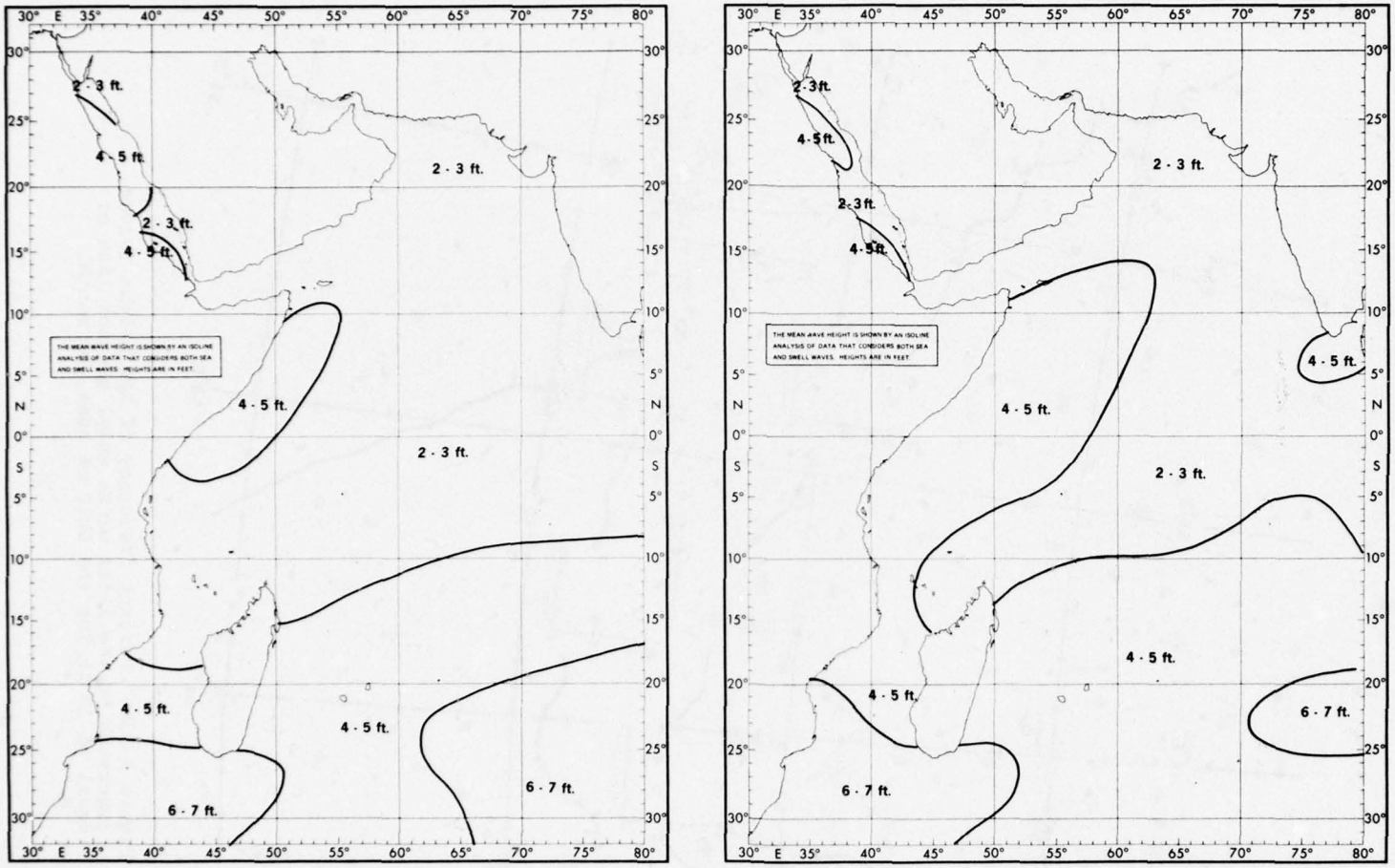

Figure A-34. Monthly charts of mean wave heights (ft). Data include both sea and swell waves. If both are present in an observation, the higher of the two is used (from U.S. Naval Weather Service Command, 1974a). (a) January and (b) February.

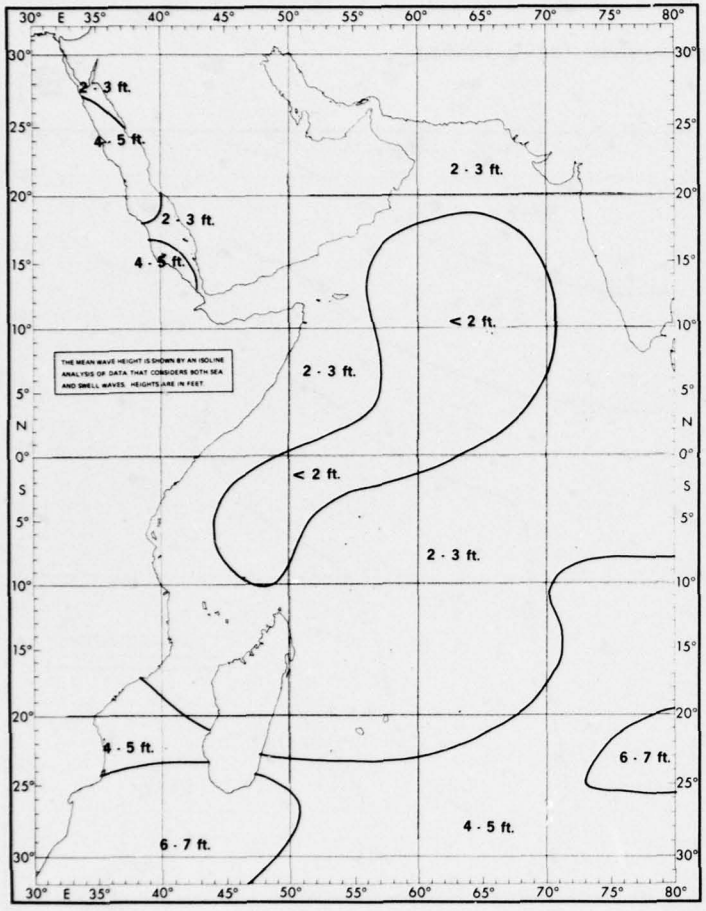

(c.)

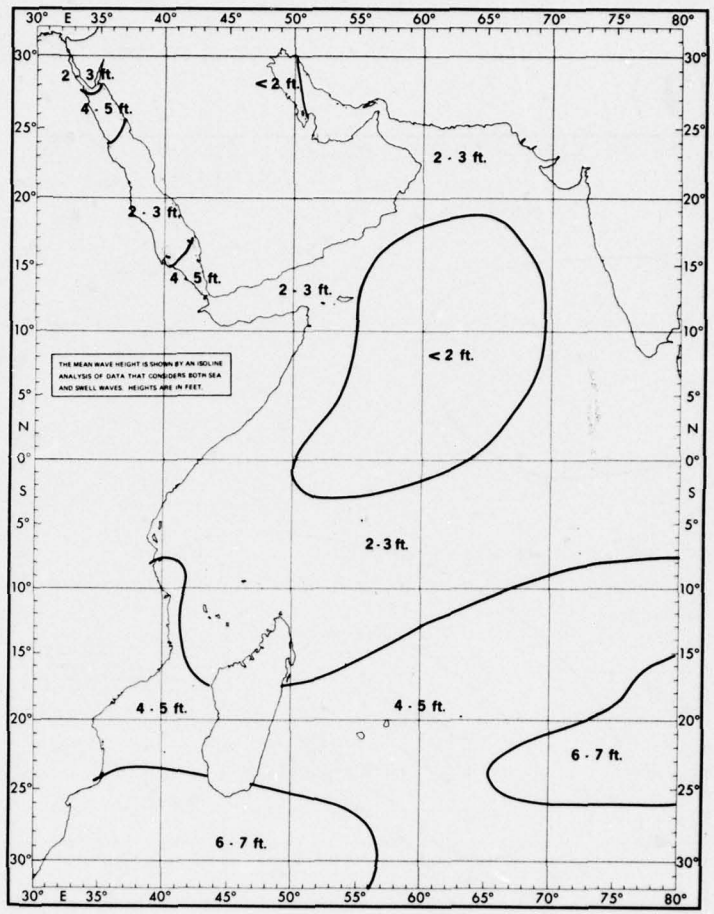

(d.)

Figure A-34, continued. (c) March and (d) April.

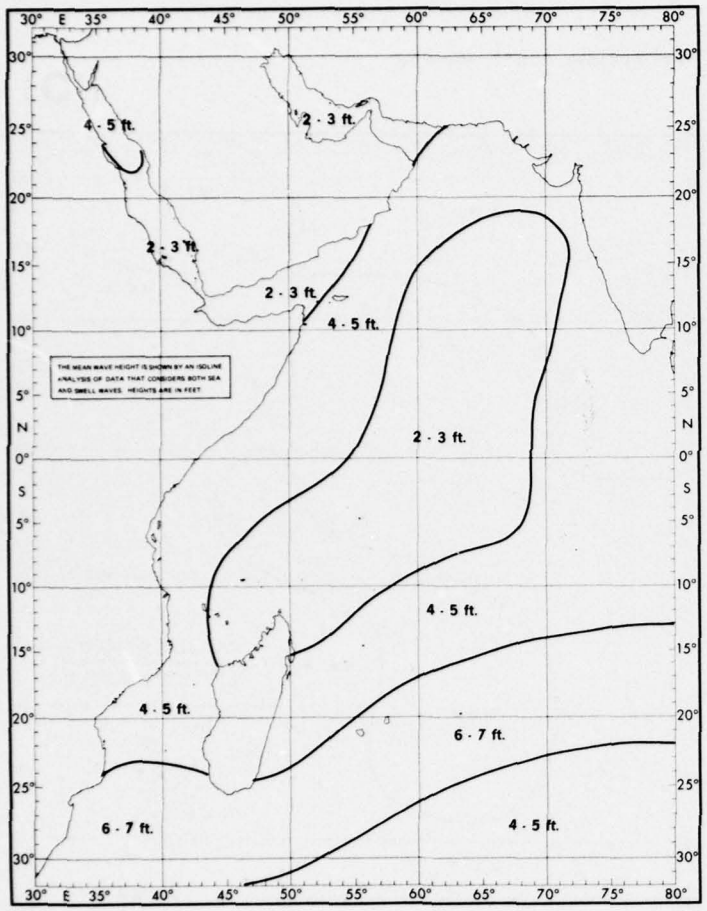

(e.)

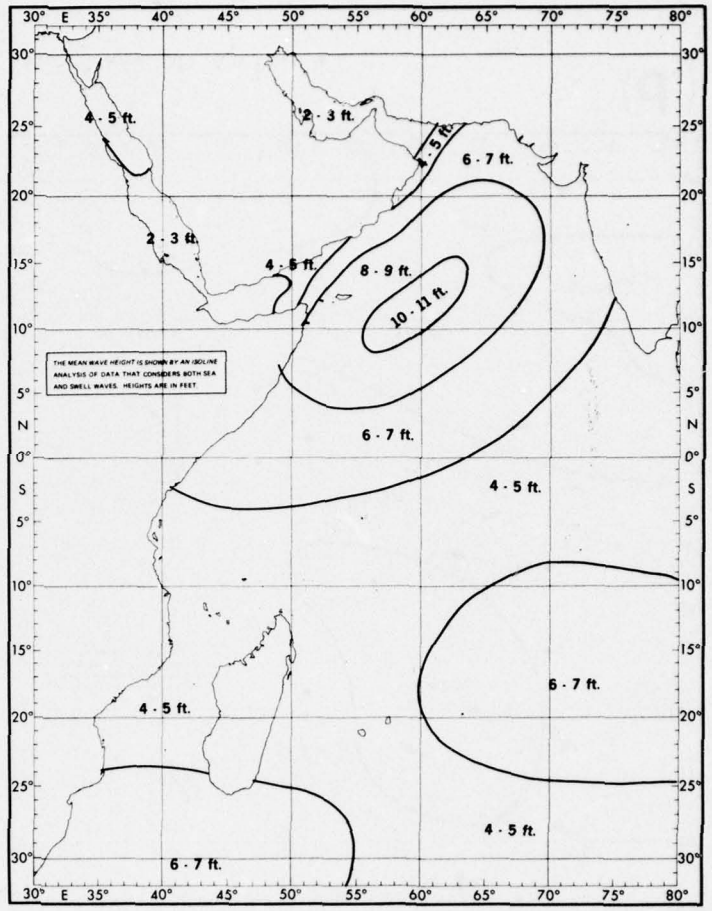

(f.)

Figure A-34, continued. (e) May and (f) June.

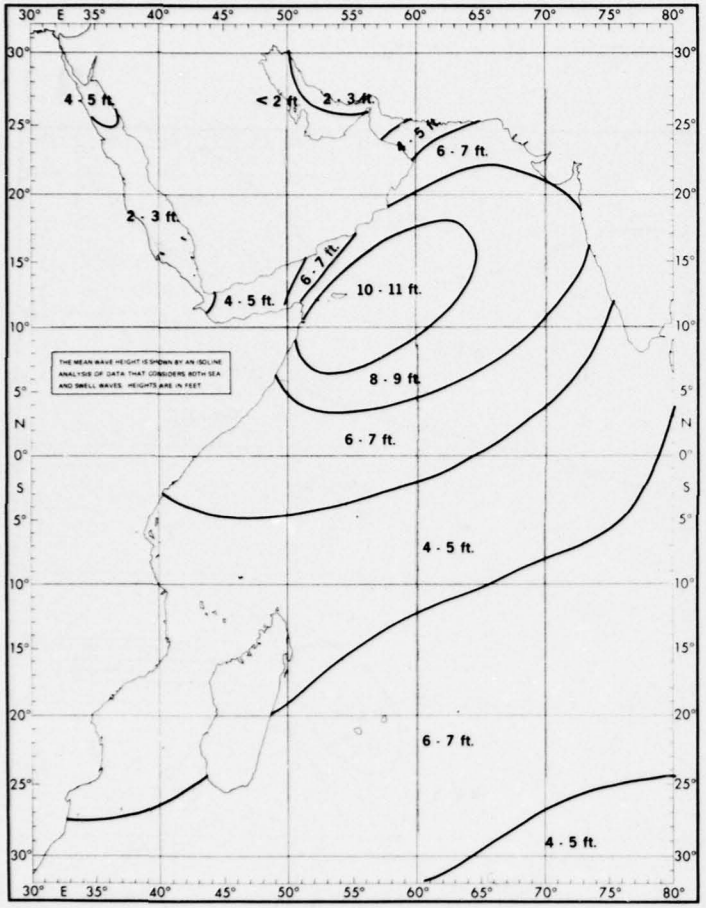

(g.)

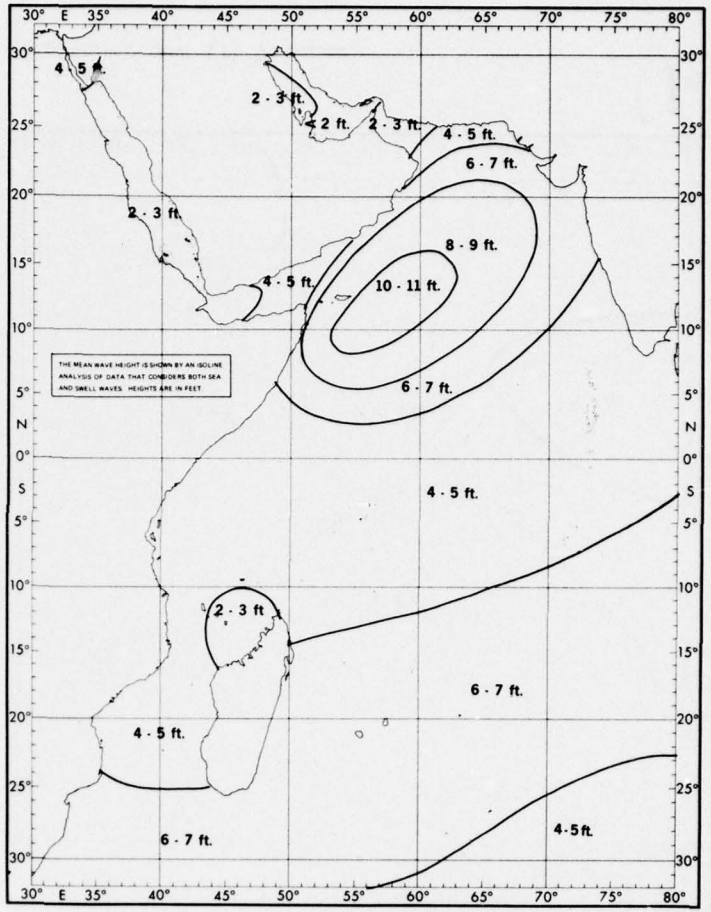

(h.)

Figure A-34, continued. (g) July and (h) August.

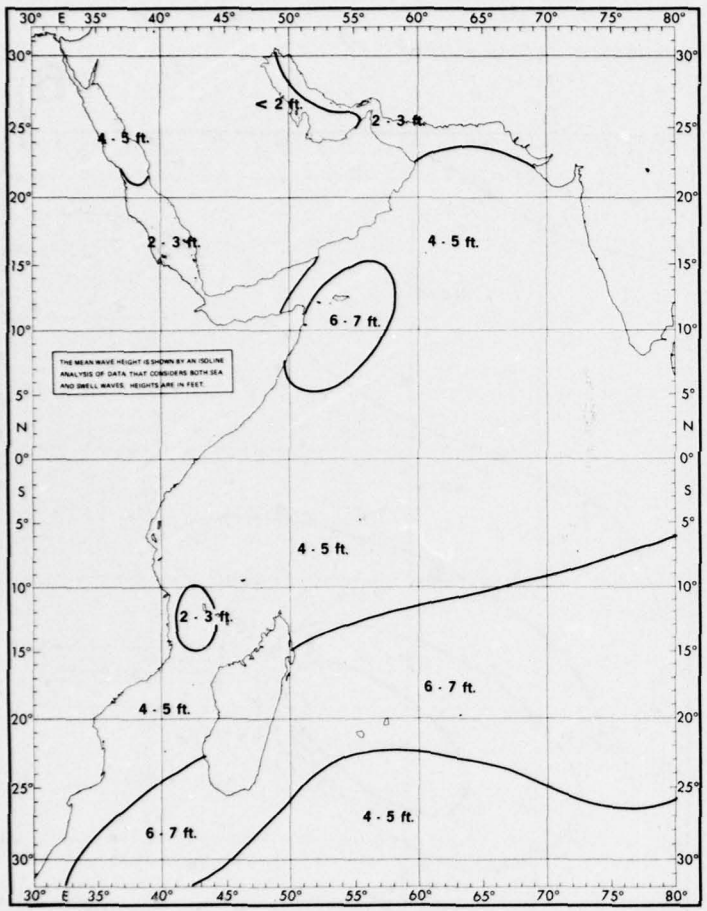

(i.)

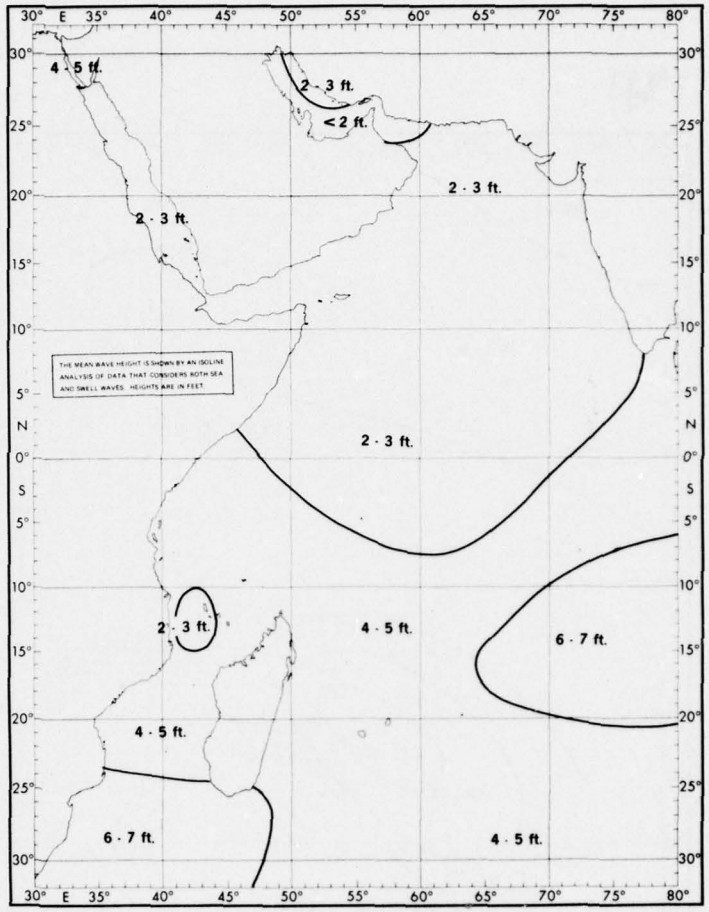

(j.)

Figure A-34, continued. (i) September and (j) October.

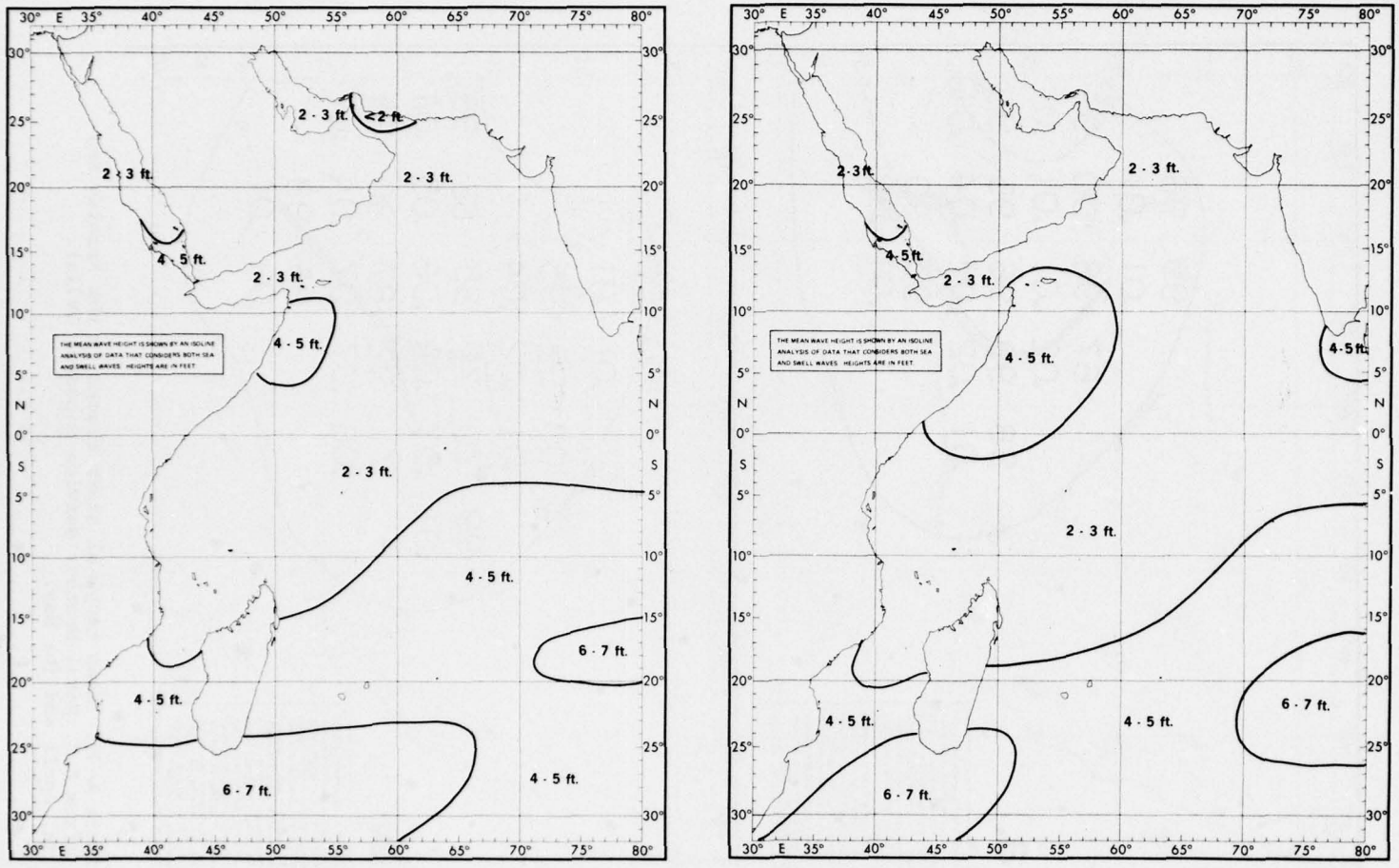

(k.) (l.)

Figure A-34, continued. (k) November and (l) December.

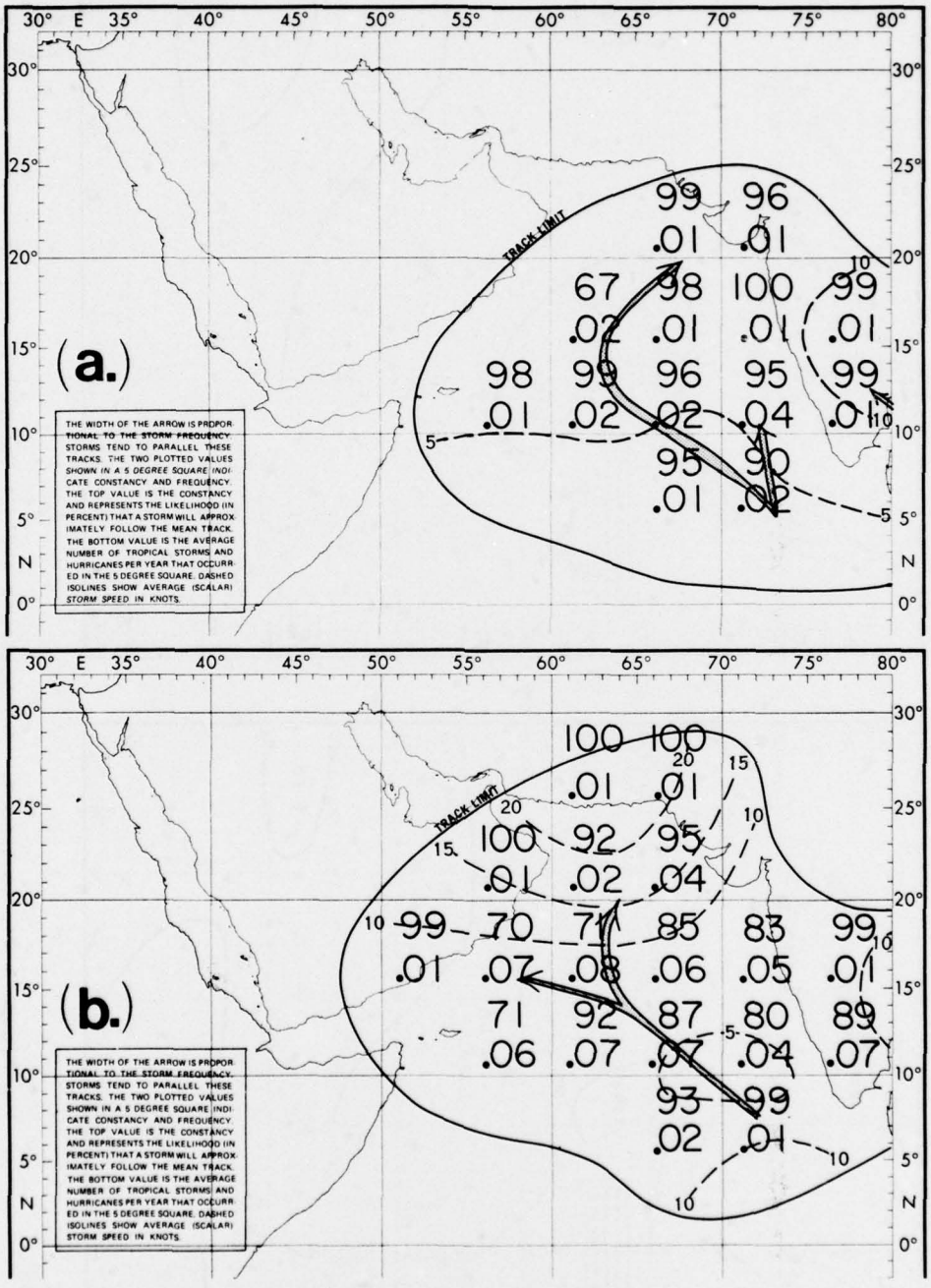

Figure A-35. Mean tropical storm tracks in the Arabian Sea (from U.S. Naval Weather Service Command, 1974a). (a) April and (b) May.

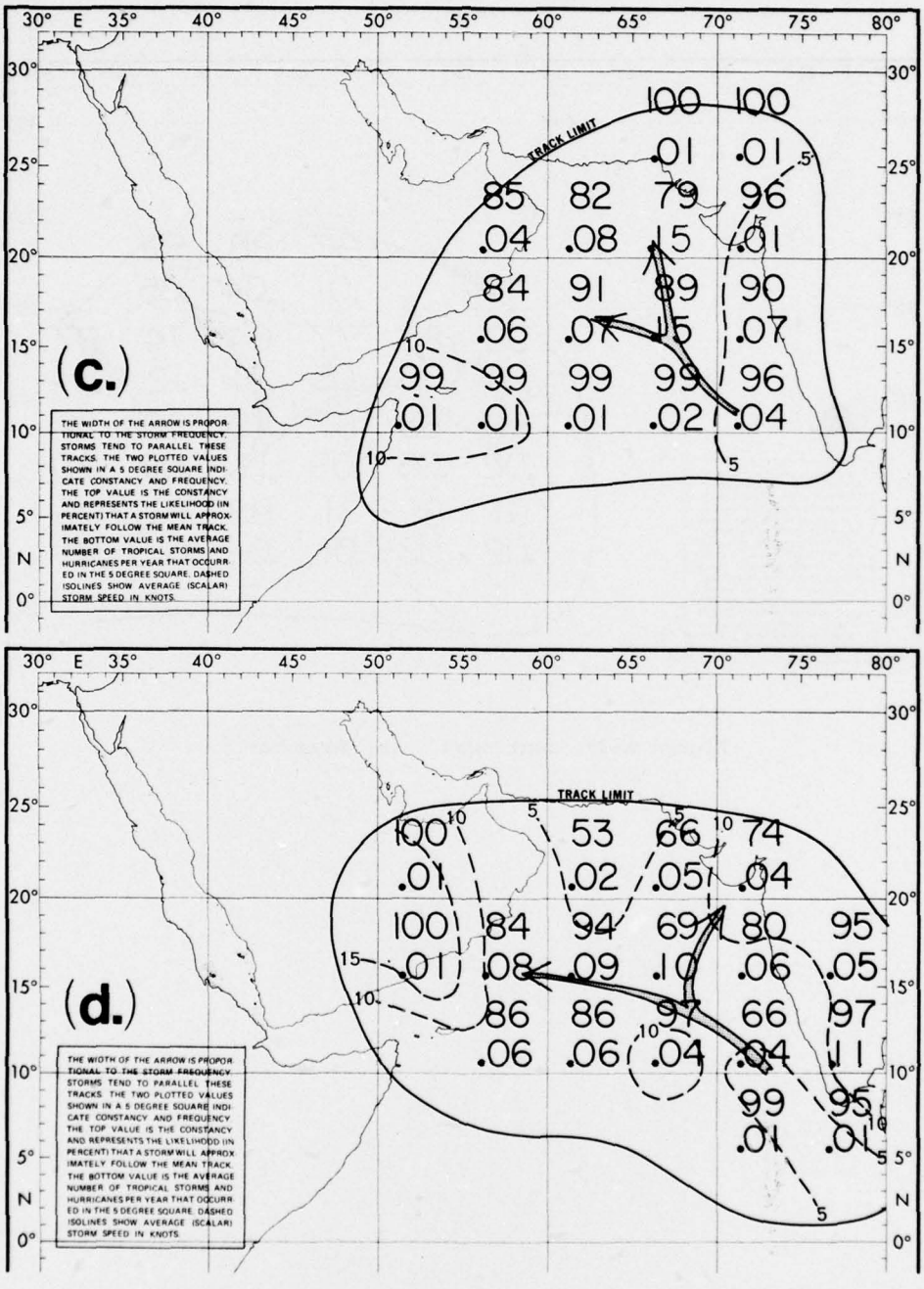

Figure A-35, continued. (c) June and (d) October.

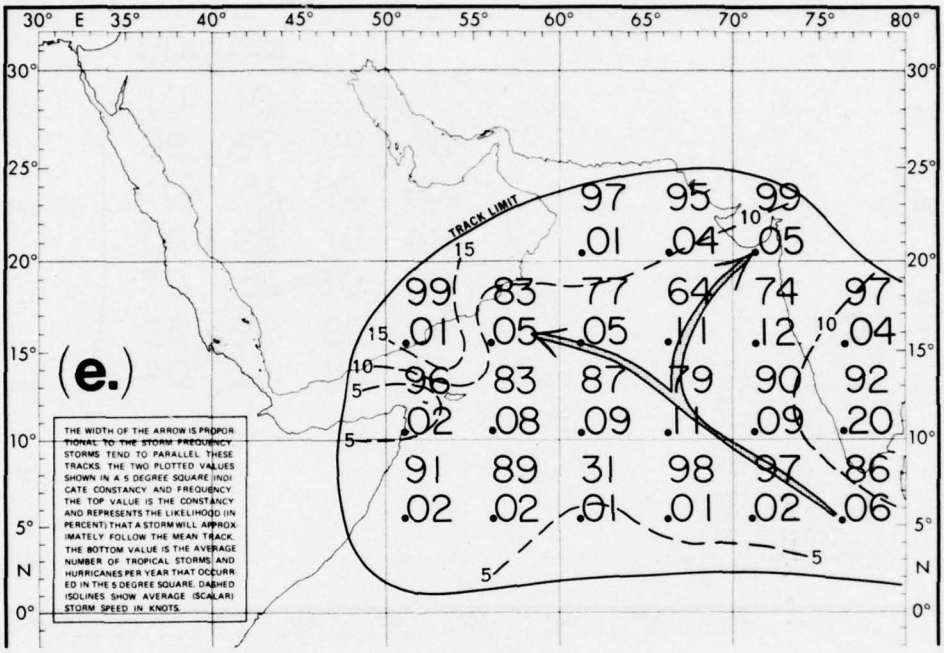

Figure A-35, continued. (e) November.

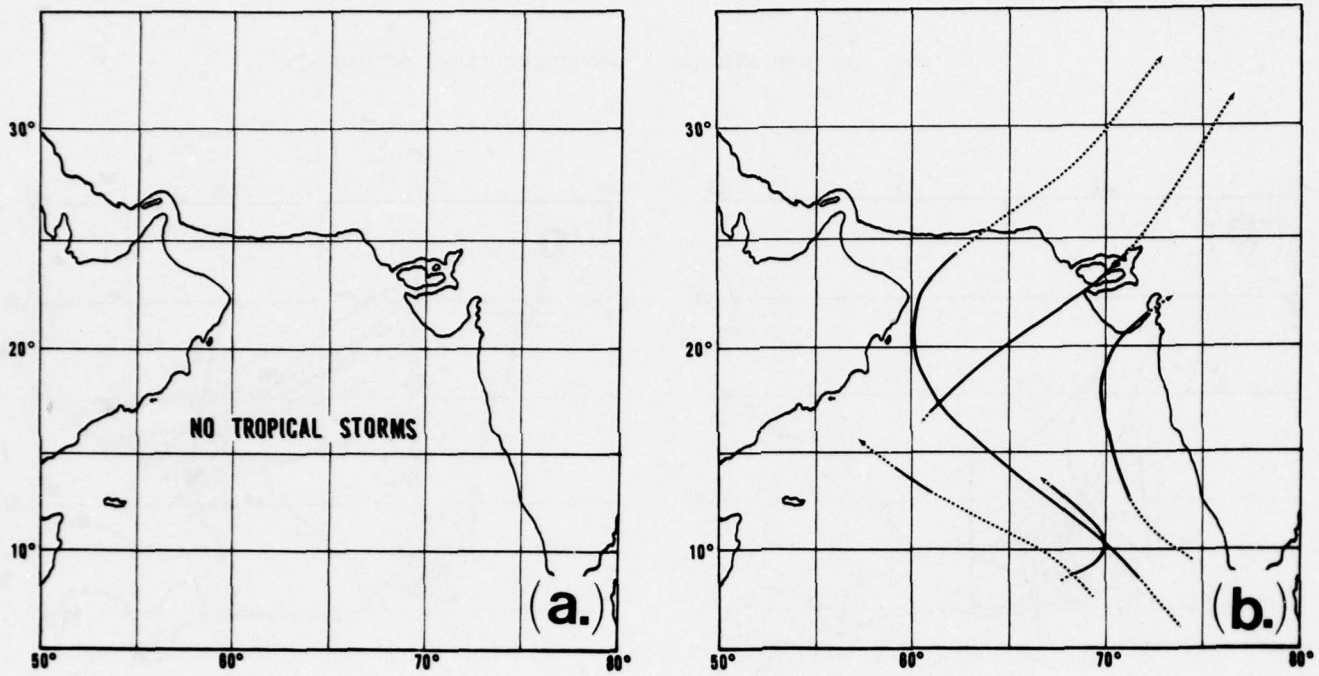

Figure A-36. Tracks of tropical cyclones which reached tropical storm intensity in the Arabian Sea (dotted line indicates depression stage). The period of record is 1891-1970. (Tracks through 1960 from Indian Meteorological Department, 1964.) (a) January, February and March; (b) April.

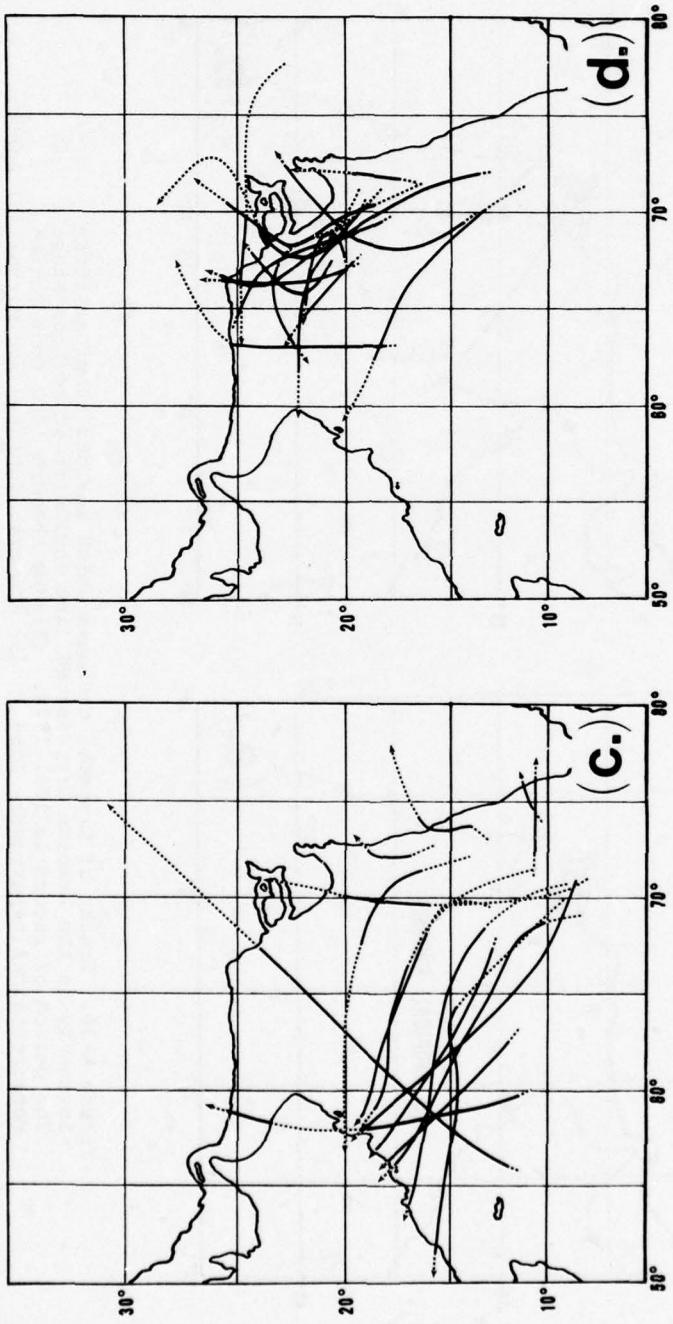

Figure A-36, continued. (c) May and (d) June.

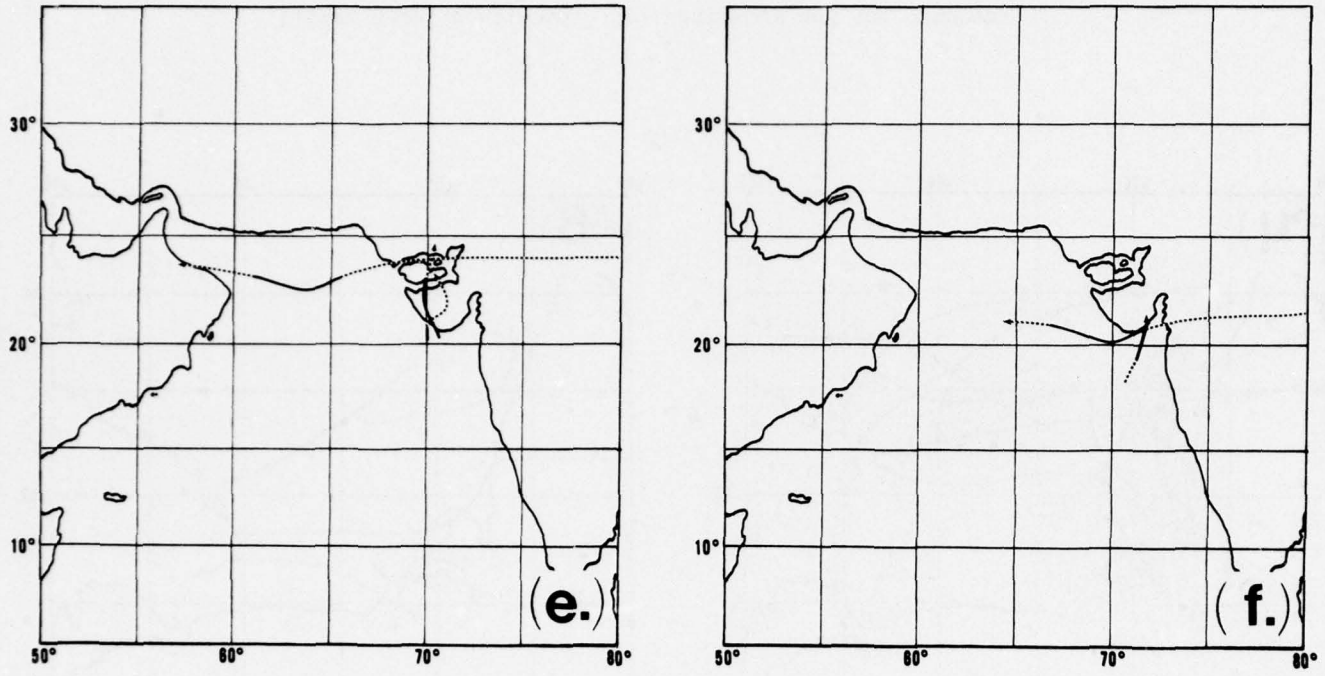

Figure A-36, continued. (e) July and (f) August.

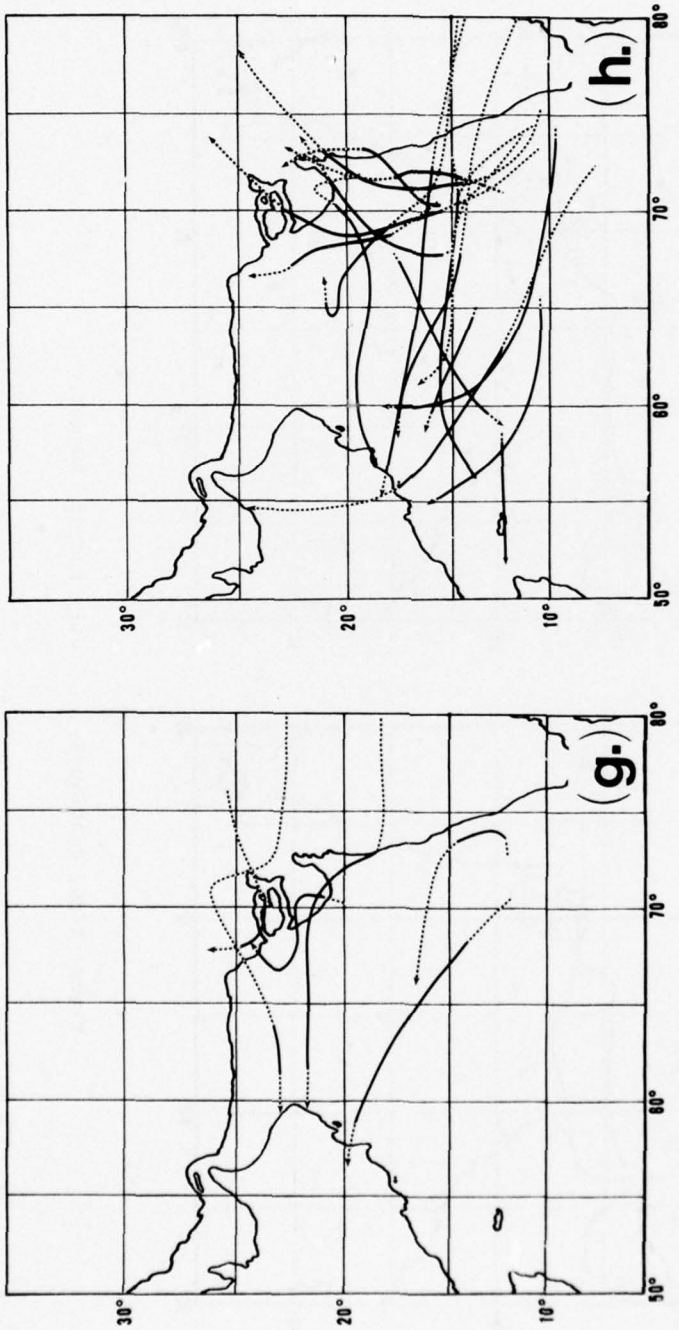

Figure A-36, continued. (g) September and (h) October.

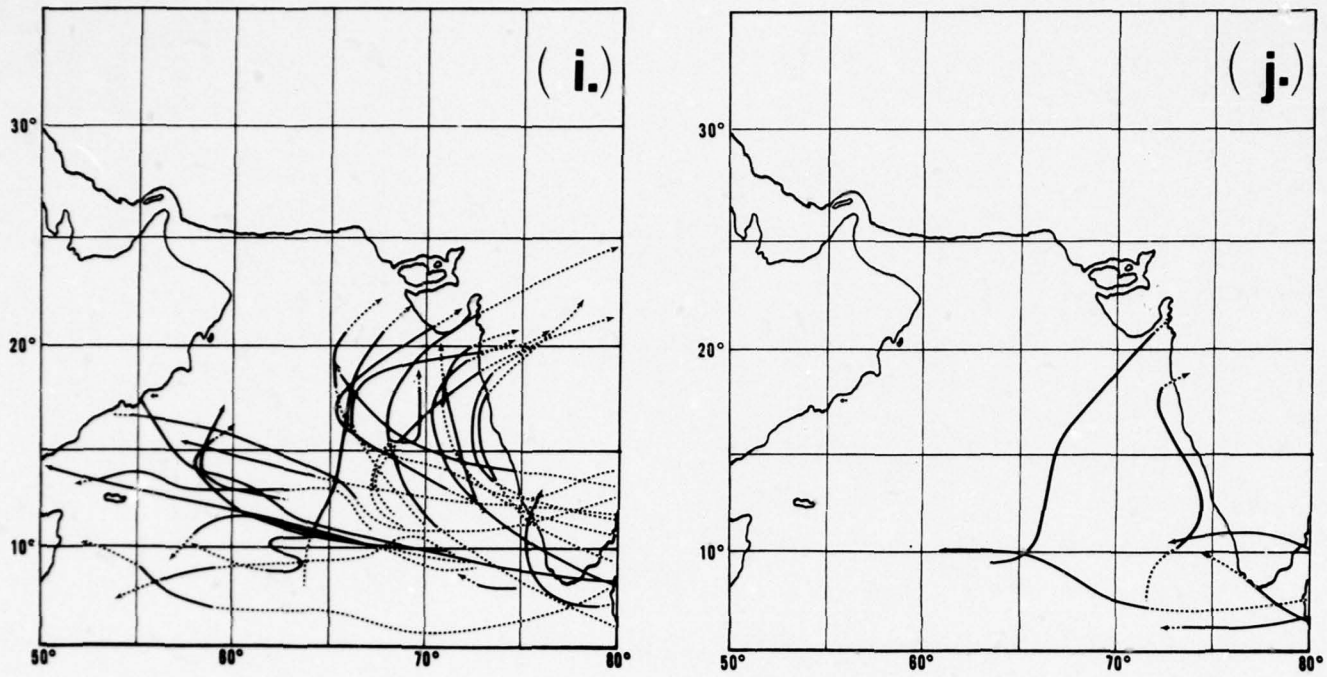

Figure A-36, continued. (i) November and (j) December.

APPENDIX B
SATELLITE PHOTOGRAPHS SHOWING TROPICAL STORM DEVELOPMENT IN THE ARABIAN SEA

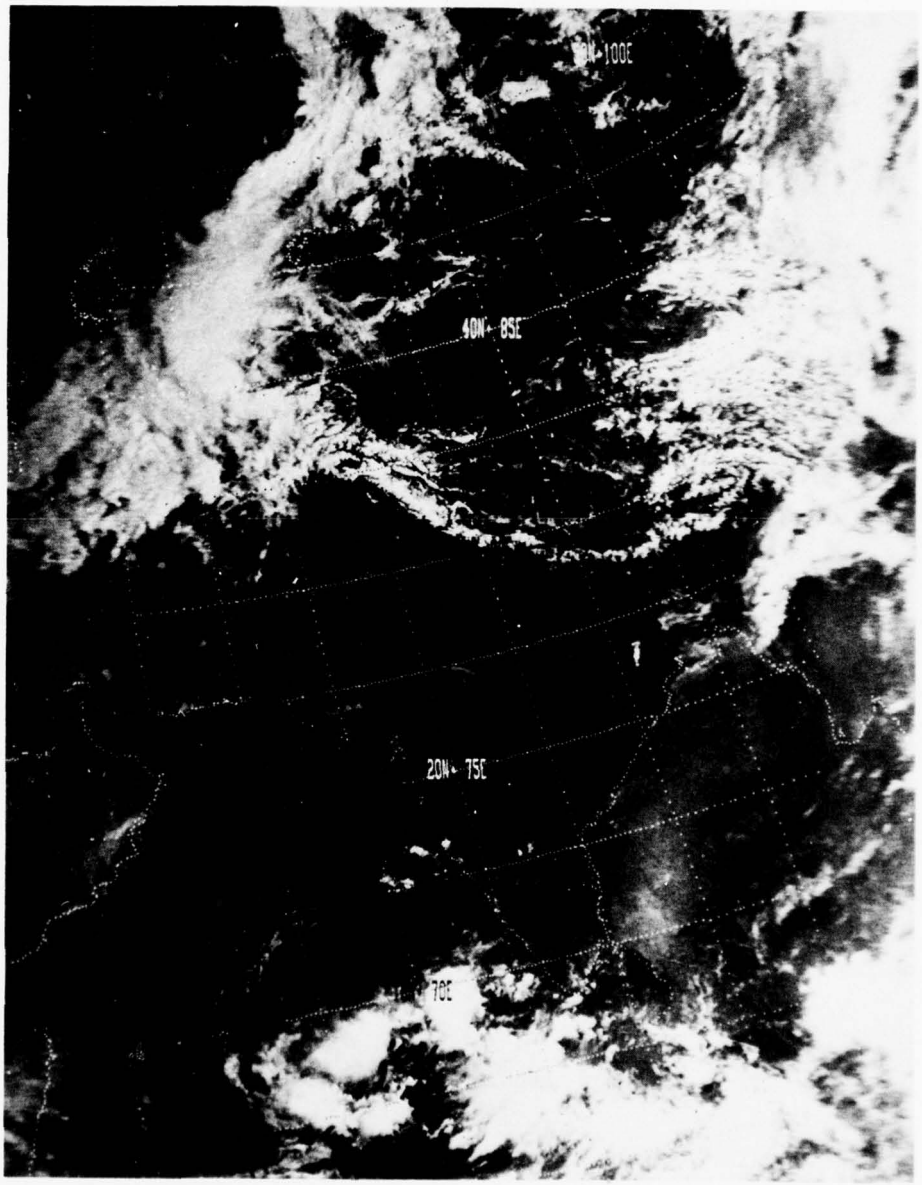

Figure B-1. 12 April 1974, 0326 GMT (NOAA-3).

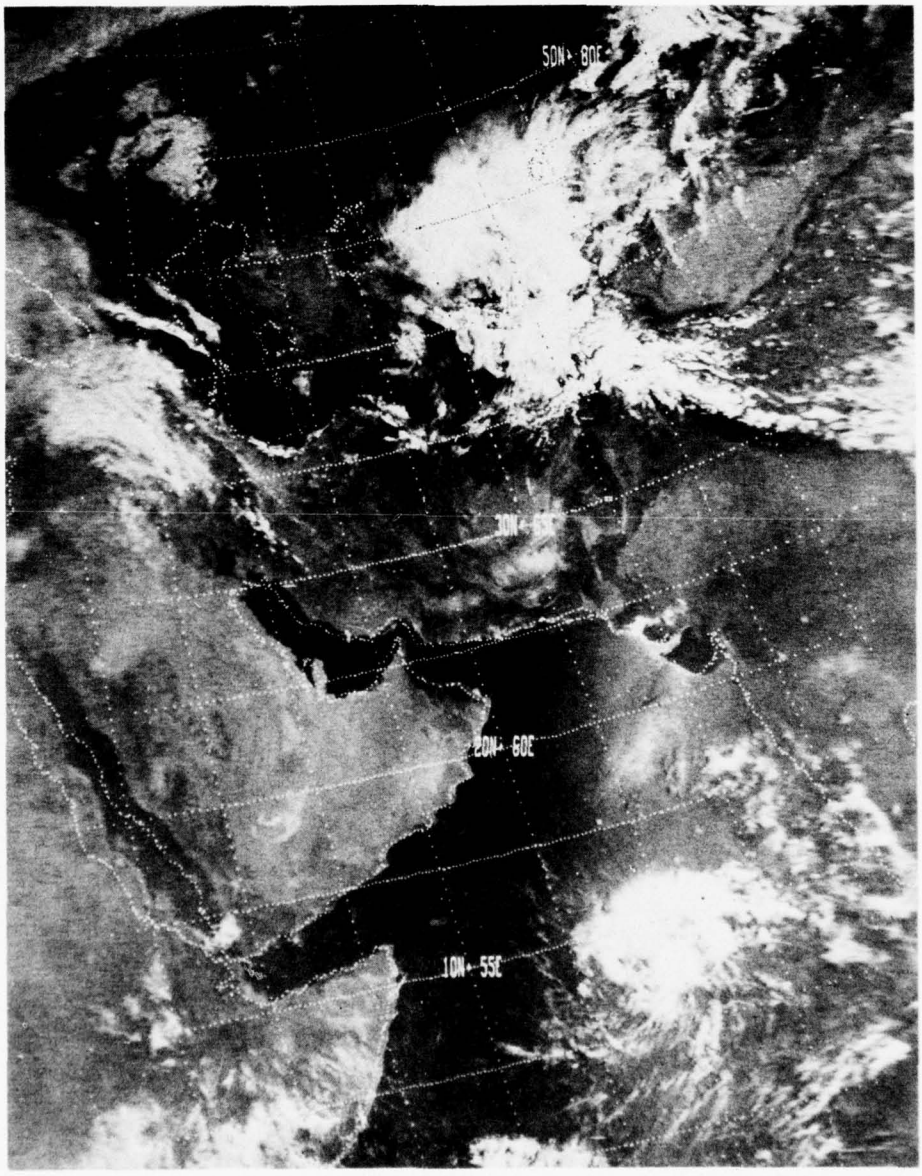

Figure B-2. 13 April 1974, 0436 GMT (NOAA-3).

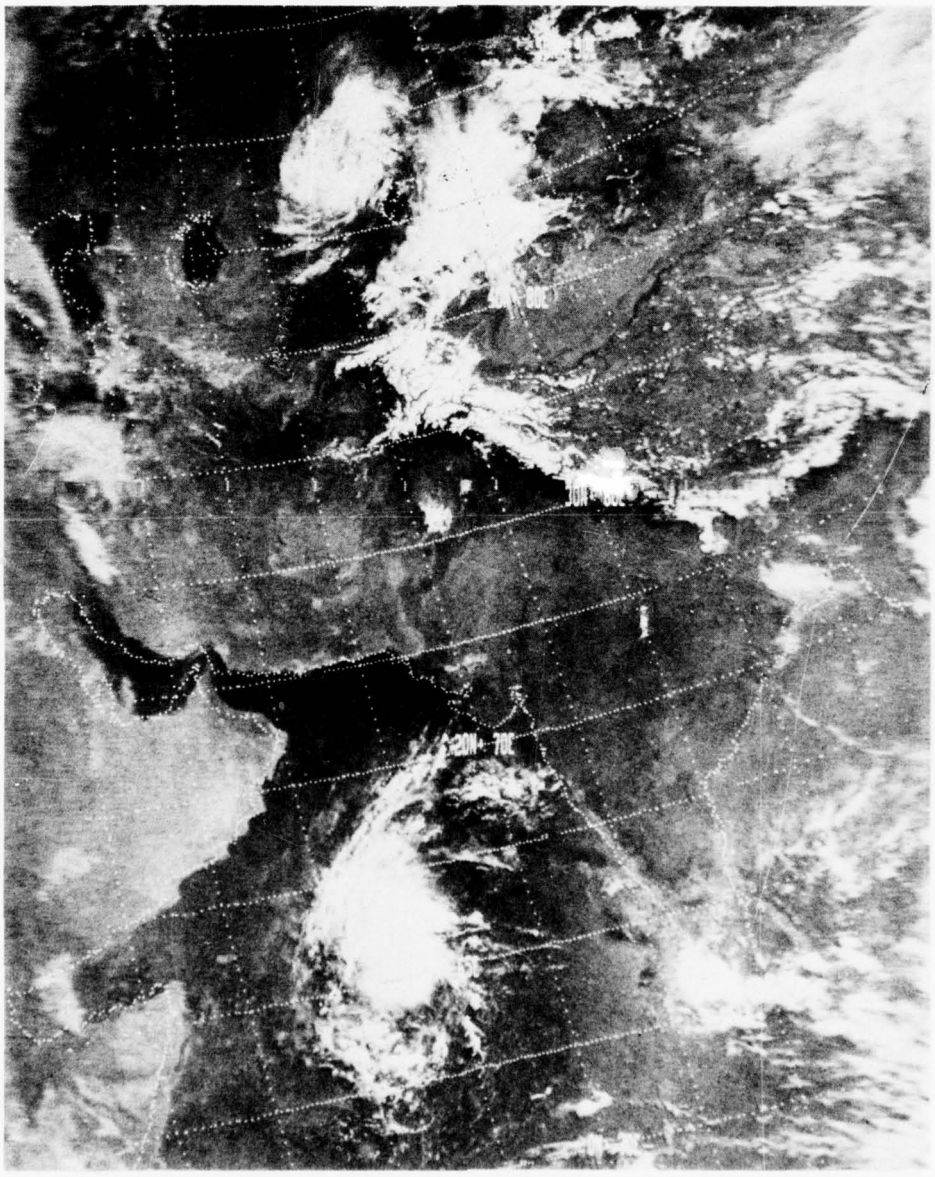

Figure B-3. 14 April 1974, 0351 GMT (NOAA-3).

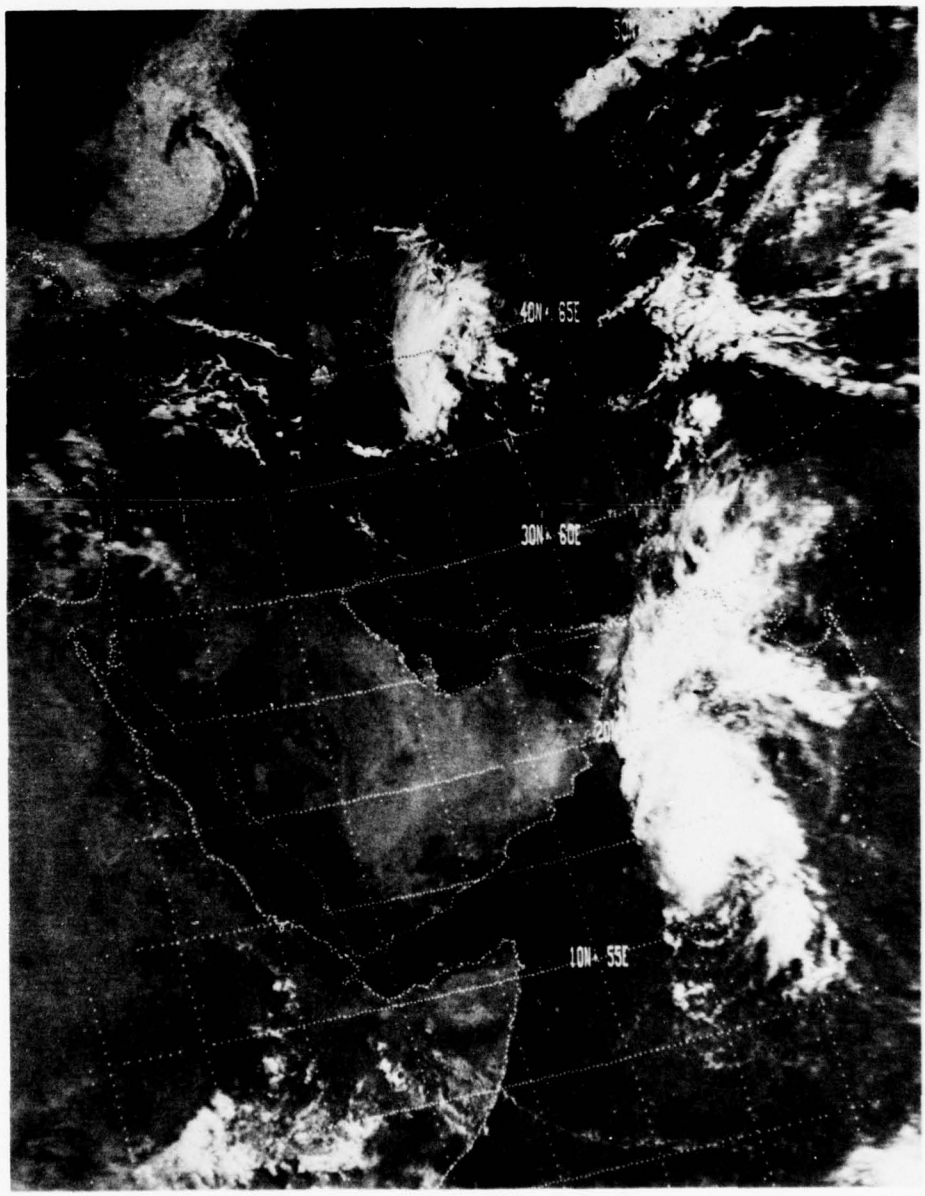

Figure B-4. 15 April 1974, 0501 GMT (NOAA-3).

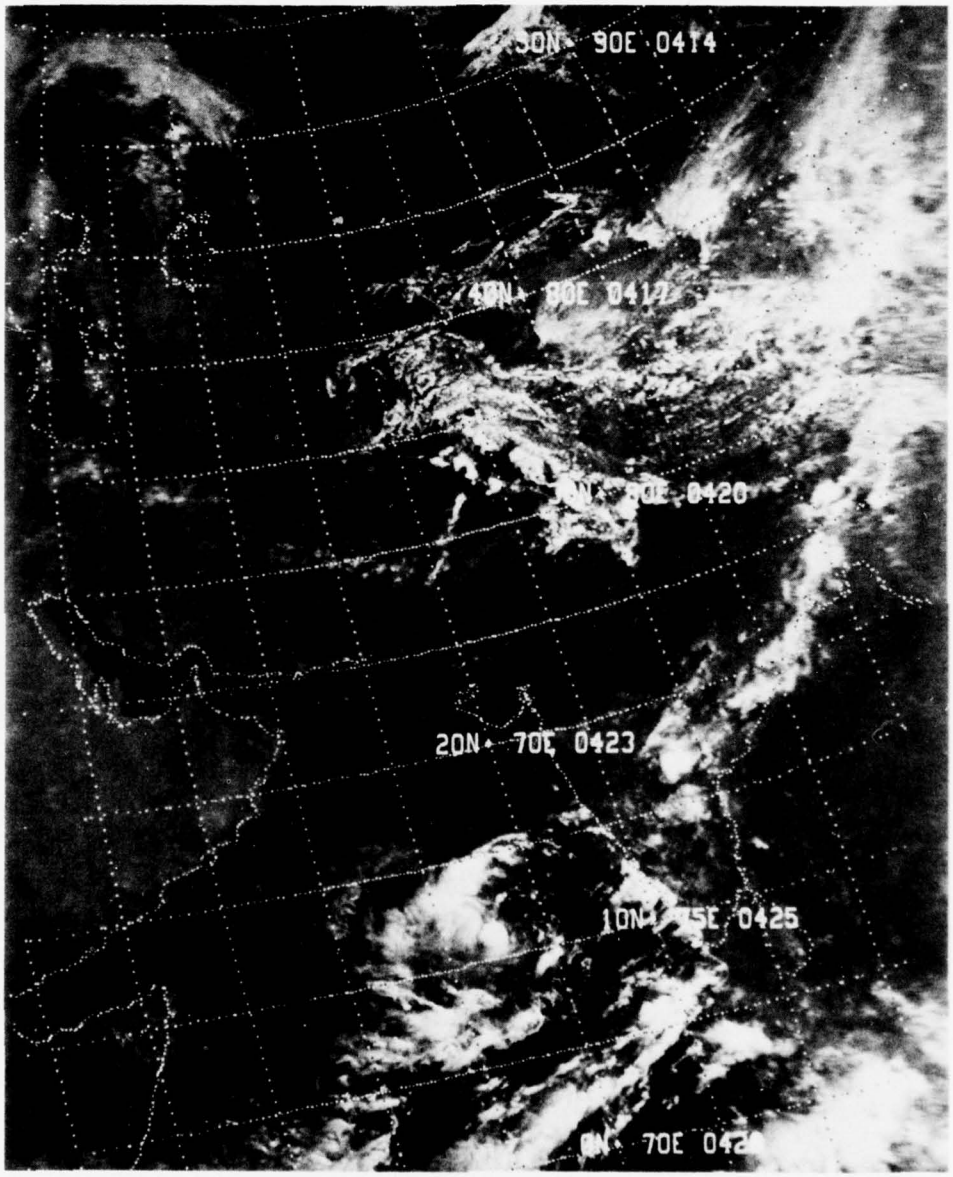

Figure B-5. 17 May 1974, 0403 GMT (NOAA-3).

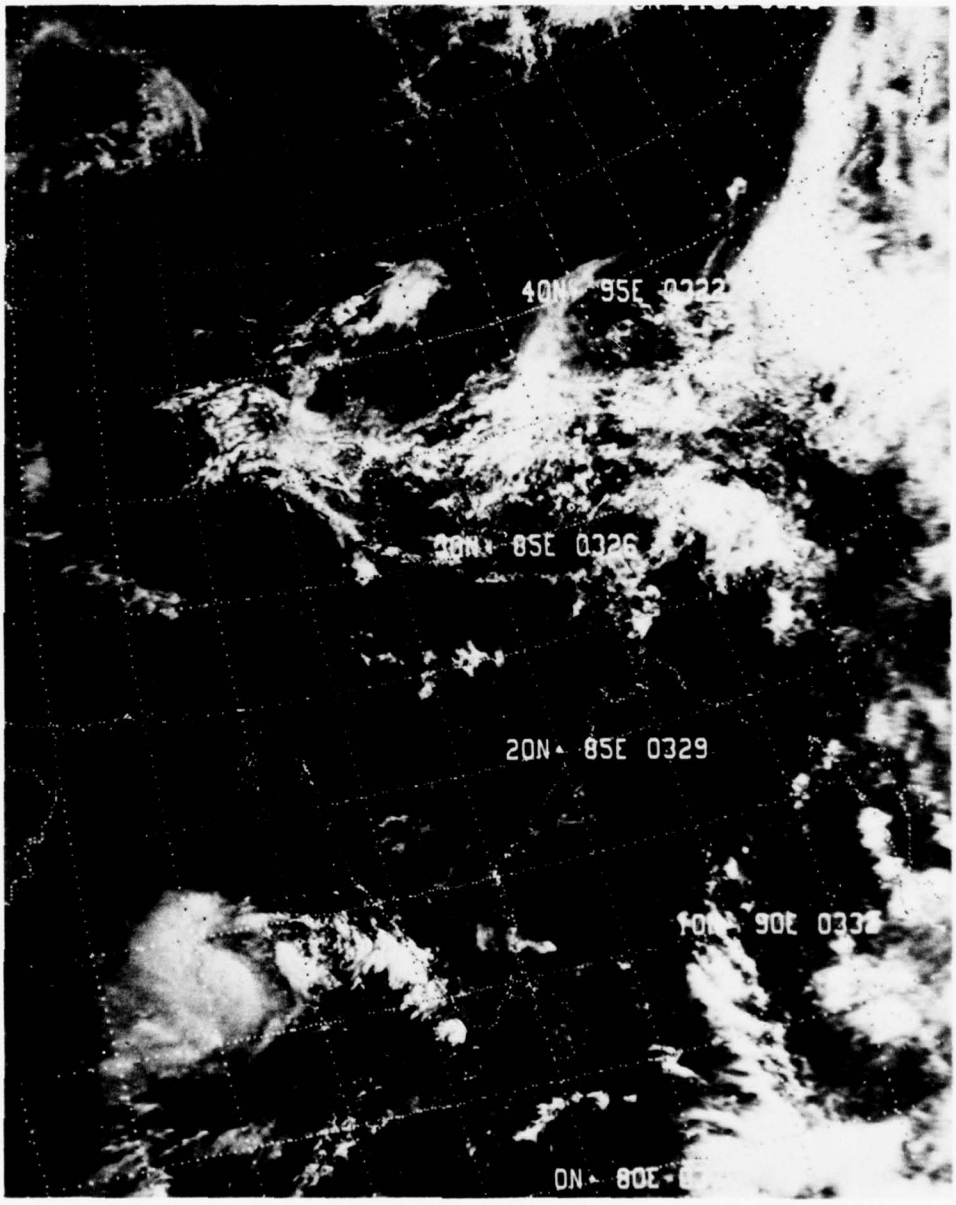

Figure B-6. 18 May 1974, 0305 GMT (NOAA-3).

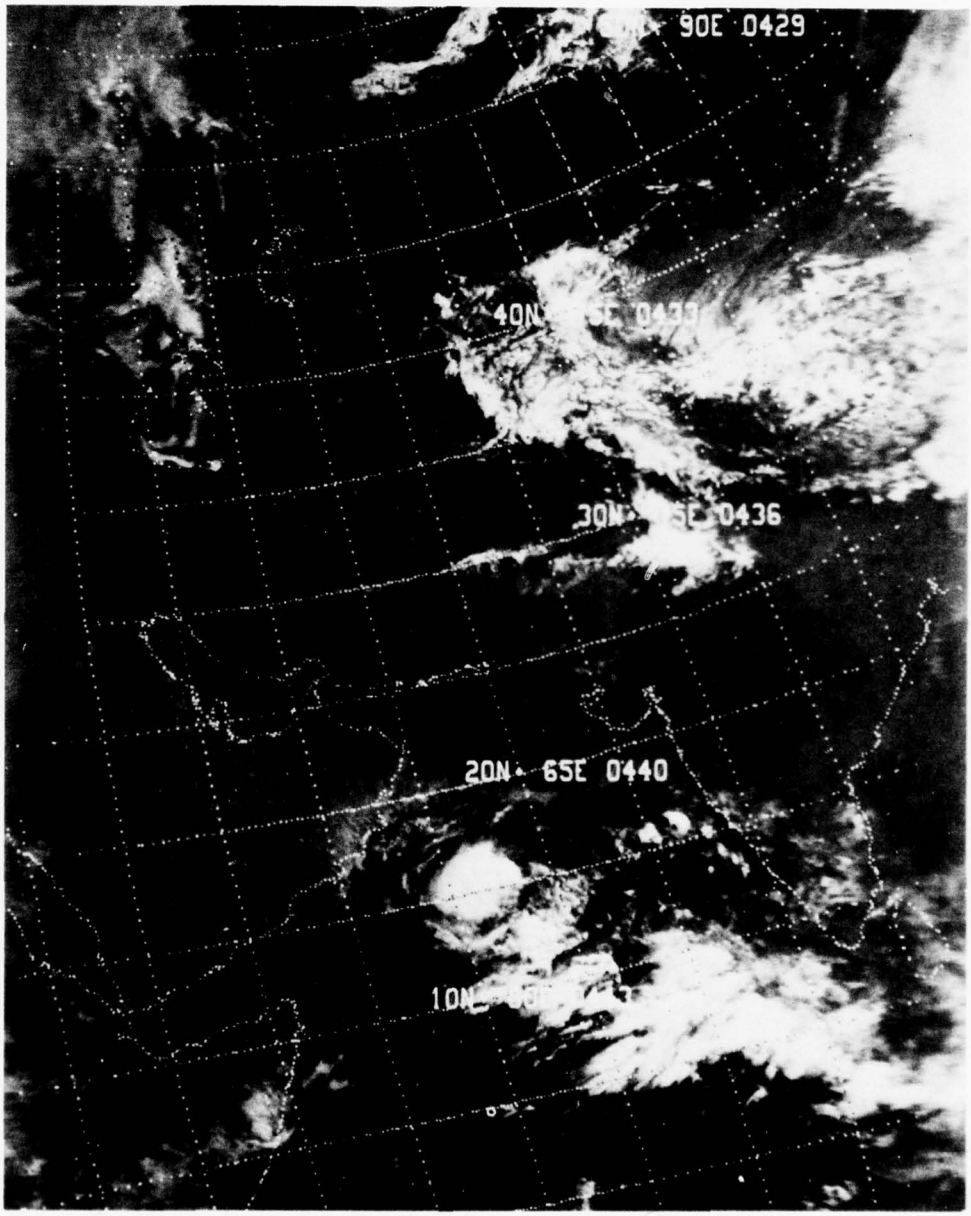

Figure B-7. 19 May 1974, 0416 GMT (NOAA-3).

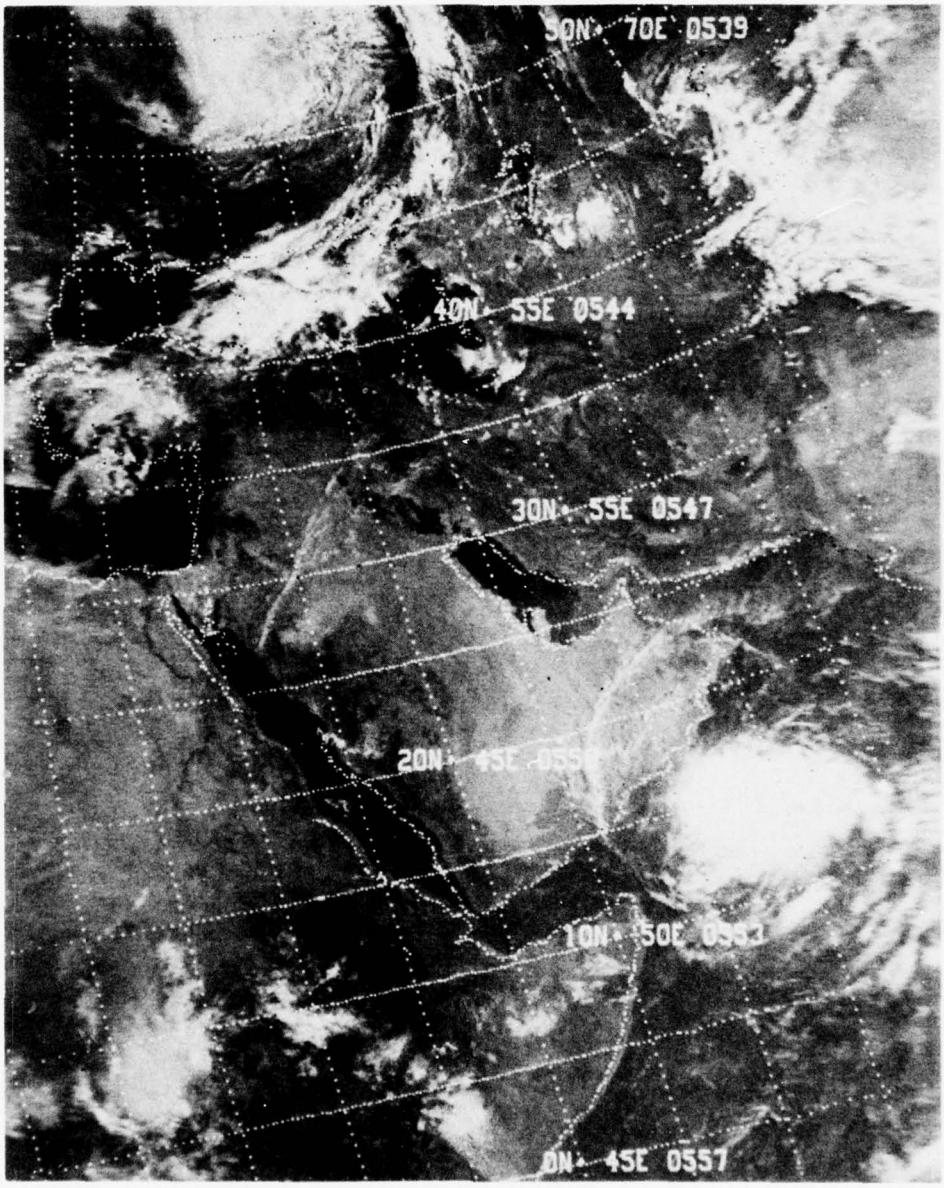

Figure B-8. 20 May 1974, 0526 GMT (NOAA-3).

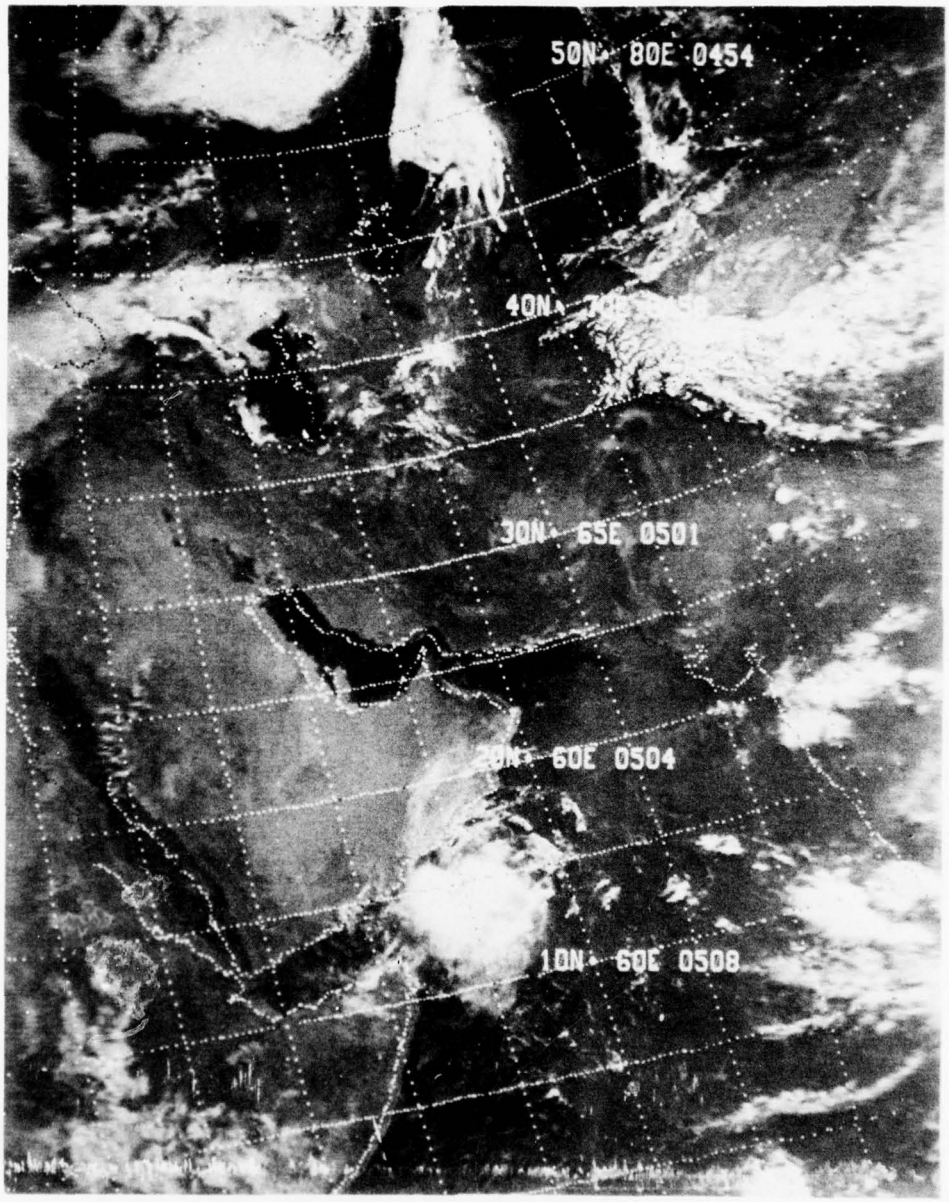

Figure B-9. 21 May 1974, 0440 GMT (NOAA-3).

APPENDIX C

TYPICAL CASE STUDIES OF WESTERN DISTURBANCES AFFECTING THE NORTHERN ARABIAN SEA

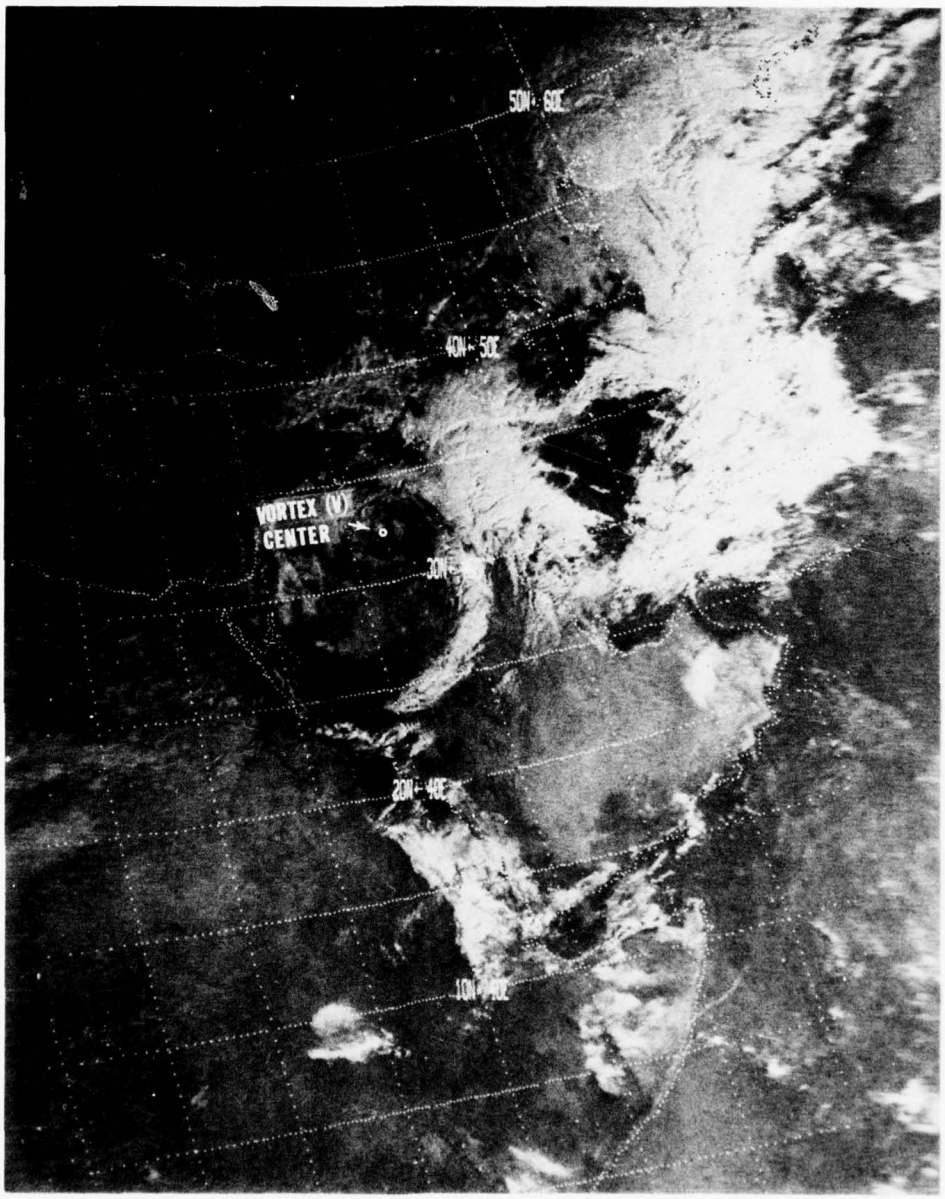

Figure C-1a. 24 January 1974, 0555 GMT (NOAA-2).

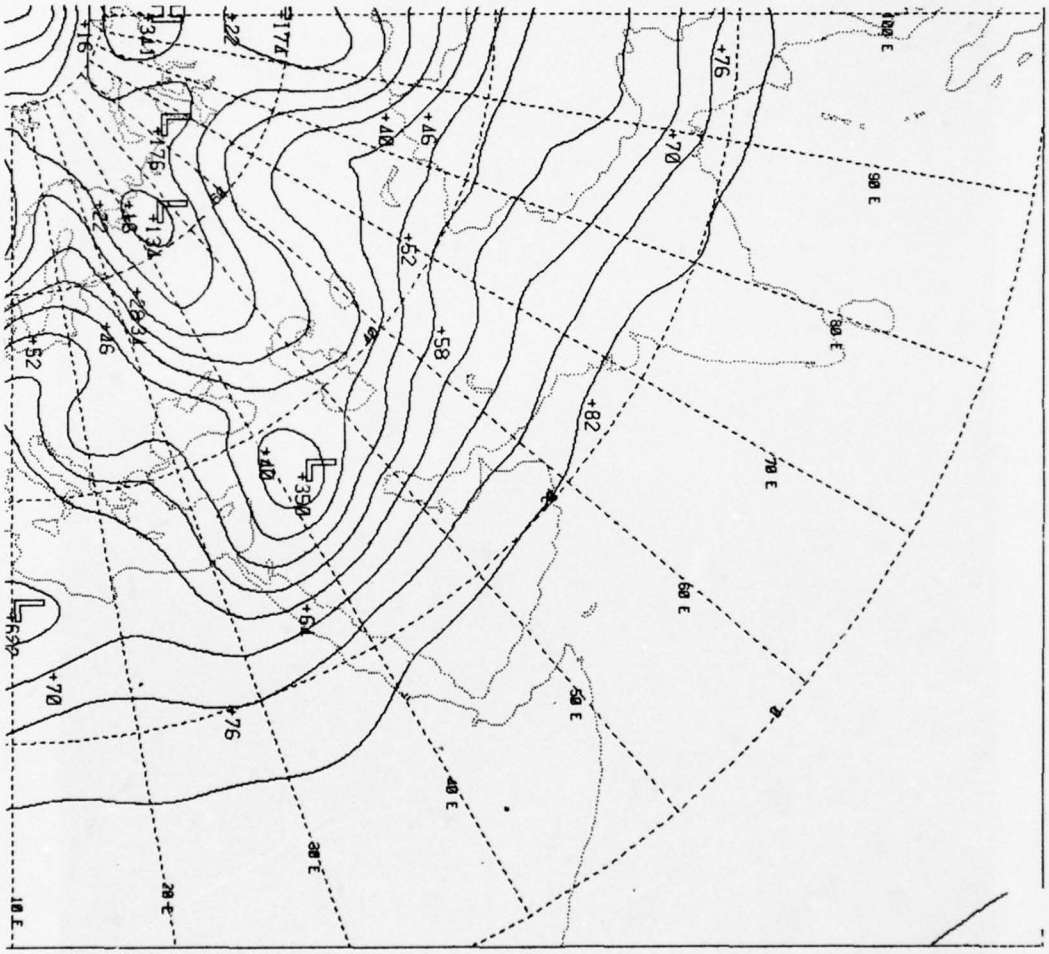

Figure C-1b. 24 January 1974, 0000 GMT, D 500.

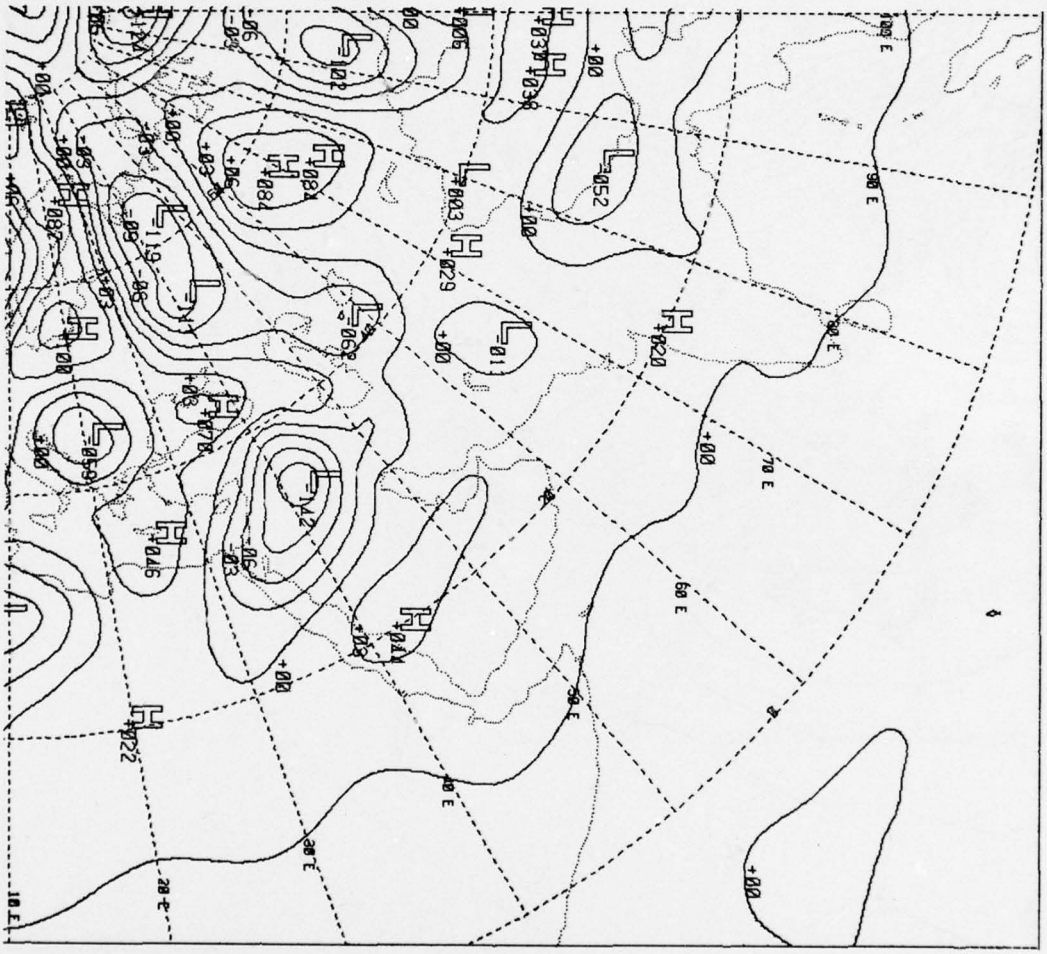

Figure C-1c. 24 January 1974, 0000 GMT, SD 500.

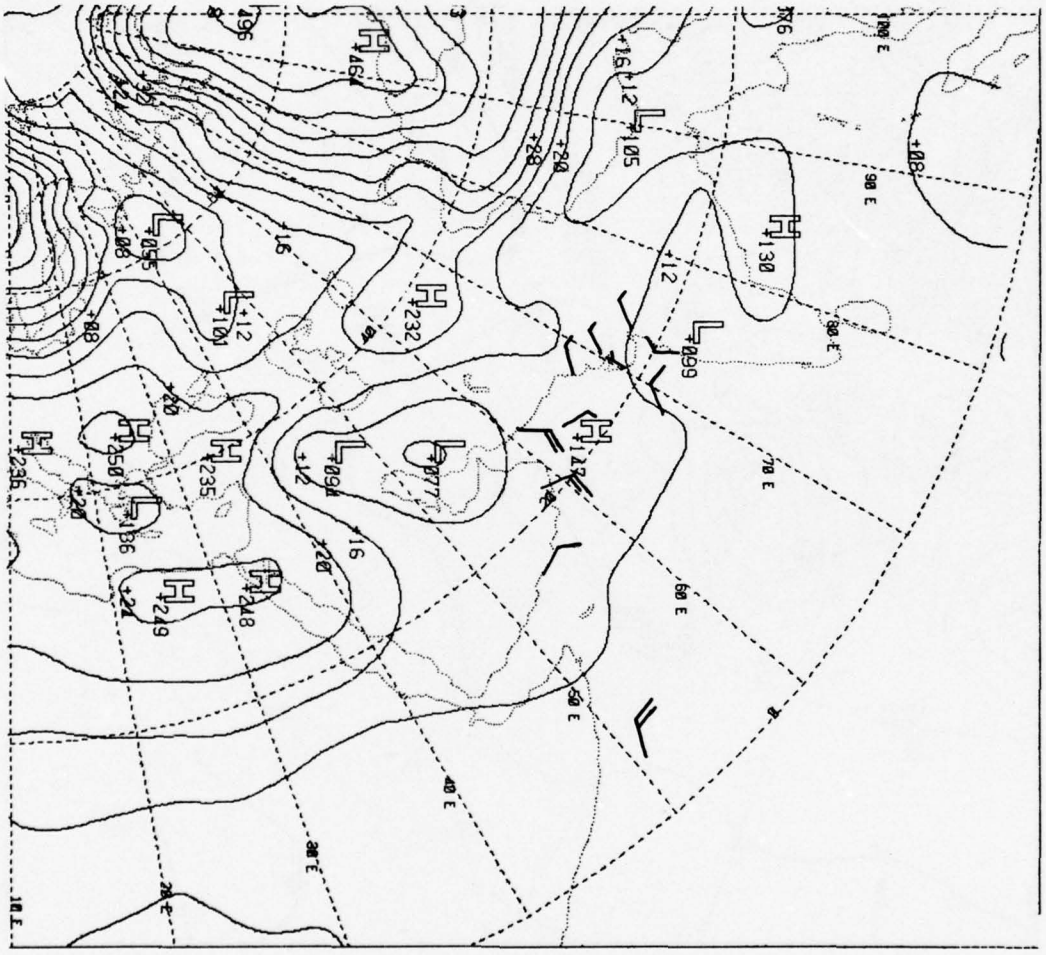

Figure C-1d. 24 January 1974, 1200 GMT, PS.

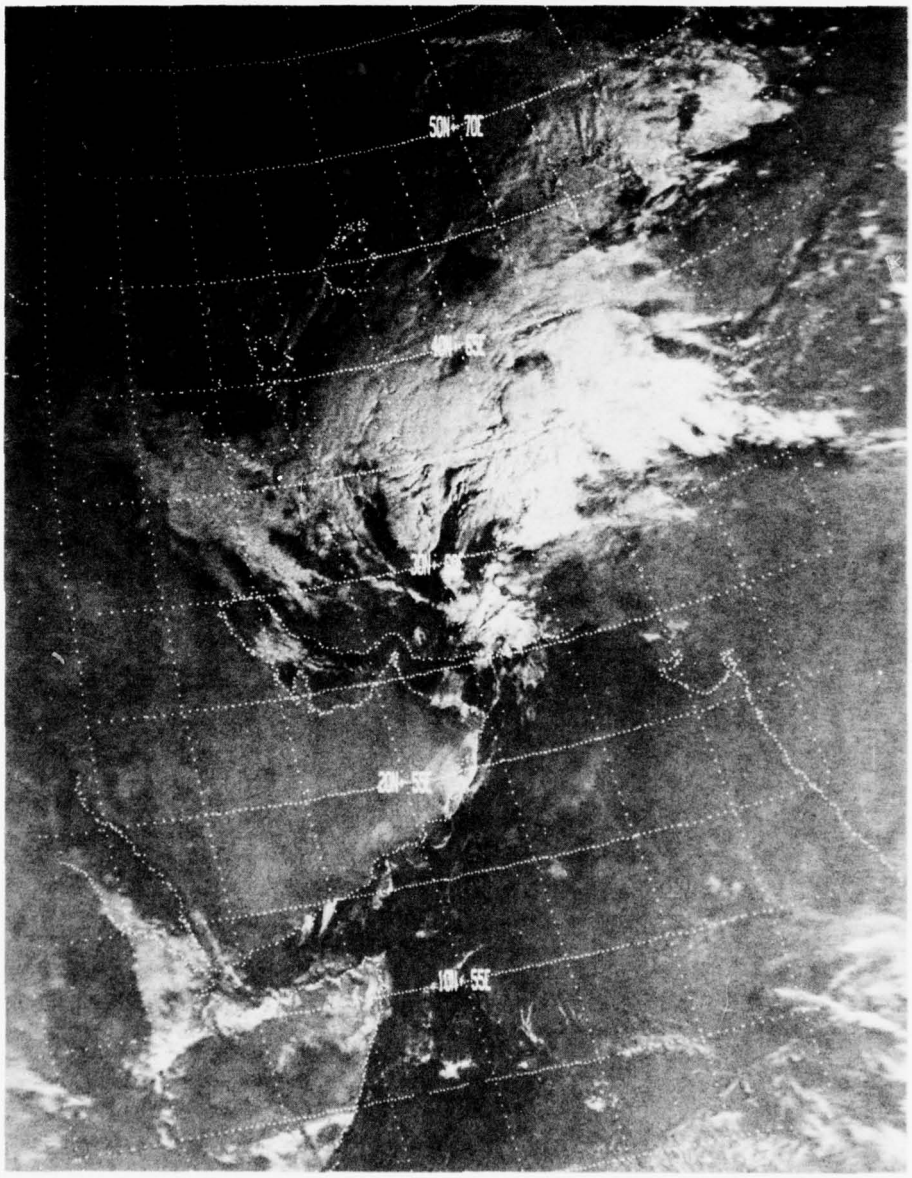

Figure C-2a. 25 January 1974, 0455 GMT (NOAA-2).

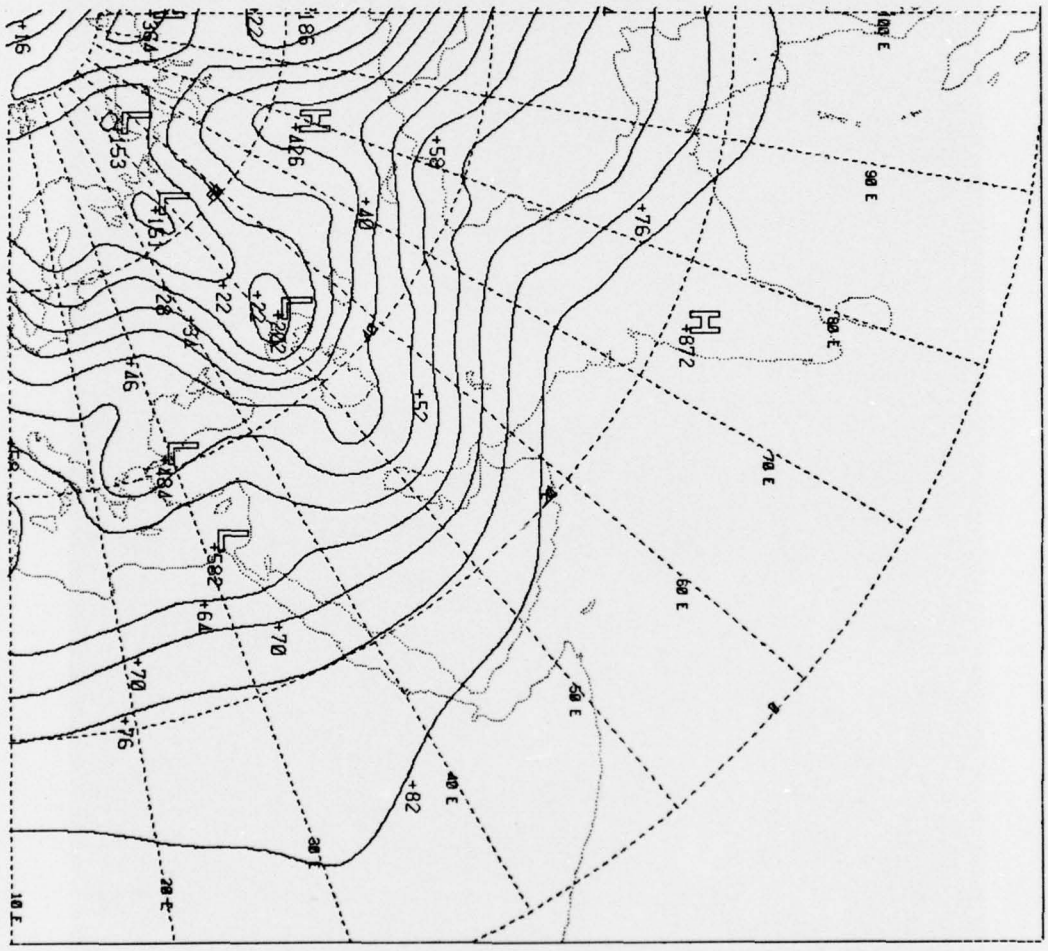

Figure C-2b. 25 January 1974, 0000 GMT, D 500.

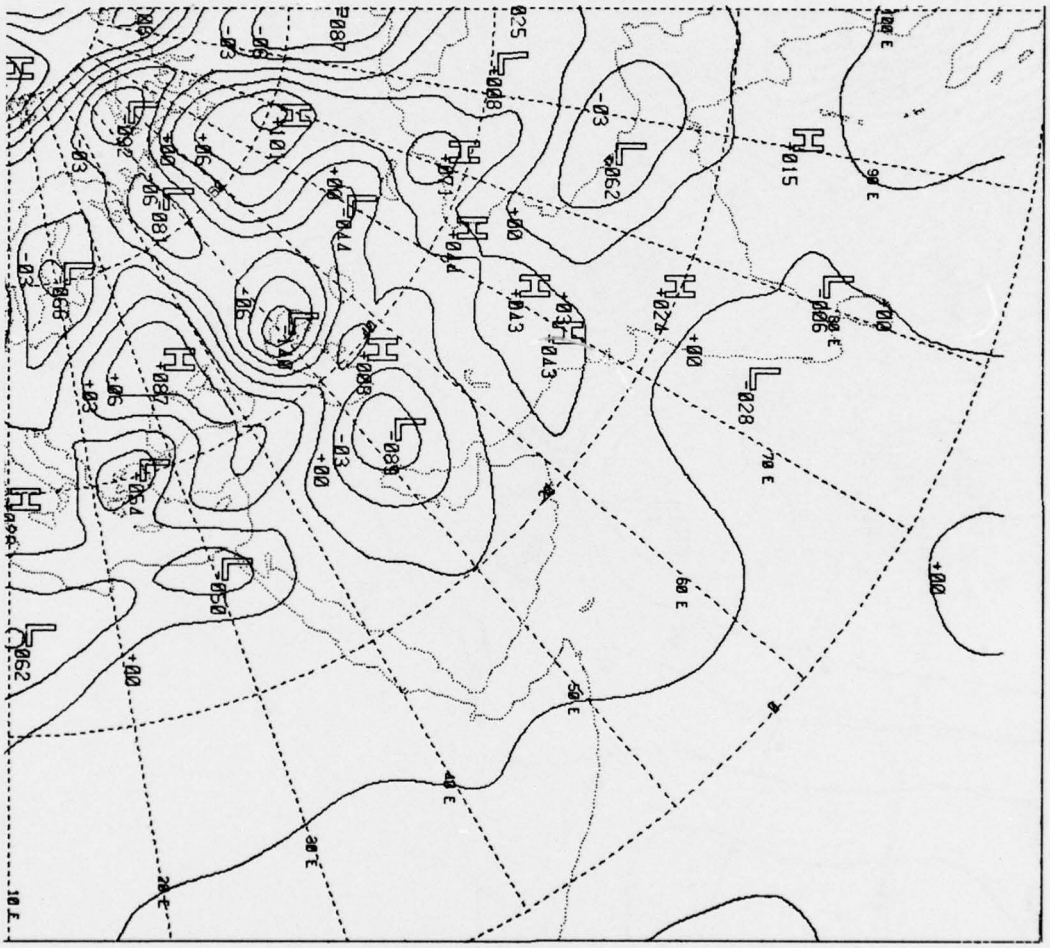

Figure C-2c. 25 January 1974, 0000 GMT, SD 500.

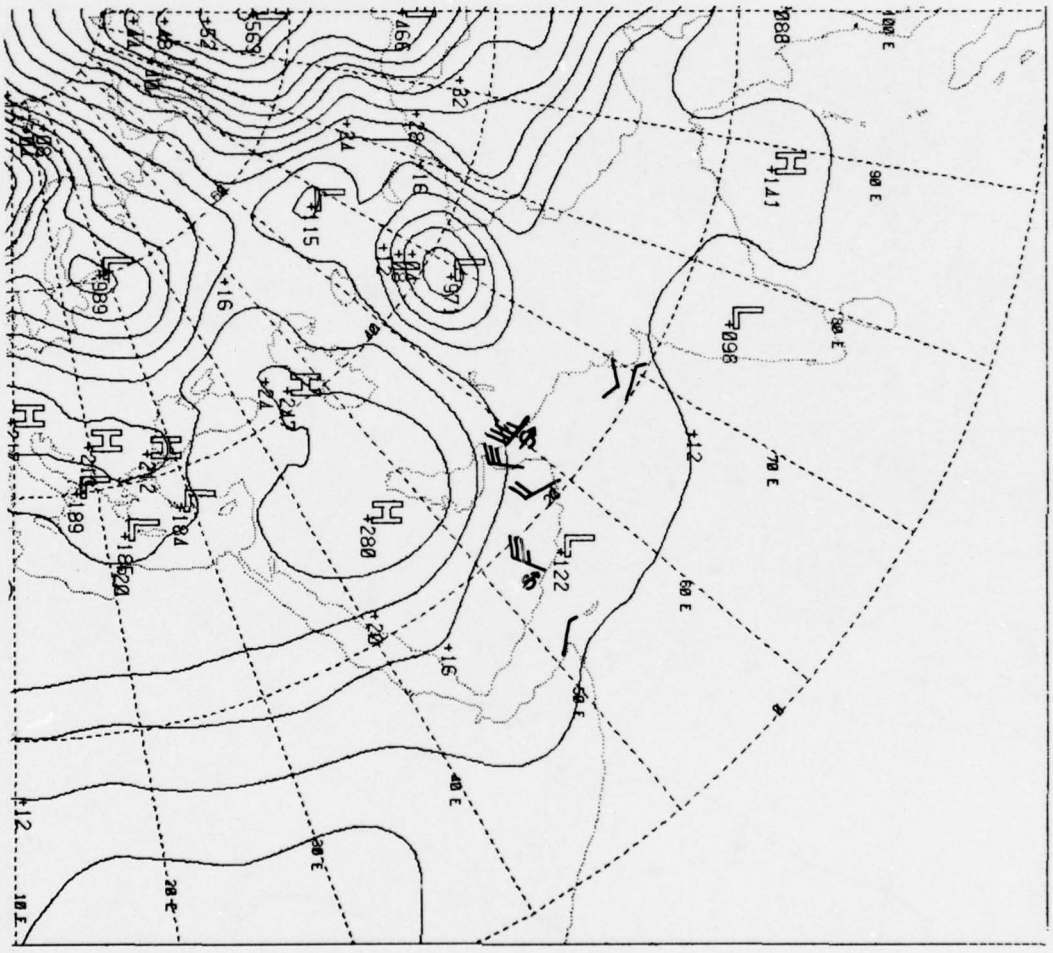

Figure C-2d. 25 January 1974, 1200 GMT, PS.

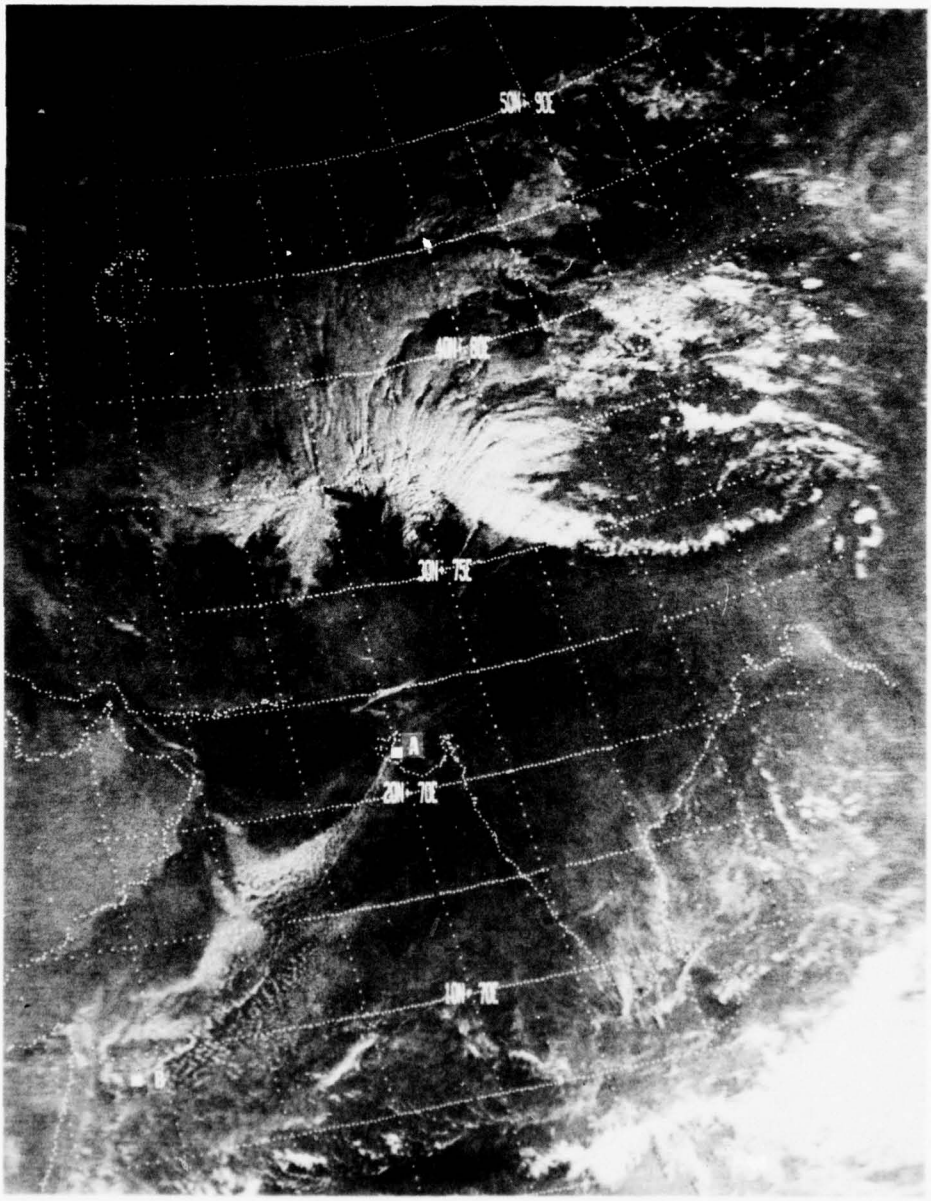

Figure C-3a. 26 January 1974, 0354 GMT (NOAA-2).

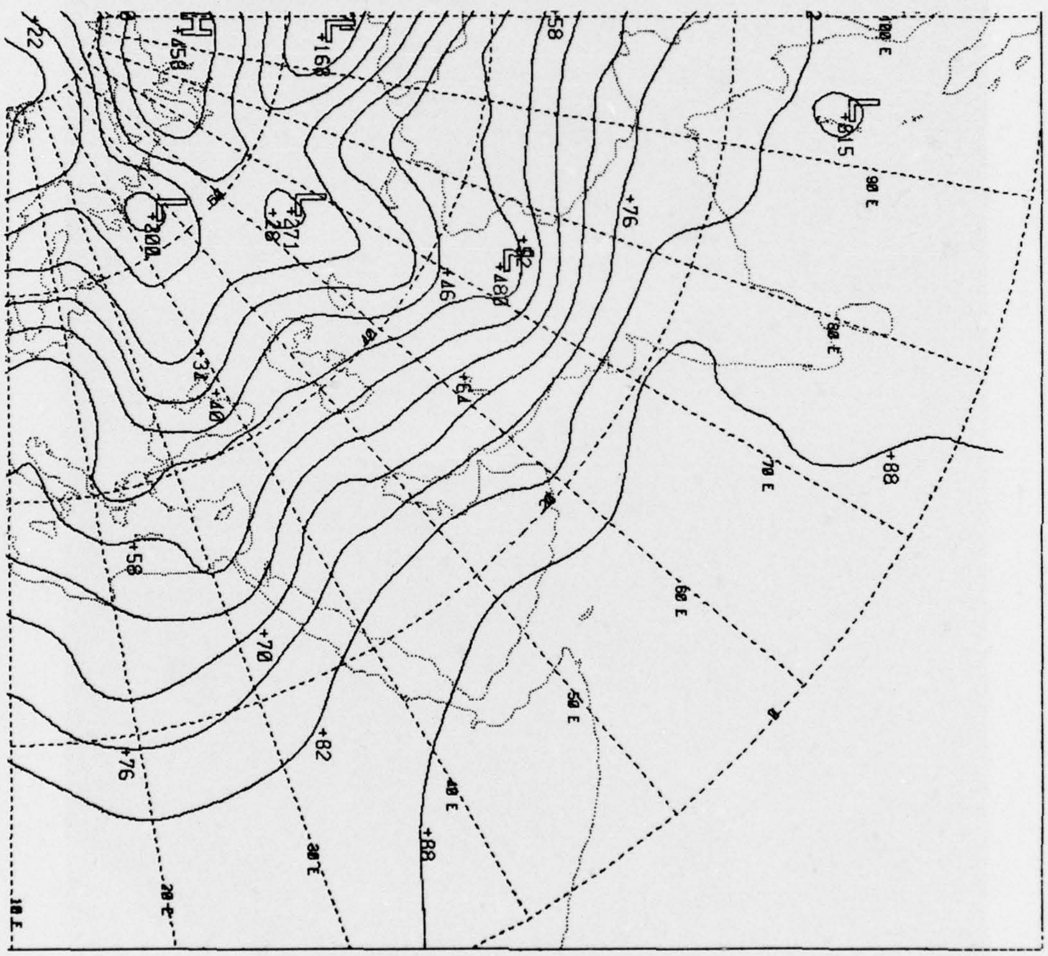

Figure C-3b. 26 January 1974, 1200 GMT, D 500.

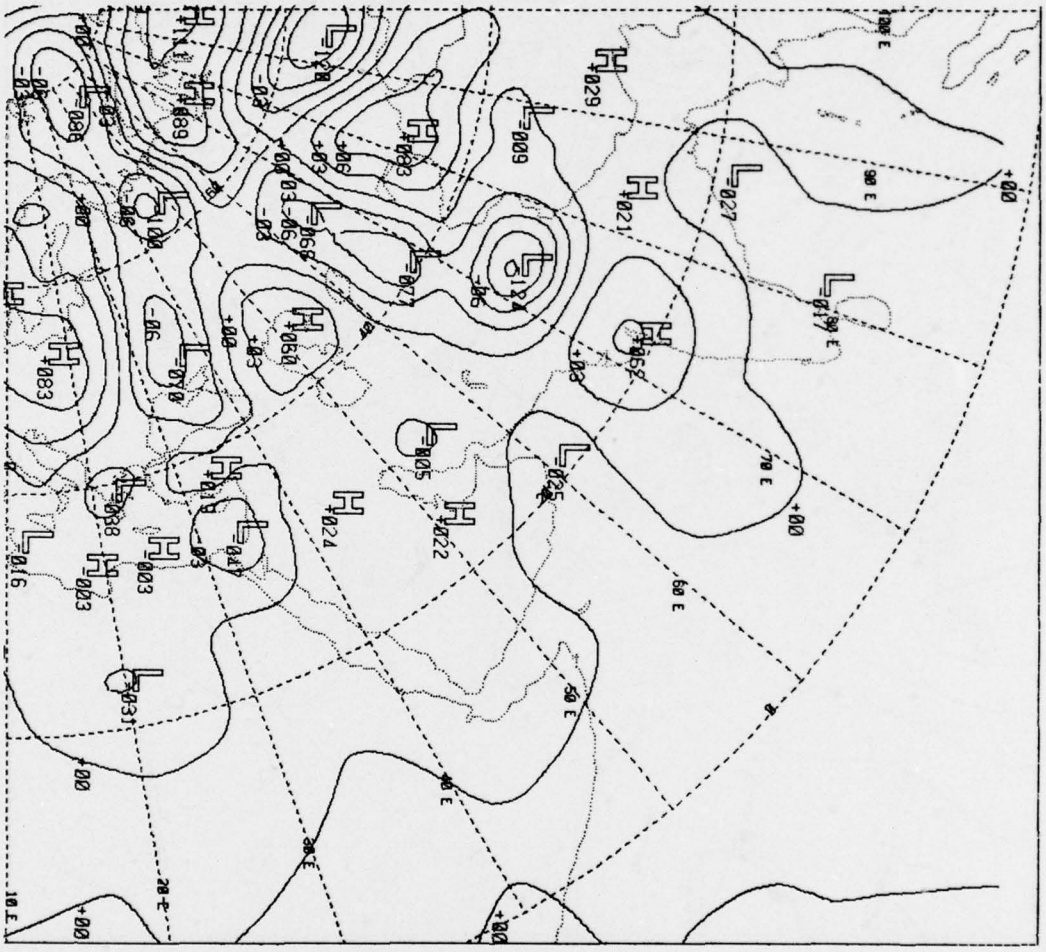

Figure C-3c. 25 January 1974, 1200 GMT, SD 500.

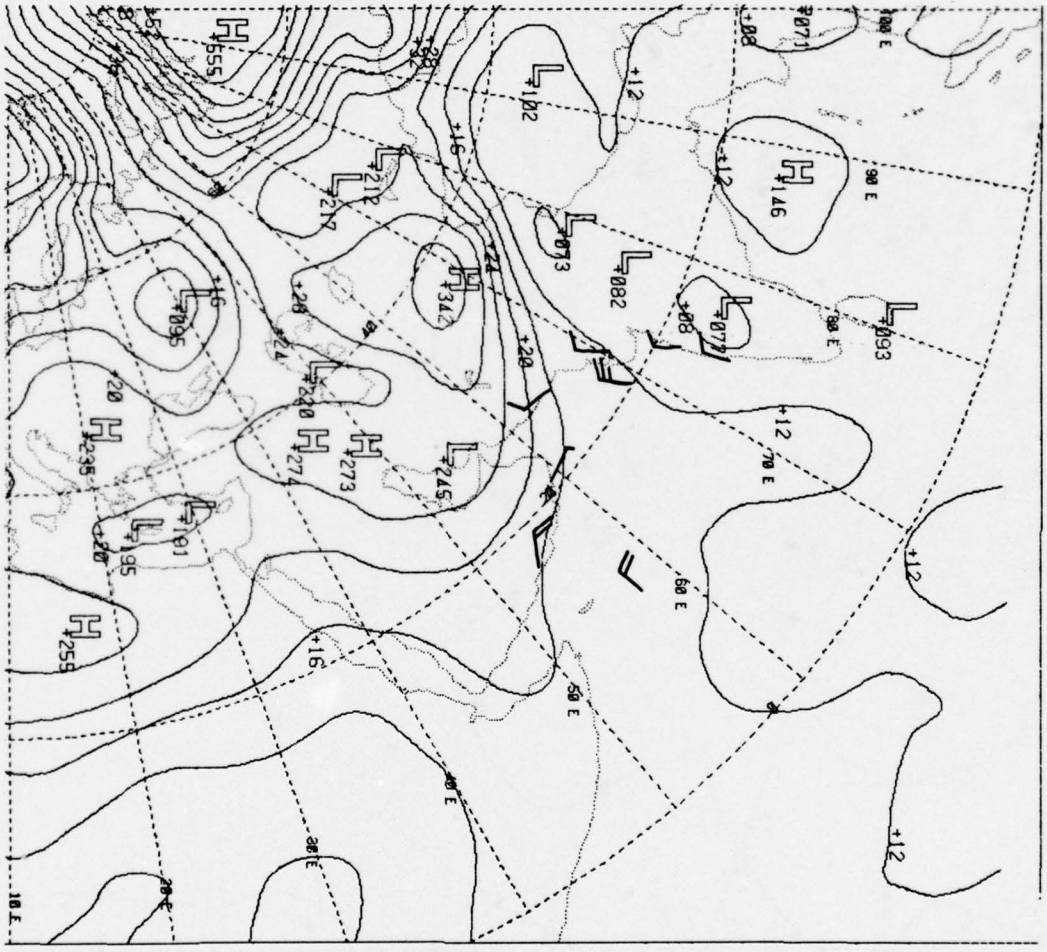

Figure C-3d. 26 January 1974, 1200 GMT, PS.

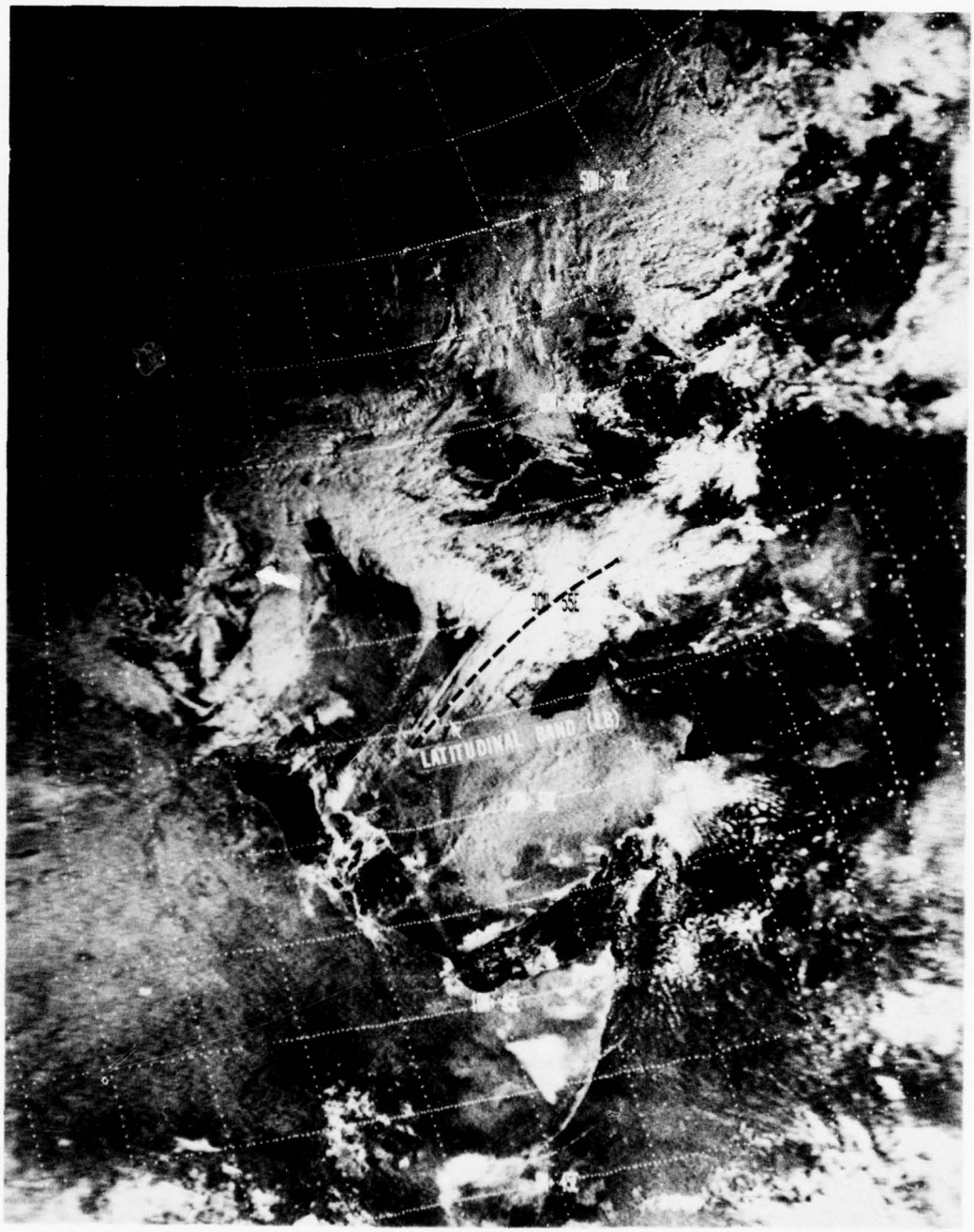

Figure C-4a. 15 January 1973, 0638 GMT (NOAA-2).

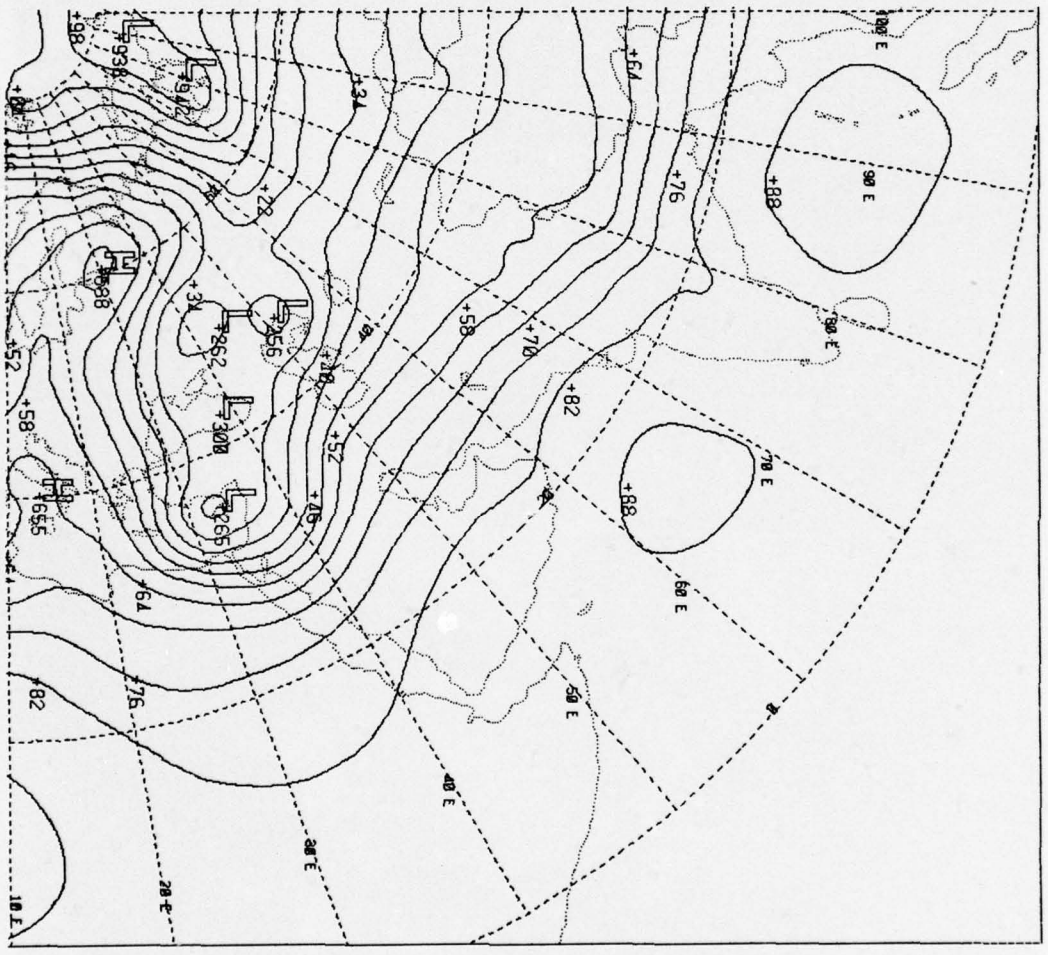

Figure C-4b. 15 January 1973, 0000 GMT, D 500.

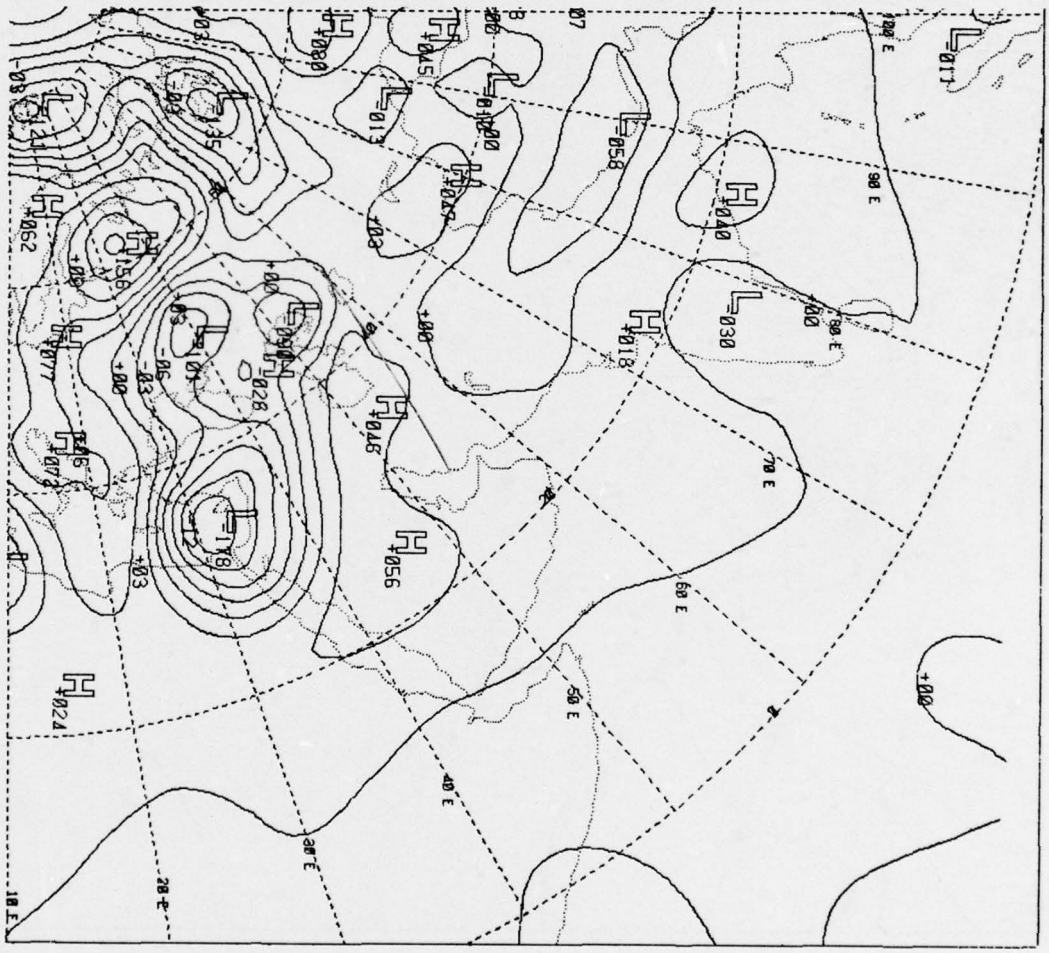

Figure C-4c. 15 January 1973, 0000 GMT, SD 500.

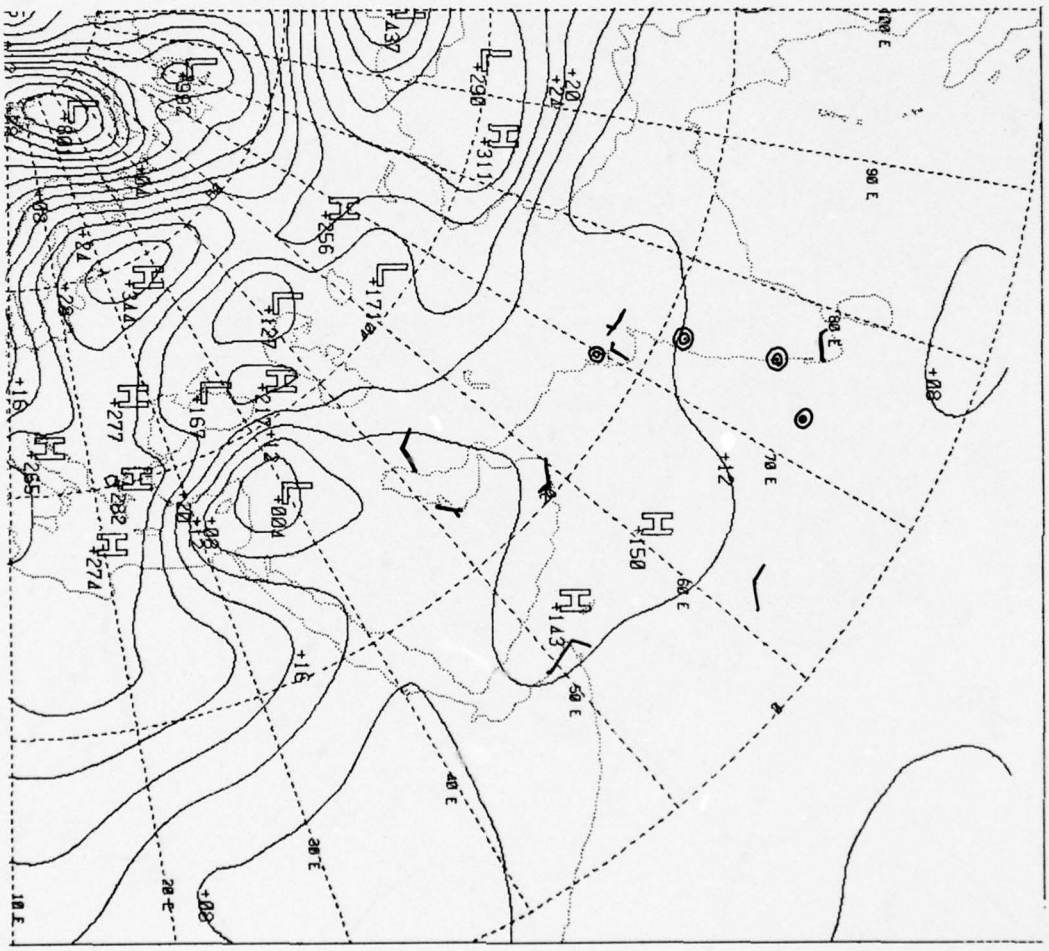

Figure C-4d. 15 January 1973, 0000 GMT, PS.

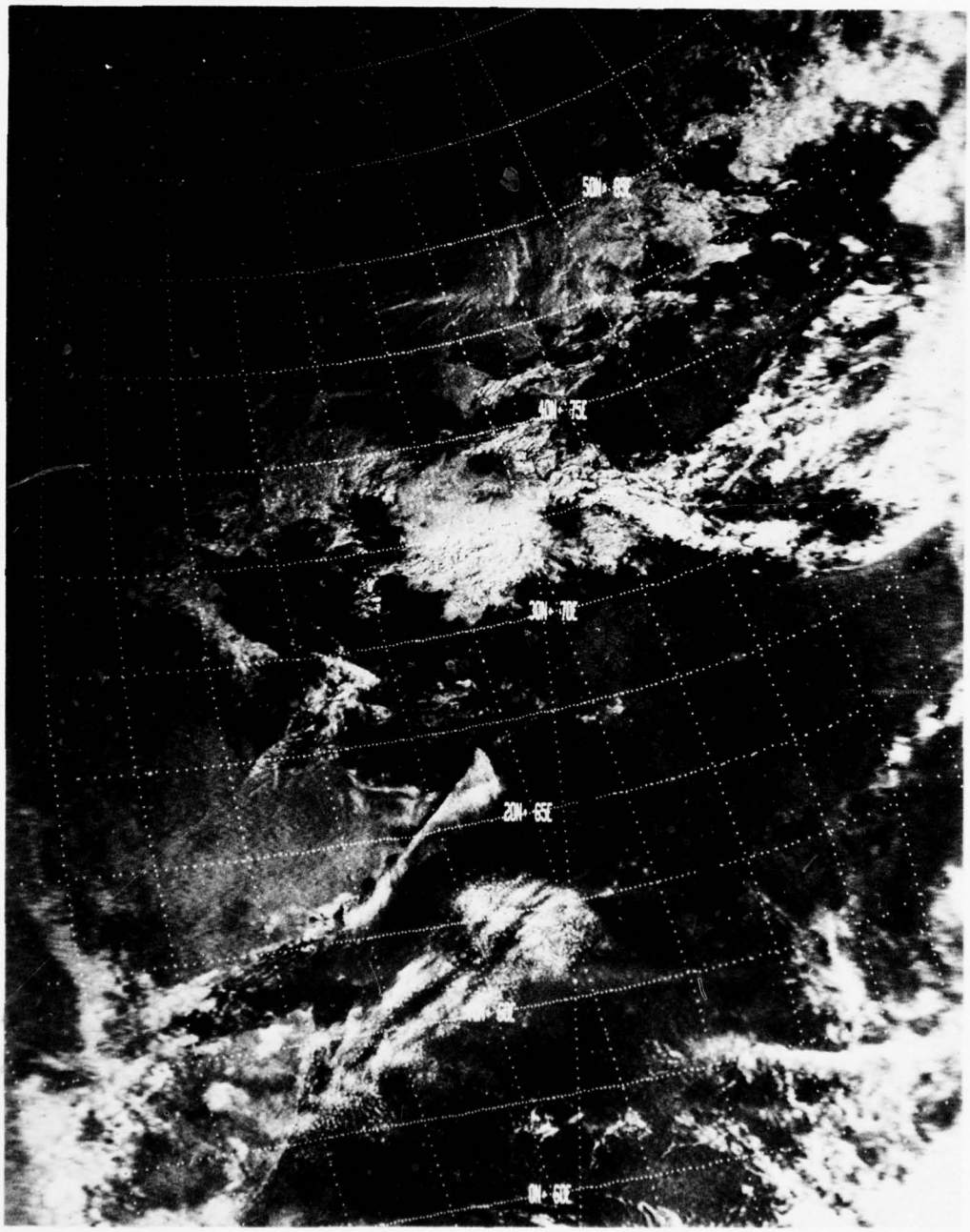

Figure C-5a. 16 January 1973, 0538 GMT (NOAA-2).

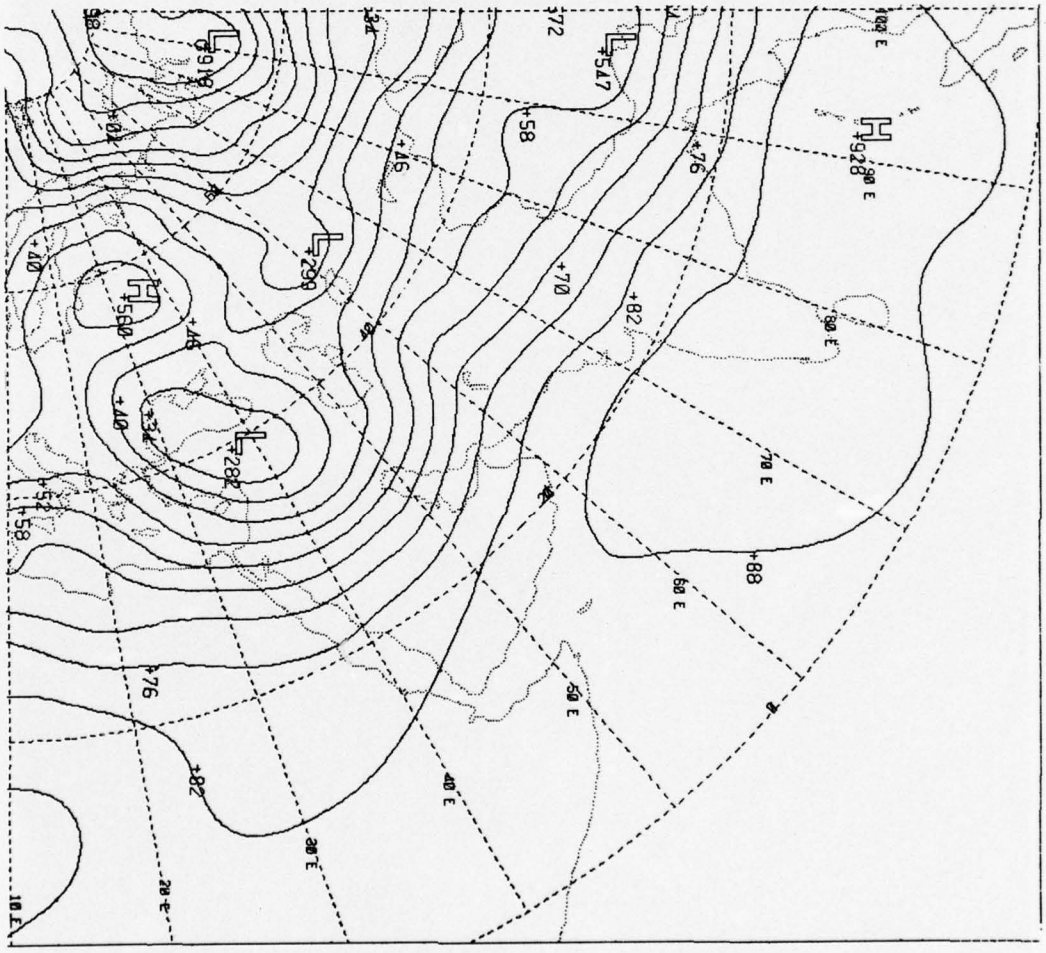

Figure C-5b. 16 January 1973, 0000 GMT, D 500.

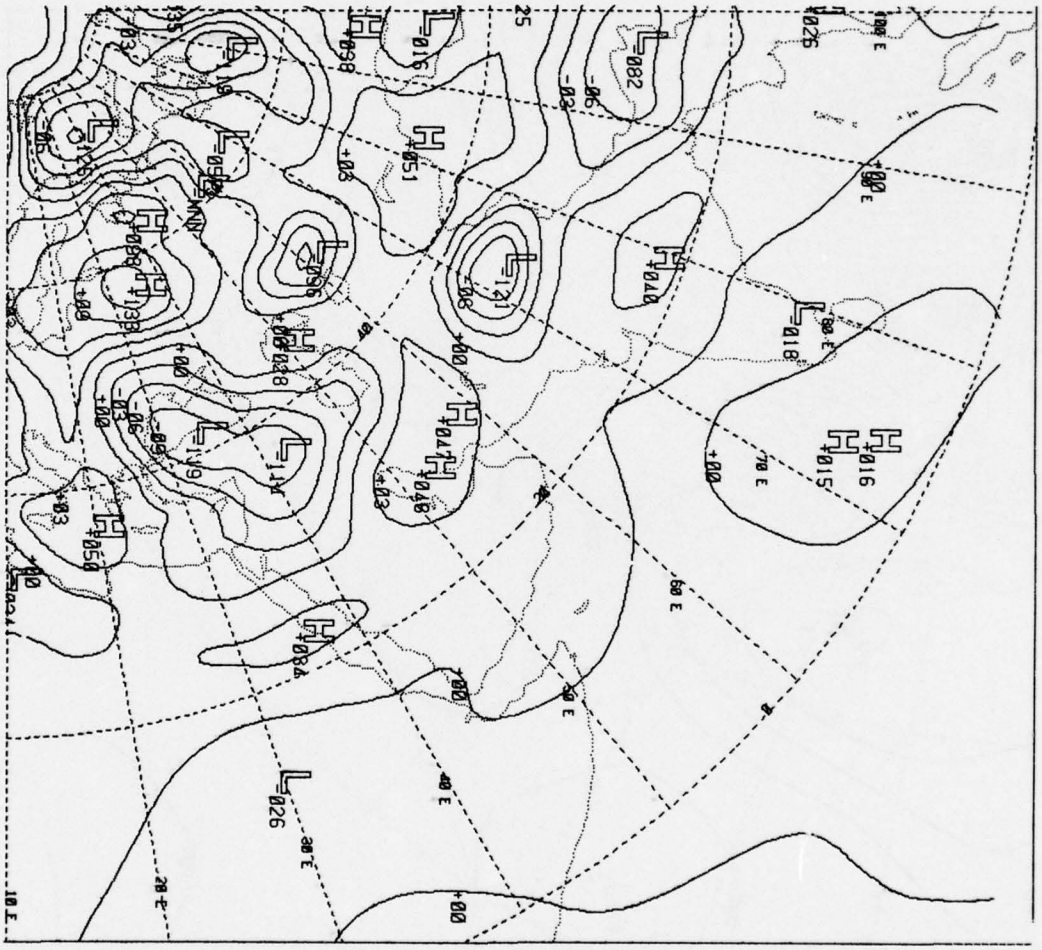

Figure C-5c. 16 January 1973, 0000 GMT, SD 500.

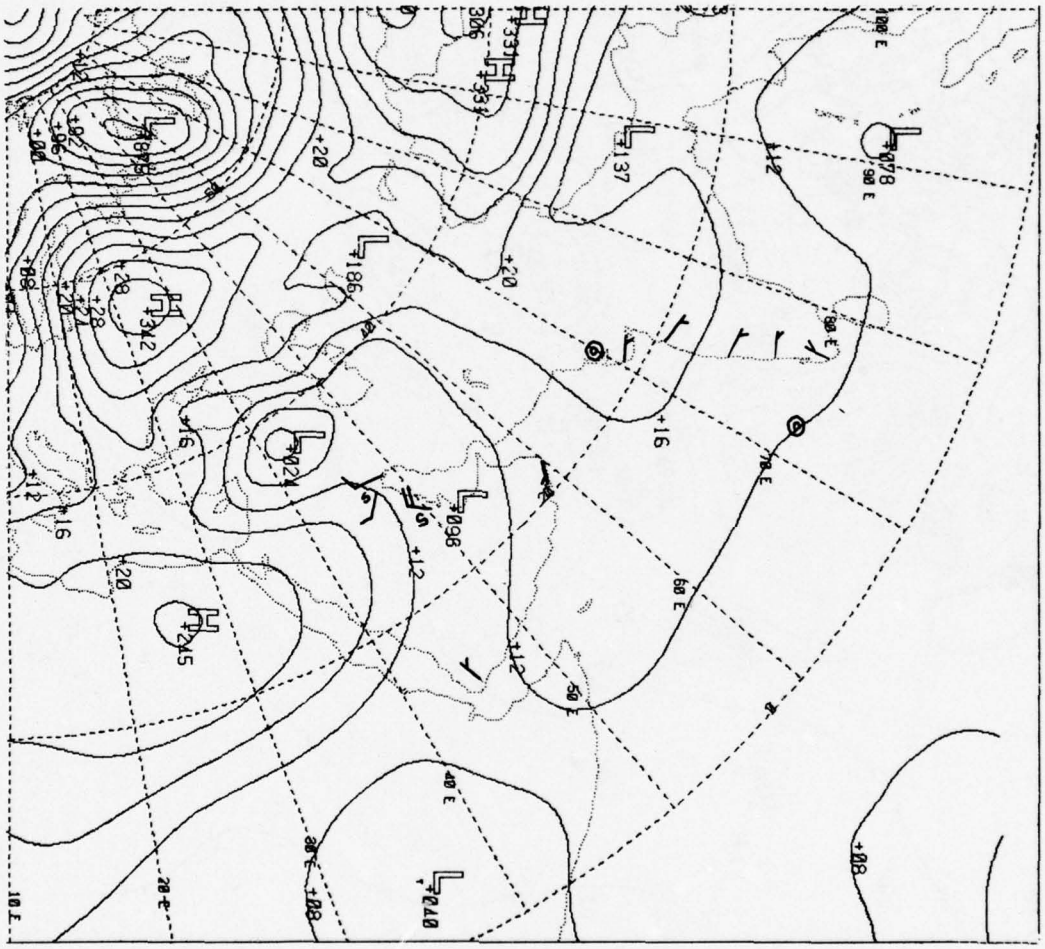

Figure C-5d. 16 January 1973, 0000 GMT, PS.

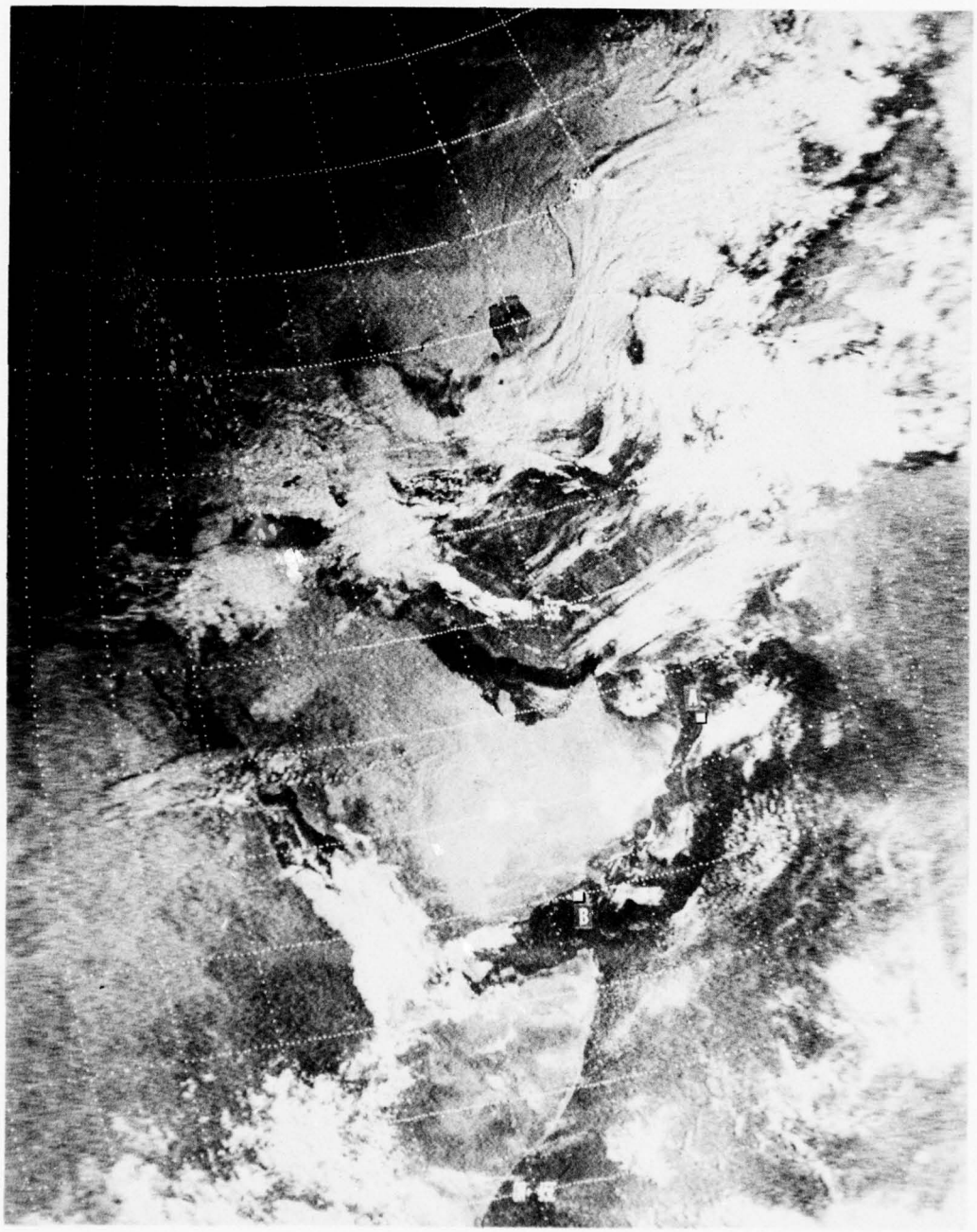

Figure C-6a. 17 January 1973, 0633 GMT (NOAA-2).

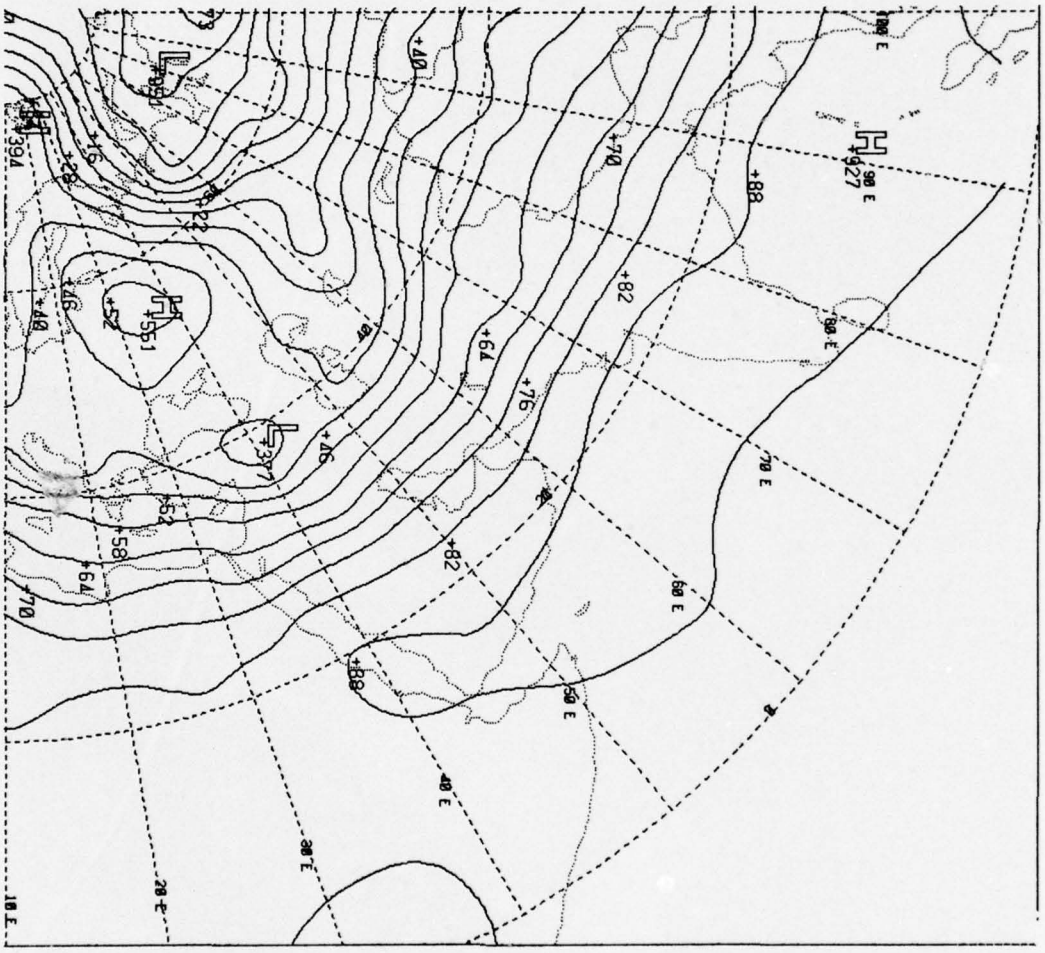

Figure C-6b. 17 January 1973, 0000 GMT, D 500.

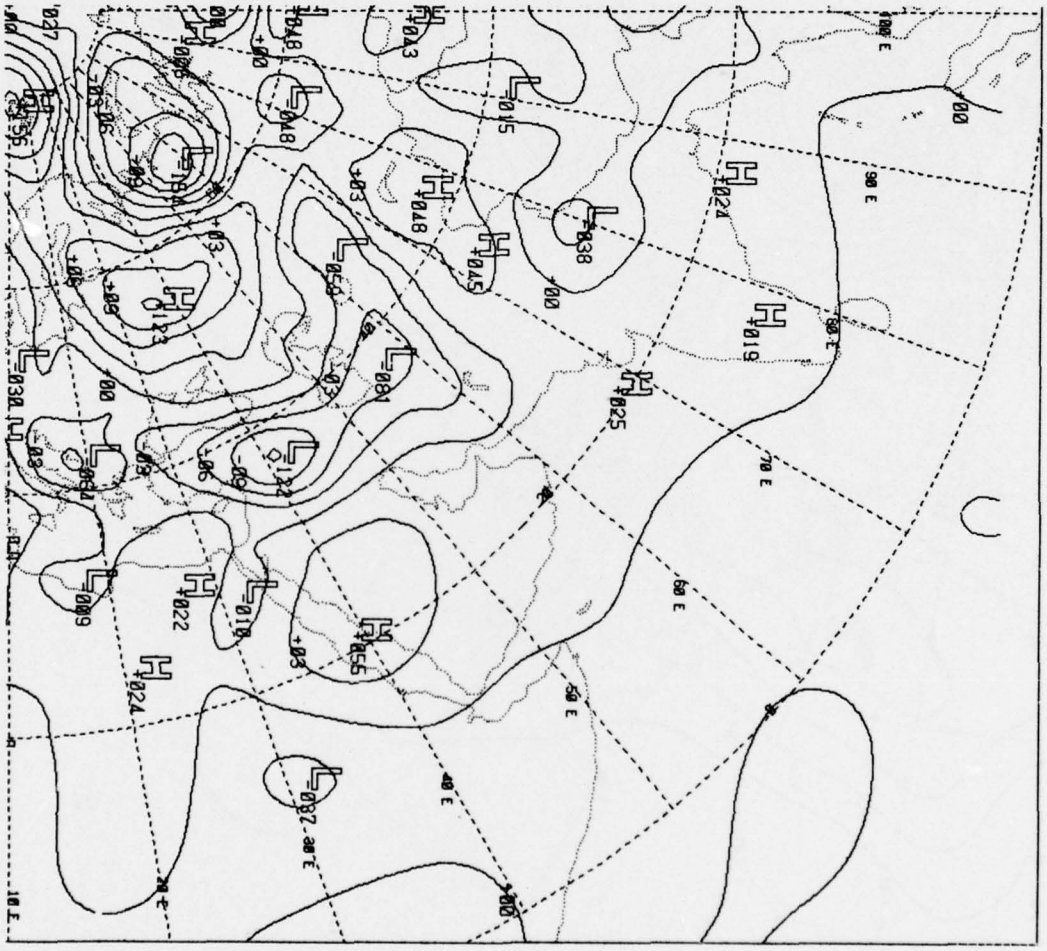

Figure C-6c. 17 January 1973, 0000 GMT, SD 500.

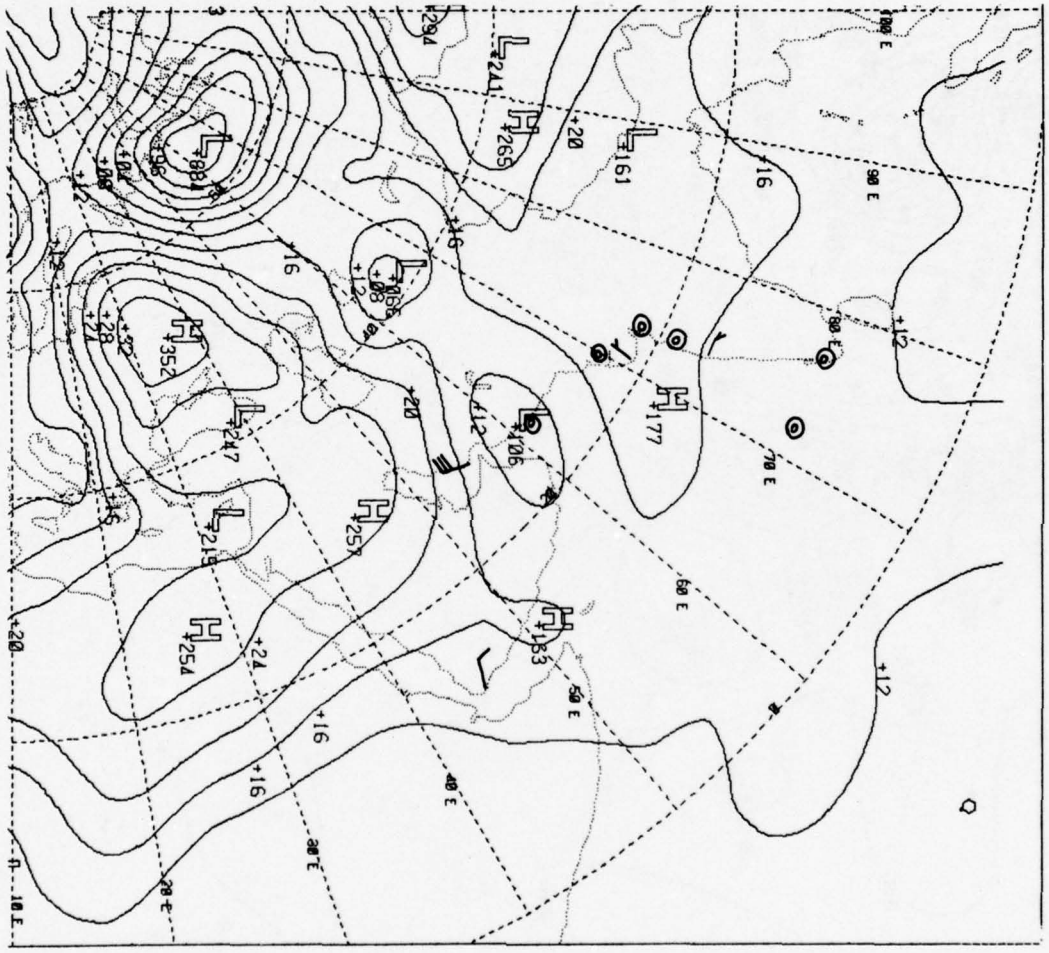

Figure C-6d. 17 January 1973, 0000 GMT, PS.

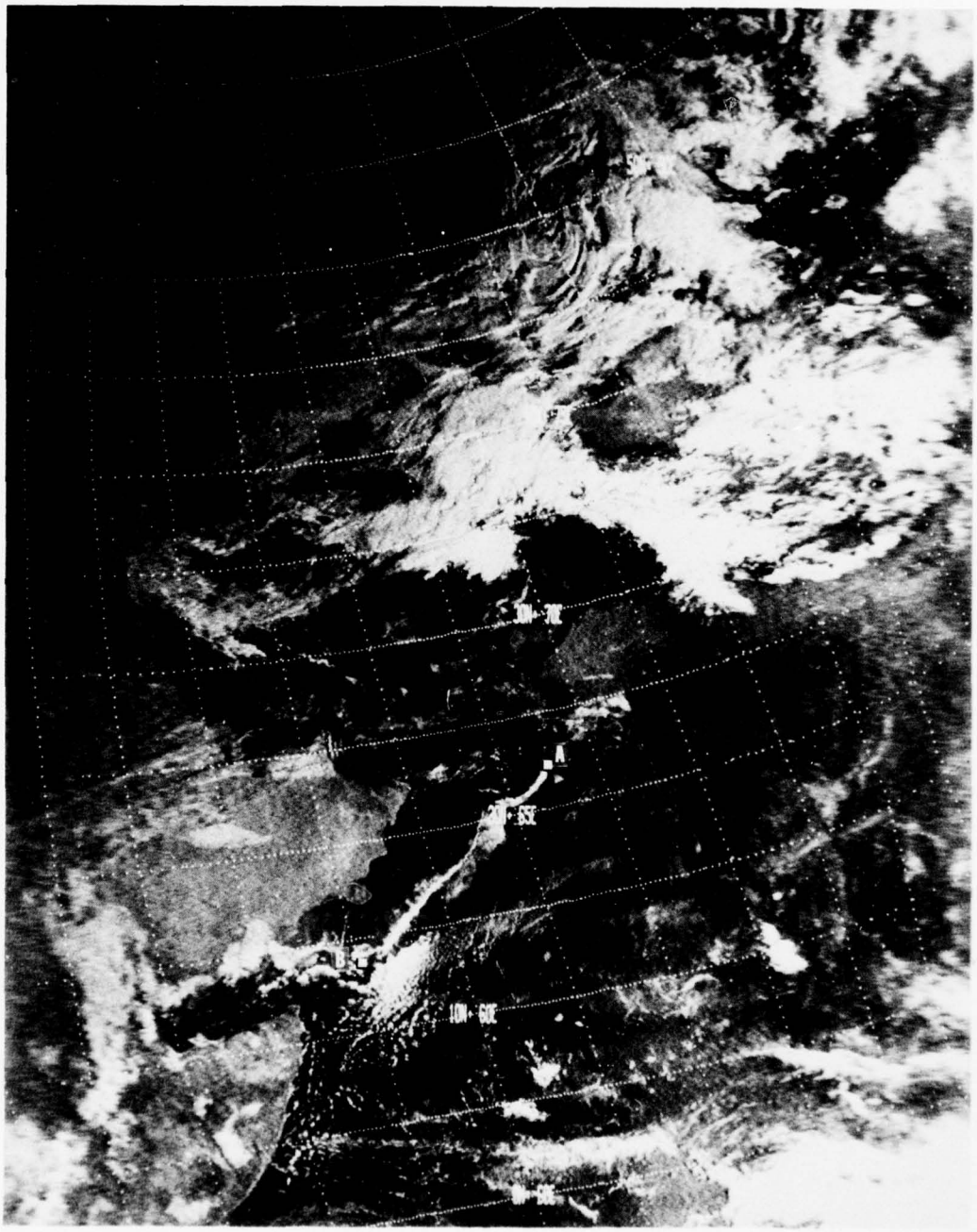

Figure C-7a. 18 January 1973, 0533 GMT (NOAA-2).

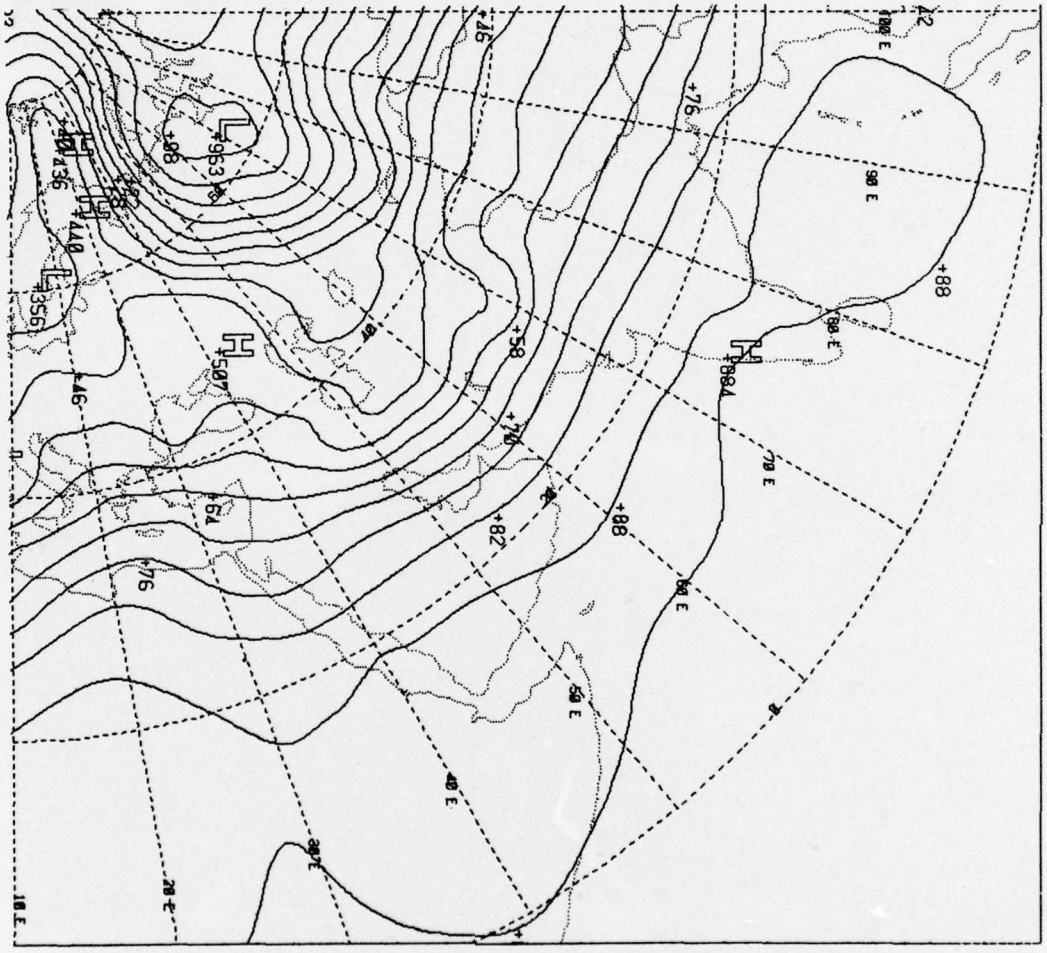

Figure C-7b. 18 January 1973, 0000 GMT, D 500.

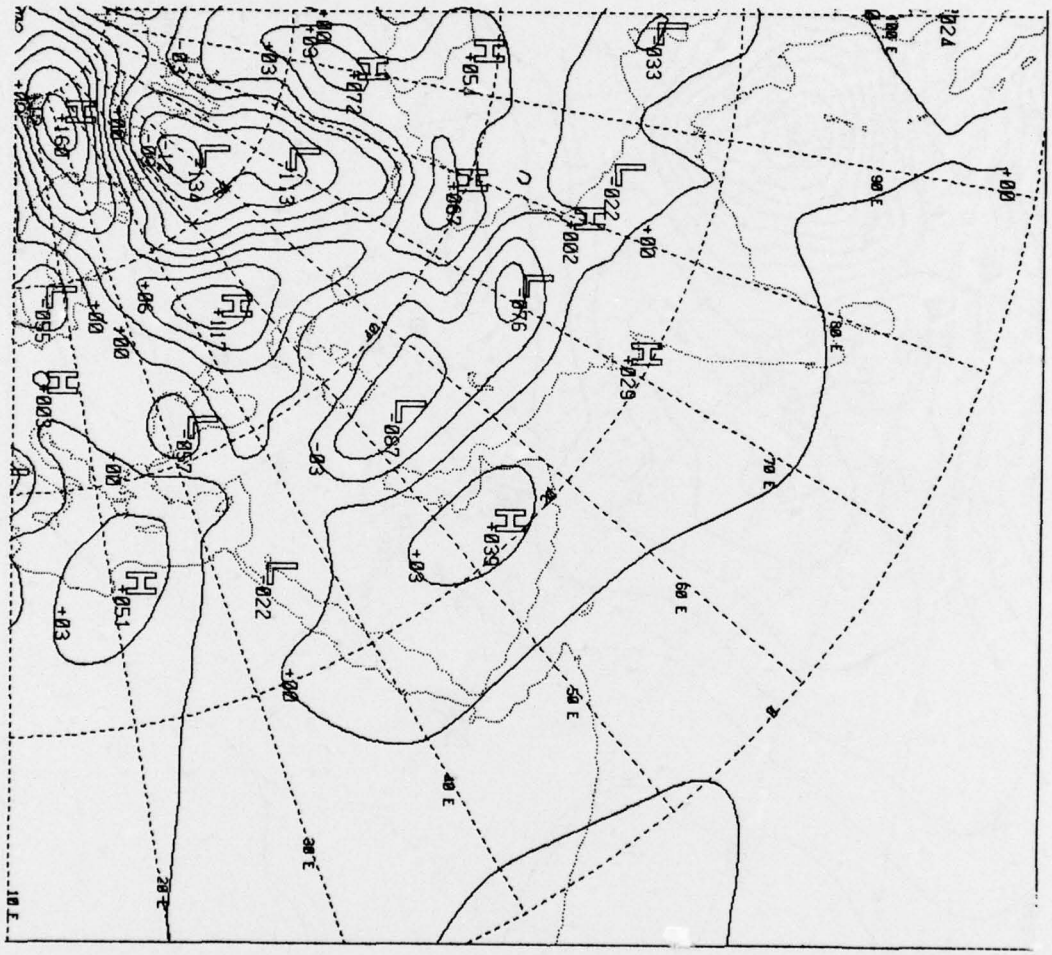

Figure C-7c. 18 January 1973, 0000 GMT, SD 500.

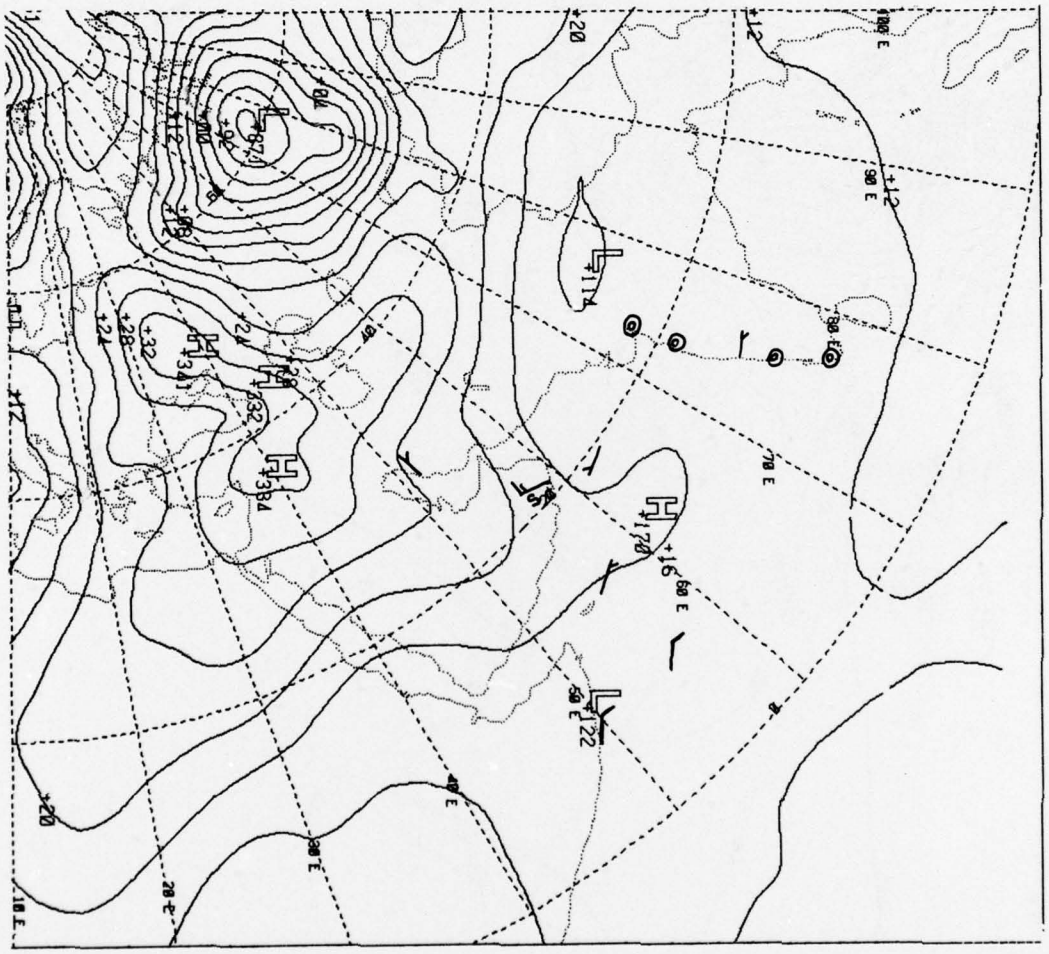

Figure C-7d. 18 January 1973, 0000 GMT, PS.

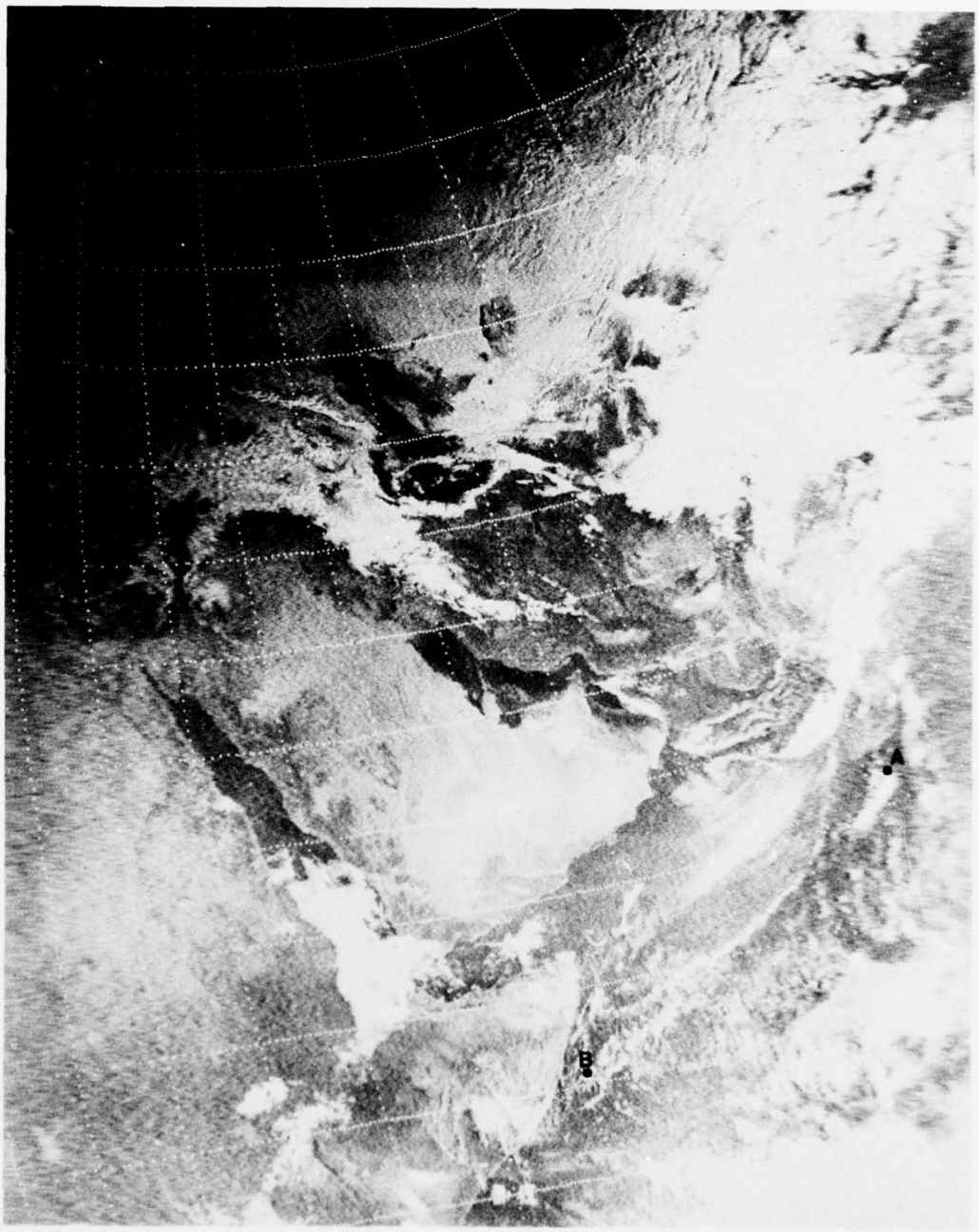

Figure C-8a. 19 January 1973, 0628 GMT (NOAA-2).

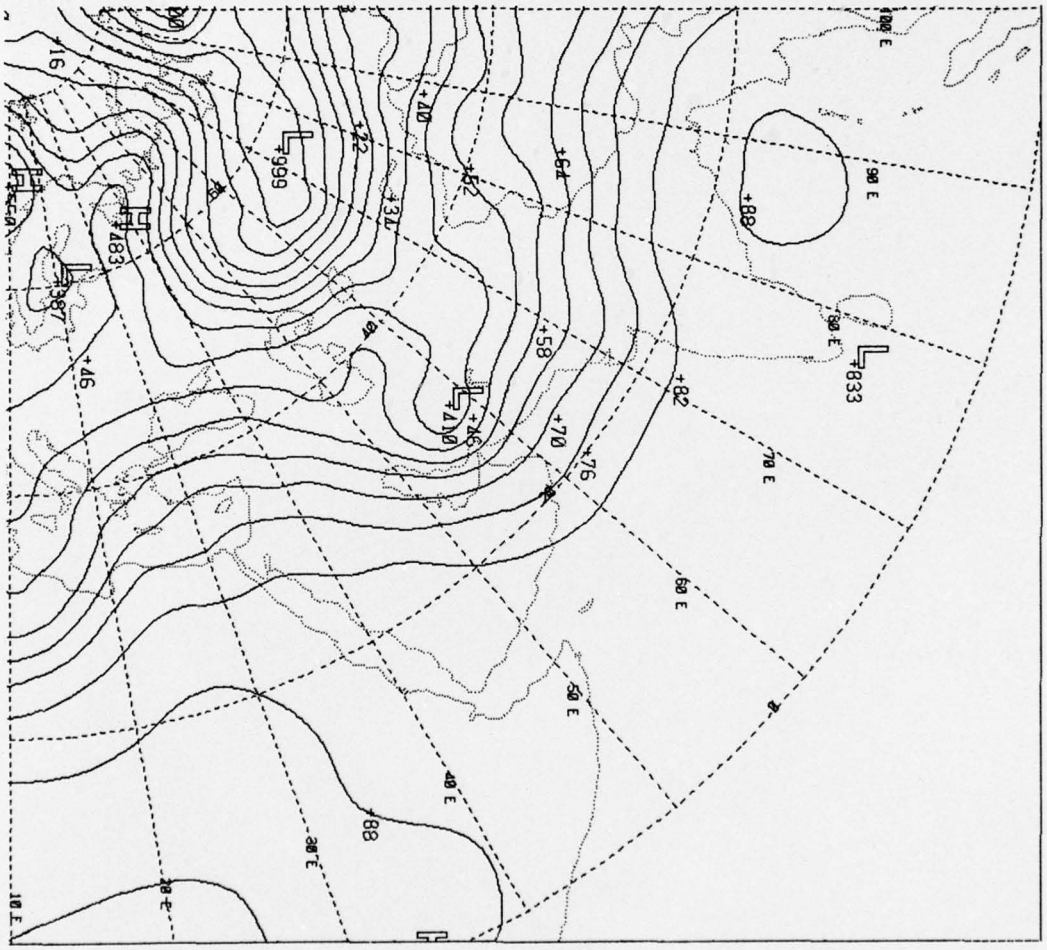

Figure C-8b. 19 January 1973, 1200 GMT, D 500.

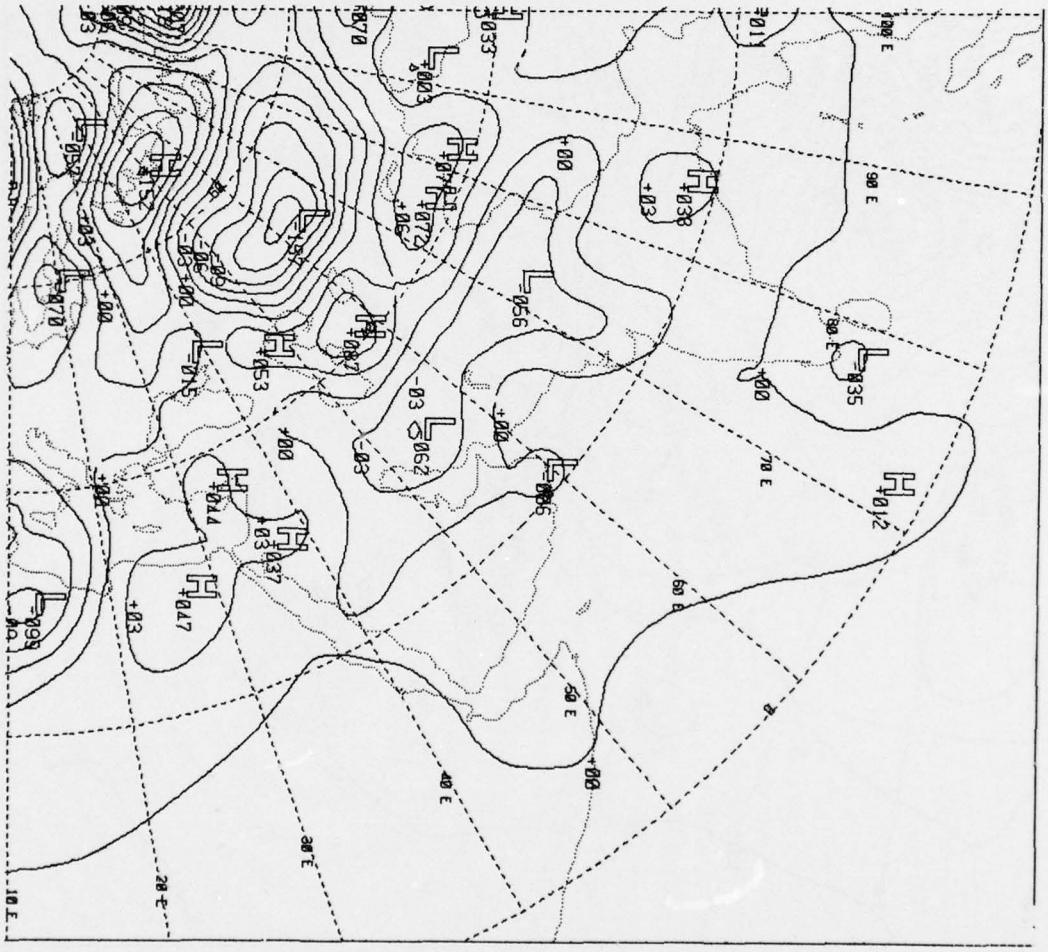

Figure C-8c. 19 January 1973, 1200 GMT, SD 500.

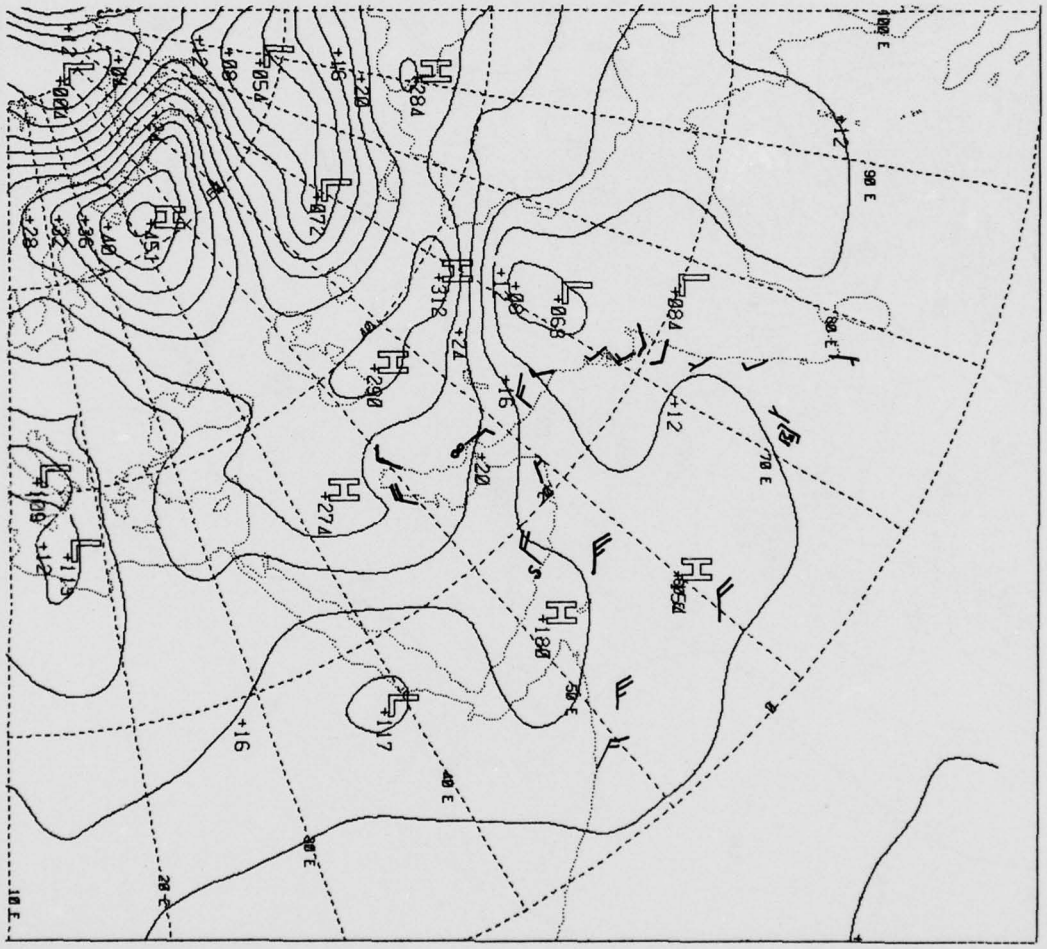

Figure C-8d. 19 January 1973, 1200 GMT, PS.

APPENDIX D

FORECASTING HIGH WINDS ASSOCIATED WITH TROPICAL CYCLONES AT KARACHI, PAKISTAN*

This study provides information useful in the prediction of high winds associated with tropical cyclones at the port of Karachi, Pakistan. All tropical cyclones passing within approximately 180 n mi of Karachi during the 21-year period 1950-1970 were included in the data sample. The usual warm-cored tropical cyclones described in Section 3.3 were investigated, and additional studies were made of the monsoon depressions that developed in the northern Bay of Bengal during the summer monsoon. These monsoon depressions (see Cuming, 1973, for a detailed description) occasionally move across the Indian subcontinent before dissipating.

Hourly wind reports, including the daily maximum, obtained from Pakistani sources were used to relate wind speed to the approach of tropical cyclones. The data sample was then divided into cyclones that produced wind speeds either equal to or greater than 22 kt, or equal to or greater than 34 kt, at Karachi. Table D-1 lists all tropical cyclones that produced wind speeds of at least 22 kt. It should be noted that the 17 cyclones listed represent 71% of the total number, 24, that moved within 180 n mi of Karachi. It is a fact of interest that in the 21-year period studied, no tropical cyclones affected the port of Karachi during the months of December through May, and that the strongest winds were generally from a northeasterly direction.

---

*To be published in Typhoon Havens Handbook for the Western Pacific and Indian Oceans, S. Brand and J. Blelloch, NEPRF, Monterey, CA.

Table D-1. List of tropical cyclones that passed within approximately 180 n mi of Karachi and produced wind speeds ≥22 kt during the 21-year period of record 1950-1970.

MONTH (1)	YEAR	DIRECTION OF APPROACH TO KARACHI (2)	PRODUCED >22 KT WINDS (3)	PRODUCED >34 KT WINDS (3)	DIRECTION/SPEED OF MAXIMUM WINDS (3)	
					DIRECTION	SPEED
JUN	56	SSE	X	X	040 060	35
JUN	59	SSE	X		090 120	30
JUN	61	SSE	X		090	28
JUN	64	SSE	X	X	020	40
JUL	50	ENE	X		290	24
JUL	54	SSE	X		070	24
JUL #1	59	SSE	X	X	360	40
JUL #2	59	ESE	X	X	060 090	35
JUL #3	59	ESE	X		360	22
JUL	62	SSE	X	X	030	45
AUG	56	ESE	X		290	30
SEP	58	ESE	X		330	24
SEP	61	ENE	X		080	25
OCT	63	SSE	X	X	090	40
NOV	51	SSE	X		070	30
NOV	58	SSW	X		050	22
NOV	63	SSE	X		070	24

(1) Date of entry into circle of 180 n mi radius centered on Karachi.

(2) Point of entry into circle of 180 n mi radius centered on Karachi.

(3) Records furnished by Pakistani sources.

Selected information from Table D-1 is summarized in Tables D-2 and D-3. Table D-2 indicates that the majority of tropical cyclones producing winds of at least 22 kt approached Karachi from the south-southeast (point of entry into 180 n mi radius circle centered on Karachi). The cyclones which approached from the east-northeast or east-southeast were monsoon depressions during the months of July through September.

Table D-2. Direction of approach (point of entry into 180 n mi radius circle) to Karachi of cyclones that occurred in the months of May through December and produced winds ≥22 kt during the period 1950-1970.

	NNE	ENE	ESE	SSE	SSW	WSW	WNW	NNW	TOTAL
NUMBER	0	2	4	10	1	0	0	0	17
PERCENTAGE	0	12	24	59	6	0	0	0	101*

*Does not total 100% due to rounding.

Table D-3. Monthly distribution of tropical cyclones entering 180 n mi radius circle centered at Karachi in the months of May through December during the period 1950-1970 (percentages shown in ( )).

Wind Speed at Karachi	MAY	JUN	JUL	AUG	SEP	OCT	NOV	DEC	TOTAL
≥22 Kt	0(0)	4(24)	6(35)	1(6)	2(12)	1(6)	3(18)	0(0)	17(101)*
≥34 Kt	0(0)	2(33)	3(50)	0(0)	0(0)	1(17)	0(0)	0(0)	6(100)

*Does not total 100% due to rounding.

The monthly occurrences of tropical cyclones producing wind speeds of either ≥22 kt or ≥34 kt are shown in Table D-3, which indicates that the peak months for both categories are June and July. It is emphasized, however, that the origins of tropical cyclones affecting Karachi are significantly different for those two months. These differences are depicted in Figures D-1, D-2 and D-3, which show the tracks of all tropical cyclones passing within 180 n mi of Karachi and producing winds of at least 22 kt.

The June cases (Figure D-1) were associated with tropical cyclones that developed off the west coast of India and in each case reached tropical storm intensity. It is likely that those systems developed in the near-equatorial trough, which is believed to reintensify occasionally over the water at the end of the spring transition season (see Para. 3.3.2). Comparing Figures D-1

and A-36d (80 years of data) it seems likely that most tropical cyclones reaching storm intensity during June are likely to approach within 180 n mi of Karachi and produce strong winds at this port.

During the height of the summer monsoon, July through September, the tropical cyclones affecting Karachi (see Figure D-2) appear to be remnants of monsoon depressions that developed over the northern Bay of Bengal. Since these cyclones occur at a rate of two or three per month at this time of year (Cuming, 1973), the sparsity of tracks over the 21-year period indicates that only a small percentage reach the vicinity of Karachi. Additionally, several monsoon depressions that passed within 180 n mi of Karachi were so weak that they did not produce winds of at least 22 kt (see Table D-4). Table D-4 shows that only during the months of July through September did cyclones that passed close to Karachi fail to produce strong winds. The single exception is one cyclone in June, 1954.

Table D-4. Monthly distribution of tropical cyclones entering 180 n mi radius circle centerd at Karachi and not producing wind speeds of at least 22 kt during the period 1950-1970 (percentages shown in ( )).

MAY	JUN	JUL	AUG	SEP	OCT	NOV	DEC	TOTAL
0(0)	1(14)	3(43)	1(14)	2(29)	0(0)	0(0)	0(0)	7(100)

During the autumn transition season of October and November, as in June, tropical cyclones that caused high winds at Karachi once again developed primarily off the west coast of India (see Figure D-3) and intensified into tropical storms. The only exception was a tropical cyclone that crossed the southern Indian peninsula before redeveloping into a tropical storm over the Arabian Sea (November, 1958). However, unlike June when most tropical cyclones that reached storm intensity apparently also produced high winds at Karachi, it appears from the 80 years of data shown in Figures A-36h and A-36i that a much smaller percentage of autumn tropical storms approach this port within 180 n mi and with resulting high winds.

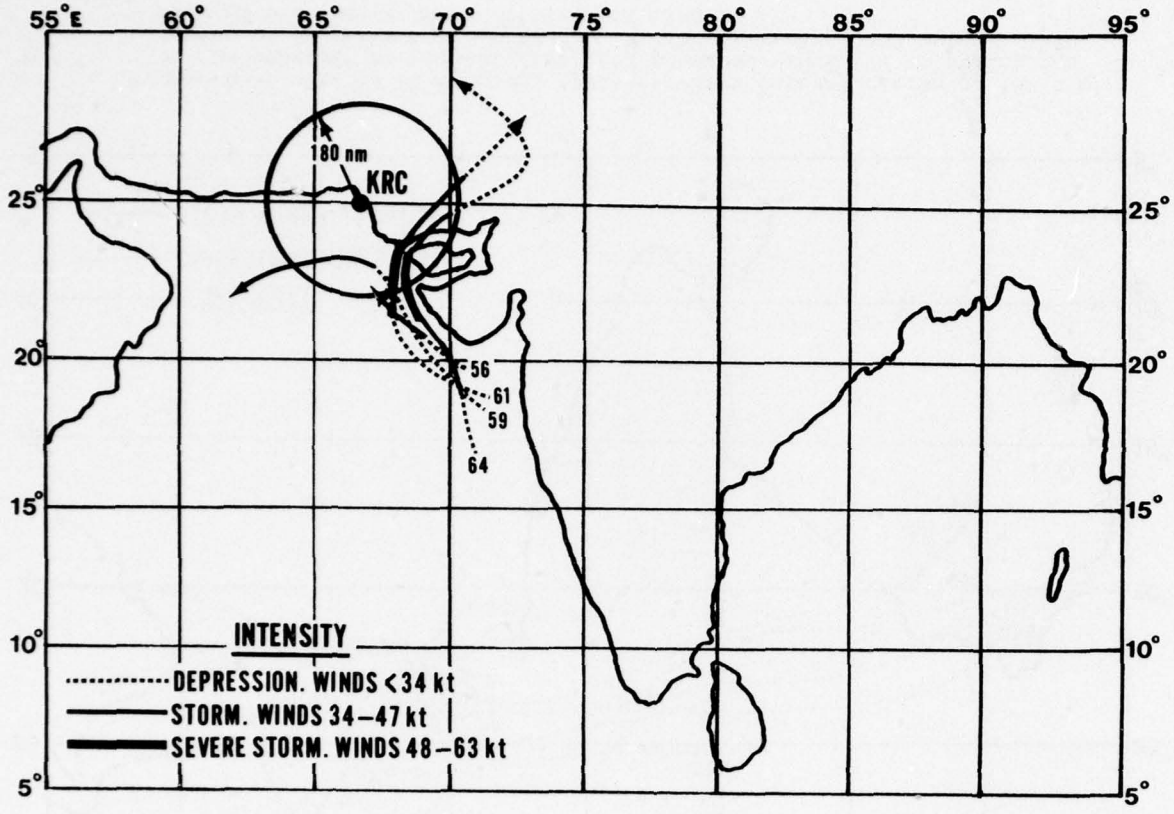

Figure D-1. Tracks of tropical cyclones which entered circle of 180 n mi radius centered on Karachi (KRC) and produced winds ≥22 kt during June. Period of record 1950 through 1970. Year of occurrence shown at start of track.

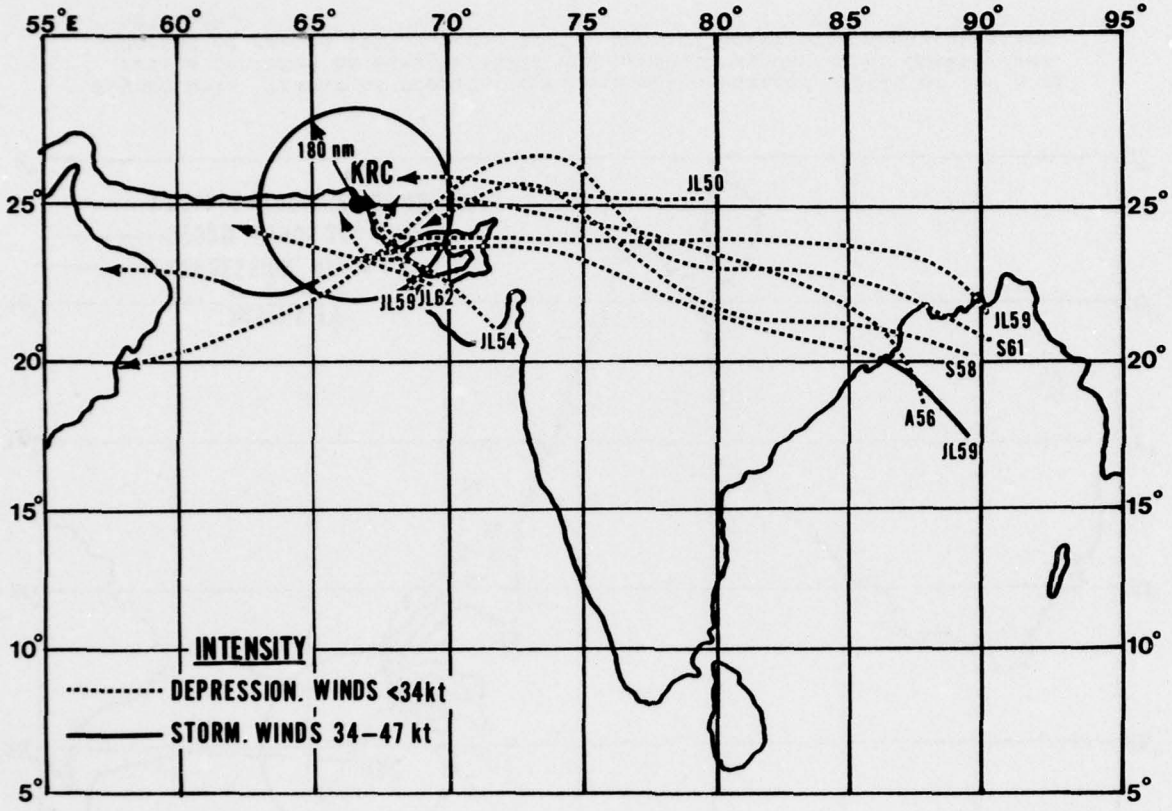

Figure D-2. Tracks of tropical cyclones which entered circle of 180 n mi radius centered on Karachi (KRC) and produced winds >22 kt during the months of July through September. Period of record 1950 through 1970. Year of occurrence shown at start of track.

☆U.S. GPO: 1977-791-511

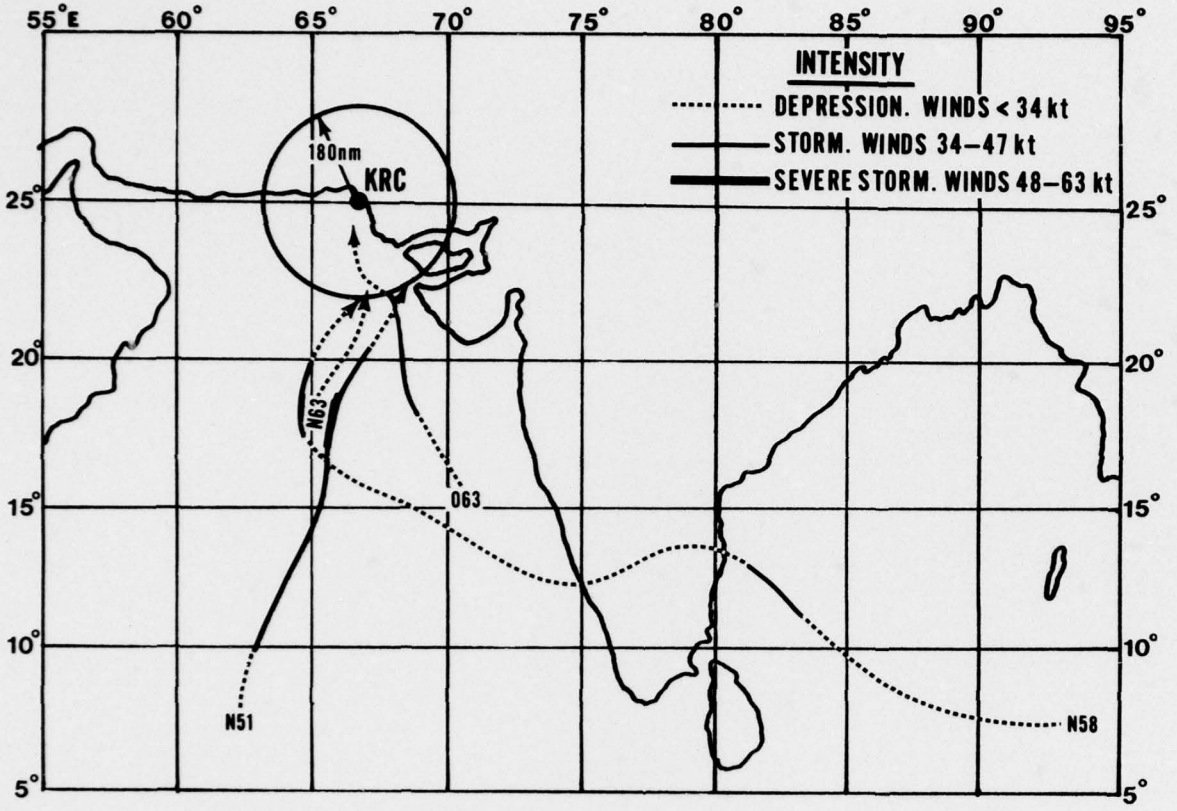

Figure D-3. Tracks of tropical cyclones which entered circle of 180 n mi radius centered on Karachi (KRC) and produced winds >22 kt during the months of October and November. Period of record 1950 through 1970. Year of occurrence shown at start of track.